Localization and Trafficking of CXCR4 and CXCR7

Lokalisation und Verteilung von CXCR4 und CXCR7

Doctoral thesis for a doctoral degree
at the Graduate School of Life Sciences,
Julius-Maximilians-Universität Würzburg,
Section Biomedicine

submitted by

Ali İşbilir

from

Tokat, Turkey

Würzburg **2021**

Submitted on:

Members of the Thesis Committee

Chairperson: Prof. Dr. Manfred Gessler

Primary Supervisor: Prof. Dr. Martin J. Lohse

Supervisor (Second): Prof. Dr. Markus Sauer

Supervisor (Third): Prof. Dr. Martine J. Smit

Date of Public Defence:

Date of Receipt of Certificates:

AFFIDAVIT

I hereby confirm that my thesis entitled “Localization and Trafficking of CXCR4 and CXCR7” is the result of my own work. I did not receive any help or support from commercial consultants. All sources and / or materials applied are listed and specified in the thesis.

Furthermore, I confirm that this thesis has not yet been submitted as part of another examination process neither in identical nor in similar form.

Place, date Signature

EIDESSTATTLICHE ERKLÄRUNG

Hiermit erkläre ich an Eides statt, die Dissertation “Lokalisation und Verteilung von CXCR4 und CXCR7” eigenständig, d.h. insbesondere selbständig und ohne Hilfe eines kommerziellen Promotionsberaters, angefertigt und keine anderen als die von mir angegebenen Quellen und Hilfsmittel verwendet zu haben.

Ich erkläre außerdem, dass die Dissertation weder in gleicher noch in ähnlicher Form bereits in einem anderen Prüfungsverfahren vorgelegen hat.

Ort, Datum Unterschrift

ABSTRACT

G protein-coupled receptors (GPCRs) constitute the largest class of membrane proteins, and are the master components that translate extracellular stimulus into intracellular signaling, which in turn modulates key physiological and pathophysiological processes. Research within the last three decades suggests that many GPCRs can form complexes with each other via mechanisms that are yet unexplored. Despite a number of functional evidence in favor of GPCR dimers and oligomers, the existence of such complexes remains controversial, as different methods suggest diverse quaternary organizations for individual receptors. Among various methods, high-resolution fluorescence microscopy and image-based fluorescence spectroscopy are state-of-the-art tools to quantify membrane protein oligomerization with high precision. This thesis work describes the use of single molecule fluorescence microscopy and implementation of two confocal microscopy based fluorescence fluctuation spectroscopy based methods for characterizing the quaternary organization of two class A GPCRs that are important clinical targets: the C-X-C type chemokine receptor 4 (CXCR4) and 7 (CXCR7), or recently named as the atypical chemokine receptor 3 (ACKR3). The first part of the results describe that CXCR4 protomers are mainly organized as monomeric entities that can form transient dimers at very low expression levels allowing single molecule resolution. The second part describes the establishment and use of spatial and temporal brightness methods that are based on fluorescence fluctuation spectroscopy. Results from this part suggests that ACKR3 forms clusters and surface localized monomers, while CXCR4 forms increasing amount of dimers as a function of receptor density in cells. Moreover, CXCR4 dimerization can be modulated by its ligands as well as receptor conformations in distinct manners. Further results suggest that antagonists of CXCR4 display distinct binding modes, and the binding mode influences the oligomerization and the basal activity of the receptor: While the ligands that bind to a “minor” subpocket suppress both dimerization and constitutive activity, ligands that bind to a distinct, “major” subpocket only act as neutral antagonists on the receptor, and do not modulate neither the quaternary organization nor the basal signaling of CXCR4. Together, these results link CXCR4 dimerization to its density and to its activity, which may represent a new strategy to target CXCR4.

ZUSAMMENFASSUNG

G protein-gekoppelte Rezeptoren (GPCRs) bilden die größte Klasse der Membranproteine und sind entscheidend an der Übersetzung extrazellulärer Reize in intrazelluläre Signale beteiligt, welche wiederum unzählige physiologische und pathophysiologische Prozesse regulieren. Die Forschungsergebnisse der letzten drei Jahrzehnte deutet darauf hin, dass viele GPCRs mittels noch weitgehend unbekannter Mechanismen miteinander Komplexe bilden können. Trotz vielfältiger Beobachtungen, die für die funktionelle Relevanz von GPCR-Dimeren und -Oligomeren sprechen, ist deren Existenz dennoch weiterhin umstritten, vor allem da verschiedene Methoden auf unterschiedliche quaternäre Anordnungen derselben Rezeptoren hinweisen. Von den derzeit verfügbaren Methoden zur genauen Untersuchung der GPCR-Dimerisierung/-Oligomerisierung, stellen die hochauflösende Fluoreszenzmikroskopie sowie die bildbasierte Fluoreszenzspektroskopie die Techniken der Wahl dar. Die hier vorliegende Arbeit beschreibt die Anwendung der Einzelmolekül-Fluoreszenzmikroskopie sowie zweier konfokalmikroskopischer Methoden zur Messung der Fluoreszenzfluktuation, mit deren Hilfe die quaternäre Anordnung zweier klinisch hochattraktiver Klasse A GPCRs untersucht wurde: der C-X-C Typ Chemokinrezeptoren 4 (CXCR4) und 7 (CXCR7), letzterer auch bekannt als atypischer Chemokinrezeptor 3 (ACKR3). Der erste Teil der Ergebnisse legt anhand Untersuchungen an einzelnen Molekülen dar, dass CXCR4 überwiegend in Form monomerer Einheiten auftritt, die bei sehr geringen Expressionsleveln kurzlebige Dimere bilden können. Der zweite Teil beschreibt die Etablierung und Anwendung räumlicher und zeitlicher Brillanzmethoden, die auf der spektroskopischen Untersuchung der Fluoreszenzfluktuation beruhen. Die Ergebnisse dieses Abschnitts deuten darauf hin, dass ACKR3 sowohl in Form beständiger Rezeptor-Cluster, und monomere Einheit an der Oberfläche lebender Zellen auftritt. CXCR4 ist bei zunehmender Rezeptordichte hingegen vermehrt in Form von Dimeren zu finden. Zudem kann die Dimerisierung von CXCR4 von dessen Liganden, als auch von der drei-dimensionalen Anordnung der Rezeptorteilstrukturen (Rezeptorkonformation) auf unterschiedliche Weise reguliert werden. Die weiteren Ergebnisse legen nahe, dass Antagonisten auf unterschiedliche Weise an CXCR4 binden können und dass der jeweilige Bindungsmodus entscheidend für den Einfluss des Liganden auf Oligomerisier-

ung und basale Aktivität von CXCR4 ist: Während Liganden, die an eine kleinere Untertasche des Rezeptors binden, sowohl die Dimerisierung als auch die Basalaktivität unterdrücken, fungieren Verbindungen, die an eine andere, größere Untertasche binden, lediglich als neutrale Antagonisten und zeigen keinerlei Einfluss auf die quaternäre Anordnung und basale Aktivität von CXCR4. Zusammenfassend verknüpfen diese Ergebnisse CXCR4-Dimerisierung mit der Rezeptordichte in Zellen und seiner Aktivität, was die Grundlage für neue Strategien zur phamakologischen Modulation von CXCR4 darstellen könnte.

TABLE OF CONTENTS

LIST OF FIGURES

LIST OF TABLES

LIST OF SYMBOLS

μg	Microgram
μM	Micromolar
μL	Microliter
Å	Ångstrom
α	Alpha
β	Beta
Δ	Delta
ε	Epsilon
γ	Gamma
κ	Kappa
λ	Lambda
μ	Mu
σ	Sigma
τ	Tau
ω	Omega

LIST OF ACRONYMS / ABBREVIATIONS

AC	Adenylyl cyclase
ACKR	Atypical chemokine receptor
ACTH	Adrenocorticotropic hormone
ADP	Adenosine diphosphate
ARF-GAP	ADP-ribosylation factor GTPase-activating proteins
ATP	Adenosine triphosphate
BRET	Bioluminescence resonance energy transfer
BN PAGE	Blue native polyacrylamide gel electrophoresis
cAMP	Cyclic adenosine monophosphate
cryoEM	Cryogenic electron microscopy
CCP	Clathrin coated pit
CCR	CC type chemokine receptor
cpFP	Circularly permuted fluorescence protein
CXCR	C-X-C type chemokine receptor
DAG	Diacylglycerol
*d*STORM	Direct stochastical optical reconstruction microscopy
ECL	Extracellular loop
EM	Electron microscopy
eN&B	Enhanced number and brightness
EPAC	Exchange factors directly activated by cAMP
GABA	Gamma aminobutyric acid
GAIN	GPCR autoproteolysis inducing
GCGR	Glucagon receptor
GDP	Guanosine diphosphate
GPCR	G protein-coupled receptor
GRK	G protein-coupled receptor kinase
GTP	Guanosine triphosphate
FCS	Fluorescence correlation spectroscopy
FFS	Fluorescence fluctuation spectroscopy

FIF	Fluorescence intensity fluctuation
FP	Fluorescent protein
FRAP	Fluorescence recovery after photobleaching
FRET	Fluorescence resonance energy transfer
FRET AB	Fluorescence resonance energy transfer acceptor photobleaching
HDX-MS	Hydrogen-deuterium exchange mass spectrometry
ICL	Intracellular loop
ICS	Image correlation spectroscopy
MD	Molecular dynamics
N&B	Number and brightness
NMR	Nuclear magnetic resonance
PALM	Photoactivated localization microscopy
PCH	Photon counting histogram
PKA	Protein kinase A
PKC	Protein kinase C
PLC	phospholipase C
PP-2A	Protein phosphatase type 2A
PCR	Polymerase chain reaction
RGS	Regulator of G protein signaling
RICS	Raster image correlation spectroscopy
SB	Spatial brightness
SpIDA	Spatial intensity distribution analysis
STED	Stimulated emission depletion
STICS	Spatiotemporal image correlation spectroscopy
TB	Temporal brightness
TICS	Temporal image correlation spectroscopy
TIRF	Total internal reflection fluorescence
TM	Transmembrane
TR-FRET	Time resolved fluorescence resonance energy transfer
VFT	Venus flytrap

1. INTRODUCTION

1.1. Receptor Theory and Signal Transduction

Cells are the basic units of life that make up a whole, functional organism. A living, functional cell processes countless number of biochemical activities within its borders, which define its physiology. Communicating with the environment is *sine qua non* of cellular functionality. The communication of a cell with a nearby peer, or with a distinctly localized one can be mediated by physical and chemical stimuli. An electrical transmission through brain cells, or a hormone that can travel via the blood through peripheral tissues are examples of these physical and chemicals stimuli, respectively. Signal transduction is the general mechanism defined by physical and biochemical reactions, evoked by the extremal stimuli, which eventually produces the physiological response of the cells, such as gene transcription, secretion of ions/peptides, cellular motility, differentiation, division, cell death *et cetera*.

But how do cells recognize their environment to activate such a cascade of signaling processes? We now know that (putting aside the transmembrane transport of certain molecules) many extracellular cues are recognized by a specialized family of transmembrane proteins called “receptors”. The first step of signal transduction is the binding of an external molecule to the extracellular surface of its receptor. This binding induces conformational changes of the receptor protein, which enables the interaction with and activation of intracellular messengers. An activated messenger, in turn, initiates a cascade of biochemical reactions, which eventually ends up as a specific cellular response (Uings and Farrow, 2000). Most of the hormones, ions, cytokines, peptides, small molecules/nucleotides and even a large number of the drugs used in medicine are now known to exert their cellular functions through binding to specific cell surface receptors (Nair et al., 2019).

The largest superfamily of membrane localized proteins are the G protein-coupled receptors (GPCRs), or the seven transmembrane receptors (7TMRs), which comprise more

than 800 members. GPCRs are transmembrane proteins that respond to numerous external cues such as light, hormones, biogenic amines, peptides, ions, fatty acids, *et cetera*, and consequently activate intracellular signaling cascades (Pierce et al., 2002). They are expressed in every tissue and cell type (Regard et al., 2008), and they modulate almost all physiological processes (Marinissen and Gutkind, 2001). Due to their involvement in a wide range of physiological functions, GPCRs are also in the center of many pathophysiologies. As a natural result of this, modern drug development strategies have focused on modulating functions of GPCRs and yielded an enormous amount of GPCR targeting drugs, which constitute more than a third of all marketed drugs (Hauser et al., 2017).

Yet, drugs that we know now to target receptors were long used before there was any knowledge of receptors. So, it is perhaps fair to say that it were the advances on the action mechanism of drugs that led to the identification of receptors. Humans had already used a number of plant-extracted pharmacological reagents that are now known to be acting on receptors. Some examples of these early drugs are the muscarinic acetylcholine receptor binding alkaloids atropine (Geiger and Hesse, 1833), scopolamine (Gerrard, 1875) and pilocarpine (Ladenburg, 1881); opioid receptor binding alkaloids morphine (Sertuerner, 1817) and codeine (Robiquet, 1832); adrenergic receptor binding alkaloids ergotamine (Dale, 1922) and yohimbine (Lewitt, 1902).

The theory of cellular receptivity was perhaps firstly coined by the German scientist Paul Ehrlich, who firstly used the German term "*Seitenkette*" ("side chains" in English), after years of observations to conceptualize the cellular entities that toxins were able to bind (Ehrlich and Morgenroth, 1900). The "side chain" theory that Paul Ehrlich hypothesized is now known to be the cell surface and secreted antibody binding to antigens. Inspired by the cell surface binding conception of Ehrlich, the British pharmacologist John Newport Langley cautiously hypothesized that the direct pharmacological actions of nicotine and curare on the denervated muscle tissue contraction might be related to the activity of a "receptive substance", similarly to the mechanism that Ehrlich had proposed:

"The relation between the receptive and the contractile substance is clearly very close, and, on the general lines of Ehrlich's immunity theory, it might be supposed that a receptive substance is a side chain molecule of the molecule of contractile substance, but at present there does not seem to me to be any advantage in attempting to refer the phenomena to molecular arrangement." (Langley, 1905)

We now know that nicotine and curare act on nicotinic acetylcholine receptors, which are membrane bound ion channel proteins.

Acknowledging the novel receptor theory of Langley, another British scientist Henry Dale, who extensively worked on neurotransmitters, also mentioned the possibility of the involvement of specific "myoneural junctions", when he described how ergot extract reversed the vessel and muscle contraction actions of adrenaline (epinephrine), while it did not alter the vasodilation and muscle relaxation actions of adrenaline:

"A sympathetic nerve-supply of mixed function may contain some fibres connected to purely inhibitor, others to purely motor myoneural junctions: or, on the other hand, the myoneural junctions may themselves be composite, containing both motor and inhibitor elements. The question as to whether these so-called myoneural junctions are morphologically differentiated, or, as Langley suggests, distributed, as "receptor substances" through the muscle-fibre is also untouched by these results." (Dale, 1906)

Over the next two decades, the receptor theory was confronted by other scientists who based the drug action on other theories, suggesting that drugs act physically on cells by changing the cell membrane structure, or by penetrating into the cell. Yet, the work of another British pharmacologist Alfred Joseph Clark in 1930s, providing an extensive quantitative conceptualization of the pharmacological action of drugs, further supported that drug action may be dependent on receptive substances on the cell surface. The mathematical approach of Clark explained the action mechanism of several drugs in terms of the law of mass action and the Hill-Langmuir equation, which was originally developed to describe cooperative O_2 binding to hemoglobin (Hill, 1913). The physiochemical concepts Clark applied on drug activity further suggested that the drug response requires a receptor mediated activity:

"Measurements of the quantities of drugs that suffice to produce an action on cells, prove that in the case of powerful drugs the amount fixed is only sufficient to cover a small fraction of the cell surface. The speed with which drugs act and the slowness with which drugs penetrate cells indicates that many drugs probably act on cell surfaces. The simples probable conception of drug action is that potent drugs occupy certain specific receptors on the cell surface, and that these specific receptors only comprise a small fraction of the total cell surface." (Clark, 1933)

One of the most direct attempts to conceptualize receptor activity perhaps came from the seminal work of the American scientist Raymond P. Ahlquist in 1948. Ahlquist was the first to classify yet-to-be hypothetical receptors that mediate the actions of sympathomimetic amines. Ahlquist tested the excitatory and inhibitory effects of 6 biogenic amines and described two classes of adrenotropic receptors (*alpha* and *beta*) depending on their activity type on different physiological systems:

"There are at least two distinct general types of these receptors. ... The alpha adrenotropic receptor is associated vasoconstriction, and stimulation of the uterus, nictitating membrane, ureter and dilator pupillae) and one important inhibitory function (intestinal relaxation). The beta adrenotropic receptor is associated with most of the inhibitory functions (vasodilation, and inhibition of the uterine and bronchial musculature) and one excitatory function (myocardial stimulation). Racemic epinephrine ... is the one amine which is the most active on both the alpha and beta receptors". (Ahlquist, 1948)

It is yet interesting to note that Ahlquist himself assumed for a long time that these "receptors" were only a concept to explain the effects of the substances in tissues (Ahlquist, 1973). What perhaps added up a large support on the hypothesis of Ahlquist was the discovery of a specific beta receptor blocker Compound 38,174, or as now known as propranolol, which inhibited the beta receptor specific cardiac sympathetic activity and reduced arterial blood pressure (Black and Stephenson, 1962).

Starting with the British scientist Ernest Henry Starling, who coined the term "hormone" in 1905 (Starling, 1905), an emerging research led to the discovery of intracellular components, now known as second messengers, such as inositol phosphate (Hokin and Hokin, 1989) and cyclic adenosine monophosphate (cAMP) (Sutherland and Rall, 1957, 1958) that mediate neurotransmitter and hormone activity inside the cell. The merging of

hormone activity and intracellular signaling even led the American pharmacologist Earl W. Sutherland to propose that adenylyl cyclase (AC), the enzyme that synthesizes cAMP from adenosine triphosphate (ATP), is the cell surface receptor for adrenaline (Robison et al., 1967). Yet, it is now known that ACs are not the direct receptors of adrenaline. Work of Lutz Birnbaumer and Martin Rodbell using α- and β-blockers displayed clear evidence that the effect of each hormone or catecholamine on cAMP production was mediated by their cognate receptors (Birnbaumer and Rodbell, 1969). The first proof that G proteins are distinct from receptors and ACs was actually provided when Thomas Pfeuffer and Ernst J. M. Helmreich isolated the G proteins in Würzburg (Pfeuffer and Helmreich, 1975). Further developments in the field by Martin Rodbell and Alfred Gilman brought up the importance of guanosine triphosphate (GTP) and GTP hydrolyzing enzymes Gs and Gi into light as essential components to modulate AC mediated cAMP catalysis. Their work on how the nucleotide GTP and G proteins modulated ligand binding to the cells further supported the indispensable role of receptors as specialized components to mediate stimulus specific cellular signaling (Rodbell, 1980). Later, it was found that G proteins were trimeric complexes that were constituted by three distinct subunits (α, β and γ) (Hildebrandt et al., 1984; Sternweis et al., 1981).

One of the most direct evidences for hormone/catecholamine specific receptor theory emerged with the advances in radioligand binding assays on cell membranes. Experiments on isolated membranes of animal cells of different tissues using radioisotope labeled glucagon, ACTH and the beta blocker alprenolol and ligands that compete with them provided a platform to quantify specific receptors on membranes, and supported the functional and physical discrimination of α- and β-adrenoreceptors even further (Alexander et al., 1975; Lefkowitz et al., 1970; Pohl et al., 1971; Williams et al., 1976). Following studies revealed more and more details of how GTP and G proteins modulated low affinity and high affinity states of the receptors (Kent et al., 1980); while the presence of nucleotide free G proteins increased the potency of ligand binding, GTP binding to G proteins reduced it. These advances in the field brought up a complex model, called the “ternary complex model”, describing the functional and cooperative relationship between the agonist, receptor, G protein and the effector (De Lean et al., 1980).

All of the studies mentioned above only functionally described the existence of the receptors. Development of affinity chromatography methods using columns functionalized with receptor ligands paved the path to isolating the first adrenoreceptors as pure proteins (Caron et al., 1979; Lomasney et al., 1986; Regan et al., 1982; Shorr et al., 1981; Vauquelin et al., 1977, 1979). Soon after, scientists were able to reconstitute these isolated proteins and prove their functionality, postulating that these receptors were intact, single unit proteins (Cerione et al., 1983). Following these, thanks to the development of novel molecular biology tools, it became possible to discover the genetic material in which these drug and hormone receptors were encoded (Dixon et al., 1986; Kobilka, Dixon, et al., 1987; Kobilka, Matsui, et al., 1987). Sequencing of the whole genome of the human (Craig Venter et al., 2001) then led to the discovery of numerous other receptor genes with similar homology to the ones that were discovered previously (Fredriksson et al., 2003; Takeda et al., 2002).

1.2. G Protein-Coupled Receptors

As mentioned in the previous chapter, GPCRs are the largest subclass of membrane proteins. In humans, genes encoding for all GPCRs constitutes approximately 3-4% of the whole protein-coding genes (Takeda et al., 2002). The function of all GPCRs in simplest terms is translate extracellular information into the cell via signal transducers and intracellular effectors that initiate a cascade of biochemical events, which in turn exert a cellular response, such as the regulation of gene expression, activation of transmembrane ion flux, secretion of hormones and neurotransmitters, cellular motility, neural activity, cell division, differentiation. These cellular processes in broad terms modulate systemic behaviors, such as vision, smell, taste, heartbeat, mood, immune response, muscle contraction *et cetera*. Because GPCRs are involved in almost every physiological function, dysregulations in their functions are associated with numerous diseases, such as hypertension, cancer, depression, autoinflammation, diabetes, migraine and many more. Not surprisingly, an enormous number of drugs used routinely in clinical practice, or being developed, target mainly GPCRs (Santos et al., 2016). This alone indicates the importance of GPCRs not only in physiology, but also in drug development and pharmacology. Currently, there are drugs in the market targeting only about a hundred of all known GPCRs. Understanding

how GPCRs function at systemic, cellular and molecular level is a crucial aspect of mapping the role of each receptor in human physiology and pathophysiology. In order to develop efficient and safer drugs, it is crucial to have a broad understanding of these proteins in terms of their structure, distribution, interactions, signaling behavior and physiological effects in living organisms.

1.3. Structural Features and Activation of GPCRs

The general topology of GPCRs exhibits a seven transmembrane (TM) alpha helical structure, in which each helical domain is connected to each other with alternating intracellular and extracellular loops (ICLs and ECLs), together with unstructured N terminal and C terminal domains, which all together assemble to a single continuous "bundle" (Figure 1-1).

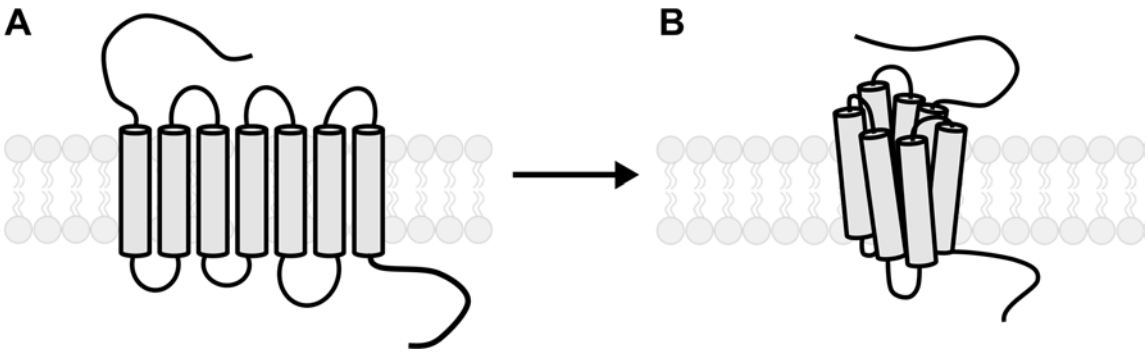

Figure 1-1. General topology and organization of the transmembrane domains of GPCRs. GPCRs consist of seven transmembrane *alpha* helical domains that are connected to each other with unstructured loops, often an intracellular helix 8 connected to an unstructured C terminal domain, and an N terminal domain.

A more detailed view of GPCR secondary and tertiary structures allowed dividing GPCRs in 6 classes (Foord et al., 2005): Class A (rhodopsin-like) GPCRs constitute the largest class with ~400 olfactory receptors and ~300 non-olfactory receptors. Class B (secretin-like) receptors exhibit usually a larger N terminal domain compared to that of the class A GPCRs, and their native ligands are peptide hormones which form extensive con-

tac s with the charact r stic N term nus of the re eptor f his class (F gure 1 2B). rel- ati e y ne subclass of clas B is th adhes on G CRs, hich o prise a much large and comp ex N te minal dom in than other class B recept rs. Adhe ion recep ors media e cel - ell or c ll-extracellu ar matrix adh sion funct ons via t eir large N termi al domai . Class C (meta otropic glutamate) receptors are characterized by their constitutively dimeric or- ganizat on and an N terminal so-called v nus fly rap (VF) dom in hat const tute the ligand bin ing cleft (Figure 1-2). Class D (fungal mating GPCRs are expressed nly in fu g and are responsible f r sensi g pheromones and nu ri nts. A recent stu y show d that th cl ss D rece to Ste2 exhib ted imeric assembly (Velazhahan et al , 2021) Class E (cAM) receptors are exp essed in slime mo ds uch as *Dic yostelium dis oid um* an hey media e d velopment, ifferenti tio and chem taxis (Hereld and Devreotes, 1993). Last y, the class F (Fr zzled a d Smoothe ed) ecep or ar activated by c steine-r ch i- p glycoprote ns a led WNT . Intrig ingly, class rece t rs lack many o the onserved m tifs req ired for GPCR acti ation nd G protein binding. Structurall , lass GPC s ex ibi a cl ss s ecif c cyste ne rich e tracel ul r domain Figure 1- D). Evolu iona y ana yses of GPCRs show that all GPCR c me from a common ance tor. Tr ces of th o de t GPC - ike re epto s wer f und i f ngi nd prot stom s (Schöne erg et l. 2007 . Humans only express the cl ss , B, C a d F G CRs. Each cl ss of GPCRs i also ivided into su groups de ined by their seq en e imilariti s (Joost nd Meth er, 2002) (Figure 1-3).

GP Rs e hibit highly class- pec fic onse ved s quences/dom ins of TM res du s. A gene ic residu nu bering s stems based on his c n ervati n scheme for each GPC class fa il tates he a ignment of d ffe ent recept rs for sequ nce compa ison. or class A PCR , Balles ero -Wein tein n mbering i wi el used (Balles ero an Weins ein, 1995 . T is numbe in sc eme con ists of wo num ers: the first umber i dicates t e M hel x nu ber, nd the econd ndic tes th po ition of t e r si ue relati e to th mo t con- er ed residue (umbere as *x*.50 *x* is helix nu ber) with n that eli . For cla s , C and F num er ng s stems ar for ed in a iden ical lo ic but with c ss specific conserved residue for anchoring as reference (Pin et al., 2003; C. Wang et al., 2014; Wootten et al., 2013).

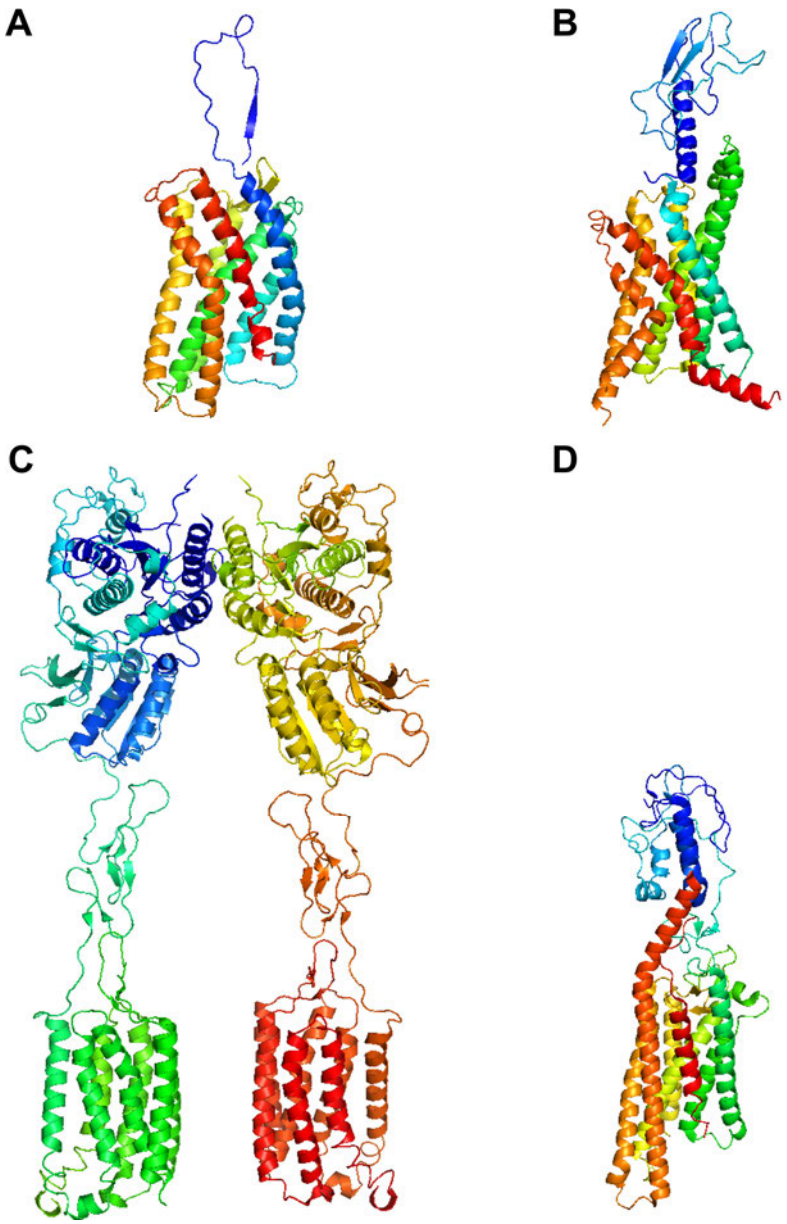

Figure 1-2. Example structures of GPCRs expressed in humans. (A) class A, CXCR4 (Ngo et al., 2020); (B) class B, Glucagon-like peptide-1 receptor (GLP1R) (Kawai et al., 2020); class C, metabotropic glutamate receptor 5 (mGluR5) (Koehl et al., 2019); class F, smoothened (SMO) (Qi et al., 2020).

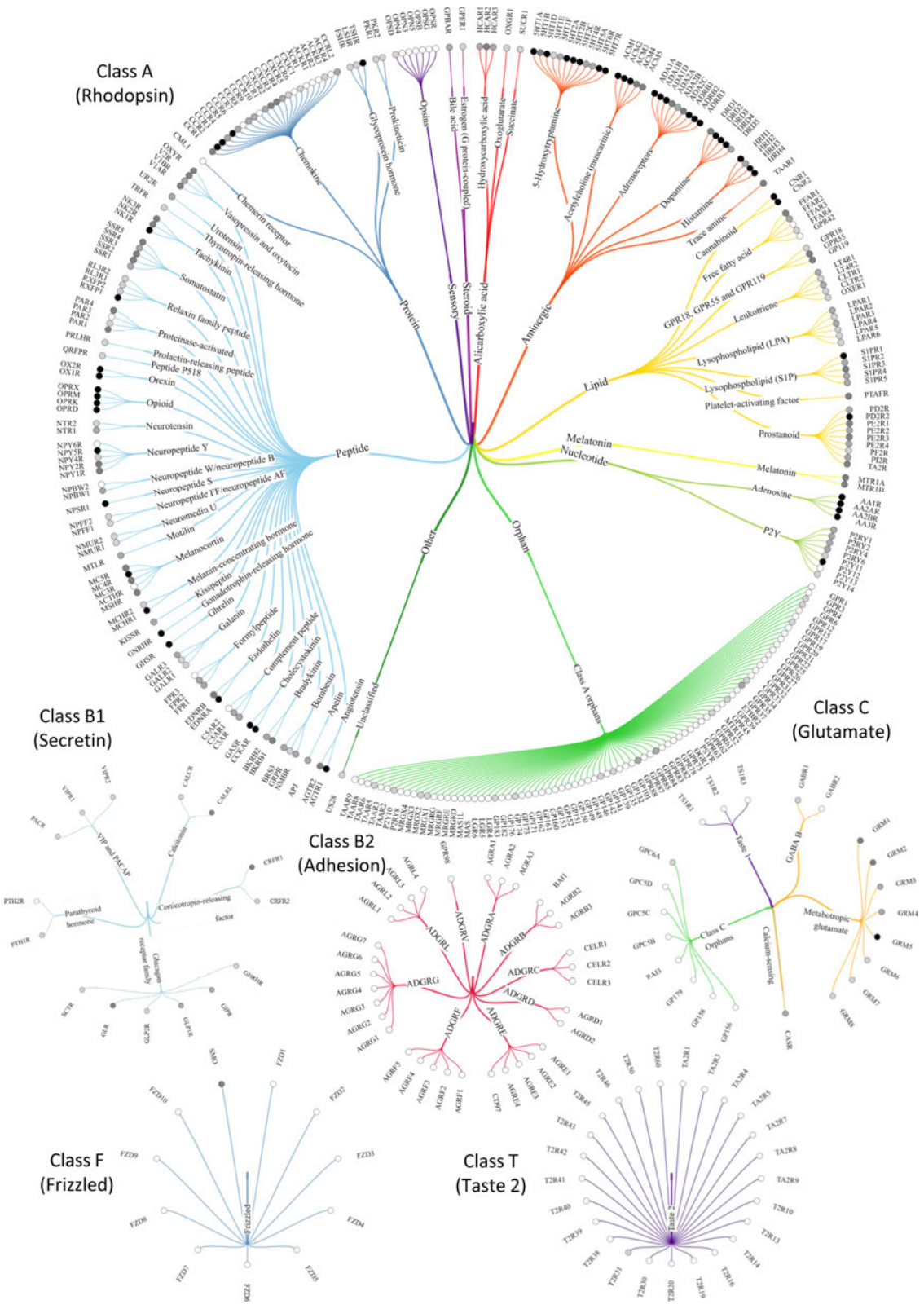

Figure 1-3. Phylogenetic tree representation of all human GPCR classes and subdivisions. Image is extracted from (Pándy-Szekeres et al., 2018).

GPCRs from all classes are activated either by light or upon binding of an endogenous extracellular agonist to a specific cleft, named ligand binding pocket, which is located mainly at the transmembrane domains of the protein. In general terms, receptor activation is defined by a series of conformational changes that occur within the receptor domains upon ligand binding, which eventually stabilizes the receptor in an "active conformation". This active conformation is able to interact with and activate the intracellular proteins to stimulate downstream signaling cascades. Years of research have shown that GPCRs do not exist only in a fixed "inactive" or an "active" conformation, but they rather exhibit a dynamic switch between several inactive and active conformations, thus causing a certain level of basal receptor activity. Agonist binding stabilizes a certain active receptor conformation, which allows effector binding and signal transduction as response. Partial agonists are the ligands that shift only a certain population of the receptors to an active conformation that is less than that of full agonists. As a consequence, the maximal receptor activity reached by partial agonists is less than that of full agonists. Another class of ligands, inverse agonists, shift the equilibrium of dynamics towards inactive receptor conformations. Finally, antagonist ligands do not cause a significant shift in the active-inactive equilibrium of the receptor population.

Agonist bound receptor conformation provides a high affinity at the intracellular site of the receptor for signal transducer coupling. This process provides the basis of an allosteric coupling feature of GPCRs. Moreover, binding of the signaling proteins at the intracellular site increases the affinity of the agonist at the ligand binding pocket of the receptor (Devree et al., 2016). According to the knowledge coming from numerous structural studies, GPCR conformations are determined by molecular interactions of varying strength between residues from different TM domains as well as ECLs and ICLs. Binding of an agonist at the extracellular site of the receptor causes a number of switches in specific residue-residue interactions. These changes cause further molecular rearrangements along the TM residues towards the intracellular end of the receptor like a defined allosteric pathway. While there are certain differences between the activation mechanisms of GPCRs from different classes, a signature indicator of GPCR activation is the outward movement of the intracellular part of the transmembrane helix 6 (TM6) (Rasmussen et al., 2011). This

movement, along with other critical conformational changes, opens a cleft at the intracellular face of the receptor that allows effector coupling. Computational analyses of ever-growing number of GPCR structures in their active, inactive and basal conformations resolve more and more details of the receptor activation mechanisms at the molecular level. These analyses helped to discriminate the common features of GPCR activation, as well as class-specific molecular signatures and rearrangements in certain "motifs".

For class A GPCRs it is now known that agonist binding can alone shift the conformational equilibrium towards the active state, and this active conformation includes outward movement of the TM6 at the intracellular side (Rasmussen et al., 2011). Yet, in the absence of the heterotrimeric G protein, the agonist bound active structure is not fully stable. Presence of the G protein further stabilizes the agonist bound active receptor conformation. A number of well conserved structural motifs that are made up of certain residues, called microswitches, govern the general allosteric activation mechanism of GPCRs. The most conserved motifs in class A GPCRs are 1) the (E)DRY motif in TM3, 2) the PIF motif formed between TM3-TM5-TM6, 3) the CWxP motif in TM6, 4) the NPxxY motif in TM7 and 5) the allosteric Na^+ binding pocket (White et al., 2018). The residues within each motif form non-covalent interactions to stabilize an inactive conformation. Upon binding to an agonist, interactions between the microswitches are weakened or broken, and in some cases rewired to form interactions with different residues, which in turn triggers rotations and movement of TM helices as well as changes in ICL secondary structures. Ligand binding triggers sequential conformational switches that translates from the ligand binding pocket to the intracellular part of the class A GPCRs (Zhou et al., 2019). According to reports from different receptors, the first step upon ligand binding is the rearrangement of the PIF and CWxP motifs as well as the Na^+ pocket, which moves the extracellular parts of the TM2, TM3 and TM7 closer. Rearrangement of these motifs triggers an allosteric rearrangement of a number of TM3 and TM6 residues, which initially form a so-called hydrophobic bridge. Meanwhile, new contacts are formed between TM3-TM7 residues at the cytoplasmic side via the Tyr7.53 of the NPxxY motif. Rearrangements in the hydrophobic bridge decrease TM3-TM6 interactions at the cytoplasmic side, mediate the loosening and the signature outward movement of the TM6. Upon these rearrangements, the well conserved ionic lock between the DRY motif of TM3 and charged residues of the

intracellular tip of TM6 breaks and allows more interactions between TM5-TM6 at the cytoplasmic side. All together, these molecular rearrangements open up a cleft that provides a high affinity docking site for the G protein (Figure 1-4).

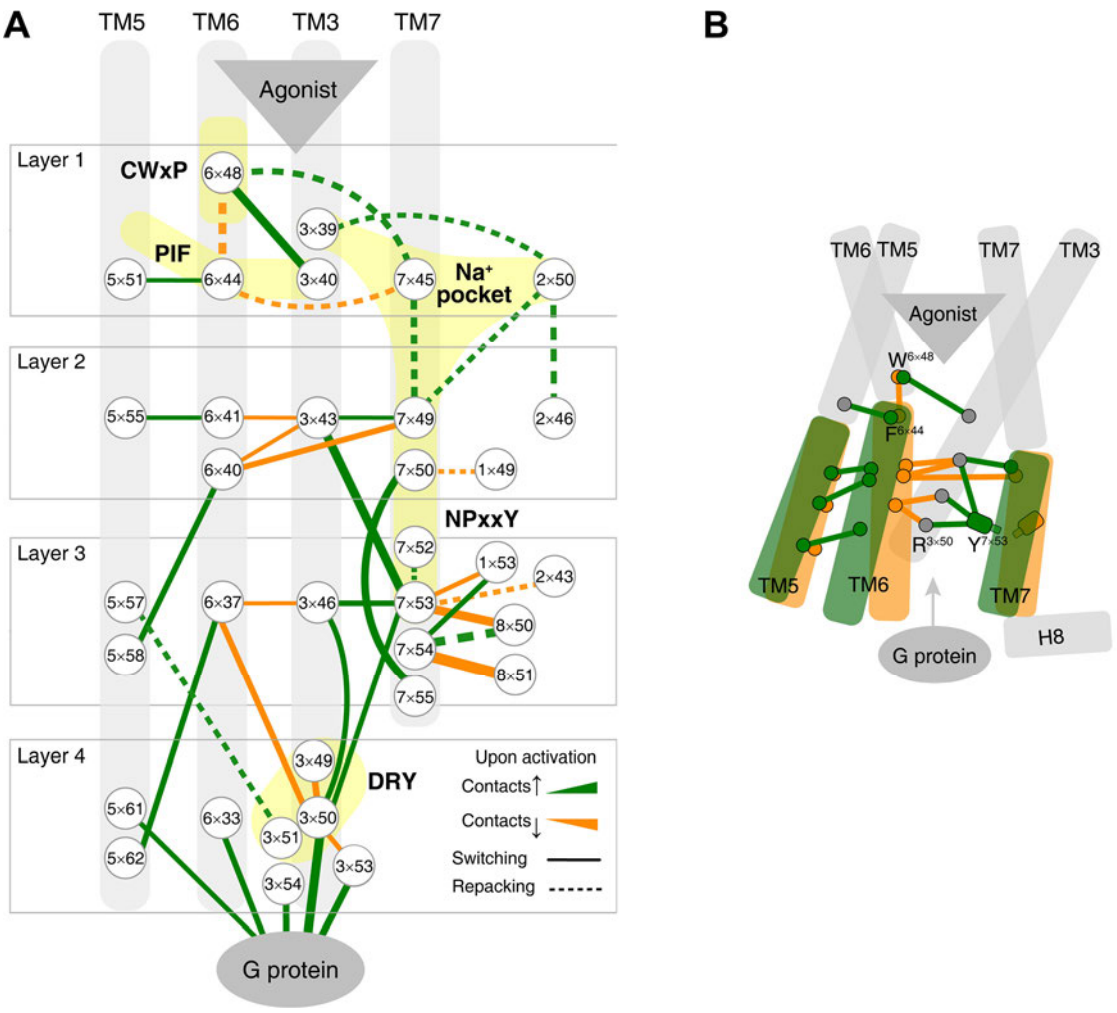

Figure 1-4. Topological model of the common activation pathway of class A GPCRs. (A) Upon agonist binding receptor activation occurs in four layers. In each layer, increasing (green) and decreasing (orange) contacts of conserved domains (yellow) and surrounding residues lead to the activation of the next layer. (B) Position and connections of conserved residues that modulate conformational changes upon agonist binding. Figure is extracted and reproduced from (Zhou et al., 2019), used under a Creative Commons Attribution-Noncommercial license: https://creativecommons.org/licenses/by/4.0/

Class B GPCRs exhibit a much larger N terminal domain compared to that of the class A GPCRs. This domain plays an important role for the binding of agonist peptide hormones. Several structures showed that the peptide agonists of class B GPCRs exhibit a

rod-like alpha helical structure. Except for calcitonin (Liang et al., 2017), the N terminal of these agonist peptides penetrates deep into the TM bundle of the receptor (Ma et al., 2020). All of the endogenous agonists of the class B GPCRs form extensive interactions with the N terminal domain of their receptor. The large N terminus of class B GPCRs contains structured and flexible domains. The structured domains consist of a short alpha helix and two beta sheets that are connected to each other via disulfide bonds. These structured domains play an important role in binding and stabilization of the peptide agonists on class B receptors. Mutations in the N terminus of these peptide agonists can turn them into antagonists, without any significant loss in their binding affinity (Seidel et al., 2017). Class B receptors do not exhibit many of the motifs that modulate class A receptor activation. Agonist bound structures of class B GPCRs display a clear distinction in terms of their activation mechanism. Firstly, agonist binding leads to an opening at the extracellular surface of the receptor, which is in contrast to the vestibule closure in class A receptors (Krumm and Roth, 2020). While agonist binding is sufficient for the signature outward movement of TM6 in class A, this is not directly the case for agonist bound class B GPCRs, as shown for the glucagon receptor (GCGR). Agonist binding indeed induces a number of conformational rearrangements in GCGR, including a very small outward movement of the TM6. This agonist induced conformation displays a high affinity at the intracellular site for G protein coupling. Binding of the G protein induces further structural rearrangements on GCGR. This includes a class specific outward opening of the TM6 (Hilger et al., 2020) (Figure 1-5A). Therefore, it can be said that agonist binding induces a low energy intermediate conformation of this exemplary class B receptor, and G protein coupling may be essential for them to reach a fully active conformation.

Another important aspect of class B receptor activation is the unusual structural change in the TM6. Unlike in class A GPCRs, in which the TM6 bends to perform the outward movement after ligand binding (Figure 1-5B), the TM6 in class B receptors undergoes a partial unwinding at the PxxG motif, and then G protein binding results in an outward kinking of the intracellular half of the helix. This structural rearrangement is the signature of class B GPCR activation (Duan et al., 2020; Liang et al., 2018; Zhang et al., 2017).

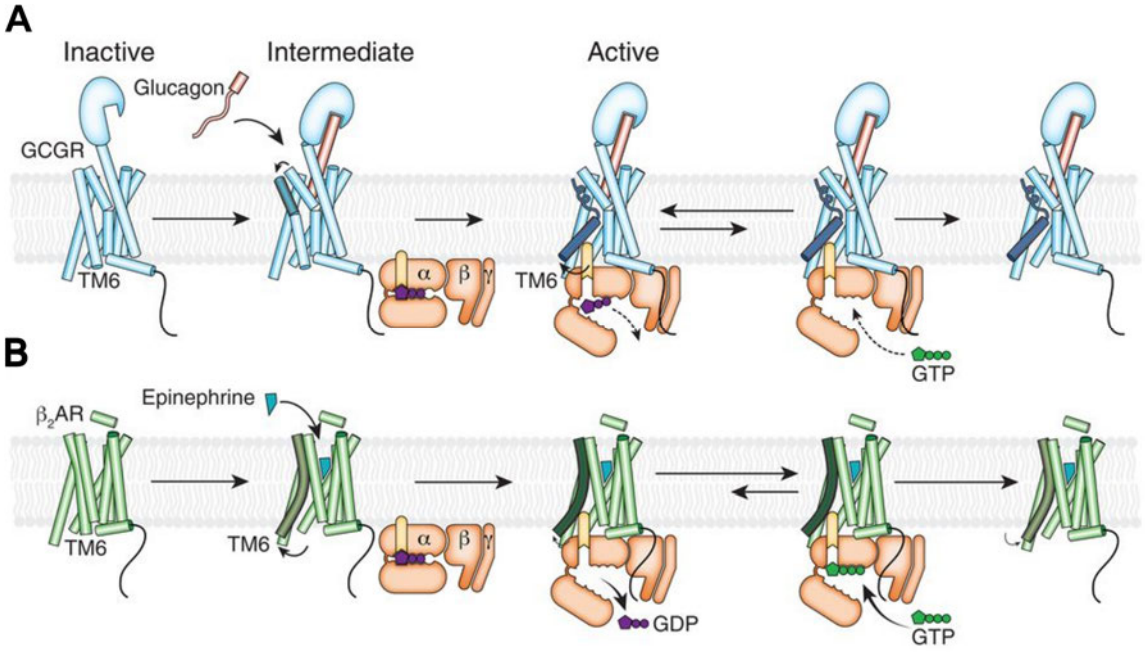

Figure 1-5. Activation models of class B and class A GPCRs according to the structural studies on GCGR and β_2AR. (A) Ligand binding to the class B GCGR induces conformational changes at the extracellular site, which leads to an intermediate conformation. G protein coupling to this conformation moves the TM6 outwards, and this complex activates nucleotide exchange in the G protein. Dissociation of the G protein causes a very slow relaxation of the active receptor conformation. (B) Agonist binding to β_2AR activates the receptor, including an outward movement of the TM6. G protein coupling further stabilizes the active conformation and allows rapid nucleotide exchange in the G protein. Dissociation of the G protein induces a rapid relaxation of β_2AR to agonist bound active state, where TM6 is not fully stable at the active position. Figure is extracted and reproduced from (Hilger et al., 2020), reprinted with permission from American Association for the Advancement of Science (AAAS).

Adhesion GPCRs, which belong to a subclass of the class B, exhibit an even larger N terminal domain compared to that of secretin like receptors. This large N terminus, which can consist of up to 1000 residues, contains distal adhesive subdomains, as well as a well conserved GPCR Autoproteolysis-Inducing (GAIN) domain, both of which define the subclass specific activation mechanism of these receptors. Adhesive subdomains are responsible for binding neighboring cell surface proteins or extracellular matrix elements. This binding starts the activation mechanism of adhesion GPCRs. Two models have been proposed to define this activation mode (Beliu et al., 2021). These models suggest that upon ligand binding of adhesive subdomains, the GAIN domain undergoes conformational changes that leads to self-catalysis, which in turn causes either 1) complete cleavage and dissociation, or 2) cleavage and remaining attachment via hydrophobic interactions of the

whole N terminal fragment. Following autoproteolysis, a beta sheet domain, which is buried within the GAIN domain at basal conformation, becomes revealed and solvent exposed. This domain, termed *Stachel*, is the "tethered agonist" and it can then interact with the ECLs and TMs of the receptor and leads to receptor activation (Liebscher et al., 2014). In line with this mechanism, truncation of the N terminal fragment displays a strong constitutive activation of adhesion GPCRs (Paavola et al., 2011). In comparison to the secretin like receptors, not much is known regarding the conformational rearrangement of the 7TM domain of adhesion GPCRs, due to the lack of structural and mutational studies. Yet, recent studies based on structure alignment, modeling and conformation simulations suggest that adhesion GPCRs retain a large number of the conserved activation motifs of secretin like receptors, which might as well modulate the conformations of the 7TM domain of adhesion GPCRs (Arimont et al., 2019).

Class C GPCRs comprise the metabotropic glutamate receptors, (mGluRs), gamma aminobutyric acid (GABA) B receptors ($GABA_BR$), a calcium sensing receptor (CaSR), taste sensing receptors (TaSRs) and a number of orphan receptors (Kniazeff et al., 2011). The most striking structural feature of these receptors is that they are obligate dimers, which means that they should form constitutive dimers to function (El Moustaine et al., 2012). Different types of mGluRs can form homo- and hetero-dimers, as well as TaSRs and CaSR. On the other hand, $GABA_BRs$ are strictly heterodimeric (Ellaithy et al., 2020). A well characterized domain that distinguishes class C receptors from others is the large N terminal portion called the "venus flytrap" (VFT) domain. VFT provides the ligand binding pocket for endogenous agonists (Takahashi et al., 1993). It is worth noting here that the TM domain of class C receptors appear to have additional, allosteric ligand binding pockets, which can be successfully targeted to modulate receptor activity (Leach and Gregory, 2017). The VFT domain contains a number of well conserved cysteines that form disulfide bonds between the dimer forming protomers in mGluRs (Romano et al., 1996) and CaSR (Bai et al., 1998). In case of mGluRs, the absence of the conserved disulfide bond does not affect dimerization remarkably, but decreases receptor activity greatly (Levitz et al., 2016). $GABA_{B1}R$- $GABA_{B2}R$ heterodimer is constituted during the protein maturation pathway via the noncovalent interactions of the C terminal domains of both receptors. $GABA_{B2}R$ heterodimerizes with $GABA_{B1}R$ in the endoplasmic reticulum (ER).

This dimerization masks an ER retention domain in the $GABA_{B1}R$ C terminus, thus facilitates the release of the homodimer to the cell surface (Bettler et al., 2004). The first step of class C GPCR activation is endogenous agonist binding to the VFT. In case of mGluRs, both VFTs bind to their agonist glutamate (Koehl et al., 2019), while only $GABA_{B1}R$ binds to GABA in case of the $GABA_BR$ heterodimer (Papasergi-Scott et al., 2020). Upon ligand binding, hinge domains of VFTs close (Kunishima et al., 2000) and a series of rapid conformational rearrangements occur between the VFTs of the dimeric protomers in sub millisecond range (Olofsson et al., 2014). Rearrangements in VFT domains propagate additional conformational changes, which bring the cysteine rich domains (bottom part of the N terminus) of both protomers closer to each other (Koehl et al., 2019; Liauw et al., 2021). In addition, intermolecular reorientations between the subunits of a dimer take place within a millisecond, which is followed by slower (20 millisecond) intramolecular rearrangements within each TM bundle (Grushevskyi et al., 2019). It is also thought that only one of the receptor protomers within a dimer can adopt an active conformation and recruit the G protein heterotrimer at a time (Ellaithy et al., 2020).

1.4. Types of GPCR Ligands

As mentioned above, GPCRs are structurally dynamic proteins: they continuously swing between several conformational rearrangements between a fully active and fully inactive arrangement. Therefore, within an observed time period, GPCRs display an equilibrium of different conformations. The fully active state is the one that displays the highest affinity to the downstream signal transducer, while the inactive state does not allow coupling or signaling. The equilibrium state of individual receptors define their basal activity: if a receptor adopts active or active like conformations more often, a basal activity at the signaling level can be observed.

Different types of endogenous and exogenous components that are able to bind GPCRs stabilize a certain receptor conformation, thus shift the conformational equilibrium to the advantage of those conformations that result in signal transduction with different efficacies (Figure 1-6). “Agonists” are the type of ligands that stabilize the most active

receptor conformation. “Partial agonists” are the ones that stabilize an “active like” conformation, which displays a lower signaling efficacy compared to that full agonists induce (Solt et al., 2017). Alternatively, it can be said that partial agonists can push the receptor to the fully active conformation less frequently than a full agonist. “Antagonists” are the molecules that bind to the receptor without changing the basal conformational equilibrium. “Inverse agonists” change the conformational equilibrium towards the inactive direction, which virtually does not allow any chance for downstream effector activation.

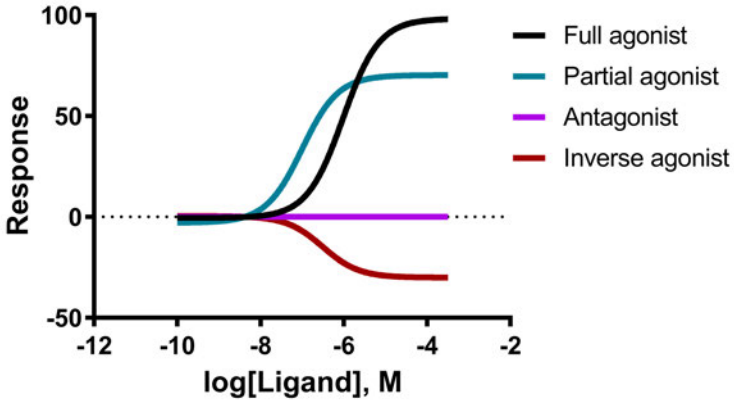

Figure 1-6. Pharmacologically distinct types of GPCR ligands. Response is the outcome of receptor activation. Ligands that change the receptor conformation induce a concentration dependent response, which can be fit to Hill equation when plotted at semi logarithmic scale. Response at zero stands for the basal activity of the receptor.

“Orthosteric” binding pocket is a term that defines the region of the receptor where the endogenous agonist binds. Molecules with other pharmacological features can also bind to this pocket. However, it is now known that many receptors contain more than one binding site. Those “non-orthosteric” ones are called “allosteric” binding pockets. Therefore, allosteric ligands are the ones that bind to these extra druggable clefts. An allosteric ligand can shift the receptor conformation towards inactive (negative allosteric modulator, NAM) or active (positive allosteric modulation) direction. While some allosteric modulators can change the basal receptor conformation alone, some of them require ligand binding to the orthosteric pocket in order to exert their effects. Recent research extended the degree of allosterism in GPCRs between pockets: binding of a ligand to the orthosteric pocket

may increase the affinity of an allosteric modulator, or vice versa (Jakubík et al., 2020; Leach et al., 2007).

1.5. GPCR Signaling

GPCRs are versatile proteins in terms of downstream signaling: they can couple to numerous intracellular proteins to initiate diverse signaling cascades with different spatio-temporal dynamics (Marinissen and Gutkind, 2001). By adopting an active conformation, GPCRs display a high affinity docking platform for downstream signaling partners. GPCR ligands with different binding modes are now known to induce diverse conformations, which can lead to the activation of a reduced number of pathways compared to that of an endogenous agonist. This phenomena is called “biased signaling”.

1.5.1. G Proteins

GPCRs were firstly found to be triggering intracellular signaling through the eponymous G proteins. G proteins are heterotrimeric proteins that consist of α, β and γ subunit. They bind to guanosine nucleotides and exert GTPase activity via the α-subunit. They become activated upon binding to an agonist bound, active GPCR. The main role of G proteins is to activate effectors that trigger downstream signaling cascades. At the basal state, heterotrimeric G protein complex is bound to GDP. Gβ and Gγ subunits form a tightly dimeric structure. Gα subunit interacts with the Gβγ complex through its N terminal α helical domain (αN), which also provides membrane localization via its myristyolated/palmitoylated residues. Gα subunit also has a Ras-like and another α helical (αH) domain that modulates nucleotide binding and catalysis (Sprang, 2010). Upon GPCR activation the heterotrimer couples to the intracellular site of the receptor. This binding is mainly mediated by the C terminal α5 helix of the Gα subunit (Weis and Kobilka, 2018). Upon coupling, Ras-like and αH domains undergo large conformational changes that allow GDP exchange with GTP. GDP to GTP exchange causes the dissociation of Gα and Gβγ subunits via molecular switches modulated by a G-R-E motif on the Gα subunit (Knight et al., 2020). Both subunits are now active and can activate a secondary messenger. Hydrolysis

of GTP by Gα is mediated with the assistance of the regulators of G-protein signaling (RGSs). This process terminates one cycle of G protein activity, and GDP bound Gα forms a trimeric complex with the Gβγ dimer again. As long as a receptor remains active, the activity cycle of G proteins continues (Figure 1-7).

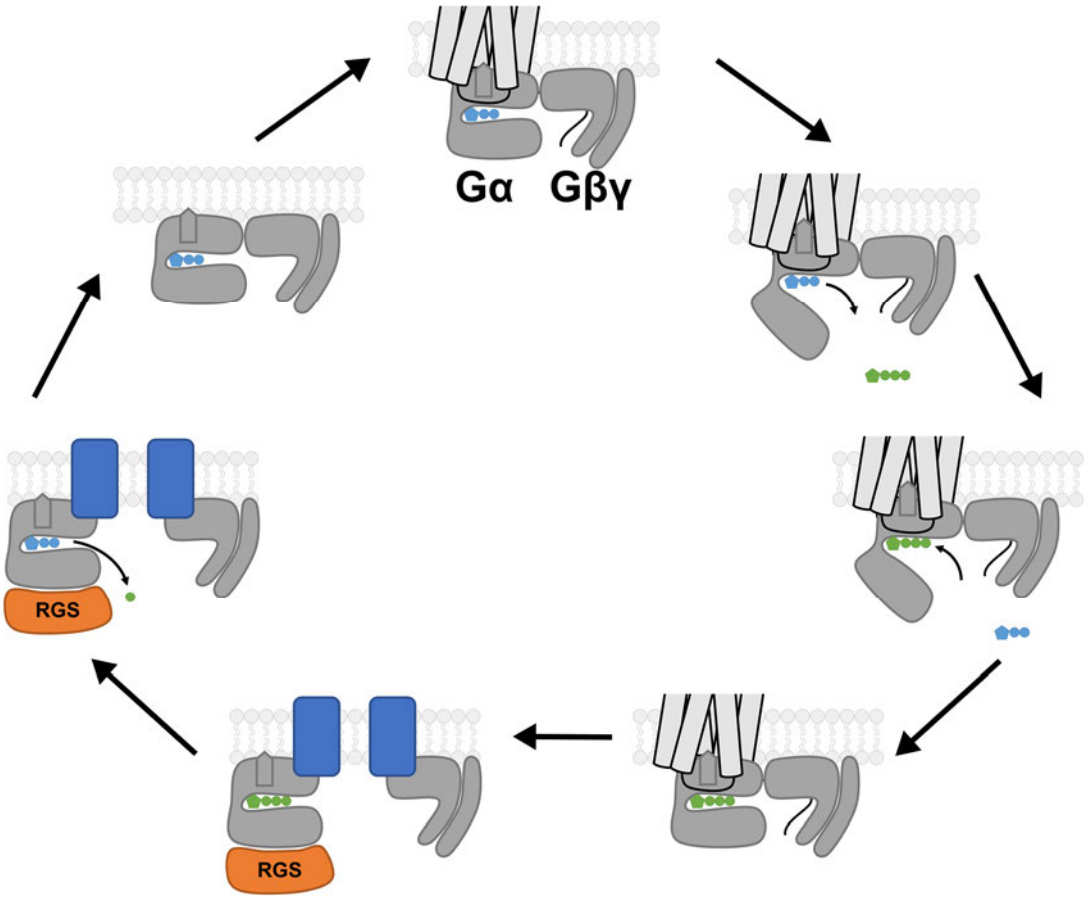

Figure 1-7. The basic G protein activation cycle. Upon receptor activation, GDP bound, inactive Gαβγ heterotrimer is recruited to the receptor. G protein stabilizes the ligand bound, active receptor conformation by inserting its α5 helix to the cytoplasmic core of the receptor. This coupling triggers a large conformational change that causes opening of the helical domain and triggers GDP release from the G protein, followed by GTP binding and closure of the α helical domain. GTP bound Gα subunit dissociates from the Gβγ subunit and these subunits activate their effectors. Meanwhile, Regulators of G protein signaling (RGS) proteins activate the GTPase activity of the Gα subunit, which causes GTP hydrolysis to GDP. GDP bound Gα then associates with the Gβγ and can bind to the active receptor again.

1.5.1.1. Gα Subunit Mediated Signaling

There are 23 Gα proteins that are categorized in four families: Gs ($G\alpha_{s\ short}$, $G\alpha_{s\ long}$, $G\alpha_{olf}$, $G\alpha_{gust}$); Gi ($G\alpha_{i1}$, $G\alpha_{i2}$, $G\alpha_{i3}$, $G\alpha_{oA}$, $G\alpha_{oB}$, $G\alpha_{z}$, $G\alpha_{t1}$, $G\alpha_{t2}$, $G\alpha_{t3}$); Gq ($G\alpha_{q}$, $G\alpha_{11}$, $G\alpha_{14}$, $G\alpha_{15}$ $G\alpha_{16}$); and G12 ($G\alpha_{12}$, $G\alpha_{13}$). Downstream signaling initiated by G proteins eventually leads to a number of changes in cell physiology and certain biological responses. It is difficult to provide a clear picture of G protein mediated signaling, because more and more research demonstrates novel coupling partners of second messenger products, which complicates the map of possible signaling cascades.

Gs family members are the first type of G proteins that were identified (Ross and Gilman, 1977; Sternweis et al., 1981). They bind to and activate 9 different types of adenylyl cyclases (ACs) that catalyze cAMP production from intracellular ATP. Increased amounts of cAMP further activate mainly the protein kinase A (PKA), exchange factors directly activated by cAMP (EPACs), and cyclic nucleotide gated channels. Members of the Gi family primarily inhibit AC activity, which in turn inhibits all cAMP mediated pathways. Interestingly, $G\alpha_o$ proteins do not directly inhibit ACs, yet they are able to reduce intracellular cAMP levels. The family of Gq proteins activates membrane bound phospholipase C β (PLCβ), and convert it into membrane bound diacylglycerol (DAG) and intracellular inositol-1,4,5-trisphosphat (IP3), which then binds to IP3 gated Ca^{2+} channels on the ER membrane and mediates intracellular release of Ca^{2+}. Gα12/13 subunits directly bind p115RhoGEF protein that activates Rho. Rho is a small GTPase that binds to its own effectors to initiate downstream signaling (Marinissen and Gutkind, 2001) (Figure 1-8).

1.5.1.2. Gβγ subunit mediated signaling

There are 5 different Gβ and 12 different Gγ subunits encoded in the human genome. Some of the subunits are restricted to certain cell types, and they can form different combinations of βγ dimers in different cells. Moreover, different βγ combinations determine the efficacy of GPCR activity and certain Gβγ combinations translocate intracellu-

larly to regulate signaling from certain compartments (Masuho et al., 2021). Upon activation of the G protein heterotrimer, the Gβγ subunit also activates a number of effectors in a fashion dependent on the partnering Gα subunit. In the case of Gi protein activity, Gβγ subunits bind and activate the G protein-coupled inwardly rectifying potassium channels (GIRKs). Gβγ subunits can also directly modulate other effectors, such as G protein-coupled receptor kinases (GRKs), PLCβ, Kir3 potassium channels, ACs, voltage gated Ca^{2+} channels, phosphoinositide 3 kinase γ (PI3Kγ) and the guanine exchange factor phosphatidylinositol-3,4,5-P3-dependent Rac exchanger 1 (PRex1) (Dupré et al., 2009) (Figure 1-8).

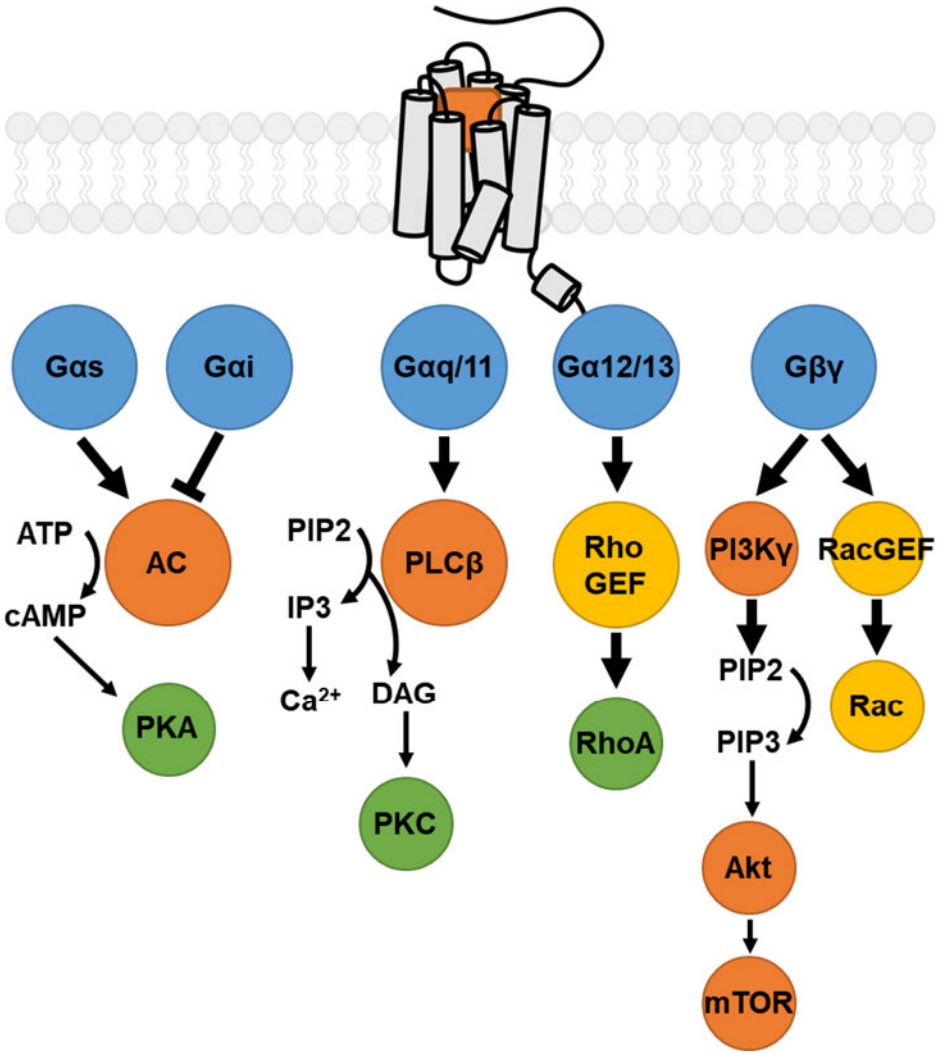

Figure 1-8. Gα and Gβγ activated pathways. While Gαs triggers AC mediated cAMP production, Gαi inhibits AC activity. Gαq/11 activates PLCβ/IP3 pathway. Gα12/13 activates RhoGEF/RhoA pathway. Gβγ subunits activate GRKs, GIRK channels, Kir3 channels, PLCβ, ACs, PI3Kγ and PRex1.

1.5.2. GRKs, Arrestins and GPCR Internalization

Shortly after the identification of GPCRs, it was found that agonist exposure decreased the number of ligand binding sites on the cell surface, and decreased the sensitivity of the cell to repeated stimulus with the same agonist (Chuang and Costa, 1979). This mechanism addressed a desensitization path, which has been explained in great detail since the discovery of its main modulators, GPCR kinases (GRKs) (Benovic et al., 1986; Kühn, 1978) and arrestins (Attramadal et al., 1992; Kühn et al., 1984; Lohse et al., 1990). Upon receptor activation, GRKs are recruited to the receptor (Daaka et al., 1997). GRKs phosphorylate specific serine and tyrosine residues mainly at the C terminal tail and intracellular loops of the receptor. An active, phosphorylated GPCR has a high affinity to intracellular proteins called β-arrestins. β-arrestins bind to the phosphorylated C terminus and the intracellular core of the receptor and then they dock to the plasma membrane (Lally et al., 2017) and adopt an active conformation (Latorraca et al., 2018; Nuber et al., 2016). Usually, β-arrestin binding terminates the G protein binding to the active receptor. Yet, new studies show that G proteins and arrestins may form signaling complexes with the active receptors (Nguyen et al., 2019; Smith et al., 2021).

A classic mechanism induced by arrestin coupling is receptor internalization via clathrin coated pits (CCPs) (Figure 1-9). CCPs are cage-like structures located on the cell membrane that modulate cargo delivery. CCPs are mainly built by the heavy and light chains of clathrin protein. With the involvement of a number of adaptor proteins, they mediate cell surface protein endocytosis (Wolfe and Trejo, 2007). Upon phosphorylation of an active GPCR, arrestin recruitment to the receptor takes place. Active arrestin displays high affinity to the adaptor protein 2 (AP2) and clathrin. Binding of several AP2 and clathrin proteins to the receptor-arrestin complex stimulates the assembly of the pit-like clathrin coated complex. This complex starts to invaginate, and another intracellular protein called dynamin sequesters the invaginated CCP from the cell membrane. Clathrin and AP2 then dissociate from the internalized vesicle. The fate of the internalized GPCR is either degradation or recycling back to the cell surface, which can be distinguished by the type of

marker proteins bound on the internalized vesicles (Moore et al., 2007). In case of recycling, phosphorylated receptor in the vesicle is dephosphorylated by intracellular protein phosphatase type 2A (PP-2A) (Pitcher et al., 1995).

1.5.2.1. GRK and Arrestin Mediated Signaling

GRKs and arrestins are not only involved in the desensitization processes. They activate numerous signaling pathways themselves. β-arrestins can interact with a number of downstream effectors, such as the non receptor tyrosine kinase Src, and mitogen-activated protein kinases (MAPKs). Although a number of recent studies, using cell lines devoid of Gα subunits or β-arrestins, challenged the necessity of β-arrestins for MAPK activity (Grundmann et al., 2018; O'Hayre et al., 2017), it is believed that β-arrestins still play an important role in propagating and maintaining the MAPK signaling, since they appear to act as scaffold proteins for the MAPK pathway components, and the lack of β-arrestins cause an impaired MAPK signaling in these knockout cell lines (Luttrell et al., 2018).

GRKs, on the other hand, have recently gained attention, since numerous studies discovered that they can interact with several cellular signaling components. Next to their indispensable role in receptor phosphorylation and desensitization, GRKs interact with a number of signaling proteins in a non-phosphorylating manner. Some of these proteins, such as the Raf kinase inhibitor protein (RKIP), negatively modulate GRK activity (Lorenz et al., 2003). Moreover, GRKs interact with molecules involved in receptor endocytosis, such as caveolin, clathrin and PI3K and they can directly modulate a number of signaling proteins, such as the serine–threonine kinase Akt, adenosine diphosphate (ADP)-ribosylation factor GTPase-activating proteins (ARF-GAP) and GRK interacting proteins 1 and 2 (GIT1 and GIT2) (reviewed in Ribas et al., 2007). In accordance with its wide interactome, dysregulations in GRK functions are known to play significant roles in cardiovascular, autoimmune and neurodegenerative diseases, as well as in a number of cancers (Métayé et al., 2005).

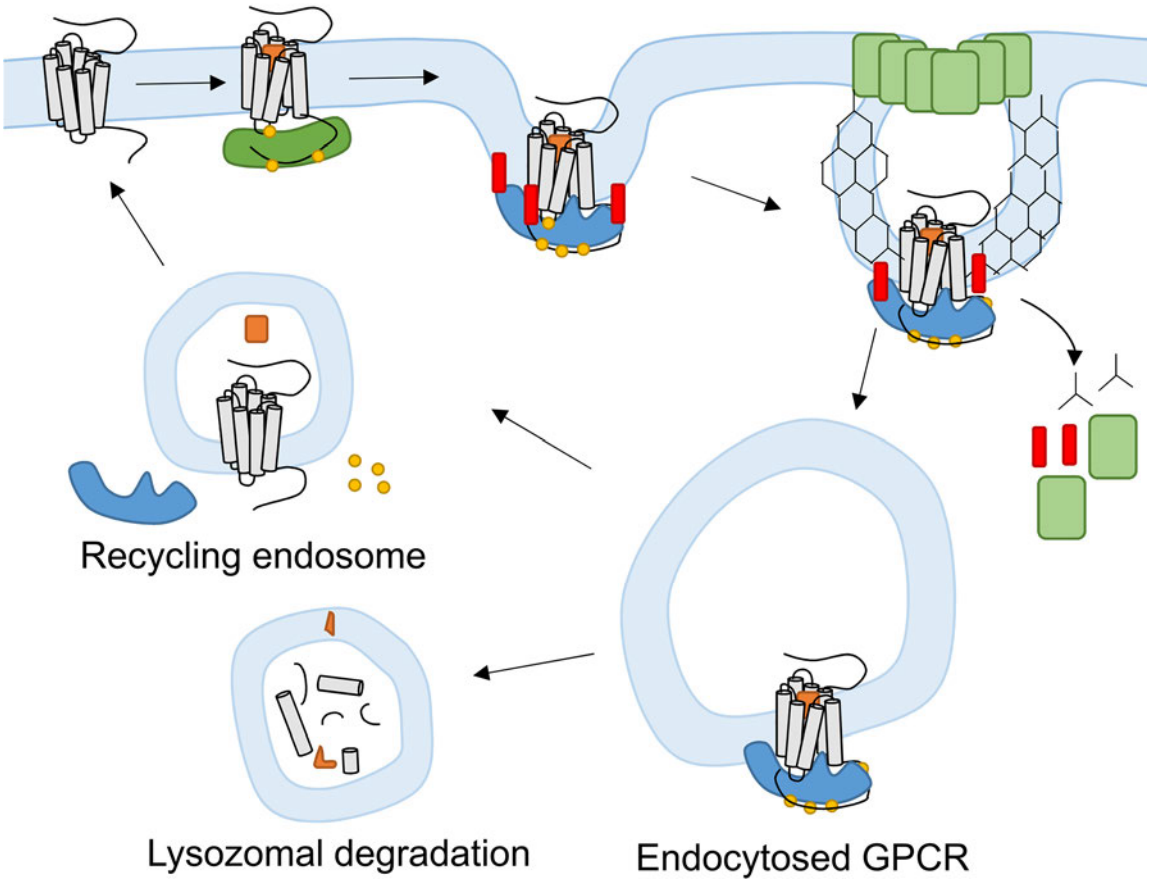

Figure 1-9. GRK and arrestin mediated signaling and internalization of GPCRs. GRK (green) is recruited to the active GPCR. GRKs phosphorylate (yellow) the GPCR. β-arrestin1/2 (blue) is recruited to the phosphorylated GPCR. β-arrestin recruits the internalization associated proteins such as the AP2, and initiates membrane invagination. Later, clathrin accumulates and forms a pit around the arrestin bound receptor. Dynamin initiates the scission of the loaded pit and finalizes endocytosis. Endosomal GPCRs are either recycled back to the cell surface in their apo form, or degraded by the lysosome.

1.5.2.2. Signaling of GPCRs From Intracellular Domains

An emerging paradigm in GPCR signaling is the signal transduction at intracellular compartments. Contrary to the early belief that suggested GPCR signaling only to be sourced from the cell surface, it is now widely accepted that GPCRs can continue signaling after being internalized. Moreover, some GPCRs are located at intracellular structures, such as the Golgi apparatus or the ER membrane, where they can bind to their agonist and mediate signal transduction. Recently, a number of Gs coupled GPCRs have been shown to induce a second wave of cAMP signaling after being internalized (Lohse and Calebiro,

2013). These studies showed that, in order to mediate a sustained, long acting cAMP signaling, and endocytosis mediated cAMP wave was indispensable. This second wave of cAMP production can be stimulated via the receptors in the early endosomes (Calebiro et al., 2009; Ferrandon et al., 2009), as well as the receptors that are translocated in Golgi/trans Golgi network after internalization (Godbole et al., 2017). For the parathyroid hormone receptor 1 (PTH1R), endosomal signaling is terminated by a retromeric protein complex that transfers the endosomal GPCR to the Golgi membrane (Feinstein et al., 2011; Ferrandon et al., 2009).

Moreover, GPCRs located at intracellular membranes can propagate distinct signaling activities. Using conformationally selective nanobodies, it was shown that β_1 and β_2 adrenergic receptors, as well as μ, δ and κ opioid receptors were shown to be located and become activated at the Golgi apparatus. In case of the beta adrenergic receptors , epinephrine and norepinephrine are transported into the intracellular space by a plasma membrane transporter called organic cation transporter 3 (OCT3), where they undergo a passive diffusion through the Golgi membrane to reach the receptor binding pocket (Irannejad et al., 2017). Moreover, endothelin receptors, metabotropic glutamate receptor 5 (mGluR5) and angiotensin II receptors were shown to be located and activated on the nuclear membrane (Merlen et al., 2013; Purgert et al., 2014; Tadevosyan et al., 2015).

The physiological role of receptor signaling from intracellular domains is still an area to be explored. Yet, a recent study suggested that blocking intracellular β_1AR may be a relevant strategy to treat norepinephrine mediated cardiac hypertrophy (Nash et al., 2019). Moreover, intracellular mGluR5 was proposed to play a role in nerve injury associated pain and neuronal hypersensitivity (Vincent et al., 2016).

1.6. Methods to Assess GPCR Activation

Development of radiolabeled ligands provided a robust platform to identify GPCRs and quantify ligand binding to them. However, ligand binding methods do not reveal in-

formation on receptor activation. Upon discovery of GPCRs, numerous biochemical, biophysical and molecular biology methods have been developed over the last 50 years in order to delineate GPCR activation at the receptor and downstream signaling levels.

1.6.1. Direct Detection of GPCR Activation

1.6.1.1. Structural Characterization of GPCR Activation

The most direct evidence of GPCR activation at the receptor level comes from the structural snapshots of GPCRs. Numerous studies in the last two decades provided more than 400 unique structures of ~90 receptors. (Kooistra et al., 2021). The general aim of structural biology is to determine the tertiary/quaternary structure of proteins at a fixed conformation, or monitoring conformational dynamics at atomic level. Commonly used methods in GPCR structural biology are X-ray crystallography, NMR spectroscopy, double electron–electron resonance (DEER) and cryogenic electron microscopy (cryo-EM). Such studies obtain density maps of the atoms of a protein in frozen/liquid solution or in crystal, and assemble all obtained positions to a final model that depicts the macromolecule structure. Structures of GPCRs in apo or ligand bound states reveal a static picture of receptor conformation at inactive and active conformations, which allows comparison at atomic level (Figure 1-10). Moreover, since structural studies reveal protein structures at atomic resolution, they facilitate the identification of critical residues that take part in conformational rearrangements. Additionally, an atomic map can also reveal the residues that form binding pockets, which can aid the development of novel drugs. Although they provide an enormous insight of receptor activation mechanisms, performing structural studies are challenging. Structural studies do not only produce a static picture of GPCRs. Adopting solution NMR and hydrogen-deuterium exchange mass spectrometry (HDX-MS) methods provided more dynamic information regarding the movements of specific residues (J. Xu et al., 2019), or temporal dynamics of global conformational changes within the receptor (Du et al., 2019).

Purification and reconstitution of GPCRs have been historically challenging (Lavington and Watts, 2020). GPCRs are intrinsically highly dynamic proteins, and many of them exhibit low thermostability after purification, which complicates obtaining a high resolution and uniform structural model in specific cases, such as working with a ligand that does not stabilize a specific conformation, or studying a receptor structure in the absence of conformational stabilizers (nanobodies, G proteins, arrestins *et cetera*) (Lebon et al., 2012). In terms of NMR based studies, labeling receptors with isotopes, which requires depletion of all cysteine residues except one for labeling, is also a challenging process, since cysteine depletion may cause alternative receptor conformations (Shimada et al., 2018). Although recent advances in cryoEM based methods provided a more rapid platform to obtain structures, they still demands highly specialized equipment, time consuming data collection and processing times and an outstanding biochemical and biophysical expertise (Grisshammer, 2020).

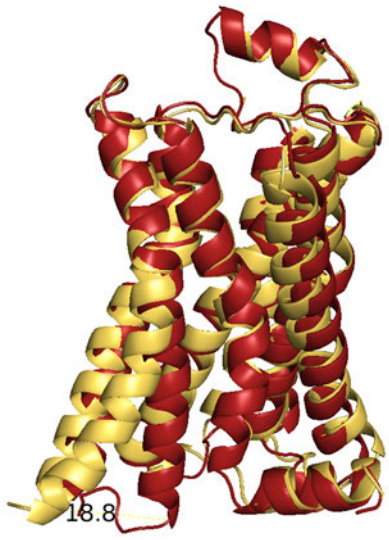

Figure 1-10. Structural characterization of receptor activation. Shown is the superimposed structural models obtained from X-ray crystal structures of the β2AR at active (bound to the agonist BI-167107) (Rasmussen et al., 2011) and inactive (bound to the inverse agonist carazolol) (X. Liu et al., 2017) conformation. Outward movement of the TM6 domain was measured on the position shift of the $K267^{6\,29}$ residue.

1.6.1.2. Fluorescence/Bioluminescence Based Characterization of GPCR Activation

Discovery of the fluorescent proteins and the development of methods that enable site specific labeling of proteins served greatly for studying GPCR activation. Moreover, adoption of fluorescence and bioluminescence energy transfer (FRET and BRET) methods in GPCR research opened the way to several robust tools that revolutionized the field and accelerated the progress in the field.

Fluorescence, in very rough terms, is photon emission by a chemical compound upon being excited by light or electromagnetic field. The chemical compound that is able to emit fluorescence is called a fluorophore. When a fluorophore is illuminated by light, electrons become promoted from ground singlet state (S_0) to an excited electronic state (S_n). Electrons at excited states undergo a number of internal transitions, such as relaxation to lower vibrational states within the excited singlet state, as well as internal conversions to lower excited states (i. e. from S_n to S_1). During these conversions, photons lose part of the energy they absorbed. When a photon undergoes a relaxation from S_1 singlet state to the ground S_0 singlet state, it releases its energy in form of photons. This released energy is defined as fluorescence. Since electrons spend part of their energy during internal conversions, the emitted energy is lower than the absorbed energy. As a result of this, wavelength of the emitted light is larger than the excitation light. This phenomena is called the Stokes shift (Stokes, 1852).

Resonance energy transfer occurs when the electrons at the excited singlet state transfer their energy in a non-radiative dipole-dipole coupling process to a neighboring (acceptor) fluorophore. This transfer excites the electrons of the acceptor fluorophore, which eventually may relax to the ground state and emit photons, or lose all the absorbed energy during internal conversions (Figure 1-11A). For non radiative energy transfer to occur, the excitation spectra of the acceptor fluorophore should overlap the emission spectra of the transferred energy, two fluorophores should be within minimal spatial distance, and the transition dipole moments of both fluorophores should display a high relative orientation (preferably parallel, for maximum energy transfer) (Förster, 1946) (Figure 1-11B-

D). The efficiency of energy transfer is also dependent on the intrinsic photophysical properties of fluorophores, such as the quantum yield (relative amount of photons emitted in comparison to absorbed) and extinction coefficient (ability of light absorption) of both donor and acceptor molecules.

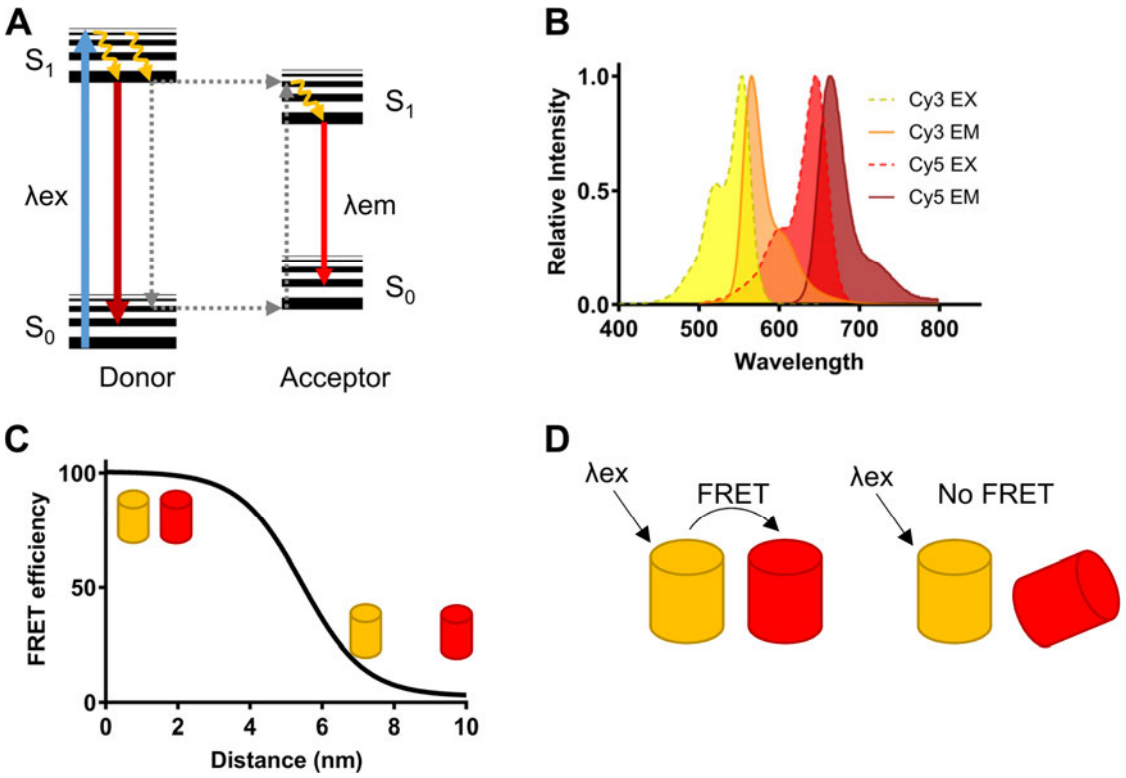

Figure 1-11. Jablonski diagram and the principles of FRET. (A) Schematic representation of fluorophore excitation (blue arrow), interstate conversions (yellow lines) and emission (fluorescence, dark red line). FRET is the non radiative transfer of donor energy at the excited state to the acceptor fluorophore (grey line), which brings the ground state electrons of the acceptor to the excited state. Transfer of this energy to the ground state exhibits acceptor emission (red arrow). (B) For FRET, the emission spectra of the donor fluorophore (orange, Cy3) should overlap with the excitation spectra of the acceptor (red, Cy5). (C) FRET decreases as a function of distance between the donor and acceptor. (D) Donor and acceptor should exhibit an appropriate dipol-dipol orientation for FRET.

Fluorescence based methods have been applied in the GPCR field soon after receptor isolation was achieved. Site specific, covalent labeling of rhodopsin and β_2AR with environmentally sensitive fluorophores allowed spectroscopic measurements of ligand induced conformational changes in these receptors (Farrens et al., 1996; Gether et al., 1995). Recent advances in protein biochemistry and microscopy methods enabled studying these

receptors in better spatiotemporal resolution. Incorporation of the environmentally sensitive monobromobimane to the conformationally dynamic domains of GPCRs aided to delineate highly dynamic conformational landscape of GPCRs, and how its equilibrium can be rapidly modulated by the ligands (Lamichhane et al., 2015; Maeda et al., 2014).

A revolutionary advance in this regard came with the characterization of the first GPCR based intramolecular FRET sensors, which were developed to measure the conformational switch of the GPCR based on the large movement of the TM6 helix. These sensors based on the α_{2A}-adrenergic receptor (α_{2A}AR) and the parathyroid hormone receptor (PTHR) reported for the first time directly that the receptor activation occurred in the millisecond range (Vilardaga et al., 2003). Starting with these biosensors, many other FRET sensors have explored many facts regarding the ligand specific and temporal characteristics of the changes in receptor conformations (Kauk and Hoffmann, 2018; Vilardaga et al., 2005; Zürn et al., 2009). FRET based GPCR sensors were further used in single molecule studies. Site specifically labeling of two intracellular residues that are supposed to undergo a significant distance change made it possible to explore the conformational dynamics of GPCRs with high signal to noise ratio. Such studies now expand the knowledge of how ligands and intracellular effectors, as well as nucleotides affect the conformational dynamics of GPCRs (Gregorio et al., 2017; Maslov et al., 2020; Vafabakhsh et al., 2015).

1.6.2. Detection of Signal Transducer Activation

G proteins are the first step of signal transduction after receptor activation. Perhaps the most historical and classical method to measure G protein activity is the measurement of a ^{35}S radioisotope labeled, non hydrolysable GTP (GTPγS) binding to the G protein. The method relies on the continuous GTPase activity cycle upon G protein activation. Presence of ^{35}S-GTPγS occupies all active G proteins, and detection of the radioactivity from the bound GTPγS successfully reports the GTPase activity (Bokoch et al., 1984). Updated versions of this method use a fluorescently labeled GTPγS that allows fluorometric measurements (Labrecque et al., 2005; McEwen et al., 2001). A novel version of this application makes use of fluorescently labeled GTPγS and a fluorescently labeled antibody

that targets only the active Gα protein. FRET between two labels reports the extent of G protein activity. This assay provides a better signal to noise ratio compared to that of the radiolabeled GTPγS method (Rozwandowicz-Jansen et al., 2010).

Novel biosensors based on FRET can also measure G protein activation using fluorescence imaging. These sensors are based on the phenomena that activated Gα and Gβγ subunits dissociate from each other (Wall et al., 1995). Labeling Gα and Gβγ subunits with donor and acceptor fluorophores allows direct monitoring of G protein with high temporal resolution (Janetopoulos et al., 2001; Lohse et al., 2008). Development of such sensors also cast doubt on the necessity of subunit dissociation phenomena for G protein activation, since the Gαi subunits labeled at certain sites led to an increase in FRET upon receptor activation, instead of a decrease (Bünemann et al., 2003; Frank et al., 2005). FRET has also been used for measuring the temporal dynamics of receptor-G protein interactions and displayed a very rapid onset of interaction upon receptor activation (Hein et al., 2005). Using more bright and photostable fluorophores and luciferases, G protein activation biosensors have been made compatible with multiwell assay plates for high throughput measurements (Olsen et al., 2020). Moreover, single molecule imaging methods allowed tracking the interactions of receptors and G proteins in a spatiotemporal manner, which allowed observing the “hotspot” regions where G proteins and receptors meet more often upon activation. This study added “location” as a new dimension to the complexity of receptor-G protein interactions (Sungkaworn et al., 2017).

1.6.3. Detection of Second Messenger Levels

Active G proteins, whose activity is triggered by GPCRs, diffuse on the cell membrane to find and activate their effectors. The result of this process is the production/inhibition of second messengers, such as cAMP and IP derivates. Numerous types of robust biochemical and biophysical assays are present to measure these processes. The most classical assays in this regard are based on radioimmunoassays, which are based on competitive binding of radioisotope labeled second messengers to messenger specific receptors or antibodies (Steiner et al., 1972). Improved version of these assays now use fluorophore

labeled metabolites instead of radioisotope labels with fluorescently labeled antibodies/receptors specifically binding to the metabolite, allowing FRET based quantification of metabolite production in high throughput manner (Degorce et al., 2009).

Second messengers can also be measured by genetically encoded fluorescent biosensors. Among these, circularly permuted fluorescence protein (cpFP) based biosensors provide a simple, single color based measurement of pathway activation. These sensors can be designed using a cpFP attached to one of the following peptide domains: a metabolite binding peptide, e.g. cAMP, or a kinase/phosphatase substrate of a signaling component, e.g. PKA (Harada et al., 2017; Ohta et al., 2018). Conformational changes in the cpFPs domain of the biosensor cause complementation of a fluorescent chromophore, as well as a shift in the excitation spectra of the pre-formed chromophore (Mehta et al., 2018). Ca^{2+} binding proteins such as calmodulin have also been used to design fluorescent biosensors (A. Takahashi et al., 1999). Ca^{2+} binding to the sensor's binding domain induces a conformational change that eventually rearranges the cpFP barrel in a manner that it becomes more fluorescent. As a result, an increase in fluorescence can be observed in an intracellular Ca^{2+} flux dependent manner (Zhong and Schleifenbaum, 2019). Intracellular Ca^{2+} can also be measured as a second messenger. Dyes of which the excitation maxima is shifted upon Ca^{2+} binding (Fura-2, Fluo-4) are widely used in live cell measurements.

Moreover, FRET and BRET based biosensors that use the substrate/binding domain principle also exist. These sensors are based on the conformational changes on the binding domain that rearranges the distance and orientation of the donor and acceptor fluorophores attached to it (Klarenbeek et al., 2015; Nikolaev et al., 2004). As a result, changes in the RET signal are observed. All fluorescent biosensors are suitable for measurements with high temporal resolution. However, RET based biosensors can also provide spatial resolution at nanometer grade, which helps understanding the location of the observed signal (Mo et al., 2017).

1.6.4. Detection of GPCR Desensitization/Internalization

Activated receptors become phosphorylated by GRKs, interact with arrestins and become internalized via the CCPs. All of these processes can also be monitored as part of receptor activation mechanism. GRK mediated receptor phosphorylation can be measured via phosphorylation sensitive receptor antibodies. This method requires phosphorylation specific antibodies for each receptor, and even each residue that is phosphorylated (Prihandoko et al., 2015). Moreover, incorporation of radiolabeled phosphorus ([^{32}P]-orthophosphate) can also be used to measure receptor phosphorylation, in combination with receptor isolation (Stadel et al., 1983).

Receptor internalization can classically be observed by radioligand binding assays. Since agonist stimulation decreases the number of receptors over time, radioligand binding at different time points after agonist stimulation can report the decrease in binding pockets on the cell surface (Mukherjee et al., 1975). Receptor internalization can also be assessed using flow cytometry or ELISA with receptor specific, labeled antibodies (Hislop and Von Zastrow, 2011; Nevins and Marchese, 2018). More advanced assays use TR-FRET and BRET technologies. Such assays make use of fluorescently labeled receptors at their C terminal domain, and a membrane localized bioluminescent/fluorescent protein (fused to lipids or a membrane bound protein). Agonist mediated internalization of the receptor would decrease the amount of fluorescently labeled receptor on the cell surface, which is reported as a decrease in RET (White et al., 2017). Moreover, using membrane impermeable dyes in cell culture medium with N terminally labeled receptors are also used in the same manner. In this case, FRET/BRET would decrease upon receptor internalization, since the number of fluorescently labeled receptors-extracellular dye interactions would decrease (Levoye et al., 2015). Such an assay can also be implemented in terms of luciferase complementation. In this case, the receptor is tagged with a peptide based on the luciferase, which can be complemented with an extracellular, purified luciferase peptide (Soave et al., 2020).

Using FRET and BRET, the early steps of receptor internalization, which are the arrestin and GRK recruitment to the receptors, can also be monitored. RET can be used with C terminally labeled receptor in combination with fluorescently labeled arrestin/GRK (Angers et al., 2000; Krasel et al., 2005; Vilardaga et al., 2003). On the other hand by-stander BRET methods make use of non labeled receptors in combination with membrane localized fluorescent proteins or luciferase labeled arrestins (Namkung et al., 2016).

1.6.5. Detection of Downstream Signaling

Further downstream signals induced by second messengers can also be measured using several assays. Western blot method is one of the best established technique in this regard, thanks to the availability of phosphor-specific and unspecific antibodies targeting the components of the signaling pathway. Signal transduction after second messenger activation involves several kinase induced pathways. These include cAMP/PKA, MAPK/ERK, PI3K/Akt/mTOR, PLC/PKC *et cetera*. Moreover, a number of novel cpFP and RET based biosensors can also be used (Harvey et al., 2008; Mehta et al., 2018). These biosensors usually make use of the substrates of kinases labeled with a cpFP or acceptor and donor fluorophores. Upon phosphorylation, these protein subunits undergo a conformational change that induces a change in fluorescence intensity of the cpFP, or in the RET signal.

1.7. Oligomerization of GPCRs

A rather new and emerging concept in GPCR biology is the ability of receptors forming oligomers. Receptor oligomers can be described in two categories: self association of protomers (homomerization) or complex formation with a different receptor type (heteromerization). The size of the complex defines the name of it: a single protomer is a monomer, and two receptors form a dimer, then trimer, tetramer, oligomer *et cetera*. GPCR oligomerization was first reported for human β_2AR isolated from lung cells (Fraser and Venter, 1982). Since then, the concept of GPCR oligomerization has been described for

several GPCRs, and the functional impact of these complexes has been explored intensively. It is now well known that class C GPCRs are constitutive homo/heterodimers (Pin and Bettler, 2016). However, in the case of class A and B GPCRs, oligomerization is a hot and still debated topic. The existence, stability and functional relevance of especially the class A GPCRs are still not well understood, despite many reports addressing these issues. One of the main problems in assessing class A receptor dimerization is the methods used to identify dimers.

1.7.1. Methods to Assess GPCR Oligomerization

Techniques that are used for identifying GPCR oligomerization can be categorized in four groups: biochemical, biophysical, structural and computational methods (Figure 1-12).

1.7.1.1. Biochemical Methods

Biochemical methods that are used for GPCR oligomerization detection are based on immunodetection with protein gel electrophoresis. The first well controlled evidences on GPCR oligomerization were reported using Western blot and coimmunoprecipitation (coIP) for β_2AR and δOR in heterologous systems using antibodies against epitope tags (Cvejic and Devi, 1997; T. E. Hebert et al., 1996). These methods have also been used to describe the oligomerization of receptors in native cells using receptor specific antibodies (Marsango et al., 2011; Nimchinsky et al., 1997). These methods have also been used in combination with cysteine-cysteine cross linking at specific residues, in order to identify possible dimer interfaces between the protomers (W. Guo et al., 2008; Mancia et al., 2008; Xue et al., 2019). A crucial point to consider while interpreting the oligomerization using biochemical methods is the solubility of proteins. Membrane proteins are hard to isolate, as they require excessive detergent treatment for full solubilization. Therefore, if protein solubility is not assessed well, it may lead to false dimers in these experiments. On the other hand, detergents can also cause excessive denaturation of the proteins, which may actually reduce the size of protein complexes, leading to artificial monomers. Moreover,

using reducing reagents in the experiments can also disrupt possible disulfide bonds between protomers, again causing a reduction in the oligomer size.

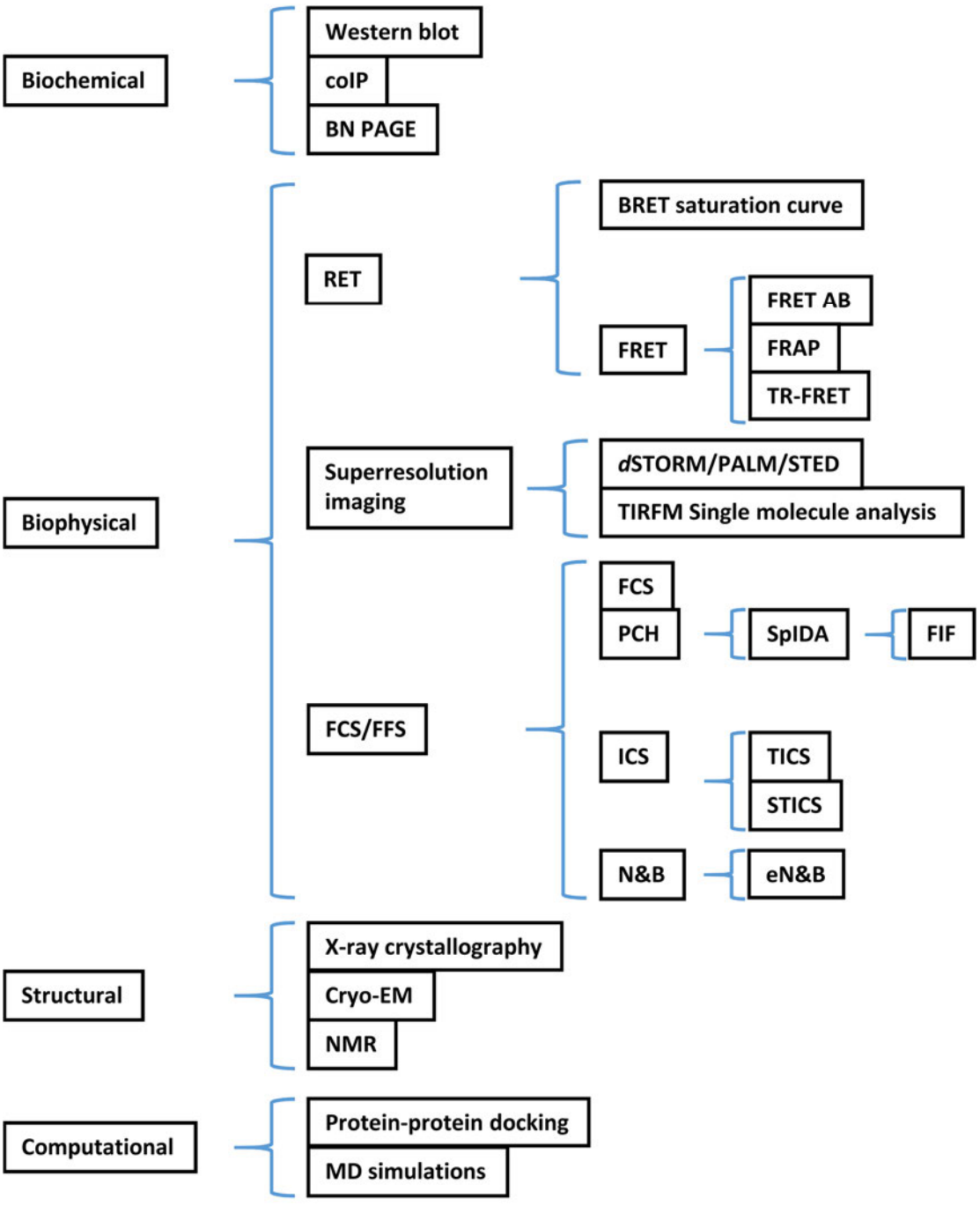

Figure 1-12. Schematic view of the methods used for identifying and characterizing GPCR oligomerization. These methods are divided in 4 categories: Biochemical, biophysical, structural and computational. Full form of abbreviations are given in the List of Acronyms / Abbreviations.

Blue native polyacrylamide gel electrophoresis (BN-PAGE) is an alternative method to Western blot for identifying GPCR oligomers. This method makes use of mild detergents and Coomassie blue, both of which are less denaturing reagents. As a result, during purification proteins retain their endogenous stoichiometry. Using this method, dimeric stoichiometry of the orexin 1 (OX1) and 5-HT_{2C} receptors were detected (Ward et al., 2015; T. R. Xu et al., 2011).

1.7.1.2. Biophysical Methods

Fluorescence based methods constitute the backbone of biophysical methods for studying GPCR oligomerization. Among these, FRET and BRET have been the pioneers. Earlier studies used exogenous expression of donor/luciferase and acceptor tagged receptors in immortalized cell lines using BRET (Angers et al., 2000; Ayoub et al., 2002; Hanyaloglu et al., 2002; Issafras et al., 2002) and FRET (Overton and Blumer, 2000; Rocheville et al., 2000). Since RET based methods require a very proximal orientation of the fluorophores, they are one of the best indicators of receptor-receptor interactions. FRET and BRET can be measured using a microscope or microtiter fluorescence/bioluminescence readers. One advantage of using microscopic imaging, especially those methods that provide high spatial resolution, is the power of identifying the location of the RET signal. Homo- and hetero oligomerization of proteins have been performed using acceptor photobleaching FRET (FRET AB), which is based on calculating the FRET efficiency from the intensity increase in the donor fluorophore upon photodestruction of the acceptor (Herrick-Davis et al., 2004, 2006; Vilardaga et al., 2008). Working with titrated and known concentrations of donor and acceptor labeled proteins, one can directly compare the average FRET AB values for a monomeric control and the protein of interest (Patel, Lange, et al., 2002). Alternatively, plotting the FRET efficiency values against the acceptor intensity or acceptor/donor intensity ratio provides a semi-quantitative calculation of oligomerization: If the FRET efficiency data follows a hyperbolically increasing trend, this indicates a specific protein-protein interaction. Another robust method is measuring the donor lifetime, which is a more quantitative indicator of FRET (Łukasiewicz et al., 2007). Combination of BRET and FRET have also been used to detect trimers or higher order oligomers (Carriba et al.,

2008). The principle of this assay is using receptors tagged with a luciferase that can transfer energy to a fluorophore, which in turn can transfer energy to another fluorophore. FRET and BRET have also been used to study the changes in dimer conformations as well as stoichiometry changes upon certain stimuli. However, it is important to consider that it is difficult to discriminate whether the RET signal change originates from stoichiometry or conformational changes. One disadvantage of these methods is the requirement of using engineered receptor constructs and overexpression of these receptors. Therefore, it becomes troublesome to estimate the receptor concentrations at which dimerization is observed. A solution to this drawback emerged by measuring FRET using donor and acceptor fluorescent dye labeled ligands. This technique allows studying oligomerization in native tissues. The important point here is that the selected ligands for RET measurement should not alter the basal receptor dimerization.

Fluorescence recovery after photobleaching (FRAP) is a confocal microscopy imaging method that has been report used to report oligomerization in a qualitative manner. FRAP is based on the diffusion of fluorophores to a region in which all fluorophores are photobleached. The fluorescence recovery at the bleached area indicates diffusion. This feature of FRAP has been used to detect GPCR oligomerization, using receptors tagged with two spectrally different fluorophores. If constraining the mobility of one receptor also causes a reduction of the mobility of the second receptor, it means that they interact with each other. If the diffusion of the second receptor is not influenced, then these receptors do not oligomerize. This method has been used to identify both homo and hetero oligomers of GPCRs (Dorsch et al., 2009; Fonseca and Lambert, 2009).

Fluorescence and bioluminescence protein complementation assays have also been used to study oligomerization (Vidi et al., 2010). These methods are based on the complementation of two fragments of the FP/luciferase. In this case, fluorescence/bioluminescence is only observed when two proteins, each carrying complementary fragments of the FP/luciferase, are in close proximity that allows the formation of functional luminescent/fluorescent protein. Split luciferase and split FP approach have been combined to detect higher order oligomers in terms of BRET (Armando et al., 2014; Bagher et al., 2019;

Gandia et al., 2008). In this assay, complementation of luciferase and FP separately indicates dimerization, and BRET between complemented luciferase and FP reports at least tetramer formation. One drawback of the bimolecular fluorescence complementation is that the complementary fragments of the FPs usually have high affinities, which causes overestimating the oligomerization. This is less of a concern for the bimolecular luminescence complementation nowadays, thanks to the development of a "split nanoluciferase", which consists of very low affinity fragments. In these assays, the main problem again is that they lack spatial information on the protein oligomerization, unless they are imaged under a high resolution microscope. Yet, these assays also require overexpression of the proteins of interests, as signal detection might not be possible at endogenous expression levels.

Single molecule based oligomer analysis is one of the most novel and informative techniques. This method is based on TIRFM imaging of receptors carrying fluorescent tags. This approach allows detecting single receptors with the size of the point spread function of the receptor. The oligomerization can be detected in two manners: 1) when two single PSFs overlap in the imaging field, they appear as a single PSF, but with the sum of the intensity of two (Calebiro et al., 2013). Therefore, comparing the cumulative single molecule intensities of a monomeric control and a protein of interest can help identify the oligomeric size of a receptor (Figure 1-13A). Other studies also make use of calculating the ratio of colocalizing receptors labeled with two different colors to the total number of fluorescent receptors detected. This way, a 33% of particle colocalization can be assigned to a perfect homodimerization (Felce et al., 2017) (Figure 1-13C). However, static TIRF images do not inform on the dynamics of single receptor interactions. Using continuous TIRFM imaging with high temporal resolution, it has been possible to calculate the time constants of particle interactions, which reported the dimer lifetimes of class A GPCRs (Figure 1-13B). Since fluorescently labeled single particles exhibit larger diameters than the real size of GPCRs (10 nm), not every single PSF collision is a productive dimerization. Simulating the movements of single PSFs that match the size of experimental ones have been informative on detecting the non-dimerization associated lifetimes of PSF collisions.

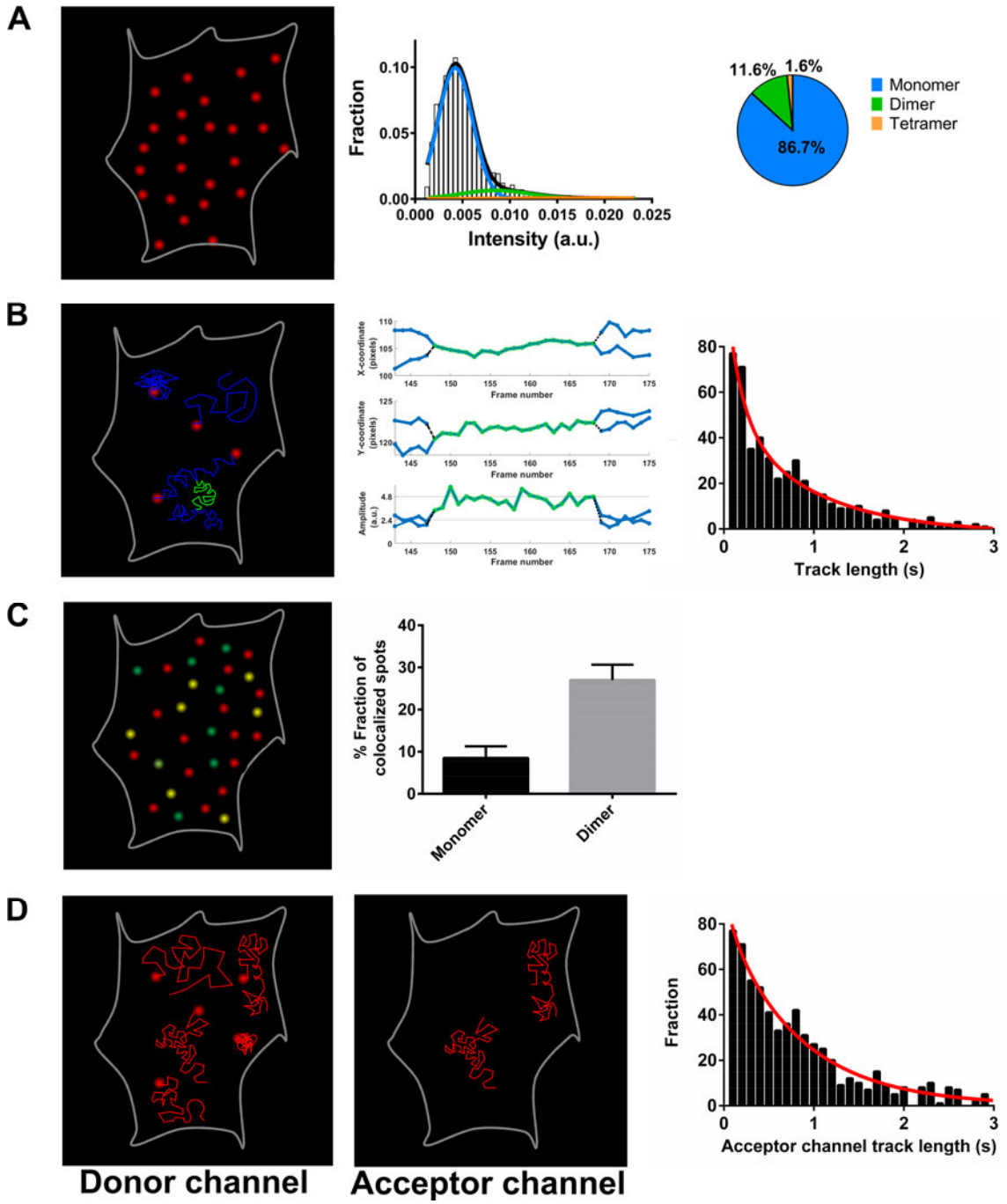

Figure 1-13. Single molecule analysis of receptor dimerization. (A) Intensity distribution and oligomer fraction calculation. (B) Calculation of dimer lifetime by single molecule tracking. (C) Dual color particle colocalization analysis. (D) FRET based dimer lifetime calculation by measuring track length in the acceptor channel.

Recently, a new method described class A GPCR interactions using single molecule FRET (smFRET) technology using highly photostable and bright organic fluorophores (Asher et al., 2021). This method can be more advantageous in comparison to the

single molecule tracking approach, as the single molecule FRET traces can only be observed if the donor and acceptor labeled proteins interact at FRET distances (Figure 1-13D). One minor disadvantage of this method is that, in terms of measuring homo oligomerization, only 33% of every receptor-receptor interaction can be detected, assuming a 1:1 donor:acceptor labeling. In general, a main advantage of single molecule studies is the power of detecting oligomers with high resolution imaging, at very low expression levels. However, the requirement for low receptor expression can be disadvantageous, since it does not allow concentration based effects on receptor dimerization. In general, single molecule based methods described a transient nature of class A GPCR dimerization, with small amount of steady state dimers at very low expression levels. Assessment of the dynamic receptor-receptor interactions suggested dimer lifetimes ranging from low millisecond to one second range (Calebiro et al., 2013; Dijkman et al., 2018; Hern et al., 2010; Işbilir et al., 2020; Möller et al., 2020; Tabor et al., 2016).

A rather newly adopted class of methods to measure GPCR oligomerization is the fluorescence fluctuation spectroscopy (FFS) based methods (T. Youker and Voet, 2020). These methods are based on the statistical analysis of fluorescence signal fluctuations in a small observation volume. Using this data as an input, FFS based methods can report the diffusion behavior, concentration and oligomeric size of the fluorescent entities measured. The ability of FFS to calculate an average concentration and oligomer size is superior to the RET methods. Moreover, since all FFS methods are compatible with confocal microscopy, they allow calculating receptor concentration and oligomerization at specific substructures of cells. Since the concentrations calculated by FFS methods are defined by the shape and size of the confocal observation volume, it is crucial to characterize the PSF profile of the confocal microscope at the wavelengths used for actual experiments. FFS methods are also versatile methods in terms of the setup. They can be implemented to microscope setups using different types of photon detectors, different illumination sources and imaging modes, such as TIRF (Zamai et al., 2019) or STED (Sezgin et al., 2019) imaging.

Fluorescence correlation spectroscopy (FCS) is perhaps the most historical FFS method, extensively used to determine the concentration and diffusion properties of fluorescent molecules (Ehrenberg and Rigler, 1974; Magde et al., 1972). FCS is based on measuring the intensity fluctuations in a small volume (i.e. confocal volume) of an open system in which fluorescent particles are freely diffusing. Diffusion of these particles in and out of the observation spot generates fluctuations in observed fluorescence intensity over time. FCS uses an autocorrelation analysis of these measured intensity fluctuations, allowing the average transit time through the observation volume and the average number of molecules over time in the observation volume to be calculated. Dividing the average intensity to the average number of molecules gives the photon counts per molecule per given time, which is called the molecular brightness value (Figure 1-14). Molecular brightness can then be used to calculate the average oligomeric size of the observed particles when compared with the brightness of a well characterized monomeric control. FCS correlates the measured intensity fluctuation with itself by shifting the signal with a certain lag time, and outputs the strength of the correlation across multiple lag times. This general autocorrelation function is as follows:

$$G(\tau) = \frac{< \delta I(t).\delta I(t+\tau) >}{< I(t) >^2} + 1$$

Where G is the autocorrelation function, I(t) is the average intensity signal at time t, and I(t+τ) is the intensity after the lag time (τ). δI (t) is the fluorescence fluctuation at the time point t, and it is calculated by the formula: $\delta I(t) = I(t) \quad < I >$, where <I> is the ensemble average intensity. Rapidly diffusing molecules exhibit a rapidly decaying autocorrelation curve, while this decay is delayed for the slower particles. The average transit time of the molecules throughout the observation volume can be calculated by fitting a diffusion model (i.e. 2D or 3D diffusion) to the autocorrelation curve. Using the calculated transient time (τ_D), an average diffusion coefficient (D) can be calculated:

$$D = \frac{\omega^2}{4\tau_D}$$

Where ω^2 is defined by the ratio of the axial and lateral dimensions of the ellipsoidal observation volume. The amplitude of the autocorrelation plot also contains the information about molecular concentration. The amplitude of the autocorrelation decreases when a sample with higher concentration is measured, because the relative contribution of each individual molecule to the total fluorescence intensity becomes less as the concentration of particles increases. This inverse relation of the autocorrelation and particle number can be seen in an alternative representation of the autocorrelation formula:

$$G(\tau) = 1 + \frac{1}{N}\left(1 + \frac{\tau}{\tau_D}\right)^{-1}\left(1 + \frac{\omega^2\tau}{\tau_D}\right)^{-\frac{1}{2}}$$

From this formula, the number of particles can be calculated at the $\lim(\tau \to 0)$ as $G(0) - 1 = {}^{1}/_{N}$, assuming free diffusion. FCS has been initially used to characterize fluorescent ligand binding to GPCRs, but since FCS gives information on the concentration and brightness of fluorescent particles, it has also been used in characterizing GPCR oligomerization as well at overexpression (Herrick-Davis et al., 2013) and native systems (Herrick-Davis et al., 2015). Moreover, an extension of FCS, called fluorescence cross-correlation spectroscopy (FCCS), which can be applied to two color imaging (Figure 1-14), was also used to characterize somatostatin receptor (SSTR) oligomerization (Patel, Kumar, et al., 2002).

A spatial analog of the FCS analysis is the image correlation spectroscopy (ICS) (Petersen et al., 1993). ICS uses single *my* confocal images (Figure 1-14). These images are generated by measuring fluorescence intensity values with a step-by-step (with a defined step distance) sliding observation spot (defined by the PSF) in a raster fashion and rendering them in a 2D matrix array as pixels. In an image, intensity fluctuations come from the relative intensity differences of the pixels across the image: $\delta I(x,y) = I(x,y) - < I >$, where $I_{x,y}$ is the fluorescence intensity of the pixel at the x,y coordinate. Therefore, ICS applies the autocorrelation function across the spatial domain. Classic ICS has also been used to study GPCR oligomerization (Chakraborty et al., 2018).

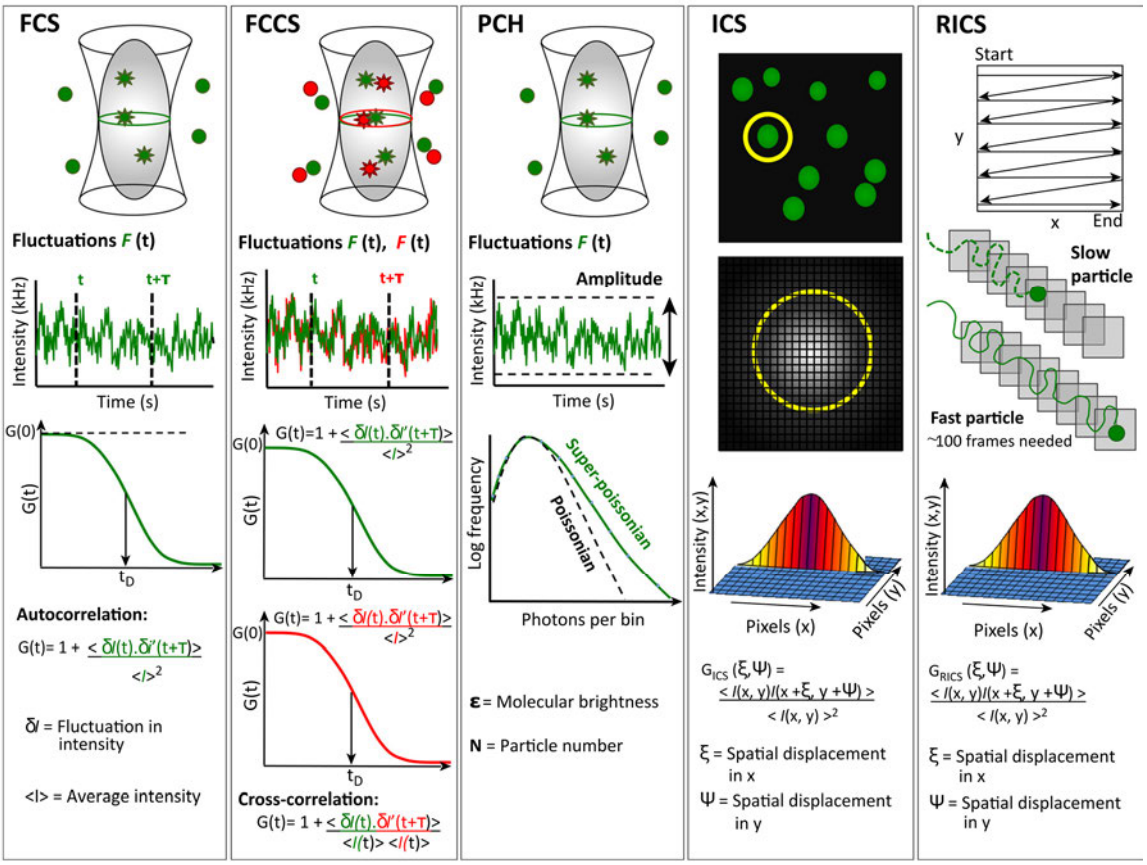

Figure 1-14. Summary of the main principles of the FCS based methods to calculate protein oligomerization and density. Figure extracted and modified from (Briddon et al., 2018), used under the license number 5034380705311 provided by Elsevier and Copyright Clearance Center.

Addition of the temporal domain to ICS brought up the method called temporal ICS (TICS) (Srivastava and Petersen, 1996). TICS autocorrelates the intensity fluctuations across time for individual pixels of an *xy* image series and extracts the diffusion data as well. As a result, it provides diffusion information for each pixel of the image, but requires an averaging of all those values. In scanning confocal microscope imaging, since the time gap that the scanner needs to arrive back at the same pixel is longer than the one that FCS requires (FCS is faster because the observation spot is stationary), TICS can measure more slowly diffusing particles but not the faster ones, which is the opposite of single point FCS. TICS was used in one instance to characterize the distribution and membrane dynamics of β_2AR, PTH1R and CaSR (Wheeler et al., 2007).

Another extension of ICS is the spatiotemporal ICS (STICS) (B. Hebert et al., 2005). STICS was developed by integrating temporal and spatial fluctuations of molecules in order to obtain not only the magnitude of diffusion, but also the directionality of the molecules moving by flow. STICS uses *xy* confocal image series and calculates average spatial correlations using each image for every time lag. From resulting correlation maps, the time resolved shift in the position of the autocorrelation fit peak can be detected. The magnitude in the shift and position of the peak directly reports the velocity and direction of the flow. Because STICS can be applied in three dimensional imaging, it can be used to distinguish a wide range of diffusion rates (Bock et al., 2020).

Photon counting histogram (PCH) is another FFS method that can calculate concentration and brightness from photon statistics (Chen et al., 1999). Data acquisition of PCH is identical to that of the FCS (Figure 1-14). Photon counts over time that stems from the constant presence of a single molecule in the observation volume follows Poisson statistics. When two or more particles are present in the system, the photon counting histogram becomes the convolution of the intensity distribution of each particle. In a free diffusion system, presence of certain number of particles at a given time also follows a Poisson distribution. Thus, fluctuation of particles creates an additional broadening of the Poissonian distribution of the photon counts. Taking this into account, PCH method fits Poissonian and super-Poissonian functions to the frequency distributions of the photon counts. Then, taking the fits into account, it calculates the probability of observing an average N number of fluorescent molecules for several configurations of N. Once calculated the optimum N value, the average intensity can be used to calculate the molecular brightness as an indicator of oligomeric size in comparison to a monomeric control that is measured under identical concentrations. This method has been used to characterize the quaternary assembly of GPCRs, and how ligands affect the oligomer size (Ilien et al., 2009; Parmar et al., 2017; Wolf-Ringwall et al., 2011). PCH has also been combined with fluorescent protein complementation to quantify higher order oligomers of GPCRs (Kilpatrick et al., 2012).

An extension of the PCH method is the spatial intensity distribution analysis (SpIDA). SpIDA, in simple terms, is the application of the PCH theory to the spatial domain. This means that the fluctuations in photon counts do not stem from observing a stationary spot over time, but rather from intensity values of individual pixels from an *xy* confocal image. This means, SpIDA uses single confocal images to generate intensity distribution histograms, from which it calculates average number and brightness of fluorescent labels in cells. Conceptually, this is similar to applying the theory of FCS to the spatial domain, which ICS is based on, as discussed above. An advantage of SpIDA is that it can also be used in chemically "fixed" cells, as it does not require diffusing particles and the fluctuation comes from the intensity variations across individual pixels. Thus, SpIDA can also be used in combination with fluorescently labeled antibodies, and measure oligomerization in native tissues.

Number and Brightness (N&B) is another FFS method based on moment analysis of fluorescence fluctuations (Digman et al., 2008; Qian and Elson, 1990). N&B also uses an *xy* confocal microscope image series as input data and calculates an average aggregate number and brightness value for each pixel of the image, using the first (center, mean) and second (variance) moments of the intensity distribution histograms generated from the fluorescence fluctuation information throughout each pixel over time. In an open volume system containing 100 monomeric or 25 tetrameric fluorescent particles of the same kind, free diffusion of these particles throughout an observation volume would generate intensity fluctuations. While the average intensity in both cases will be the same, the intensity fluctuations of the tetramers would result in a higher variance than that of the monomers. Although the first moment of these scenarios are the same, the second moment, the variance values, are different, and informative of the number of aggregates as well as the aggregate size of the particles. Here, the ratio of the squared mean intensity to the variance results in the average number of particles (for monomers) or aggregates (for oligomers). N&B has recently been used to determine GPCR quaternary structure as well (Calizo and Scarlata, 2013; Møller et al., 2018). N&B calculates a number and brightness map using confocal image series. An extended version of N&B, called enhanced N&B (eN&B), is applied for the cases where the oligomerization dynamics in a sample is not homogenous (Cutrale et al., 2019). To uncover the dynamic changes in aggregation, eN&B subsamples the data

and calculates the N&B at each subsample and iterates the same process by shifting subsampling by a factor of one frame, until all possible subsamples are covered. Another extension of the N&B method is based on the application of the moment analysis theory to the spatial domain, called fluorescence intensity fluctuation spectrometry (FIF) (Stoneman et al., 2019). FIF also uses single confocal microscope images. One of the unique features of FIF is to segment the image into smaller regions, and calculate the number and brightness values for each segments. The goal behind this rationale is to identify the proportions of different oligomeric entities. FIF has also been successfully applied to determine basal and ligand induced stoichiometry of GPCR oligomers.

1.7.1.3. Structural Methods

A number of structural studies reported homodimeric organization of class A GPCRs (Figure 1-15). Importantly, all of the homodimers observed in structural studies were obtained with X-ray crystallography. This technique provided homodimeric/oligomeric assembly of human CXCR4 (Qin et al., 2015; B. Wu et al., 2010), murine μ-opioid receptor (μOR) (Manglik et al., 2012), human κOR (H. Wu et al., 2012), turkey β_1 adrenergic receptor (Huang et al., 2013) and squid rhodopsin (Murakami and Kouyama, 2008). Interestingly, dimer interfaces observed in these studies were always formed between either TM5-TM6, or TM1, TM2-H8, or both. The only dimeric GPCR structure coming from cryoEM so far belongs to the yeast GPCR Ste2. In this structure, homodimer interface was observed between TM1-TM7 (Velazhahan et al., 2021).

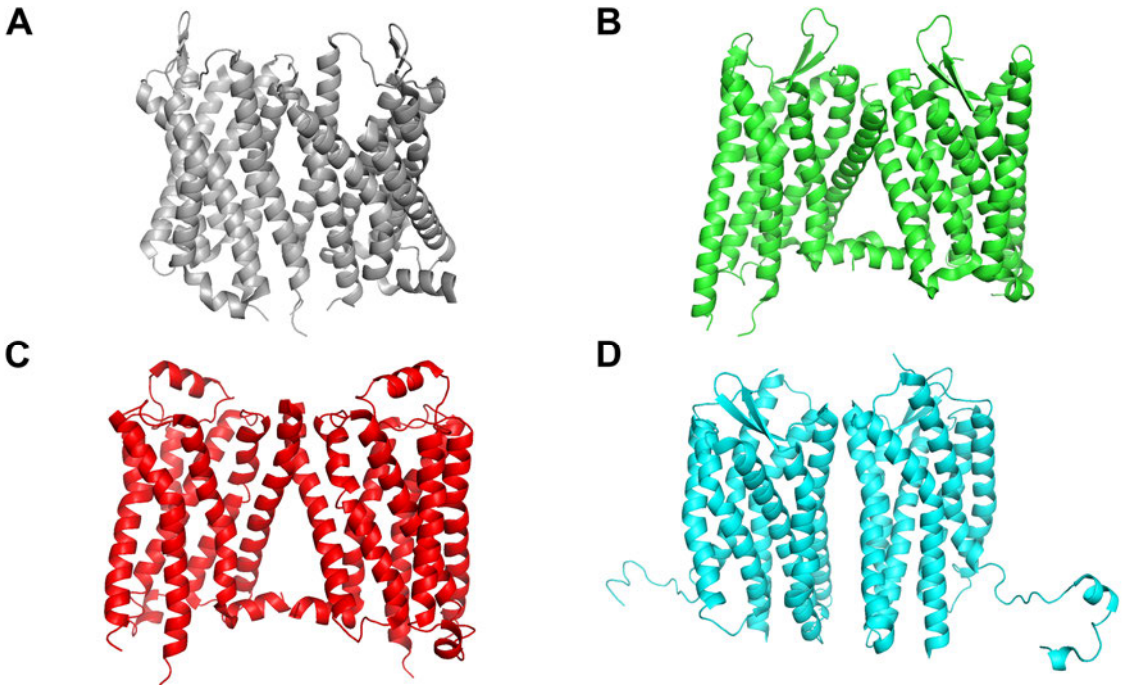

Figure 1-15. Dimeric X-ray structures of class A GPCRs: (A) μOR (PDB: 4DKL), (B) κOR (4DJH), (C) β1AR (4GPO) and (D) CXCR4 (3ODU).

1.7.2. Functional Implications of Class A GPCR Oligomers

Class C GPCRs are constitutive dimers, and their dimerization is essential for cell surface targeting (Bettler et al., 2004) and signal transmission (Levitz et al., 2016). mGluRs can form functional homo and heterodimers. Heterodimerization of mGluRs usually occurs between specific subunit groups, such as mGluR1,5; mGluR2,4; and mGluR7,8 (Delgado et al., 2017; Yin et al., 2014), and these heterodimers mediate distinct functions, such as location specific neural transmission (Yin et al., 2014). Activation mechanisms of class C GPCR homo- and heterodimers are described in great detail. In case of $GABA_BR$, binding to $GABA_{B1}R$ is sufficient to activate the heterodimer. This binding transactivates the $GABA_{B2}R$, which can then couple to the G protein (Geng et al., 2013). In the case of mGluRs, ligand binding to one of the protomers is sufficient to start signaling, but binding to both protomers in the dimer is necessary for full activation (Kniazeff et al., 2004). Upon activation, only one mGluR protomer adopts an active conformation at a time, and ligand binding to one protomer can cross activate the adjacent protomer regardless of ligand binding to the second one. This mechanism is termed asymmetric activation (Brock et al.,

2007). Therefore, eventually one protomer couples with the G protein. Asymmetric activation is thought to activate a specific protomer, as in case of the mGluR2,4 heterodimer, in which the G protein coupling is mediated by the mGluR4 (J. Liu et al., 2017).

Functional significance of class A GPCRs is a highly debated topic (Bouvier and Hébert, 2014; Lambert and Javitch, 2014). GPCRs are allosteric proteins that can work in a dynamically cooperative manner. Yet, how much is receptor dimerization involved in this cooperative modulation of activity? Numerous studies showed that individual class A GPCRs can function as active signaling units (Hanson et al., 2007; Kuszak et al., 2009; Whorton et al., 2008). However, this does not exclude the potential effect of dimerization on the receptor function by other means, i.e. alterations in ligand or effector affinity, activation kinetics, surface delivery or internalization dynamics. Recent studies based on fluorescence microscopy imaging revealed that all studied class A GPCRs form only transient homodimers with each other (Calebiro et al., 2013; Dorsch et al., 2009; Fonseca and Lambert, 2009; Işbilir et al., 2020; Kasai et al., 2011; Möller et al., 2020; Tabor et al., 2016). Yet, a number of studies based on FFS methods suggested that at higher expression levels a few of those receptors can form dimeric and high order oligomeric assemblies (Işbilir et al., 2020; Marsango et al., 2017; Stoneman et al., 2019; Ward et al., 2015). A number of high technology methods were able to show receptor dimers even in native tissues (Albizu et al., 2010). Therefore, it is possible that specific dimerization of class A dimerization follow the law of mass action, with varying specific affinity to each other. On the other hand, to date, no dynamic information for heterodimerization is present, yet a similar scenario as observed for class A receptor homodimers can be expected. A study demonstrating the negatively cooperative binding of alprenolol to β_2AR brought up the possibility of pocket to pocket cooperativity as a result of possible receptor oligomerization (Limbird et al., 1975). Although more studies followed this example and suggested negative binding cooperativity as a consequence of dimerization (George et al., 2002; Springael et al., 2006), others challenged this idea by suggesting that the competition for G protein may be the reason for observed negative cooperativity (Chabre et al., 2009). Yet, a large number of studies have explored the relevance of GPCR dimers at functional level, especially for heterodimers. For example, in case of the dopamine D_2 receptor (D_2R), activation of both protomers within a D_2R dimer shows less efficacy in signaling than that of the

situation where only one receptor is active (Han et al., 2009). This addresses a negative cooperativity between the dimeric protomers. In contrast, another study focusing on the 5-HT_4 receptor (5-HT_4R) demonstrated that this receptor can form dimers, and activating both protomers of the dimer is more efficient in recruiting and activating the heterotrimeric G protein (Pellissier et al., 2011). Melatonin receptors 1 and 2 (MT_1R and MT_2R) also received great attention in terms of their heterodimeric function. MT_1R and MT_2R heterodimer is one of those few that were shown to be functionally essential *in vivo*. In retina, MT_1R and MT_2R heteromer modulates the effect of melatonin on light sensitivity. This effect was moreover shown to be due to the heteromer specific activation of PLC/PKC pathway (Baba et al., 2013). Moreover, GPR50 was shown to heterodimerize both with MT_1R and MT_2R, and even negatively modulate the ligand binding and G protein mediated signaling of the MT_2R (Levoye et al., 2006). Another example of functional cooperation was shown between the α_{2A}AR and the μOR (Vilardaga et al., 2008). In this case, activation of the μOR by morphine was shown to partially inhibit the norepinephrine mediated activation of the α_{2A}AR. This cross-inactivation was also shown to be reflected as a reduction in G protein and MAPK activation. Another striking example comes from a study focusing on luteinizing hormone receptor (LHR) homodimers. In this study, expression of binding deficient and signaling deficient LHR mutants in a LHR knockout mouse restored the activity of LH, demonstrating a positive functional cooperativity between two mutants (Rivero-Müller et al., 2010). Apart from the function, dimerization was proposed to be necessary for cell surface delivery of receptors (Jin et al., 2018; Salahpour et al., 2004) and even internalization (Sartania et al., 2007).

1.8. Chemokines and Chemokine Receptors

1.8.1. Chemokines

Chemokines are a class of cytokines that primarily modulate motility related functions of bone marrow derived cells. In humans, the chemokine family consists of approximately 50 individual members. Although chemokines and their receptors mainly regulate the cells of the immune system, they are also widely expressed in other cell types, such as

epithelial and endothelial cells, progenitor cells and even astrocytes and neurons. Next to their function of controlling cellular migration, chemokines are also involved in numerous physiological processes, such as apoptosis, survival, exocytosis, angiogenesis, development, differentiation *et cetera* (Hughes and Nibbs, 2018).

The size of chemokine peptides varies from 8 to 12 kiloDaltons (kDa). Although chemokines share a similar structural architecture, they are divided in three groups according to their highly conserved cysteine residues that form two disulfide bonds: CC, C-X-C and C-X3-C chemokines (Zlotnik and Yoshie, 2000). Overall, chemokines consist of a long unstructured N terminal motif connected to a single turn 3_{10} helix, which is connected to three antiparallel β sheets connected to each other with two short loops, and a C terminal α helix domain that folds onto the triple β sheets. Typically, the first two Cys residues are located at the N terminal domain. The first disulfide bond forms between the first and the third Cys, and the second bond forms between the second and the fourth Cys residues. Cys residues are numbered according to the order of appearance in the polypeptide sequence.

Chemokines exert their activity as monomeric peptides. However, they are able to form dimers and oligomers (Figure 1-16). Dimerization of chemokines can occur in solution, but it is known that the cell surface glycosaminoglycans (GAGs) also contribute to chemokine oligomerization (Hoogewerf et al., 1997). Different chemokines have different GAG binding affinities (Kuschen et al., 1999), and GAG mediated chemokine oligomerization is thought to be essential for the function of a number of chemokines (Ali et al., 2005). Emerging evidence shows that di-/oligomeric chemokines interact with their receptors in distinct orientations and induce different cellular functions, such as chemokine retention during inflammation (Proudfoot et al., 2003). Usually, while chemokines in solution, i.e. in blood, mediate directed cell migration by forming a chemokine concentration gradient, cell surface bound chemokines may act as a docking site for the recruited cells, and mediate cell arrest and migration into tissues.

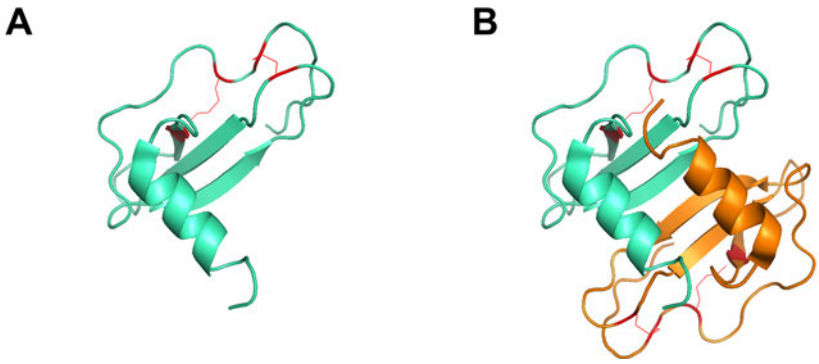

Figure 1-16. Structures of the (A) monomeric and (B) dimeric C-X-C chemokine 12 (CXCL12) (PDB: 2K01). Shown are two CXCL12 protomers (cyan and orange) that form a dimer via their βsheets. Conserved double disulfide bonds in each chemokine structure are shown in red.

Chemokines can be divided in two groups regarding their function: homeostatic chemokines are constitutively produced and they balance the basal trafficking and homing of leukocytes as well as B and T cell maturation (Mantovani, 1999), and inflammatory chemokines are the ones that are produced upon inflammation and they trigger immune cell responses. At resting state, cells of the immune system exhibit a certain profile of chemokine expression in order to maintain the immune surveillance, leukocyte homing, hematopoiesis (Figure 1-17A). In case of inflammation, chemokine profile can drastically change in order to activate the immune system and recruit leukocytes to the inflammation site (Lam et al., 2010; Øvrevik et al., 2009). The altered chemokine profile generates a gradient of chemokines to mediate chemotaxis, fixation of certain chemokines on the endothelial cells for cell arrest and extravasation, and different chemokine content at the inflammation site to activate the innate immunity (Figure 1-17B). Although the inflammatory *versus* homeostatic chemokine discrimination is applicable to a certain degree, a number of chemokines with dual functions do exist (Constantin et al., 2000). Therefore, a major determining factor of the immune response and basal surveillance must be maintaining the correct balance of different chemokines.

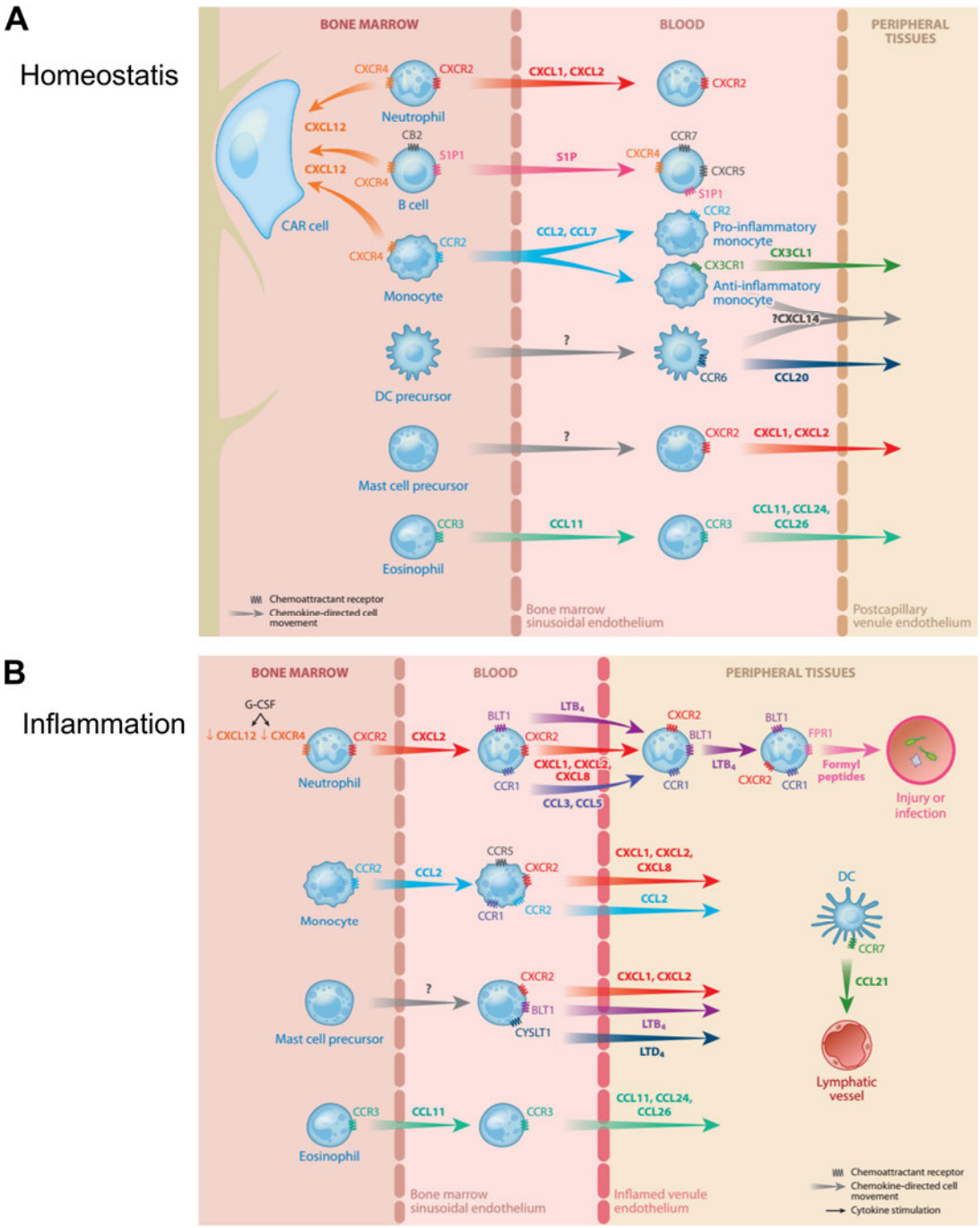

Figure 1-17. Homeostatic and inflammatory roles of chemokines in the immune system. A number of chemokines, i.e. CXCL12 as one of the most central ones, mediate bone marrow homing and retention of blood cells. Other chemokines also play role in i.e. trafficking of immune cells to blood and other peripheral tissues, such as lymph node, where immune cells differentiate and maturate. Differentiated cells also change their chemokine receptor expression pattern, which allows them to migrate to blood, where they mediate their immune surveillance duties. Upon inflammation, expression of homeostatic GPCR CXCR4 and its ligand CXCL12 decreases. Inflammatory chemokines generate a concentration gradient, which activates immune system cells and allows their migration toward peripheral tissues until the site of inflammation to start the immune response. Figure is extracted and modified from (Griffith et al., 2014), used under the license number 1106246-1 provided by Annual Reviews, Inc. and Copyright Clearance Center.

1.8.2. Chemokine Receptors

Chemokines are the agonists of the cell surface chemokine receptors, which are class A GPCRs. The first chemokine receptors identified from the human genome were the interleukin 8 (IL-8, or CXCL8) receptors CXCR1 and CXCR2 (Holmes et al., 1991; Murphy and Tiffany, 1991). Since then, a total of 22 chemokine receptors have been identified (Arimont et al., 2017). Chemokines interact with chemokine receptors promiscuously; most of the chemokines can bind to multiple receptors (Figure 1-18). This promiscuity complicates the functional outcomes of chemokine signaling, yet it is thought to be a factor for fine tuning of the immune system (Proudfoot and Uguccioni, 2016).

Except the four atypical chemokine receptors, which activate alternative signaling pathways, all chemokine receptors are primarily Gi protein couplers (Francoise Bachelerie et al., 2014). The expression profile of chemokine receptors in the immune system is in accordance with the function of their cognate chemokines. Some chemokine receptors, such as CXCR4, are widely expressed throughout the immune cells. In contrast, expression of the receptors like CCR3 and CXCR1 is more restricted to certain cell types (Figure 1-18). This tightly regulated expression pattern allows the immune system to respond correct chemokine profiles under inflammatory and basal conditions.

Over decades, structural and biophysical studies provided a great understanding of how chemokines interact with their receptors. Many of these studies proved that similar architecture of all chemokines also follows a similar mode of binding with their receptors. Overall, chemokine receptors form extensive contacts with their chemokines through the receptor N terminal domain, extracellular loops and TM domains. Earlier studies described chemokine binding to its receptor with a “two-site, two-step” mechanism that involved sequential binding of the chemokine via two chemokine recognition sites (CRSs): The receptor N terminal domain, which is called the CRS1, interacts with the globular domain of the chemokine, but this interaction does not activate the receptor. Mutations at this site, or at the adjacent chemokine site of it, was shown to reduce chemokine binding affinity(Hemmerich et al., 1999; Mayer and Stone, 2001). TM core domain of a chemokine receptor,

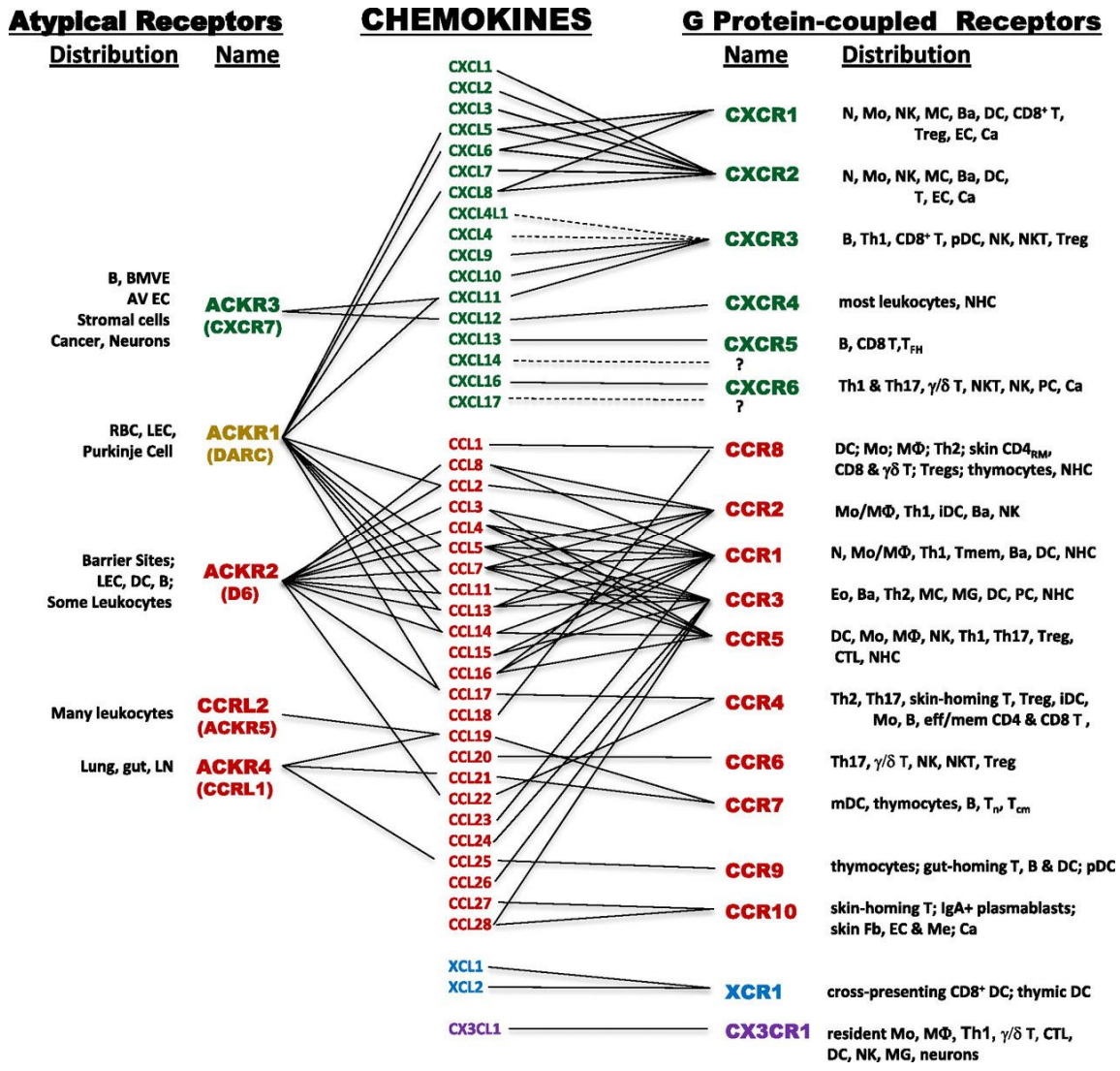

Figure 1-18. Chemokines and their promiscuous relationship with chemokine receptors. "Distribution" is the cell types in which each chemokine receptor is expressed. Abbreviations are: Ba, basophil; Ca, cancer; $CD4_{RM}$, resident memory CD4 T cell; EC, endothelial cell; Eo, eosinophil; Fb, fibroblasts; iDC, immature DC; MC, mast cell; Me, melanocyte; MG, microglial cell; Mo, monocyte; MΦ, macrophage; N, neutrophil; NHC, nonhematopoietic cells; PC, plasma cell; pDC, plasmacytoid DC; T_{cm}, central memory T cell; Th1, type 1 helper T cell; T_n, naive T cell; eff/mem, effector/memory; thym, thymocytes. Figure and the abbreviations are extracted from (Francoise Bachelerie et al., 2014), used under the license number 1121457-1 provided by American Society for Pharmacology and Experimental Therapeutics and Copyright Clearance Center.

which constitutes CRS2, forms interactions with the N terminus of a chemokine, and this binding promotes receptor activation (Crump et al., 1997). Indeed, mutating the N terminal residues of a few chemokines turned them into high affinity antagonists, suggesting the importance of CRS2 for receptor activation (Clark-Lewis et al., 1991; Gong and Clark-Lewis, 1995; Proudfoot et al., 1996). Despite many more evidence in favor of this model,

recent studies challenged this simplistic binding and activation model by identifying other sites on chemokine receptors that are also contributing to chemokine binding and receptor signaling efficacy (Kleist et al., 2016).

Structural studies shed light on experimentally supported models of receptor-ligand interactions. To date, 5 chemokine and G protein bound, 9 antagonist bound, and one ligand free chemokine receptor structures have been reported:

Table 1-1. Reported active chemokine structures.

Receptor	**Ligand**	**G protein**	**Reference**
CXCR2	$CXCL8_1$	$miniG_o$	(K. Liu et al., 2020)
CXCR2	$CXCL8_2$		
CCR5	[6P4]CCL5	G_{i1}	(Isaikina et al., 2020)
CCR6	CCL20	G_{i1}	(Wasilko et al., 2020)
US28	CX3CL1	-	(Burg et al., 2015)

Table 1-2. Reported inactive chemokine receptor structures.

Receptor	**Ligand**	**Reference**
CXCR1	-	(Park et al., 2012)
CXCR4	vMIPII	(Qin et al., 2015)
CXCR4	CVX15	(B. Wu et al., 2010)
CXCR4	IT1t	
CCR2	BMS-681	(Zheng et al., 2016)
CCR2	CCR2-RA-[R]	
CCR5	Maraviroc	(Q. Tan et al., 2013)
CCR5	[5P7]CCL5	(Zheng et al., 2017)
CCR5	gp120	(Shaik et al., 2019)

CCR7	Cmp2105	(Jaeger et al., 2019)
CCR9	Vercirnon	(Oswald et al., 2016)

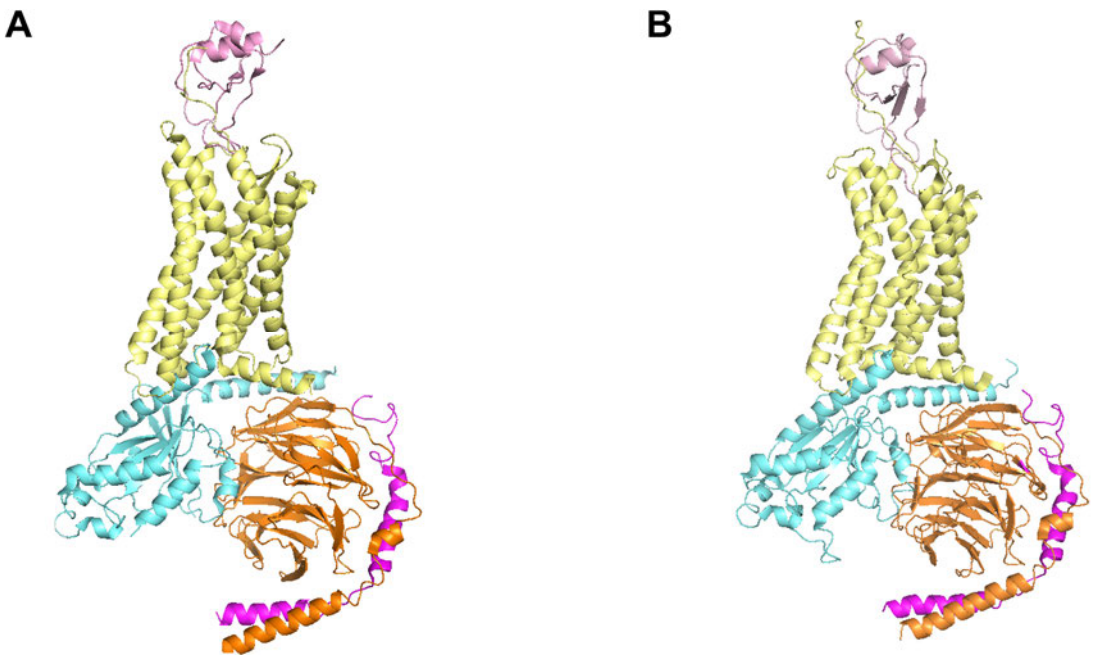

Figure 1-19. Active structures of (A) CCR6 (bound to CCL20) and (B) CXCR2 (bound to $CXCL8_1$) coupled to $G_{i/o}$ proteins. Shown structures are chemokines (pink), receptors (yellow), Gα (cyan), Gβ (orange) and Gγ (magenta).

Chemokine:chemokine receptor complex structures revealed a previously unknown mechanism of receptor activation: In CCR6:CCL20 (Figure 1-19A) and CXCR2:CXCL8 (Figure 1-19B) complexes, although the described CRS1 contacts were present, the N terminal domain of these chemokines did not display any contact with the so-called binding pocket located within the TM domains (Liu et al., 2020; Wasilko et al., 2020), in contrast to [6P4]CCL5 on CCR and CX3CL1 on US28 (Burg et al., 2015; Isaikina et al., 2020). The active structures of CCR6 and CXCR2 suggested that ligand binding to the N terminus and extracellular loops of these receptors induced a force that is translated through the TM domains and activate the receptor. This is in contrast to the activation mechanism of CCR5, in which the agonist binds both to extracellular and TM domains and

triggers a canonical microswitch cascade that eventually stabilize an active receptor conformation. This major difference is thought to be a result of short N terminus of CCL20 and CXCL8 compared to that of CCL5. Moreover, a well conserved rotamer toggle switch at the position 6.48 is a Trp in CCR5, while it is a Gln in CXCR2 and CCR6.

1.8.3. CXCL12/CXCR4/ACKR3 Axis

Among all chemokines and their receptors, CXCR4 and ACKR3 have exceptionally diverse functional roles. Despite the large promiscuity among chemokines and chemokine receptors, CXCR4 binds to only CXCL12, and ACKR3 binds to CXCL12 and CXCL11 (Scholten et al., 2012).

1.8.3.1. CXCR4

CXCR4 was discovered in 1996, originally with the name “fusin” or “leukocyte-derived seven-transmembrane domain receptor” (LESTR), as an human immunodeficiency virus 1 (HIV-1) entry cofactor protein (Feng et al., 1996). The only native chemokine of CXCR4 is CXCL12, or the stromal cell derived factor 1 (SDF-1), which was discovered the same year as CXCR4 (Bleul et al., 1996; Oberlin et al., 1996).

CXCL12 and CXCR4 are ubiquitously expressed in tissues at embryo and adult stages. As a result of this, they modulate numerous physiological processes beyond the immune system. CXCR4 expression and function is thought to be vital for mammalians, as homozygous knockout of *Cxcr4* causes perinatal fatality in mice with cerebellar, cardiovascular and hematopoietic defects (Zou et al., 1998). As an indispensable component of the immune system, CXCR4 is responsible for the survival and homing of the hematopoietic progenitor cells in the bone marrow (Broxmeyer et al., 2003; Sugiyama et al., 2006) as well as progenitor T cell localization and survival in thymus (Plotkin et al., 2003; Trampont et al., 2010). Apart from the ones in the immune system, other examples of physiological processes that CXCR4 plays a role in are angiogenesis (Tachibana et al.,

1998), cerebellar development (Q. Ma et al., 1998; Zou et al., 1998), cardiac myocyte function (Pyo et al., 2006) and neurogenesis (Stumm and Höllt, 2007).

Because of its key homeostatic and regulatory functions, alterations in CXCR4 expression and function are associated with numerous pathologies. Naturally occurring nonsense and frame shift heterozygous mutations in CXCR4 that cause truncations of its C terminal domain are associated with the human papilloma virus (HPV) induced warts, hypogammaglobinemia, infections, and myelokathexis (WHIM) syndrome (Hernandez et al., 2003; Q. Liu et al., 2012). These gain-of-function variants of CXCR4 cause diminish desensitization of CXCR4, cause abnormal retention of bone marrow cells and alter immune synapse formation between T cells and antigen presenting cells (Balabanian, Lagane, Pablos, et al., 2005; Kallikourdis et al., 2013). CXCR4 is also a known coreceptor for the entry of X4 strain of HIV-1 in humans. Binding of the HIV-1 glycoprotein gp120 to the main HIV-1 entry receptor CD4 and, in addition, to CXCR4 allows the virus to stabilize itself on the surface of $CD4^+$ T lymphocytes and fuse with the cell membrane to release its material inside the cell (Wyatt and Sodroski, 1998). It is now well established that overexpression of CXCR4 is a prognostic marker in more than 23 types of cancers, including leukemia, lymphoma, melanoma, glioma, myeloma, sarcoma as well as prostate, cervical, ovarian, pancreatic, lung, gastrointestinal, renal and breast cancers (Chatterjee et al., 2014). In cancer, CXCR4 causes the survival, growth and proliferation of cancer cells and cancer stem cells, as well as angiogenesis, metastasis and recurrence of cancers (Chatterjee et al., 2014). CXCR4 is also involved in cardiovascular (Döring et al., 2014) and neurodegenerative (Bonham et al., 2018) diseases, in which the absence of CXCR4 usually causes developmental or post-injury specific pathologies, which are associated with the chemotactic ability of CXCR4.

Activation of CXCR4 by its agonist CXCL12 transduces signals to the cell interior via a number of signaling pathways (Figure 1-20). The signaling of CXCR4 may vary depending on the cellular context (Heuninck et al., 2019). In response to CXCL12, CXCR4 primarily couples to inhibitory G proteins, except Gαz (Armando et al., 2014). A more efficient coupling was observed with $G\alpha_{i1}$ and $G\alpha_{i2}$ than with $G\alpha_{i3}$ and $G\alpha_o$ (Perpiñá-

Viciano et al., 2020). Activation of $G\alpha_{i2}$ via CXCR4 can trigger Src activation that is followed by ERK phosphorylation (Conley-LaComb et al., 2016). Other studies using more endogenous settings showed that CXCR4 can also activate $G\alpha_{13}$, which is necessary for CXCR4 induced migration of Jurkat T cells (W. Tan et al., 2006). Although a number of studies showed that CXCR4 can signal through $G\alpha_q$ mediated PI3K pathways in physiologically relevant cells (Soede et al., 2001; Vicente-Manzanares et al., 1999), *in vitro* experiments could not report any direct $G\alpha_q$ activation in HEK293 cells (Perpiñá-Viciano et al., 2020). It is possible that some cell types, such as dendritic cells, require both $G\alpha_q$ and $G\alpha_i$ for CXCR4 functions, while $G\alpha_i$ may suffice in other cells, such as T and B cells (G. Shi et al., 2007).

Agonist bound CXCR4 is targeted by GRKs and protein kinase C (PKC), which phosphorylate intracellular serine/threonine (S/T) residues of it (Busillo et al., 2010). It was shown that specific S/T residues are targeted by specific kinases with specific order: upon agonist binding S346/347 are rapidly phosphorylated by GRK2/3, which is followed by PKC and GRK6 mediated S324/325 phosphorylation, and then S338/339 by GRK6 (Mueller et al., 2013). Upon phosphorylation, CXCR4 interacts with β-arrestin1/2. Interestingly, β-arrestin2 recruitment occurs with faster kinetics than that of β-arrestin1. Moreover, GRK2/3 mediated phosphorylation of S346/347 appears to be essential for β-arrestin recruitment to CXCR4. β-arrestin recruitment to CXCR4 also plays a role in chemotaxis, since knocking out β-arrestins reduces T and B cell migration towards CXCL12 in mice (Fong et al., 2002).

CXCR4 can also induce a number of non canonical signaling pathways. Among these, an interesting one is the non receptor tyrosine kinase JAK. It was proposed that CXCL12 binding to CXCR4 activated JAK2 and JAK3 by physically interacting with them, which eventually led to nuclear transport of phosphorylated STAT proteins (Vila-Coro et al., 1999a). Moreover, this pathway was proposed to be independent from the G protein activation, and inhibition of Gi by pertussis toxin (PTx) led to a prolonged JAK/STAT activation.

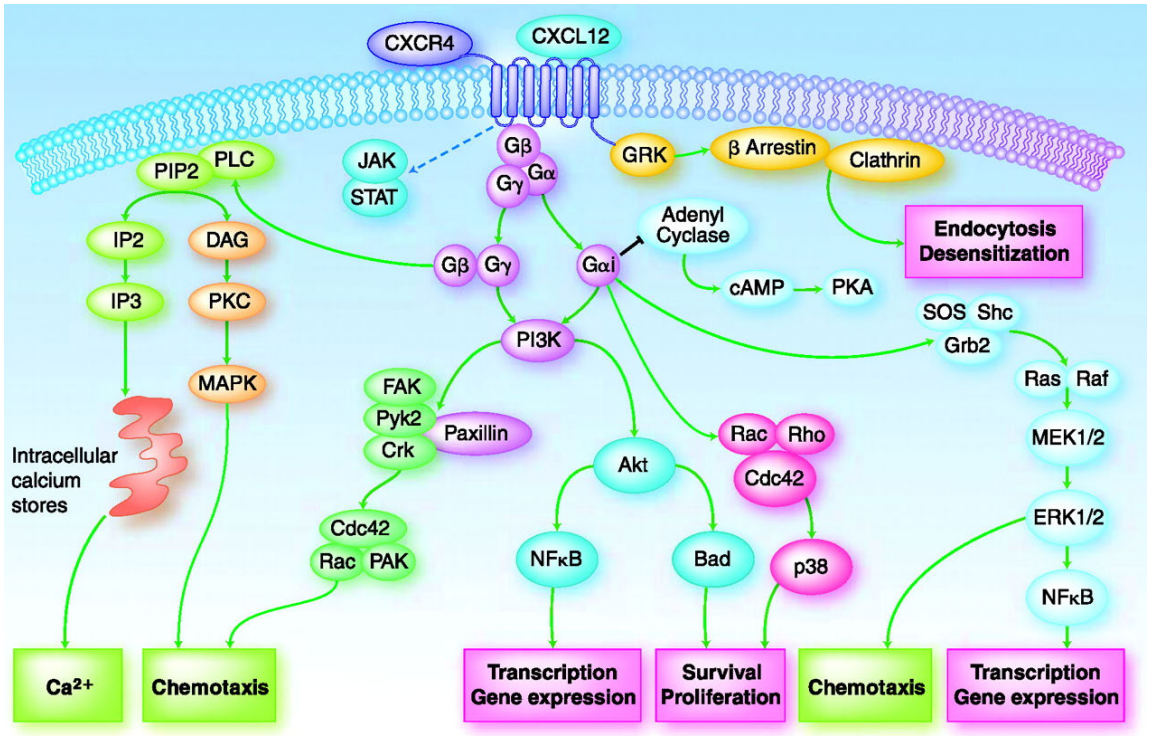

Figure 1-20. Schematic view of the signaling pathways activated by CXCL12/CXCR4 pair. Figure is extracted and modified from (Teicher and Fricker, 2010), used under the license number 5034461011761 provided by American Association for Cancer Research and Copyright Clearance Center.

1.8.3.2. ACKR3 (CXCR7)

ACKR3, or its old name CXCR7, is an atypical chemokine receptor. Atypical chemokine receptors contain mutations in the highly conserved DRYLAIV domain of class A GPCRs, which is essential for G protein mediated signaling (Françoise Bachelerie et al., 2014). ACKR3 binds to only two chemokines: CXCL12, which it shares with CXCR4, and CXCL11, which binds also to CXCR3. ACKR3 exhibits higher affinity for both of these chemokines than does CXCR3 or CXCR4 (Balabanian, Lagane, Infantino, et al., 2005; Burns et al., 2006). Upon ligand binding, ACKR3 interacts with GRKs for receptor phosphorylation (Zarca et al., 2021), which is followed by β-arrestin recruitment, and a rapid internalization follows (Rajagopal et al., 2010). Although ACKR3 does not activate G proteins, it was shown to be able to interact with Gi protein in *in vitro* assays (Levoye et al., 2009). It is possible that this interaction is needed for GRK recruitment to ACKR3 (H. T.

Nguyen et al., 2020). Independently from β-arrestin mediated pathway, ACKR3 is continuously internalized and recycled back to the cell surface in the absence of ligands. The continuous trafficking of ACKR3 is mediated by constitutive ubiquitination/deubiquitination (Canals et al., 2012). Yet, activation via its chemokines accelerates its internalization via β-arrestin dependent pathways (K. E. Luker et al., 2010). However, CXCL11 mediated internalization occurs more rapidly in comparison to that of CXCL12 (Montpas et al., 2018). Truncation of the C terminus of ACKR3 impairs continuous internalization of the receptor, and enhances ligand induced ERK phosphorylation (Ray et al., 2012). Arrestin coupling to ACKR3 was shown to activate Akt and ERK pathway activation (Rajagopal et al., 2010; Torossian et al., 2014). Due to its high affinity to chemokines and continuous internalization cycle, it is thought that ACKR3 acts as a "chemokine scavenger", which by simple means is a fine tuner of chemokine concentration in the surrounds of cells (Naumann et al., 2010).

ACKR3 is mainly expressed in astrocytes (Puchert et al., 2017), B cells and granulocytes (Humpert et al., 2012), and stromal cells such as fibroblasts and endothelial cells (Berahovich et al., 2014). Similarly to *Cxcr4*, knockout of *Ackr3* also leads to fetal or postnatal mortality and developmental defects in cardiac and renal tissues as well as in brain (Quinn et al., 2018). Endogenous expression of ACKR3 modulates chemokine concentrations in the vicinity of the cells it is expressed in. Moreover, ACKR3 is required for mature B cell functioning (Infantino et al., 2006). Next to scavenging chemokines, ACKR3 is also able to scavenge a number of natural opioid peptides in the brain (Meyrath et al., 2020).

Just like CXCR4, dysregulated expression and activity of ACKR3 is associated with numerous pathologies. Elevated expression levels of ACKR3 were found in cancer, inflammatory bowel disease, viral infections and rheumatoid arthritis (Freitas et al., 2014; Sánchez-Martín et al., 2013). High expression of ACKR3 is also associated with tumor growth (Neves et al., 2019). In cancer cells, ACKR3 overexpression causes cancer cell proliferation and metastasis. Moreover, although ACKR3 is not expressed in healthy vascular endothelial cells, it is expressed in tumor vasculature and increases angiogenesis (Miao et al., 2007). Moreover ACKR3 has been shown to increase EFG and VEGF signal-

ing especially in the vasculature, upregulating matric metalloproteases and cell-cell adhesion proteins, which further enhances tumor growth and vascularization (Wani et al., 2014). ACKR3 is also involved in viral pathologies, such as human herpes virus 8 (HHV8), human T lymphotropic virus type 1 (HTLV1), human papilloma virus (HPV) and Epstein-Barr virus (EBV), all of which carry oncogenic potential. In all carcinomas associated with above mentioned virus infections, ACKR3 overexpression was observed. ACKR3 overexpression is thought to contribute to proliferation and survival, as well as immortalization of virus induced carcinomas by enhanced signaling via CXCL12. (Freitas et al., 2014).

1.8.4. Chemokine Receptor Oligomerization

Oligomerization concept in the chemokine world is not limited to chemokine peptides itself. There is now evidence from a wide range of studies in favor of chemokine receptor homo- and heterooligomers. Again, a variety of biochemical (i.e. coIP) and biophysical methods (i.e. FRET and BRET) were used to demonstrate chemokine receptor oligomerization (Stephens and Handel, 2013). The only *in vivo* evidence for chemokine receptor dimerization was reported using proximity ligation assay (M. A. Hauser et al., 2016; Hayasaka et al., 2015). For a number of chemokine receptors oligomerization occurs at the basal state, as well as after binding to chemokines (Martínez-Muñoz, Villares, et al., 2018). Mutagenesis studies also showed the relevance of predicted dimerization interfaces of CCR2 and CCR5 (Hernanz-Falcón et al., 2004; Hurevich et al., 2013). Oligomerization of chemokine receptors is thought to influence receptor function by crosstalk at ligand binding and signaling stages. Ligand induced tetramerization of CCR7 was shown to be necessary for dendritic cell migration via tetramer associated Src and SHP2 signaling (M. A. Hauser et al., 2016). Homodimerization of CCR5 was associated with a reduction in HIV infection (Vila-Coro, 2000). CCR5 and CCR2 forms heterodimers and agonist binding to CCR5 negatively influences agonist binding to CCR2 (Springael et al., 2006). In case of CXCR1 and CXCR2 heterodimers, their common agonist CXCL8 disrupts heterodimers and stabilizes homodimers of both receptors (Martínez Muñoz et al., 2009).

1.8.4.1. Oligomerization of CXCR4 and ACKR3

Numerous studies reported homo- and heterooligomerization of CXCR4 and ACKR3. In case of CXCR4, earlier studies using coIP suggested both basal and ligand induced CXCR4 multimerization (Babcock et al., 2003; Vila-Coro et al., 1999b). Later studies based on FRET and BRET also supported the steady state dimerization of CXCR4 (Felce et al., 2017; Hamdan et al., 2006; Hammad et al., 2010; Lagane et al., 2008; Tanaka et al., 2010). CXCR4 dimerization was also shown in cancer cells using FRET (J. Wang et al., 2006). Additional analogous studies reported an increase in BRET and FRET signal between CXCR4 protomers upon CXCL12 treatment. This signal increase was interpreted as either an increase in the oligomeric size of CXCR4, or a conformational change between the protomers within dimeric units (Isik et al., 2008; Kalatskaya et al., 2009; Percherancier et al., 2005; Toth et al., 2004). A number of studies using bimolecular luminescence complementation (BiLC) and BiLC-BRET also described spontaneous formation of higher order oligomers as well as ligand stabilized ones (Hamatake et al., 2009; Sohy et al., 2009). Moreover, CXCR4 crystal structures also show a dimeric receptor assembly, with a TM5,6 dimer interface (Qin et al., 2015; B. Wu et al., 2010) (Figure 1-21). Isolated and liposome reconstituted CXCR4 also appeared to be dimeric (Zhukovsky et al., 2010). CXCR4 dimers were described to be formed in lipid rafts, as depletion of sphingomyelin from cell membrane increased CXCR4 dimerization (Asano et al., 2012). Recent studies based on single molecule analysis showed that CXCR4 is monomeric at low expression levels (Beletkaia et al., 2016; Ge et al., 2017; Lao et al., 2017). These studies also reported agonist induced dimers and oligomers. An excellent study also used single molecule imaging and showed that CXCR4 exhibits a balanced distribution of monomers, dimers and higher order oligomers (Martínez-Muñoz, Rodríguez-Frade, et al., 2018). This study also showed that ligand induced oligomer formation is essential for CXCR4 mediated migration, and oligomerization-deficient mutants of CXCR4 did not induce migration. Steady state homodimerization was described during cell surface delivery of CXCR4 as well (Charette et al., 2011), implying that dimerization may play in receptor translocation from Golgi to the cell surface.

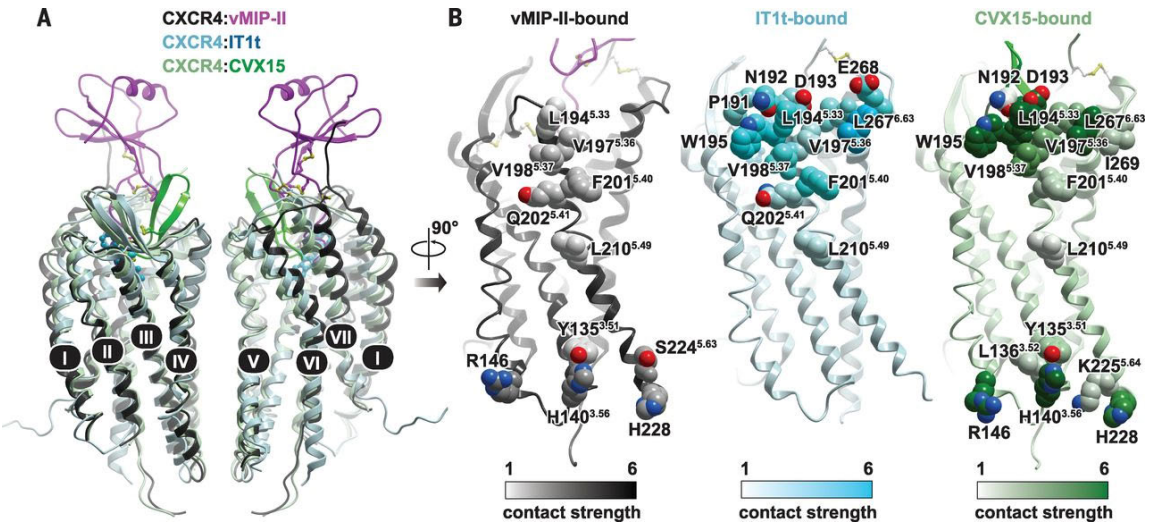

Figure 1-21. Dimer interfaces of CXCR4 obtained from three different crystal structures. The structures suggest that dimers are formed by a TM4-TM5 interface involving mainly the extracellular and intracellular portions of the helices. Figure is extracted and modified from (Qin et al., 2015), reprinted with permission from American Association for the Advancement of Science (AAAS).

CXCR4 also forms heteromeric complexes with other GPCRs and membrane proteins. Constitutive interactions of CXCR4 with CCR2 (Rodríguez-Frade et al., 2004; Sohy et al., 2009, 2007), CCR5 (Charette et al., 2011; Contento et al., 2008; Hammad et al., 2010; Isik et al., 2008; Kuang et al., 2012; Sohy et al., 2009), α_{1A}-adrenoceptor (Gao et al., 2020; Tripathi et al., 2015), μ- and κ-opioid receptors (Toth et al., 2004), as well as CD4 (Martínez-Muñoz, Rodríguez-Frade, et al., 2018; Toth et al., 2004) and T cell receptor (TCR) (Kumar et al., 2006) were reported. Heterocomplexes between CCR2/CCR5/CXCR4 (Sohy et al., 2009) as well as CD4/CCR5/CXCR4 (Martínez-Muñoz et al., 2014).

Numerous studies, mainly based on BRET and FRET, also suggested that ACKR3 can form oligomers with itself (Kalatskaya et al., 2009; Levoye et al., 2009) as well as with CXCR4 (Décaillot et al., 2011; Sierro et al., 2007). The studies of Décaillot et al. and Sierro et al. suggested that CXCR4/ACKR3 heteromers exhibit enhanced CXCL12 signaling, which appears to be necessary for cellular migration and the development of cardiovascular tissue. Yet, another study suggested that ACKR3 negatively regulates the G protein signaling of CXCR4 as well as T cell migration (Levoye et al., 2009). A recent study

showed that in cancer cell epithelium, where both CXCR4 and ACKR3 are overexpressed, heterodimers of these receptors increase histone demethylation and lead to an increased transcription of inflammatory and oncogenic genes (Song et al., 2019). It was shown that both ACKR3 agonists, as well as the CXCR4 antagonist AMD3100 increases BRET between two ACKR3 protomers (Kalatskaya et al., 2009; Kathryn E. Luker et al., 2009). However, a recent study could not verify CXCR4/ACKR7 heteromer, while ACKR3 homomers were present in their assays using BiLC (H. T. Nguyen et al., 2020).

Chemokine mediated signaling is already complicated due to the diverse binding promiscuity. On top of this, chemokine receptor oligomerization adds another layer of complexity to the whole chemokine system. As mentioned in earlier chapters, determination of oligomerization should be performed with tools that can provide spatial visualization, verified monomeric and dimeric controls. Moreover, assessing chemokine oligomerization should ideally be performed in functionally relevant cells, under endogenous expression conditions. Yet, heterologous systems that rely on microscopic analysis of oligomerization serve for characterizing the biophysical dynamics of oligomerization by allowing the observation of single receptor-receptor interaction timelines, or oligomerization dynamics as a function of receptor concentrations. In summary, chemokine receptors are involved in numerous physiological and pathophysiological processes, and understanding their mechanism of work is essential for developing drugs. Oligomerization of chemokine receptors appears to be one of the layers that contribute to the complexity of the chemokine system. Thus, it is an interesting and relevant topic to focus on.

2. AIM AND STRATEGY

During the last 20 years, numerous research teams addressed that G protein-coupled receptors can exist as monomers, yet form dimers and even oligomers. While these receptor complexes can be formed among the receptor protomers of the same type, called homo-oligomers, hetero-oligomers can also exist. Shortly after the first reports on GPCR complexes, the idea of receptor oligomerization was started to be challenged, especially in terms of its significance regarding receptor function. Growing output within the field described contradictory oligomerization behaviors for the same receptors. One key aspect of this controversy has been different types of methods used for identifying receptor oligomers. Thus, before studying whether a receptor forms homo- or hetero-oligomers, one main aspect to consider is the method of choice.

As described above, different methods can greatly affect the outcome of oligomerization analysis. Chemokine receptors CXCR4 and CXCR7 are also the receptors suffered from this fact. While a number of studies using biochemical and biophysical methods suggested that these two receptors can dimerize with themselves as well as with each other (Stephens and Handel, 2013), more recent biophysical studies suggested a monomeric organization for CXCR4 (Ge et al., 2017; Lao et al., 2017). A main criticism on the ensemble methods used in these studies is the fact that they do not quantify the exact expression levels of these receptors while detecting their oligomer size. Yet, it is known that such methods require overexpression of the receptors under investigation.

This thesis work aimed on two main questions: 1) Establishment of an experimental protocol based on microscopy imaging to assess membrane protein dimerization at various expression levels, with exact quantification of receptor density. 2) Assessment of the quaternary organization of two class A GPCRs: CXCR4 and CXCR7.

Several drawbacks of the previous literature focusing on GPCR oligomerization has been the motivation of this study. First of all, many biophysical and biochemical methods used for studying receptor oligomerization only describe a qualitative assessment of receptor expression at overexpression levels. Moreover, several methods described GPCR oligomerization only qualitatively, without focusing on the actual size of the possible complexes observed. To address these aspects, more recently a robust and high resolution microscopy method, called single molecule imaging, was used. This method is based on high resolution microscopy that allows imaging fluorescently labeled receptors on the surface of living cells. Because it is a high resolution method, it allows precise quantification of how many receptors are monomeric, or oligomeric. Moreover, this method allows tracking the motion of individual receptors, which in turn can quantify the interaction dynamics and kinetics of individual receptors. This method was selected as one of the methods to assess GPCR oligomerization in the present work.

When one has to deal with higher expression levels to study receptor oligomerization, single molecule tracking does not provide a feasible platform. In this case, methods that rely on statistical analysis of fluorescence fluctuations in confocal mode are a better choice. Despite being a robust method to study oligomerization, fluorescence fluctuation spectroscopy may suffer from complicated analysis procedures that are available only under unclear protocols and user-unfriendly softwares. One of the aims of this thesis work was to cover the above mentioned pitfalls. Firstly, a method that can precisely describe receptor oligomerization at high expression, but in a quantitative fashion, was needed. For this, two molecular brightness analysis methods were established. These methods can quantify the average concentration and oligomer size of fluorescently labeled receptors, in single cell resolution. While the first method, spatial brightness, can identify concentration and oligomer size from singe images, the second method, spatial brightness, can reveal these from image series of single cells expressing the labeled receptors. Here, this method was established for different fluorescence labeling strategies, as well as with reference monomeric and dimeric controls for each labeling. Next, using these methods, oligomerization of CXCR4 and CXCR7 were quantified. Especially for CXCR4, not only the basal oligomerization was assessed, but also the ligand and mutation mediated effects.

3. MATERIALS

3.1. Molecular Biology Materials

Table 3-1. Plasmids

DNA	Vector	Source
β_1AR-EYFP	pcDNA3	(Dorsch et al., 2009)
β_1AR-2xEYFP	pcDNA3	This work
FLAG-SNAP-β_1AR	pcDNA3	(Calebiro et al., 2013)
CD86-EYFP	pcDNA3	(Dorsch et al., 2009)
CD28-EYFP	pcDNA3	(Dorsch et al., 2009)
FLAG-SNAP-CD86	pcDNA3	(Calebiro et al., 2013)
FLAG-2xSNAP-CD86	pcDNA3	(Calebiro et al., 2013)
FLAG-SNAP-CD28	pcDNA3	(Calebiro et al., 2013)
CXCR4	pcDEF	Françoise Bachelerie
CXCR4	pcDNA3	This work
CXCR4-mTurquoise2	pcDNA3	This work
CXCR4-nLuc	pcDNA3	This work
3xHA-CXCR4-ECFP	pcDNA3	(Perpiñá-Viciano et al., 2020)
CXCR4-EYFP	pcDNA3	This work
CXCR4-SYFP2	pcDNA3	This work
FLAG-SNAP-CXCR4	pcDNA3	This work
CXCR4-Y116S	pcDNA3	This work
CXCR4-Y116S-SYFP2	pcDNA3	This work
CXCR4-N119S	pcDNA3	This work
CXCR4-N119S-SYFP2	pcDNA3	This work
CXCR4-V242D	pcDNA3	This work
CXCR4-V242D-SYFP2	pcDNA3	This work

CXCR4-L246P	pcDNA3	This work
CXCR4-L246P-SYFP2	pcDNA3	This work
Gi2 sensor (pGβ1-2A-cp173Venus-Gγ2-IRES-Gαi2-mTurquoise2Δ9)	pEGFP-N1	(Van Unen et al., 2016)
$G\alpha i_2$	pcDNA3	(Bünemann et al., 2003)
$G\beta_1$	pcDNA3	(Bünemann et al., 2003)
$G\gamma_2$-SYFP	pcDNA3	(Bünemann et al., 2003)
β-arrestin2-HaloTag	pcDNA3	(Möller et al., 2020)
Lyn-Halo-SAH60-Halo-CAAX	pcDNA3	(Möller et al., 2020)
AP2μ2-mCherry	pIRESneo3	(Taylor et al., 2011)

Table 3-2. List of primers

Primer set (F, forward primer; R, reverse primer)	**Purpose**
F: 5'-AATAATAAGCTTATGGGCGCGGGGGTGCTC-3' R: 5'-AATAATGGATCCCACCTTGGATTCCGAGGCGAA-3'	To PCR-amplify the β_1AR cDNA for generating the β_1AR-2xEYFP vector.
F: 5'-AATAATGGATCCGTGAGCAAGGGCGAGGAG-3' R: 5'- AATAATGAATTCCTTGTACAGCTCGTCCATGCC-3'	To PCR-amplify the first EYFP cDNA for generating the β_1AR-2xEYFP vector.
F: 5'P-aattcGCAGAGGCCGCGGCTAAGGAGGCCGCTGCGAAAGAAGCTGCAGCGAAGGAAGCTGCAGCGAAGt-3'	To generate the rigid linker cDNA for generating the

R: 5'P-ctagaCTTCGCTGCAGCTTCCTTCGCTGCAGCTTCTTTCGCAGCGGCCTCCTTAGCCGCGGCCTCTGCg-3'	β_1AR-2xEYFP vector.
F: 5'-AATAATTCTAGAGTGAGCAAGGGCGAGGAGCTG-3' R: 5'-AATAATGGGCCCTTACTTGTACAGCTCGTCCATGCC-3'	To PCR-amplify the second EYFP cDNA for generating the β_1AR-2xEYFP vector.
F: 5′- AAAGAATTCATGGAGGGGATCAGTATATACAC -3 R: 5′-AAATCTAGAGCTGGAGTGAAAACTTGAAGA-3	To PCR-amplify the CXCR4 cDNA for generating the pcDNA3-CXCR4-EYFP vector
F: 5′- CTAGCTAGCGATGAGGGGATCAGTATATA -3′ R: 5′- CCCTCGAGTTAGCTGGAGTGAAAACTTGAA -3′	To PCR-amplify the CXCR4 cDNA for generating the pcDNA3-FLAG-SNAP-CXCR4 vector
F: 5′-AAATCTAGAGTCTTCACACTCGAAGATTTCGTTGGGGAC-3 R: 5′-AAAGCGGCCGCTTACGCCAGAATGCGTTCGCACAG-3′	To PCR-amplify the nLuc cDNA for generating the pcDNA-CXCR4-nLuc vector
F: 5′-CCATGTCATCTCCACAGTCAACC-3′ R: 5′- ACTGCCTTGCATAGGAAG-3′	To generate the CXCR4 Y116S mutant
F: 5′-CTACACAGTCTCTCTCTACAGCAGTG-3′ R: 5′-ATGACATGGACTGCCTTG-3′	To generate the CXCR4 N119S mutant

F: 5′-CAAGACCACAGACATCCTCATCCTGG-3′ R: 5′-AGGGCCTTGCGCTTCTGG-3′	To genearate the CXCR4 V242D mutant
F: 5′-CATCCTCATCCCAGCTTTCTTCGCCTG-3′ R: 5′-ACTGTGGTCTTGAGGGCC-3′	To generate the CXCR4 L246P mutant

Table 3-3.List of enzymes

Enzyme	**Supplier**	**Catalog number**
ApaI	New England Biolabs	R0114S
BamHI-HF	New England Biolabs	R0136S
EcoRI-HF	New England Biolabs	R3101S
HindIII-HF	New England Biolabs	R3104S
NheI-HF	New England Biolabs	R3131S
NotI-HF	New England Biolabs	R3189S
XbaI	New England Biolabs	R0145S
XhoI	New England Biolabs	R0146S

Table 3-4. List of kits

Kit	**Supplier**	**Catalog number**
1 kb Plus DNA Ladder	New England Biolabs	N3200S
Q5 High-Fidelity PCR Kit	New England Biolabs	E0555S
Quick Ligation Kit	New England Biolabs	M2200S
Q5 Site-Directed Mutagenesis Kit	New England Biolabs	E0554S
Monarch Plasmid Miniprep Kit	New England Biolabs	T1010S

QIAquick Gel Extraction Kit	QIAGEN	28704
QIAGEN Plasmid Plus Midi Kit	QIAGEN	12945

3.2. Biological Materials

3.2.1. Bacterial Strains

Table 3-5. List of bacterial strains

Strain	**Supplier**	**Catalog number**
NEB 5-alpha Competent E. coli (High Efficiency)	New England Biolabs	C2987U

3.2.2. Cell Lines

Table 3-6. List of cell lines

Cell line	**Supplier**	**Cat. No. / Reference**
CHO-K1	ATCC	ATCC CCL-61
HEK 293AD	Biocat	AD-100-GVO-CB
HEK293 ΔGα	Dr. Asuka Inoue	
HEK293 Δarrestin	Dr. Asuka Inoue	

3.2.3. Antibodies

Table 3-7. List of antibodies

Antibody	Supplier	Catalog number
CXCR4 Antibody (44717) [Alexa Fluor 488]	Research And Diagnostic Systems, Inc.	FAB173G-025

3.3. Chemicals

3.3.1. Chemicals

Table 3-8. List of chemicals

Chemical	Supplier	Catalog number
Agar	Applichem	A0949
Agarose	Thermo Fisher Scientific	16500
Ampicillin	Sigma-Aldrich	A0166
Bovine Serum Albumin	Sigma-Aldrich	A7030
Calcium Chloride ($CaCl_2$)	Sigma-Aldrich	449709
Dimethyl Sulfoxide (DMSO)	Sigma-Aldrich	D8418
Ethanol	Sigma-Aldrich	1024282500
Ethidium Bromide	Thermo Fisher Scientific	15585011
Glucose (α-D)	Sigma-Aldrich	158968
Glycerol	Sigma-Aldrich	G5516
HEPES (4-(2-hydroxyethyl)-1-piperazineethanesulfonic acid)	Sigma-Aldrich	H3375

Isopropanol	Sigma-Aldrich	W292912
Kanamycin	Sigma-Aldrich	K1377
Magnesium Chloride ($MgCl_2$)	Sigma-Aldrich	M8266
Methanol	Sigma-Aldrich	M1775
Modified Tris-Acetate-EDTA (TAE) Buffer	Merck Millipore	LSKMTAE50
Poly-D-Lysine	Thermo Fisher Scientific	D8418
Potassium Chloride (KCl)	Sigma-Aldrich	P3911
Sodium Chloride	Sigma-Aldrich	S7653
Tryptone	Merck Millipore	T7293
Yeast Extract	Sigma-Aldrich	Y1625

3.3.2. Ligands

Table 3-9. List of ligands

Ligand	**Description**	**Supplier**	**Cat. No.**
Human CXCL11	CXCR7 agonist	Peprotech	300-46
Human CXCL12	CXCR4 and CXCR7 agonist	Peprotech	300-28A
AMD3100	CXCR4 antagonist	Sigma-Aldrich	239820
AMD3465	CXCR4 antagonist	Tocris	4179
TC14012	CXCR4 inverse agonist	Tocris	4300
LY2510924	CXCR4 inverse agonist	MedChemExpress	HY-12488
IT1t	CXCR4 inverse agonist	Tocris	4596
FC131	CXCR4 inverse agonist	Tocris	4320

3.3.3. Fluorescent Dyes

Table 3-10. List of organic fluorescent dyes

Dye	Supplier	Catalog number
HaloTag NanoBRET 618 Ligand	Promega	G9801
Rhodamine 6G	Sigma-Aldrich	83697
SNAP-Surface Alexa Fluor 488	New England Biolabs	S9124S
SNAP-Surface 549	New England Biolabs	S9124S

3.4. Consumable Materials

Table 3-11. List of consumable materials

Material	Supplier	Catalog number
96-well plate	Sarstedt AG	83.3924.005
6-well plate	Sarstedt AG	83.3920.005
35 mm dish	Sarstedt AG	83.3900
60 mm dish	Sarstedt AG	83.3901
100 mm dish	Sarstedt AG	83.3902
T75 flask	Sarstedt AG	83.3911
96-well plate, black	Brand GmbH	781668
96-well plate, white	Brand GmbH	781665
Cryogenic tubes	Thermo Fisher Scientific	375418
0.2 mL PCR tubes	Eppendorf	0030124359
0.5 mL microcentrifuge tube	Eppendorf	0030121023
1.5 mL microcentrifuge tube	Eppendorf	0030120086
2 mL microcentrifuge tube	Eppendorf	0030120094

5 mL microcentrifuge tube	Eppendorf	0030119401
Protein LoBind Tubes	Eppendorf	0030108116
15 mL centrifuge tube	Corning	352096
50 mL centrifuge tube	Corning	352070
Attofluor cell chamber	Thermo Fisher Scientific	A7816
Glass cover slips	Hartenstein	???
0.22 µm syringe filters		

3.5. Media, Buffers and Solutions

3.5.1. Cell Culture Media and Solutions

Table 3-12. List of cell culture media and solutions

Medium	**Supplier**	**Catalog number**
DMEM/F12	Thermo Fisher Scientific	21041033
Dulbecco Modified Eagle's Medium (DMEM)	PAN Biotech	P04-03500
Dulbecco's Phosphate-Buffered Saline (DPBS)	Gibco	14040174
Fetal Bovine Serum	Biochrom AG	S0115
Fluorobrite DMEM	Thermo Fisher Scientific	A1896701
Hank's Buffered Saline Solution (HBSS)	Thermo Fisher Scientific	14025092
L-Glutamine	PAN Biotech	P04-80050
Opti-MEM Reduced Serum Medium	Gibco	11058021
Penicillin/Streptomycin	PAN Biotech	P06-07050
Trypsin/EDTA	PAN Biotech	P10-020100

3.5.2. Bacterial Growth Media

Table 3-13. List of bacterial growth media

Media	**Formulation**
Luria Bertani (LB) Medium	25 g NaCl 50 g Tryptone 25 g Yeast Extract Distilled water up to 1 L, autoclaved
LB Agar Medium	15 g Agar LB Medium up to 1 L, heated

3.5.3. Immunofluorescence Media

Table 3-14. List of immunofluorescence media

Medium	**Formulation**
Medium for Labeling with Antibody	2.5 g BSA 55.5 mg $CaCl_2$ 2.2 g Glucose 2.4 g HEPES 7.5 g KCl 47.6 mg $MgCl_2$ 3.1 g NaCl Distilled Water up to 1L, autoclaved

3.6. Assay Kits

Table 3-15. List of assay kits

Kit	Supplier	Catalog number
MycoAlert Mycoplasma Detection Kit	Lonza	LT07-318
NanoBRET PPI Starter System Flexi	Promega	N1821
NanoBRET Nano-Glo Detection System Standard	Promega	N1661
Effectene Transfection Reagent	QIAGEN	301427
Lipofectamine 2000 Transfection Reagent	Thermo Fisher Scientific	11668019

3.7. Key Devices

Table 3-16. List of key devices

Device	Supplier	Catalog number
Plate reader	Biotek	
Fluorescence/FRET microscopy setup	Visitron	
Perfusion System OctaFlow II	ALA Scientific	
TIRF microscopy setup	Nikon Instruments	

3.8. Software and Databases

Table 3-17. List of software's and databases

Software	**Supplier**
CorelDraw Graphics Suite	Corel
Gen5	Biotek
ImageJ	National Institute of Health
Matlab 2019	Mathworks
OriginPro 2017	OriginLab
SnapGene	GSL Biotech LLC
VisiView	Visitron

4. METHODS

4.1. Molecular Biology Methods

4.1.1. Primer Design and PCR

4.1.1.1. Primer Design

All primers used for PCR-amplification of the DNA were designed *in silico* using the SnapGene software. In case of cloning with restriction digestion, a restriction enzyme recognition sequence followed by a triple Adenine (A) nucleobase sequence was inserted to the 5' end of each forward and reverse primer. Primers for site-directed mutagenesis were designed using the NEBaseChanger tool (http://nebasechanger.neb.com/). All primer oligonucleotides were synthesized by Biotez. Primers were dissolved in double distilled water (ddH_2O) to a stock concentration of 100 µM.

4.1.1.2. Polymerase Chain Reaction

Standard PCR experiments were performed to amplify DNA fragments of interest, with the purpose of cloning them into a new vector plasmid by restriction digestion followed by ligation. Briefly, PCR mixtures were prepared in 0.2 mL tubes on ice according to the Table 4-1. Reaction mixtures were mixed thoroughly by pipetting, spun down and placed into the thermal cycler block.

Table 4-1. Q5 polymerase PCR mixture

Reagent	**Volume**	**Final concentration**
5X Q5 Reaction Buffer	10 µL	1X

10 mM dNTPs	1 µL	200 µM
10 µM Forward Primer	2.5 µL	0.5 µM
10 µM Reverse Primer	2.5 µL	0.5 µM
Template DNA	1 µL	< 20 ng/µL
Q5 High-Fidelity DNA Polymerase	0.5 µL	0.02 U/µL
ddH_2O	To 50 µL	

Thermocycling was performed according to the protocol given in Table 4-2. Primer annealing temperature is a unique feature of each primer pair, and should be optimized depending on the melting temperature of each primer. It is also important that the difference in melting temperatures of the forward and reverse primers within a pair should not exceed 2-3°C.

Table 4-2. Thermocycling protocol using the Q5 High-Fidelity DNA Polymerase

Step	**Temperature**	**Time**
Initial denaturation	98°C	30 seconds
Denaturation Primer annealing Elongation (35 cycles)	98°C 50-72°C 72°C	10 seconds 20 seconds 30 seconds/kb
Final elongation	72°C	2 minutes
Hold	4°C	∞

Site-directed mutagenesis reactions were performed in order to introduce single/multiple mutations, deletions or insertions in the gene of interest. The method used by the Q5® Site-Directed Mutagenesis Kit includes a PCR-based amplification of the target vector using the mutation-inducing primers, circularization and ligation of the amplified single-strand mutant DNA, and DpnI-mediated digestion of the template vector. For the PCR step, mixtures were prepared according to Table 4-3, mixtures were spun down and the thermocycling reaction was performed according to the protocol given in Table 4-4.

Table 4-3. Q5® Site-Directed Mutagenesis Kit PCR mixture

Reagent	**Volume**	**Final concentration**
Q5 Hot Start High-Fidelity 2X Master Mix	12.5 µL	1X
10 µM Forward Primer	1.25 µL	0.5 µM
10 µM Reverse Primer	1.25 µL	0.5 µM
Template DNA	1 µL	10 ng/µL
ddH_2O	9 µL	

For the thermocycling step, primer annealing temperature calculated by the NE-BaseChanger tool should be used.

Table 4-4. Thermocycling protocol using the Q5 Site-Directed Mutagenesis Kit

Step	**Temperature**	**Time**
Initial denaturation	98°C	30 seconds
Denaturation Primer annealing Elongation (25 cycles)	98°C 50-72°C 72°C	10 seconds 20 seconds 30 seconds/kb
Final elongation	72°C	2 minutes
Hold	4°C	∞

After the PCR step, the amplified DNA was subjected to the Kinase-Ligase-DpnI (KLD) reaction by incubating the mixture given in Table 4-5 for 10 minutes at the room temperature.

Table 4-5. Kinase-Ligase-DpnI (KLD) reaction mixture

Reagent	**Volume**	**Final concentration**
PCR Product	0.5 µL	
2X KLD Reaction Buffer	2.5 µL	1X
10X KLD Enzyme Mix	0.5 µL	1X
ddH_2O	1.5 µL	

4.1.2. Restriction Enzyme Digestion

For the cloning path with restriction enzyme digestion, PCR products were subjected to two restriction enzymes, in order to generate PCR products and target vector plasmids with compatible 5' and 3' ends. The reaction mixture was prepared according to Table 4-6, was spun down and incubated at 37°C for 1 hour. Only the ApaI enzyme was used in 2X concentration.

Table 4-6. Restriction enzyme digestion mixture

Reagent	**Volume**	**Final concentration**
PCR Product/ Vector		1 µg
Restriction enzyme 1	1 µL	20 units
Restriction enzyme 2	1 µL	20 units
10X CutSmart Buffer	5 µL	1X
ddH_2O	to 50 µL	

4.1.3. Agarose Gel Electrophoresis

Agarose gel electrophoresis was performed to isolate the digested vector and the PCR product from the reaction mixture. To prepare the agarose gel, 0.75 g agarose powder was mixed in 100 mL 1X TAE buffer (prepared in ddH_2O). The mixture was heated until the agarose was completely dissolved. Then, the mixture was cooled down and 10 µL ethidium bromide was added and mixed. The solution was cast into an agarose gel tray with a gel comb to form the sample wells. After polymerization, the gel was taken into an electrophoresis tank filled with 1X TAE buffer. Samples were mixed with loading dye to a final dye concentration of 1X, and then they were loaded in the agarose gel wells along with the 1kB DNA ladder. The electrophoresis was performed at constant 120V for 45 minutes.

4.1.4. Extraction of DNA from Agarose Gel

After the electrophoresis, the gel was placed under a UV light box, wearing a plastic face protection. The fluorescent DNA bands corresponding to the digested vector backbone and the gene were cut out by using a scalpel. The excised agarose piece was taken into a 1.5 µL microcentrifuge tube, and then weighed. DNA extraction from this gel was performed using the QIAquick Gel Extraction Kit according to the manufacturer's instruction.

4.1.5. Ligation of DNA

Ligation reaction was performed using the T4 DNA Ligase kit. To do so, the digested, compatible PCR product and the vector backbone were mixed in different molar ratios (from 1:1 to 1:7 ratio of vector:insert), reaction mixture was prepared according to Table 4-7 (as an example, 1:3 ratio of vector:insert is given), and the mixture was incubated at room temperature for 1 hour.

Table 4-7. DNA Ligation reaction mixture

Reagent	**Volume**	**Final concentration**
T4 DNA Ligase Buffer	2 µL	1X
Vector DNA (6 kb)		2.5 ng/µL
Insert DNA (1kb)		1.25 ng/µL
T4 DNA Ligase	1 µL	400 units

4.1.6. Bacterial Transformation

NEB 5-alpha Competent *E. coli* were transformed with the constructs generated *in vitro* by the mutagenesis or the ligation reaction. Thawed competent cells were mixed with 10 µL of the mutagenesis or ligation mixture, and the suspension was incubated on ice for 20 minutes. Next, the mixture was placed into a 42°C heat block for 45 seconds, and then placed back on ice for a 2 minute incubation. Then, 950 µL LB medium was added, and the mixture was incubated at 37°C for 1 hour. 50µL of this mixture was added and spread onto a LB agar plate containing the appropriate antibiotic, and the plate was incubated at 37°C overnight.

4.1.7. Preparation of Plasmid DNA from E. coli

Bacteria colonies containing the transformed DNA were picked up from the LB agar plate using a pipette tip, and placed into bacterial culture tubes containing 5 mL (for miniprep) or 50 mL(for midi prep) LB medium supplemented with appropriate antibiotic. The mixture was incubated with shaking at 400 rpm at 37°C overnight. Plasmid isolation from these cultures were performed using the Monarch Plasmid Miniprep Kit or the QIAGEN Plasmid Plus Midi Kit according to the manufacturers' instructions. Plasmid concentrations and quality were assessed using a microvolume spectrophotometer by measuring the

sample absorbance at light wavelengths of 260 and 280 nm. Plasmid sequences were verified by performing a Sanger sequencing through LGC Genomics.

4.2. Cell Culture Methods

4.2.1. Growth and Maintenance of Cell Lines

HEK293AD cells were cultured in DMEM supplemented with 10% (vol/vol) fetal bovine serum (FBS), 1% L-glutamine, penicillin (100 U/mL), and streptomycin (100 µg/mL) in a sterile incubator at 37 °C and 5% CO_2. CHO-K1 cells were cultured in phenol red-free DMEM/F12 medium supplemented with 10% FBS, 1% L-glutamine, 100 U/mL penicillin, and 100 µg/mL streptomycin in a sterile incubator at 37 °C and 5% CO_2.

In order to start culturing cryopreserved cells, tubes containing cells were taken from liquid nitrogen and the cells were quickly thawed in a water bath at 37°C for 2 minutes. Thawed cell suspension was taken into a 15 mL centrifuge tube and supplemented with 10 mL pre-warmed cell culture medium in a sterile laminar flow hood. Cell suspension was centrifuged at 900 rpm for 3 minutes at room temperature. Supernatant was discarded using a sterile glass Pasteur pipette connected to a suction pump. Pelleted cells were resuspended in fresh cell culture medium. Cell counting was performed using an automated cell counter by loading a 1:1 mixture of cell suspension:methylene blue to a cell counting slide.

For maintenance, firstly the medium in T75 flasks with cells was removed. Cells were then washed with 2 mL PBS, and treated with 2 mL trypsin/EDTA solution for 30 seconds. After removing the trypsin/EDTA, cells were detached by tapping the flask a few times. Then, cells were resuspended in 10 mL cell culture medium. Two million cells were resuspended in a total volume of cell culture medium in a T75 cell culture flask, which was maintained in a sterile incubator at 37 °C and 5% CO_2 and passaged every 2 to 3 days.

4.3. Live Cell Microscopy Methods

4.3.1. Transfection of Cells for Fluorescence Microscopy

For single-cell analysis using fluorescence, FRET, confocal and TIRF microscopy, cells were prepared at a density of 250,000 cells/well in 6-well plates containing 24 mm (Ø) round glass coverslips. Sixteen hours later, cells were transfected. HEK 293AD cells were transfected using Effectene Transfection Reagent. Briefly, 0.5µg plasmid DNA was mixed with 55 µL EC Buffer and 4 µL Enhancer. After 3 minutes incubation at room temperature, 6 µL Effectene was added to the mixture and further incubated for 7 minutes, and then the mixture was added drop-wise into one well, mixed by gently shaking the plate. CHO-K1 cells were transfected using the Lipofectamine 2000 Transfection Reagent according to the manufacturer's instructions. Briefly, in one 2 mL microcentrifuge tube, 2 µg plasmid DNA and 0.5 mL OptiMEM medium were added. In another tube, 6 µL Lipofectamine Transfection Reagent and 0.5 mL OptiMEM medium were added. After incubating for 5 minutes, both solutions were combined and the final mixture was further incubated for 20 minutes. During this incubation, cell culture medium in 6-well plates with cells was replaced with the antibiotic-free DMEM/F12 supplemented with FBS and L-Glutamine. After incubating the cells for 20 minutes, transfection mixture was added to one well. Four to five hours after transfection, the transfection medium was replaced with the antibiotic-free DMEM/F12 medium. For fluorescence, FRET and confocal microscopy imaging, cells were transfected for 16 to 48 hours. For TIRF experiments, cells were transfected for 4 to 6 hours.

4.3.2. SNAP and HaloTag Labeling of Cells

For SNAP tag labeling, dye stocks were prepared using DMSO at a final concentration of 1 mM. Stocks were preserved at -20°C. After appropriate time of transfection, the medium was removed from the 6-well plates and cells on coverslips were rinsed three times using pre-warmed PBS solution. Then, cells were supplemented with 1 mL cell culture medium containing 1 µM SNAP-Surface labeling reagent, or 1 µM HaloTag ligand.

After incubating for 20 minutes, labeling medium was removed, and cells were incubated with PBS for 3 times, each for 5 minutes in a cell culture incubator at 37 °C and 5% CO_2.

4.3.3. Single Color Fluorescence and FRET Microscopy

In order to perform time-course imaging of cpGFP-based sensors, FRET-based biosensors or FRET measurements of two proteins with fluorescent tags in intact single-cells a fluorescence microscope was used.

4.3.3.1. Microscope Setup

The microscope is a semi-customized commercially-available setup from Visitron, Germany. It contains a Leica DMi8 microscope body with inverted objectives. Illumination unit contains a 75 Watt Xenon lamp and a VisiChrome polychromator that is connected to the microscope body where the excitation filter turret is located. Signal is detected by a Prime 95B scientific complementary metal-oxide semiconductor (sCMOS) camera that is connected to the microscope body with an OptoSplit II emission beam splitter. The beam splitter is used for simultaneous two-color (i. e. FRET) imaging (Figure 4-1). This unit contains a filter cube that allows in the light between certain emission wavelengths defined by the first filter. The allowed light is further filtered through a dichroic mirror inside: while the light within a certain wavelength window is allowed through to one half of the camera chip, another is reflected. The reflected light at higher wavelength is then filtered through another emission filter, and beamed to the other half of the camera chip. This way the same camera can detect light with different wavelength windows at distinct parts of the camera chip. The filer sets used in this study are given in the section 4.3.3.3.

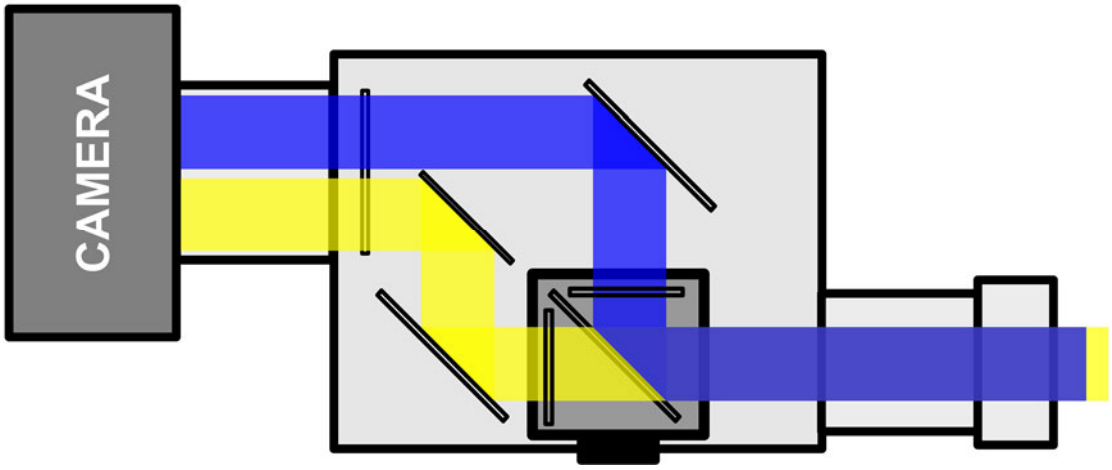

Figure 4-1. Schematic view of the OptoSplit II that is used for dual-color widefield fluorescence imaging. The beam with mixed wavelengths enters the filter cube (inner box in dark grey) and hits the dichroic mirror, which reflects the wavelengths lower than a certain threshold (blue) and allows the higher wavelengths (yellow). Both filtered beams pass through allows the light within a defined wavelength window. Filtered emission beams are then reflected via full mirrors to the top and bottom halves of the camera chip.

4.3.3.2. Perfusion Setup and Application

The fluorescence microscope setup is complemented with an external liquid handling unit (OctaFlow II, ALA Scientific, USA) that allows ultra-fast drug application during time-course imaging of living cells. The setup is connected to a computer with a USB interface that allows the digital control of valves. The liquid handling unit contains a board with air-pressurized sample reservoirs, each of which is connected to a pinch valve and a microdiameter tubing. These tubings are then connected to a micromanifold where all channels are clustered to a single opening. The micromanifold opening is then connected to an output tube of 100 µm diameter that can be placed closely to the cell that is to be imaged, in order to allow direct drug application. Solution switching speed of OctaFlow is in the range of hundreds of microseconds.

In order to use the perfusion setup, the first step is to load the reservoirs with a 5 mL volume of the drug solution. Then, the first 1 mL is run through the system to assure

that the drug has reached to the tip of the output, which will ensure ultrafast exchange from buffer to drug.

4.3.3.3. Image Acquisition

After 16 to 24 hours of transfection and then labeling in case of experiments with SNAP and HaloTag, glass coverslips containing cells were taken into an imaging chamber and supplemented with HBSS. The chamber with coverslip was placed on the microscope, with a drop of immersion oil between the objective and the coverslip. Image acquisition was performed using the VisiView software.

For cpGFP biosensor imaging, only the single-color imaging settings were used. The cells were illuminated at 450-490 nm and emission was detected between 500-550 nm. For CFP/YFP FRET imaging, cells were illuminated at 430-440 nm and CFP was detected between 450-480 nm, while FRET was detected between 520-560 nm. For kinetic experiments, constant illumination was applied. Signal was collected with 10 millisecond intervals for kinetic measurements.

After detecting a cell with appropriate fluorescence signal, the perfusion tip was aligned very closely to the cell. Cells were subjected to a continuous buffer superfusion at the beginning of the imaging. During the imaging, buffer was switched with drug superfusion for different durations, and then the drug was washed out with buffer superfusion until the signal reached the baseline value. Time points at which buffer and drug solutions were exchanged were stamped during imaging via the imaging software (VisiView, Visitron, Germany).

4.3.3.4. Image Correction

All acquired image series were corrected to background signal using the ImageJ software. Background fluorescence intensity was detected by selecting a cell/fluorescence-

free region in the image and the mean value was subtracted from the intensity value of each pixel within the image. Same procedure was applied to each image within an image series.

CFP/YFP FRET images were additionally corrected to donor bleed through to the acceptor channel, and direct excitation of the acceptor. Bleed through is the direct donor emission that is detected in the acceptor channel, which occurs due to spectral spillover of the donor emission in the acceptor channel. On the other hand, direct excitation of YFP occurs because of the beginning of the YFP excitation spectra at the 430-440 nm. To calculate the donor bleed through, cells expressing only CFP was imaged using the FRET imaging settings. After background correction, bleed through factor (BTF) was calculated by dividing the YFP intensity ($F_{YFP(435,540)}$) by the CFP intensity ($F_{CFP(435,465)}$). Direct excitation was measured by imaging cells expressing only YFP. YFP emission at 490-510 nm excitation ($F_{YFP(500,540)}$) was divided by the YFP emission 430-440 nm ($F_{YFP(435,540)}$) to calculate the direct emission factor (DEF).

In FRET image series, after background correction, the corrected YFP signal was calculated using the formula:

$$F_{YFP(corr)} = F_{YFP(435,540)} - BTF \times F_{CFP(435,465)} - DEF \times F_{YFP(500,540)}$$

Final FRET ratio for each image within an image series was calculated by dividing $F_{YFP(corr)}$ by F_{CFP}.

In time-lapse fluorescence imaging, exposure to the excitation light causes irreversible damage of fluorophores that causes an exponential decay of the fluorescence intensity over time. This exponential decay is reflected likewise in the FRET signal. In order to accurately calculate the onset and offset kinetics of fluorescence intensity and FRET changes over time, this photobleaching effect should be corrected. To do this correction,

firstly an exponential decay function was fit on the manually-selected baseline fluorescence/FRET signal, and then the calculated fit was subtracted from the trace, using Origin Pro 2017 software.

4.3.3.5. Onset and Offset Kinetics Calculation

In order to calculate the kinetics of fluorescence/FRET changes upon drug application/removal, Origin Pro 2017 software was used. Firstly, corrected intensity/FRET values were plotted over time. In order to calculate the kinetics of any change in the signal, a mono-exponential function was fit from the data point where the change in signal started, until the data point where the signal exhibited a linear behavior. After applying this calculation on several measurements, obtained tau (τ) values were plotted as a scatter dot plot using the GraphPad Prism 7 software.

4.3.4. Confocal Microscopy

Confocal microscopy was used for imaging the samples prepared for immunofluorescence and spatial and temporal brightness experiments. The setup that was used is a commercial Leica SP8 laser-scanning confocal microscope equipped with two photon-counting and two analog (with photomultiplier tube) multiwavelength detectors, scanning head, white light laser (WLL), 405 nm diode laser and multiple objectives.

4.3.4.1. Immunofluorescence

HEK293AD or CHO-K1 cells were seeded on glass cover slips in 6-well plates, and the next day they were transfected with pcDNA3 or 3xHA-CXCR4-ECFP or β_1AR-ECFP construct as given in the section 4.3.1. Next day, cells were washed 3 times with pre-warmed PBS, and then were supplemented with 1% BSA in FluoroBrite medium, and were incubated at 37 °C and 5% CO_2. One hour after incubation, the medium was replaced with the immunofluorescence medium supplemented with 20 μg/mL CXCR4 Alexa Fluor

488-conjugated antibody, and then further incubated for 1 hour at 37 °C and 5% CO_2. Next, the antibody-containing medium was discarded, cells were washed 3 times with PBS, and then were incubated with the immunofluorescence medium for 10 minutes. This step was repeated 3 times and after each step the medium was refreshed. After the last incubation, a coverslip containing labeled cells was placed into a cell chamber and supplemented with immunofluorescence buffer. The chamber was carefully placed on the microscope stage right above the 40X/1.3 NA objective with a drop of immersion oil. For ECFP excitation, a 405 nm diode laser was used at 10% power, and ECFP emission was detected between 430-490 nm using the first hybrid detector in photon counting mode. For Alexa Fluor 488 excitation, WLL was set to 492 nm laser line at 10% final power output. Alexa Fluor 488 emission was detected between 500-650 nm using the second hybrid detector in photon counting mode. Line sequential imaging option was used, in order to prevent the spillover of the ECFP signal into the Alexa Fluor 488 channel. Image size was 512×512 pixels, zoom factor was 11.37, pixel size was 50 nm, and pixel dwell time was 4.88 µs.

4.3.4.2. FRET Acceptor Photobleaching

To perform FRET acceptor photobleaching (FRET AB), HEK293AD cells were seeded on glass cover slips in 6-well plates, and the next day they were transfected with two GPCR constructs, one with ECFP at the C terminus, and the other with EYFP. 16 to 24 hours after transfection, cells were taken to a cell chamber and supplemented with HBSS, or HBSS with a drug at certain concentration. For imaging the FRET AB module of the Leica SP8 confocal microscope was used. FRET AB imaging was performed on the basal membranes of the cells expressing ECFP and EYFP-tagged receptors. .A pre-bleaching snapshot of donor and acceptor channels were sequentially acquired at 700 Hz scanner rate with 1% 405 nm laser output and 1% output of 514 nm line of the WLL. Detection was performed using the PMT detectors at 700 V gain. ECFP was detected between 450-490 nm and EYFP was detected between 520-600 nm. Next, photobleaching of the acceptor was performed by acquiring 10 frames of the whole imaging field using the 514 nm line of the WLL at 50% output. After photobleaching, post-bleaching images of the donor and acceptor were acquired using the same settings as in the pre-bleaching imaging. Image size was 512×512, pixel size was 50 nm. To calculate the FRET efficiency, a region of

interest (ROI) was selected by hand, avoiding the heterogeneous, high-intensity areas such as clusters, membrane ruffles etc. FRET efficiency was calculated according to the following formula, where $I_{ECFP(pre)}$ is the intensity of ECFP before acceptor photobleaching, and $I_{ECFP(post)}$ the intensity of ECFP after acceptor photobleaching within the ROI:

$$\%FRET = \frac{I_{ECFP(post)} - I_{ECFP(pre)}}{I_{ECFP(pre)}}$$

4.3.4.3. Spatial and Temporal Brightness Imaging

For spatial and temporal brightness imaging, cells were seeded on glass cover slips in 6-well plates, and the next day they were transfected with constructs carrying a SNAP- or EYFP-tagged GPCR gene according to the section 4.3.1. 16 to 24 hours after transfection, cells were washed with pre-warmed PBS, were mounted on a cell chamber and supplemented with HBSS. Then, the cell chamber was placed on the microscope stage, over the 40X/1.3 NA objective with a drop of immersion oil. For SNAP Surface Alexa Fluor 488-labeled cells, the 488 nm line of the WLL was used at 10% power for excitation. For EYFP, 514 nm laser line was used at 10% output. While searching cells, laser power for either wavelength line was used at 0.3% to minimize photobleaching, the scan frequency was increased to 700 Hz and the zoom factor was set to minimum to allow a more rapid cell search. Using the z-axis scanning module, the bottom membrane (membrane area that contacts the coverslip) of the cells were assessed. Only the cells that exhibited a homogenous morphology at this area were imaged. Once a suitable cell was found, the zoom factor was set to achieve 50 nm pixel size, the cell was centered in the imaging field, and then the acquisition was stopped. Next, the following settings were applied and image acquisition was started: For spatial brightness imaging, laser output was 10%, image size was 512×512 pixels, zoom factor was 11.37, and pixel dwell time was 4.88 µs. For regular brightness analysis, only one frame was acquired. For experiments with photobleaching, a series of 10 consecutive frames were acquired. For temporal brightness imaging, laser output was 0.75%, image size was 256×256 pixels, zoom factor was 22.8, and pixel dwell time was 2.43 µs. For both imaging approaches, emission was detected using the hybrid

detectors in photon counting mode, between 520-600 nm for EYFP and 500-650 nm for SNAP Surface Alexa Fluor 488. For each cell, 100 consecutive frames were acquired. During acquisition, autofocus was set to a well-focused lane on the z-axis, in order to prevent the defocusing of the sample during imaging.

4.3.4.4. Spatial and Temporal Brightness Analysis

Spatial image analysis was performed using a custom-written analysis routine in Matlab and Igor (can be found at Işbilir et al., 2021). First, a single frame image was opened in Matlab or Igor. A polygonal region of interest (ROI) was marked by hand, avoiding the inhomogeneities that are obvious to the eye. After masking the selected ROI, the analysis code was run to calculate the number and the brightness values.

Temporal brightness analysis was performed manually using the ImageJ software. First, an image stack was opened in ImageJ and the image type was set to 32-bit. Intensity profile was plotted over frame number to assess the photobleaching level. If photobleaching was less than 70%, then a detrending routine was applied without any thresholding using the Detrendr plugin on ImageJ. Average fluorescence across the image stack was always checked after "detrending". Detrending is applied on the image series to normalize the photobleaching-induced decrease in fluorescence. Image series that display is 30% or more photobleaching were not used in the analysis. Using the photobleaching-corrected image stack, average intensity and standard deviation images were generated. The variance image was then generated by calculating the square root of the standard deviation image. Also, a squared mean intensity image was generated. Then, using the image calculator on ImageJ, a brightness image was generated by dividing the variance image by the average intensity image. The "number of molecules" image was generated by dividing the squared mean intensity image by the variance image. To calculate the average number and brightness, aligned ROIs on both number and brightness images were selected and mean pixel values were calculated.

4.3.5. TIRF Microscopy

4.3.5.1. TIRF Microscope Setup

To image fluorescently-labeled receptors at single molecule resolution, TIRF microscopy approaches were used. The commercial, modified microscopy setup used here is equipped with a 100X/1.49 NA TIRF objective with automated correction collar, a laser box with 405 nm: 20 mW, 488 nm: 45 mW, 561 nm: 45 mW, 647 nm: 40 mW diode laser lines connected to a single fiber output to the N-STORM module, and 4 electron multiplying charge-coupled devices (EMCCD). EMCCDs were connected to the microscope body via a camera splitter equipped with dichroic mirrors for detection of certain wavelength windows at each camera.

4.3.5.2. TIRF Microscopy Imaging

CHO-K1 cells were seeded on clean cover slips in 6-well plates and transfected 24 hours after seeding with plasmids containing N-terminally SNAP-tagged GPCR DNA. Four to six hours after transfection, transfection medium was removed, cells were washed with pre-warmed PBS, and supplemented with cell culture buffer containing 1 μM SNAP Surface 549 dye. After incubating the cells for 20 minutes at 37 °C and 5% CO_2, the labeling medium was removed, cells were washed 3 times with DPBS, and then they were incubated with cell culture medium for 5 minutes to remove excess and non-specifically bound dye. This incubation was repeated 2 more times with fresh medium. After the last incubation, the medium was removed, cells were rinsed with PBS, the cover slip was taken to an imaging chamber and it was supplemented with HBSS. Using a low laser power, the focus was set, and the focus position was fixed on the software for continuous autofocus. Imaging was performed at different time intervals ranging from 10 to 50 ms, and 400 to 800 frames were acquired. Image size was 512×512, pixel size was 106 nm.

4.3.5.3. Single Molecule Intensity Analysis

In order to quantify receptor oligomerization via single molecule imaging, first frames of the TIRF movies acquired with 40 ms and 50 ms integration time were used, as these images provided the sufficient signal-to-noise ratio for robust quantification of single fluorescent particle intensities. Analysis was performed using the u-track software, which detects single particles and calculates their mean intensities. After obtaining the intensity values of each particle from the first or the last frame of the image series, their frequency distribution was plotted. By fitting multiple Gaussian distributions with experimentally-defined center of mass and standard deviation, proportions of different oligomeric states were obtained by calculating the area under each mono-Gaussian.

4.3.5.4. Single Molecule Tracking Analysis

Single molecule tracking was performed in order to calculate the kinetics of single molecule interactions. For this analysis, TIRF movies acquired with 10 ms to 40 ms were used. The u-track software was used for detecting single particles at each frame of the movie, and corresponding particle trajectories for each single molecule were assigned. This software can also assign particles association and dissociation in terms of track merging and splitting. Using a second software, named Polytracker, the length of the tracks from the moment two particles merged until they split were calculated. Polytracker uses the tracking information from u-track to retrieve track merging and splitting information. It calculates the number of frames starting from the frame where two individual tracks merge until they split. By manually entering the frame rate in the script, it calculates the “lifetime” of each dimer track. The frequency of lifetimes with a bin size of 50 ms was then plotted, and a bi-exponential curve was fit to this in order to calculate the τ value of the dimerization lifetime. The τ of the fast monoexponential phase of this function was fixed to 112 ms, which is the τ value obtained by fitting the dimer lifetimes of simulated single molecule particles that exhibit a mixed diffusion behavior. From this constrained bi-exponential fit, the slow phase of the fit revealed the τ of the true dimer lifetimes of the measured receptor.

4.4. Plate Reader-Based FRET and BRET Analysis

4.4.1. Plate Reader Setup

In order to assess the drug concentration-response relationship of biological pathways using FRET or BRET, a multi-well plate reader was used. This commercial Biotek Neo2 plate reader is equipped with a Xenon lamp and a monochromator to facilitate fluorophore excitation with a defined wavelength. Emission light is filtered through monochromators and detected via photomultiplier tubes (PMT) with adjustable voltage gain. Excitation and emission can also be controlled using filter blocks equipped with dichroic mirrors that can filter appropriate light wavelengths and direct them to separate PMT detectors. For BRET measurements, no external excitation light is used, since it is produced by an enzymatic reaction via the nanoluciferase enzyme and its substrate furimazine. For CFP/YFP FRET, an excitation filter cube with 420/50 nm bandpass filter was used. The emission filter had two filters: 485/20 nm bandpass for donor (CFP) and 540/25 nm bandpass for acceptor (YFP). For nanoBRET, a full pass-through excitation filter cube was used. For nanoBRET emission (BRET between nanoluciferase and HaloTag 618 dye) an emission filter cube with the following filters was used: 450/50 nm bandpass for donor (nanoluciferase) emission and 610 nm longpass filter for acceptor (HaloTag 618) emission.

4.4.2. Preparation of Cells for the Multiwell Plate Measurements

Two million HEK293AD cells were seeded in 10 cm cell culture plates and were transfected with plasmids containing the appropriate FRET or BRET pair. Twenty-four hours after transfection, cells were resuspended in cell culture medium and 50,000 to 100,000 cells were seeded into each well of a 96-well plate. If a NanoBRET assay was to be performed, cell suspension was supplemented with HaloTag 618 dye with a final concentration of 1 µM. After seeding to the 96-well plate, cells were incubated for 24 hours at 37°C and 5% CO_2. For plate reader measurements, cell medium was discarded and cells were washed using HBSS, supplemented with 90 µL pre-warmed HBSS and incubated at 37°C and 5% CO_2 for 10 minutes. If a NanoBRET assay was to be performed, HBSS was

supplemented with furimazine solution (1:1,000 vol/vol). Next, measurement was performed by placing the 96-well plate in the reader and applying an appropriate, pre-set assay protocol. All measurements were performed at 37°C. Detector distance from the plate was set to 4.5 mm. For FRET, measurements per data point per well was set to 20, and lamp energy was set to high. For BRET, residence time of the detector on each well was set to 0.3 seconds. For FRET, donor and acceptor PMT gain were both set to 100. For BRET, donor PMT was set to 90 and acceptor PMT was set to 120.

To assess drug response, firstly a basal measurement with no drug was performed. For this, each well was measured 4 times. Then, each column (8 wells) of the plate was supplemented with different concentrations of the drug (in total 11 concentrations and vehicle). An automatic, 5-second bidirectional shake was applied to allow uniform distribution of the applied drug. For G protein activation FRET assays, a 5-minute measurement was performed post-drug application. For BRET-based β-arrestin recruitment and internalization assays, this measurement was performed for 45 minutes after drug addition.

4.4.3. Plate Reader Data Analysis

After the measurement was done, an Excel file containing the whole assay data was extracted. To calculate a drug-induced change of FRET or BRET, the mean basal and post-stimulus response were calculated by averaging the basal and post-stimulus signal from different time points. Data points at the linear saturation were used for averaging in case of post-stimulus response. Next, the net signal change (%Δ Response) was calculated using the formula below:

$$\%\ \ Response = \left(\frac{Response_{post} - Response_{basal}}{Response_{basal}}\right) \times 100$$

Where $Response_{post}$ is the average BRET or FRET ratio after ligand stimulus, and $Response_{pre}$ is the average FRET or FRET ratio observed at the basal state. Calculated %Δ

Response values were plotted against corresponding logarithmic drug concentration value in Molar unit, and a Hill equation was fit on the data to calculate the EC50 and Emax values.

5. RESULTS

5.1. TIRFM-Based Assessment of CXCR4 Oligomerization

CXCR4 is expressed in diverse tissues and cell types, and the expression levels of CXCR4 varies greatly from one cell type to another. Due to this, one of the first aspects to consider before assessing oligomerization is the expression level of a receptor of interest. A robust technique to precisely quantify membrane protein oligomerization at very low expression levels is the TIRFM based single particle analysis. At expression levels below 0.5 particle per micron square (μm^2) membrane area, this method provides sufficient resolution to observe single receptor protomers labeled with a fluorophore. To investigate CXCR4 oligomerization using single molecule analysis, an N-terminally SNAP-tag incorporated CXCR4 construct was cloned and used. This protein tag was expressed in cells and covalently labeled with a selection of organic dyes to facilitate live cell TIRFM imaging.

5.1.1. Single Particle Intensity Analysis

As the first method of choice, single particle intensity analysis was employed to quantify oligomerization. For this, intact CHO-K1 cells expressing SNAP-tagged receptors were imaged after labeling with SNAP Surface 549 dye (Figure 5-1A). This analysis makes use of single-frame TIRF images (Figure 5-1C), from which the single particles are detected, and then their intensities are calculated (Figure 5-1D). Due to the resolution limit, each receptor, which in reality has a diameter of 10 nm, appears as a sphere with a diameter of approximately ~550 nm diameter, which is defined by the point spread function (PSF). Therefore, when two particles physically interact, in the imaging field they appear as one single PSF that present the intensity value corresponding to the sum of those two overlapping particles. Because of the cell architecture and intrinsic properties of fluorophores, as well as the illumination profile of the microscope and other setup dependent effects, these particles do not exhibit a homogeneous intensity value. Rather, the intensity values of the

particles of a particular size are normally distributed. By fitting a Gaussian distribution to the particle intensity distributions, one can calculate the characteristics of intensity distributions of known monomeric/oligomeric controls. Such an analysis requires well-characterized monomeric and dimeric membrane proteins in order to quantify oligomeric states with precision. Therefore, previously-established controls were used here: N-terminally SNAP-tagged β_1AR (SNAP-β_1AR) as the monomeric, and SNAP-CD28 as dimeric control (Calebiro et al., 2013).

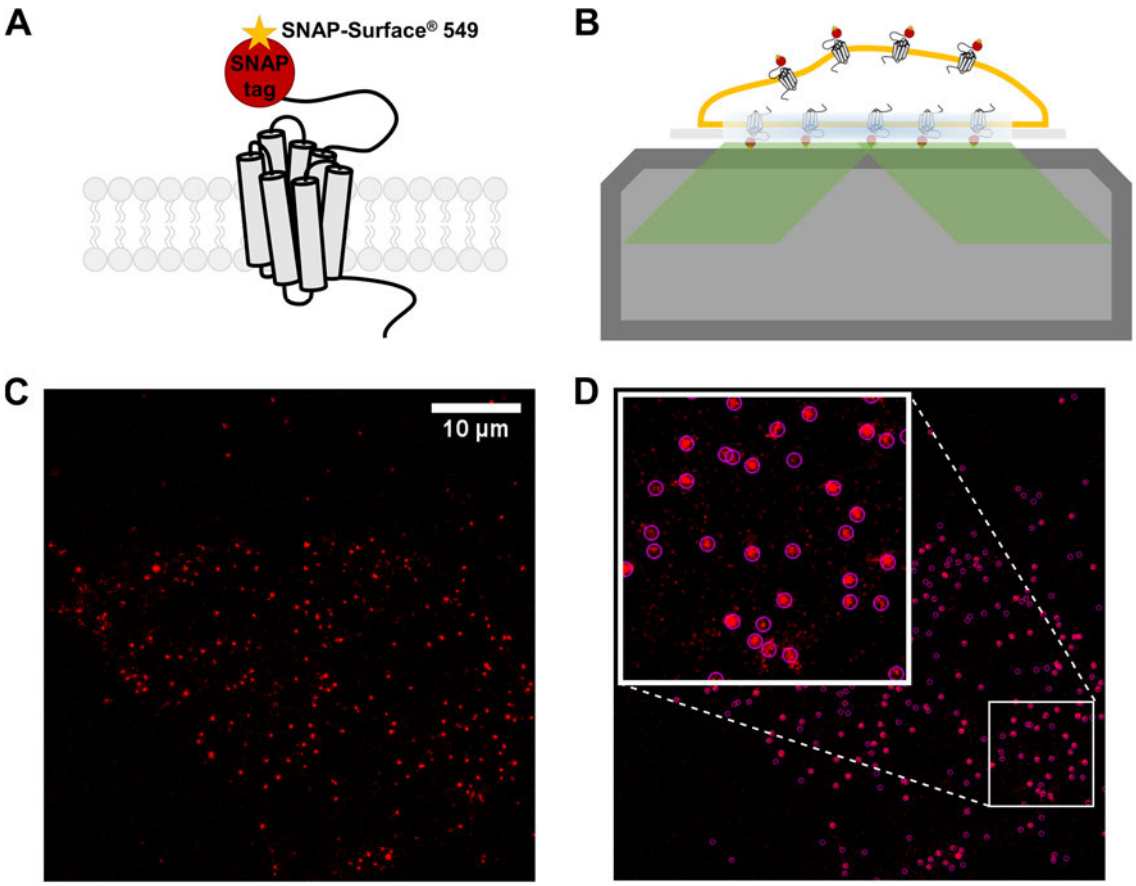

Figure 5-1. Single molecule imaging using TIRFM. (A) Schematic view of a SNAP (red)-CXCR4, labeled with SNAP-Surface 549 (yellow). (B) Schematic representation of TIRFM imaging of single molecules. Laser beam is directed to the specimen at a certain incidence angle. Depending on this angle and the refractive index of the immersion oil between the specimen and the objective, the excitation beam is partially reflected. A portion of the non-reflected light generates an electromagnetic evanescence field (light blue), with a depth of ~100 nm, which allows observing fluorescent particles in single molecule resolution on the surface of an intact cell (yellow). (C) A representative single molecule TIRFM image of SNAP-CXCR4 in an intact CHO-K1 cell, displaying single fluorescent particles (red) and (D) particle detection from this image. Each purple circle indicates a detected particle above the background threshold. Inlet: zoomed in view of the image within the white box.

After transfecting CHO-K1 cells with one of these constructs each for 4-6 hours, expressed and cell surface localized SNAP-tagged receptors were labeled using the SNAP Surface 549 dye, and imaging was performed on the TIRF microscope. To deconvolute each of the oligomer states of a given receptor using this method, multiple Gaussian fits on the single molecule intensity frequency distributions are applied. In such a fit, each Gaussian component corresponds to an oligomeric state. Firstly, the properties (center (*c*) and full width at half maximum (FWHM)) of the Gaussian fit that corresponds to an exclusively monomeric receptor (using certain image acquisition settings) needs to be defined as reference. To do this, multiple consecutive frames of the highly monomeric SNAP-β_1AR were acquired (Figure 5-2A and B), and the particle intensity distribution was calculated from the last frame of those movies, because TIRF imaging at high laser power causes photobleaching, and this increases the probability of having all remaining SNAP-β_1AR particles in the last image frame to be exclusively monomeric.

When analyzed, the intensity distribution of the 400th frame of SNAP-β_1AR movies displayed, indeed, a single Gaussian trend, which corresponded to an exclusively monomeric behavior (Figure 5-2C). This Gaussian fit resulted in the following values: *c*= 0.00425 and FWHM=0.0043. These values then served to define the properties of the Gaussian fit profiles of larger oligomeric fractions as fixed values, such as dimers (*c*= 0.0085 and FWHM=0.0086) or tetramers (*c*= 0.017 and FWHM=0.0172).

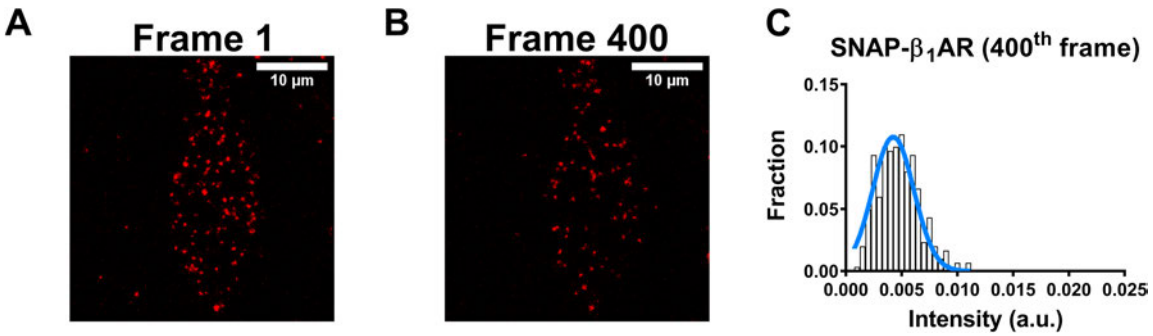

Figure 5-2. Determination of monomeric single molecule intensity distribution fitting values. (A) First and (B) last (400th) images of a CHO-K1 cell expressing the SNAP-β_1AR labeled with SNAP Surface 549. (C) Intensity distribution of the 400th image can be fit with a mono-Gaussian distribution, which indicates that there are only monomeric species in this sample. The properties of this fit corresponding to the monomeric intensity character are then used as constrains for the experiments with unknown species characteristics.

Next, the first frames of SNAP-β_1AR movies were analyzed to identify the basal oligomeric behavior of this receptor. After fitting multi-Gaussian distributions with defined *c* and FWHM values on the intensity frequency distributions, the area under the curve (AUC) of each Gaussian component was calculated. This calculation revealed a 94.4% monomeric and 5.6% dimeric fraction, and no larger oligomers (Figure 5-3A and D). This analysis confirmed the largely monomeric behavior of SNAP-β_1AR. The same analysis on the dimeric control, SNAP-CD28, revealed a 92.6% dimeric and 3.8% tetrameric population for it. A small, monomeric SNAP-CD28 fraction of at 3.6%, which is probably caused by substantial photobleaching, or incomplete labeling, was also observed (Figure 5-3B and D). These experiments revealed the reliable use of the control constructs used here and also confirmed the validity of the approach. Finally, the analysis of SNAP-CXCR4 images revealed a highly monomeric fraction at 86.7%, and a fraction of dimers at 11.6%, as well as a negligible amount of higher order oligomers (1.7%) (Figure 5-3C and D).

All together, these results suggest that at very low expression levels (below 0.3 particles per μm^2) SNAP-CXCR4 exhibits a dominant monomeric behavior in intact CHO-K1 cells.

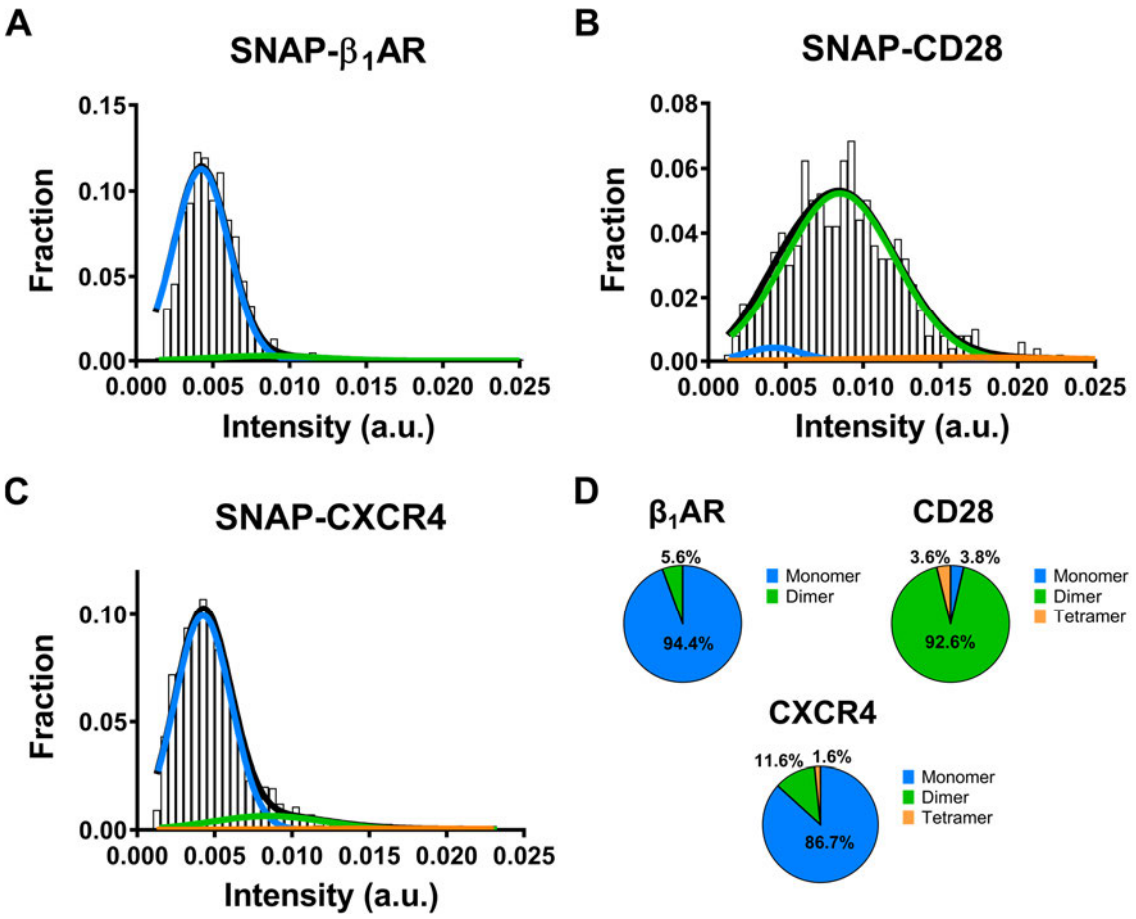

Figure 5-3. TIRFM single molecule intensity analysis. Intensity distributions of SNAP-Surface 549 particles corresponding to (A) SNAP-CXCR4, (B) SNAP-β_1AR, and (C) SNAP-CD28. A mixed Gaussian fit distinguishes fractions of oligomeric populations. From the global fit (black line), monomeric (blue), dimeric (green), and tetrameric (orange) fractions were derived. (D) Pie chart view of the fractions of oligomeric species, calculated from the areas under Gaussian fit curves. Intensity values were collected from 27 different cells for SNAP-CXCR4, 8 cells for SNAP-β_1AR, and 13 cells for SNAP-CD28 in seven independent experiments.

5.1.2. Dynamic Interactions of CXCR4 Protomers

Static analysis of single molecule intensities displayed a prevalently monomeric organization of CXCR4. Therefore, it was essential to assess whether these monomeric CXCR4 molecules ever interact with each other, and if they do so, with what temporal kinetics those interactions would occur. To assess this, lateral movements of individual SNAP-CXCR4 molecules in living cells were assessed from TIRF image series acquired at 10-50 ms intervals per frame (Figure 5-4A and B). Using the Polytracker software

(Möller et al., 2020), time points where individual tracks colocalized and split were analyzed. Then, the durations in which two tracks remained merged were calculated and their frequencies were plotted. Since TIRFM cannot resolve particles below 50 nm, not every merging information revealed by Polytracker actually corresponds to a specific interaction. Due to this, some of the interactions observed in TIRF movies correspond to random colocalizations. The duration of these random, nonspecific colocalizations of PSFs were calculated previously (for identical imaging settings) by computationally simulating the single molecules with experimentally-determined diffusion speeds (Möller et al., 2020). The distribution of random colocalization times displayed a single exponential decay behavior, with a τ value of 112 ms. Then, a bi-exponential decay on the SNAP-CXCR4 data with a constrained τ value of the random colocalizations was fitted. This revealed the true interaction kinetics of SNAP-CXCR4, as the τ value of the second exponential component from the fit, which was ~900 ms (Figure 5-4C). This dimerization time is almost twice as long as that observed for the strictly monomeric μ opioid receptor under identical experimental conditions.

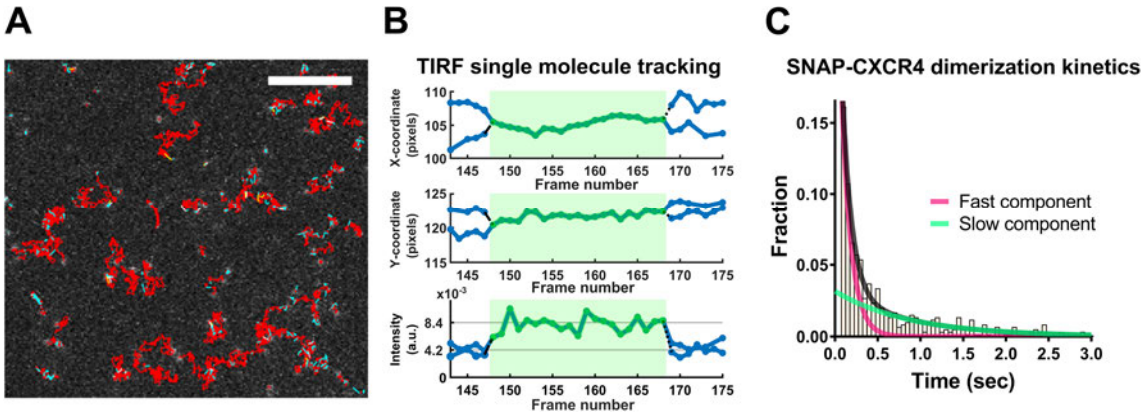

Figure 5-4. TIRFM single molecule tracking and dimerization kinetics. (A) A representative TIRF image and single molecule tracks (red) overlaid on its source TIRF movie. (B) Representative tracks of two SNAP-CXCR4 transiently homodimerizing. Shown are the coordinates of two tracks (blue lines) in X (upper) and Y (middle) dimensions. Intensity doubling (lower) upon particle merging (color change from blue to green) demonstrates receptor interactions. (C) Distribution of colocalization times obtained from the length of individual dimerization events. A biexponential decay function (black) with a constrained rate constant (magenta), derived from simulated randomly colocalizing particles (magenta), resulted in a slow component (green), representing specific interactions of SNAP-CXCR4, with a lifetime (τ-value) of 890 (730 to 1,088) ms (mean and 95% CI).

In summary, these results suggest that CXCR4 organization is largely monomeric at low densities, but the individual protomers can form specific interactions with each other in the order of 1 second kinetics.

5.2. Molecular Brightness-Based Assessment of CXCR4 Oligomerization

Single molecule imaging using TIRFM is an excellent method to precisely analyze receptor oligomerization at very low expression levels. This method provides a robust approach to understand dynamic and kinetic features of receptor protomer interactions. However, at receptor densities higher than ~0.5 protomers per μm^2 membrane area, the individual PSFs within the TIRF illumination field start to overlap, thus detecting single entities separately becomes impossible. Moreover, depending on the receptor and tissue type, expression levels of GPCRs usually exceed the expression levels that are generally optimal for TIRF imaging. This is indeed the case for CXCR4. For example, CXCR4 levels in leukocytes can range from a few thousands to above 100.000 receptors, which corresponds to a range between ~4 to >300 receptors per μm^2 of membrane area (assuming that the surface area of a T cell is ~250 μm^2). Therefore, single molecule fluorescence imaging would not be suitable to explore CXCR4 oligomerization at high expression levels. For this reason, molecular brightness analysis, which is a method based on fluorescence fluctuation spectroscopy, was the method of choice for further experiments.

5.2.1. Implementation of Spatial and Temporal Brightness Protocols

Molecular brightness methods implemented here are based on the mathematical theory of the Number & Brightness (N&B) analysis (Digman et al., 2008), which is a fluorescence fluctuation spectroscopy method. N&B method relies on the statistical analysis of fluorescence intensity fluctuations within the confocal beam volume determined by the confocal beam volume, to calculate the concentration and brightness of fluorescent particles.

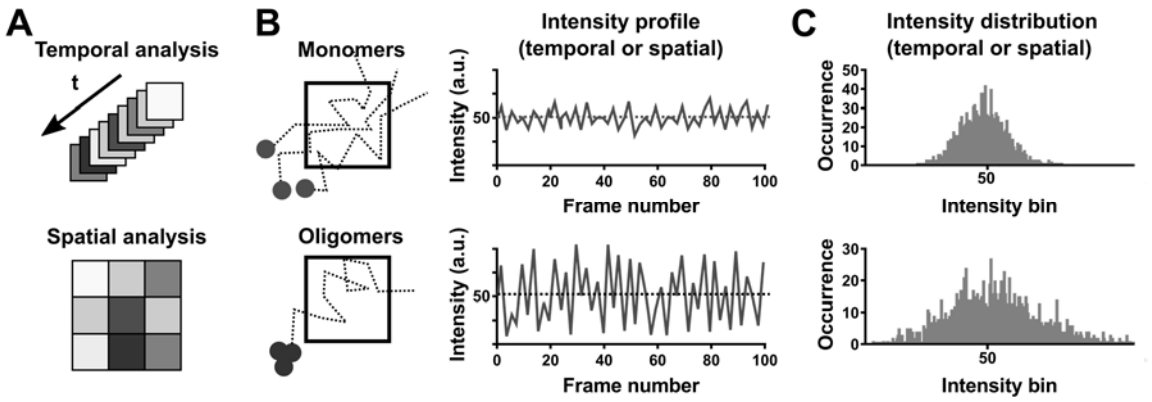

Figure 5-5. The basis of fluorescence fluctuation analysis. (A) Intensity fluctuations can be measured in individual pixels over time (top), or among different pixels of an image (bottom). (B) In temporal measurements, diffusion of several monomeric proteins or a single trimeric protein through the observation volume produces the same average intensity, while the intensity fluctuations in case of trimers is larger. (C) Intensity histograms of these two cases clearly indicate that the variance of intensity distributions is larger for the case where trimers are present, compared to where monomers are present.

Originally, N&B was developed to measure the intensity fluctuations within individual pixels of an image over time. However, a pool of pixels with individual intensity values can be treated similarly, thus the theory behind N&B may apply to a single confocal image as well (Figure 5-5A). The fluctuations, within a pixel over time or within several pixels over a single image, produce intensity variations (Figure 5-5B). The variation of the fluorescence intensity is defined by the oligomeric size of the fluorescent particles traveling through the confocal volume over time, or the presence of particles in a given moment over space. This means, over time, whenever a large particle (i.e. tetramer) travels through the observation spot, high jumps in the fluorescence intensity are observed, while smaller complexes (i.e. monomer) produce smaller intensity changes (Figure 5-5C). Same applies in the spatial domain: compared to monomeric species, the presence of the amount of trimeric species in individual pixels of a static image in a given time exhibits a larger variance in fluorescence intensity.

Based on this theory, the number and brightness calculations, where the ratio of the variance (σ^2) to average intensity (k) results in the apparent brightness, and the ratio of the square of the average intensity (k^2) to variance, results in the apparent number of particles within the observation volume. σ^2 and k are calculated by Gaussian fitting on the intensity histograms. In an ideal model, where all the fluorescence fluctuations arise purely from the

photon counts, apparent number, *N*, and apparent brightness, B, are calculated with the formulas given below:

$$N = \frac{k^2}{\sigma^2} \qquad B = \frac{\sigma^2}{k}$$

The variance σ^2 is proportional to the square of intrinsic molecular brightness (real photon counts per particle per time), ε^2, and the number of particles, n. So, σ^2 is calculated as: $\sigma_n^2 = \varepsilon^2 n$. However, the variance in fluorescence intensity does not solely emerge from photon counts. In a photon counting detector, detector shot noise also contributes linearly to the variance ($\sigma_d^2 = \varepsilon n$). Because εn is actually equal to the average intensity k, the detector shot noise contributes to the variance equally to the k. Thus, the apparent B is calculated with the contribution of both variances:

$$B = \frac{\sigma_n^2}{k} + \frac{\sigma_d^2}{k} = \frac{\varepsilon^2 n}{k} + \frac{\varepsilon n}{k} = \frac{\varepsilon k}{k} + \frac{k}{k} = \varepsilon + 1$$

$$N = \frac{k^2}{\sigma^2} = \frac{\varepsilon n \times \varepsilon n}{\varepsilon^2 n + \varepsilon n} = \frac{\varepsilon n \times \varepsilon n}{\varepsilon n(\varepsilon + 1)} = \frac{\varepsilon n}{\varepsilon + 1}$$

The intrinsic brightness ε is independent from the number of particles n, and it is defined by the photophysical properties of the fluorescent entity (fluorescent protein or dye). On the other hand, N is directly proportional to n. So the ε and n can be defined as:

$$\varepsilon = \frac{\sigma^2 - k}{k} \qquad n = \frac{k^2}{\sigma^2 \quad k}$$

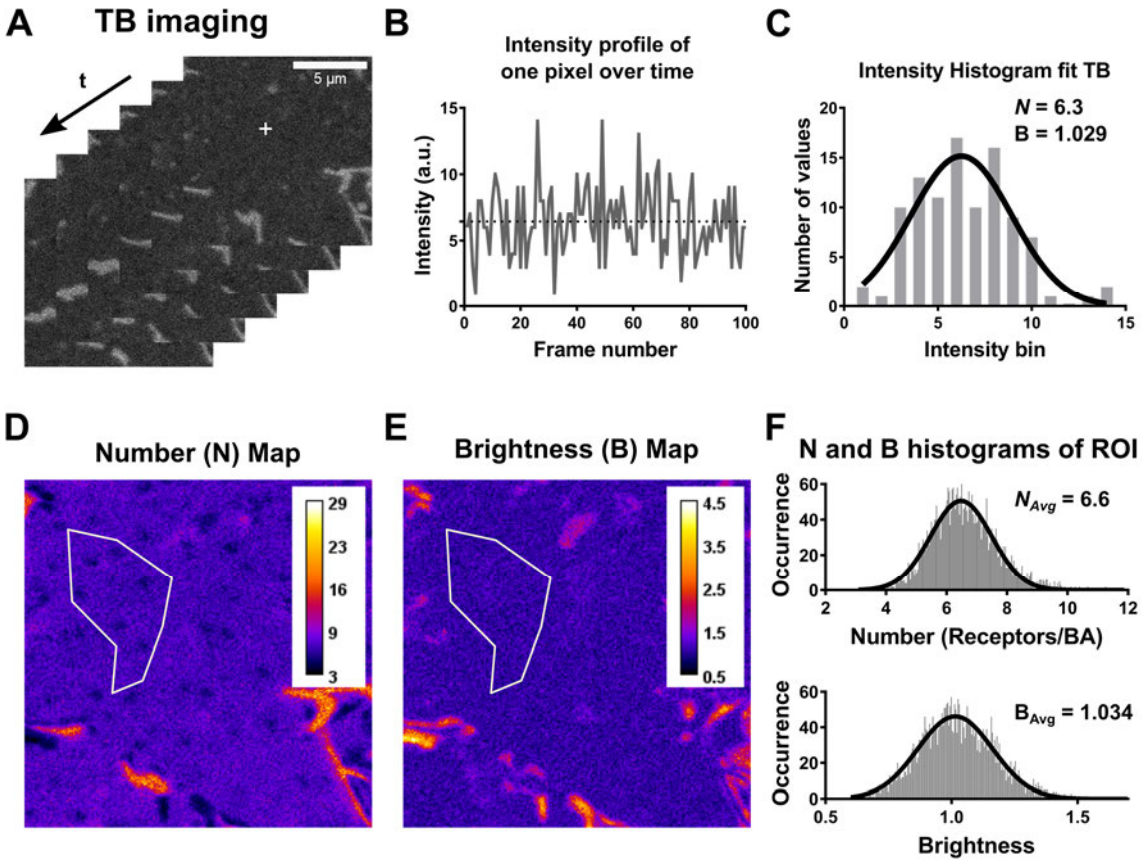

Figure 5-6. Image acquisition and data curation for temporal brightness analysis. (A) Confocal image series of the basolateral membrane of an intact HEK293AD cell expressing a C-terminally EYFP tagged GPCR. (B) Intensity profile and the mean intensity (black dashed line) of an individual pixel over time. (C) Distribution of the intensity values obtained from (B) and Gaussian fitting. Center of and the variance of the Gaussian fit are used to calculate the *N* and B values for this individual pixel. Same calculations are iterated for all the pixels within the image. (D and E) Number and Brightness maps generated from the calculations in (C). (F) Distribution of *N* and B values obtained by appointing a ROI on the *N* and B maps in (D) and (E). A Gaussian distribution fitting revealed the average number (N_{Avg}) and average brightness (B_{Avg}) for the marked ROI.

The temporal brightness (TB) method uses image series (Figure 5-6A) and calculates average number of fluorescent molecules as well as their average brightness for individual beam areas (Figure 5-6B and C), and assigns these values to each pixel. When this analysis is performed over time with several pixels that constitute an image, it generates number and brightness maps of individual cells (Figure 5-6D and E). It is then possible to calculate the average number and brightness at certain regions of the cells (Figure 5-6F). On the other hand, spatial brightness (SB) calculates an average *N* and apparent B from a pool of pixels of a single image (Figure 5-7A and B), and produces a single, average number and brightness value for each ROI on individual cells (Figure 5-7C).

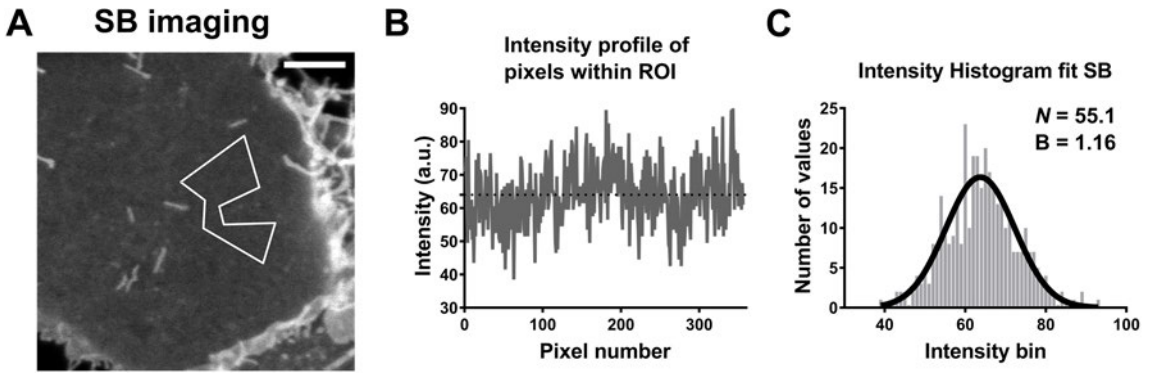

Figure 5-7. Image acquisition and data curation for spatial brightness analysis. (A) A single confocal image of the basolateral membrane of an intact HEK293AD cell expressing a C-terminally EYFP tagged GPCR. (B) Intensity profile and the mean intensity (black dashed line) of the pixels within the ROI (white) marked on the image in (A). (C) Distribution and Gaussian fitting of the intensity values obtained from (B). Center of and the variance of the Gaussian fit are used to calculate the *N* and B values for this individual ROI.

To successfully apply a molecular brightness method, it is essential to verify the validity of the theory under certain imaging conditions first. To verify whether this method can calculate the concentration (number of fluorescence molecules within the confocal beam area), firstly the microscope resolution, thus the PSF beam volume was calculated by imaging single 0.5 µm TetraSpeck microspheres on confocal microscope. Fluorescent microspheres were diluted 1:1000 (vol/vol) in ethanol and 10 µL of the mixture was added on a glass coverslip, and then it was allowed to drop. Then, the coverslip was mounted on a microscope slide and an xyz image of a single bead was acquired using the imaging settings for Alexa Fluor 488 (excitation with 488 nm at 10% laser power, emission at 500-650 nm) and EYFP (excitation with 514 nm at 10% laser power; emission at 520-600 nm) (Figure 5-8A). Then, using the MetroloJ plugin of ImageJ (Matthews and Cordelières, 2010), an *xz* and a *yz* projection from the center of the microsphere was taken to calculate the *x*, *y* and *z* dimensions of the PSF, which are used for calculating the confocal volume (V) and the beam area (ω^2) (Figure 5-8B). The calculated PSF dimensions are given in Table 5-1. After deconvoluting 0.25 µm (radius of the microspheres) from these values, the PSF volume was calculated using the spheroid volume formula, and the beam area was calculated using the ellipsoid area formula. The "number" value calculated by TB and SB corresponds to the amount of fluorescent molecules within the size of one beam area. This calculated number per beam area can then be converted to number of particles per μm^2 membrane area.

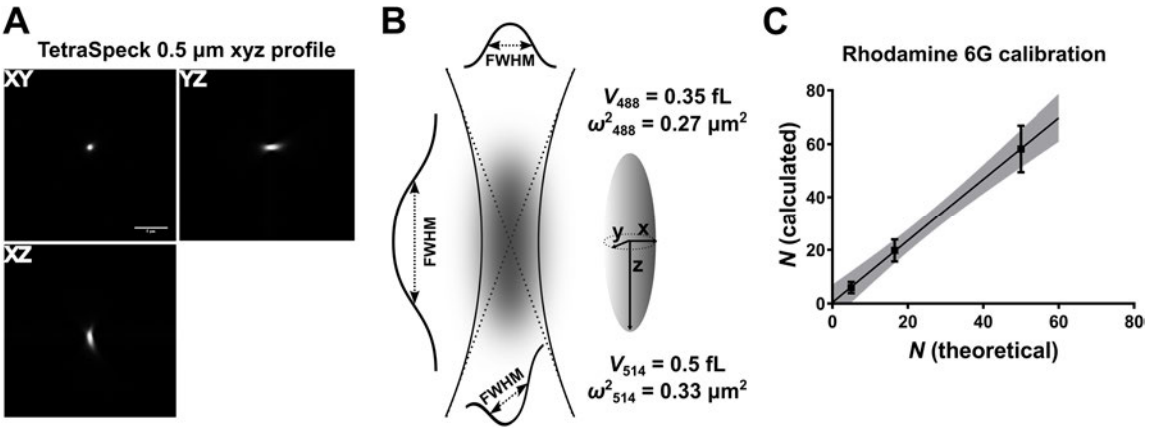

Figure 5-8. Confocal beam volume/beam area calculation and verification. (A) *xyz* intensity profile of a 0.5 µm Tetraspeck bead acquired under SB imaging settings with 488 nm and 514 nm laser lines.(B) Theoretical shape of the confocal beam and calculation of the confocal volume and area based on the Rayleigh criterion. Gaussian fitting of the bead intensity profiles at *x*, *y,* and *z* axes calculates the beam dimensions (FWHM of the Gaussian fit for each axis). From these dimensions both the beam area ($\omega^2 = \pi xy$) and volume ($V = \pi^{3/2} xyz$) are calculated. (C) Verification of the calculated beam volume by measuring the Rhodamine 6G. Theoretical number was calculated considering the molar concentration of Rhodamine 6G solution and the observation volume calculated from the beads. Each data point is the mean±standard deviation (SD) calculated from 3 different images per condition. The straight line is the fit of the data points with 95% confidence intervals (CI, gray shade). The fit resulted in a line with a slope of 1.16 (0.94 to 1.38 CI).

Table 5-1. Confocal PSF dimensions calculated by imaging fluorescence microspheres.

Laser Line	***x* (corr.)**	***y* (corr.)**	***z* (corr.)**	**Volume**	**Beam Area**
488 nm	0.545 µm (0.295 µm)	0.548 µm (0.289 µm)	1.226 µm (0.976 µm)	0.35 fL	0.27 µm^2
514 nm	0.579 µm (0.329 µm)	0.566 µm (0.316 µm)	1.389 µm (1.139 µm)	0.65 fL	0.33 µm^2

Once the confocal volume was calculated, the next step was to verify whether the solution concentrations could be accurately measured using the brightness methods. For this, Rhodamine G solutions at different concentrations prepared in glycerol:water (9:1 vol/vol) were prepared and imaged with spatial brightness imaging settings using the 514 nm laser line and 520-600 nm detection window. Ideally, since the concentration of the confocal volume is known, the calculated number using the brightness analysis should

correctly correspond to the concentration of the solution. Indeed, the calculated number of Rhodamine 6G at each concentration correlated with the theoretical number of molecules at given confocal volume. These experiments verified that the implemented imaging settings for molecular brightness measurement can calculate fluorescent particle concentrations accurately, and can be used for studying the oligomerization of fluorescently-labeled GPCRs (Figure 5-8C).

5.2.1.1. Selection and Verification of Monomeric and Dimeric Controls

Once the calibration measurements verified the concentrations calculated by brightness measurements, the next step was to test the method to quantify the membrane protein oligomerization and density. The apparent brightness (ε) values produced by the method can be used to quantify the average oligomerization only when it is compared with a fully characterized and validated, true monomeric and, ideally, a dimeric control protein. By normalizing the observed brightness value to which observed for the monomeric control, one can describe an average oligomeric state for the protein of interest: $Oligomer\ state = \frac{\varepsilon_{GPCR}}{\varepsilon_{monomer}}$.

Recent studies displayed that a majority of GPCRs display similar diffusion properties (Yanagawa et al., 2018). In view of previous studies, the single-transmembrane protein CD86 and a class A GPCR β_1 adrenergic receptor (β_1AR), were tested as candidate monomeric controls (Calebiro et al., 2013; Dorsch et al., 2009). Both β_1AR and CD86 displays monomeric stoichiometry according to the single molecule studies. To evaluate their potential as monomeric controls, an N-terminally SNAP-tagged, or a C-terminally EYFP-tagged β_1AR and CD86 constructs were cloned. Moreover, in order to have a dimeric control, a β_1AR construct with two tandem EYFPs at the C-terminus (β_1AR-2xEYFP) was also cloned. A rigid, alpha helical linker sequence that is made up of $A(EAAAK)_4A$ protein sequence was inserted between two EYFPs in order to limit the interactions between the two EYFPs within the same protein (Arai et al., 2001). Therefore, SNAP-CD28 and CD28-EYFP constructs were also cloned to be tested as dimeric control constructs (Figure 5-9A). Confocal microscopy imaging of these constructs expressed in

HEK293AD cells showed that these tags did not alter the expression or the plasma membrane localization of this receptor (Figure 5-9B).

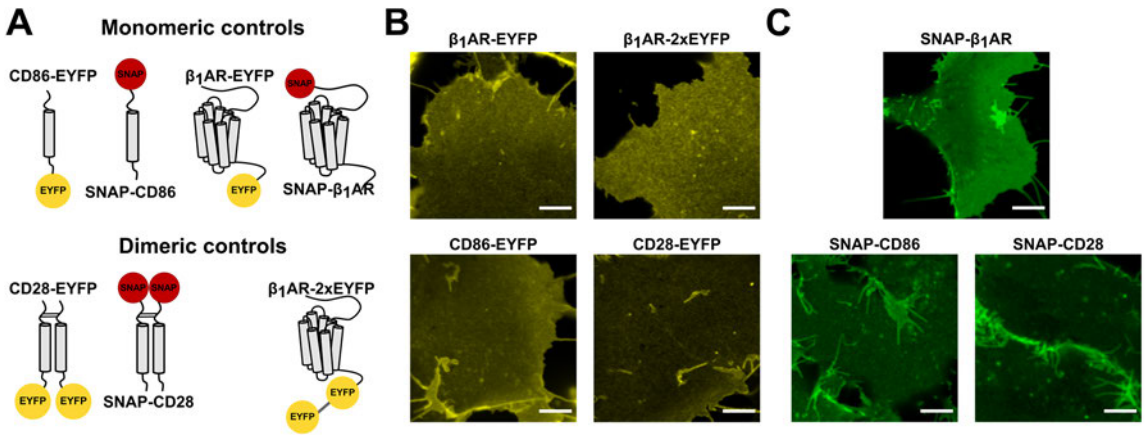

Figure 5-9. Candidate monomeric and dimeric calibration constructs for brightness analyses. (A) Cartoon view of the designed control constructs. EYFP was always inserted C-terminally. SNAP tag was inserted N-terminally for extracellular labeling with organic dyes. (B and C) Confocal microscopy images of the basolateral membranes of HEK293AD cells expressing the (B) C-terminally EYFP tagged constructs and (C) N-terminally SNAP tagged constructs, labeled with SNAP Surface Alexa Fluor 488 dye. The scale bar in each image is 5 μm.

Firstly, C-terminally EYFP-tagged constructs were characterized. Several single confocal images of the cells expressing each construct were acquired for SB analysis. Results of SB analysis showed that the β_1AR-EYFP displayed the lowest average brightness ($\varepsilon = 0.99 \pm 0.21$ SD). The average brightness calculated for β_1AR-2xEYFP was double of was measured for β_1AR-EYFP (2.01 ± 0.34). CD28-EYFP displayed brightness values slightly above β_1AR-2xEYFP (2.21 ± 0.39). On the other hand, the average brightness of CD86-EYFP was roughly 20% higher than that of β_1AR-EYFP (1.17 ± 0.22) (Figure 5-10A). Brightness values for each of these construct also displayed a consistent average brightness along increasing densities, calculated as number of receptors per square micron basolateral membrane area (Figure 5-10B). These results at the first glance suggest that β_1AR-EYFP was a better monomeric control than CD86-EYFP at expression levels needed for brightness analysis. In order to confirm that β_1AR-EYFP is truly monomeric, a stepwise bleaching approach with SB was used. This approach relies on the following fact: If the imaged protein is truly monomeric, photobleaching causes only a reduction in the number of fluorescent molecules, but not the brightness. On the other hand, if there are

more complex assemblies, bleaching would reduce not only the number of fluorescent particles, but also the brightness, as at each step of photobleaching fluorescent molecules within oligomers will become dim and they would not produce decreased brightness. For this approach, 3 consecutive frames of individual cells expressing CD86, CD28, β_1AR-EYFP and β_1AR-2xEYFP were acquired, ensuring photobleaching after each frame (assessed by comparing average intensity values of each frame), and average brightness was analyzed for the first and the third frame (Figure 5-10C). This analysis showed that β_1AR-EYFP displayed identical average brightness in both frames (ε change from 1.01 to 0.99), while a remarkably decreased brightness was observed for CD28 (from 2.37 to 1.51) and β_1AR-2xEYFP (from 2.14 to 1.18). On the other hand, CD86 displayed a non-negligible decrease in brightness from first to the last frame (from 1.31 to 0.96). These experiments confirmed the dimeric nature of CD28-EYFP and β_1AR-2xEYFP, as well as the monomeric behavior of β_1AR-EYFP. To test the reliability of these results, the same experiments were performed with TB analysis. The results of the TB analysis were in good correlation with that of the SB analysis. The bleaching analyses using TB also supported the notion that β_1AR-EYFP is highly monomeric, while CD86-EYFP displays a slightly higher oligomer state (Figure 5-10D).

In order to further verify whether the 3-step bleaching was sufficient to characterize the monomeric structure of β_1AR-EYFP, this time a 10-step bleaching was performed. Analysis of 10 consecutive frames from individual cells showed that the brightness of β_1AR-EYFP remains stable (Figure 5-10E), and β_1AR-2xEYFP decreases (Figure 5-10F), while the total number decreases over bleaching steps for both conditions. These results further confirmed that β_1AR-EYFP and β_1AR-2xEYFP are reliable monomeric and dimeric controls for brightness analysis.

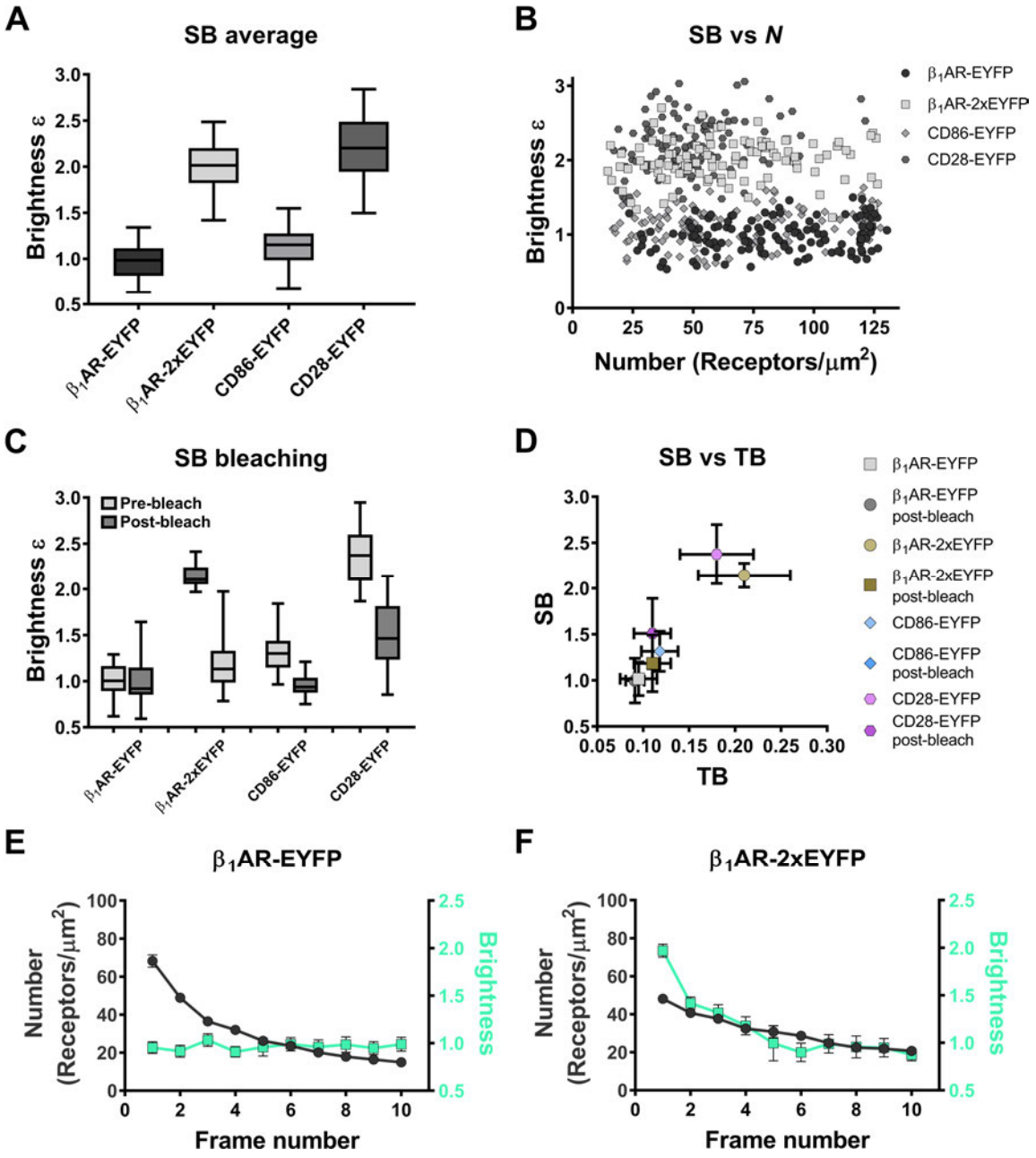

Figure 5-10. Characterization of the monomeric and dimeric controls of the EYFP tagged constructs. (A) The box and whiskers representation shows the median and 5-95 percentile of brightness (ε=B-1) values of multiple single cells calculated with SB for each construct. (B) Concentration-brightness plot. Each data point represents the N and ε values of each cell image for different constructs. (C) Box and whiskers plot of average brightness values calculated from the pre- and post-bleached images. Whiskers show the 5-95 percentiles of the median. (D) Comparison of the ε values calculated from spatial and temporal brightness analysis before and after bleaching. Each data point is the average ε value with SD. (E and F) Time-course plot of brightness and density of the time-series images. Despite the density of β_1AR-EYFP molecules decrease, its brightness remains the same (coefficient of variation: 3.81%), while β_1AR-2xEYFP exhibits declining brightness (coefficient of variance: 29.43%) and number. Four different membrane regions corresponding to the same spots within each frame was analyzed and obtained brightness-density values were averaged. Black and blue lines connect data points. Each data point is the mean ± SD of three independent experiments.

Next, N-terminally SNAP-tagged constructs were tested. Firstly, SB analysis of these constructs showed that SNAP-β_1AR (ε = 0.52 ± 0.11) exhibited relatively lower brightness than that of SNAP-CD86 (0.67 ± 0.10). On the other hand, a double-SNAP tagged CD86 construct (2xSNAP-CD86) displayed an average brightness notably higher than the double of that of SNAP-β_1AR (1.04 ± 0.23). Moreover, it displayed a density-dependent increase in its brightness, suggesting that it would not be a reliable control candidate (Figure 5-11A). The post-photobleaching SB experiments further showed that SNAP-CD86 brightness decreased in post-bleach images, while the SNAP-β_1AR brightness remained stable (Figure 5-11B).

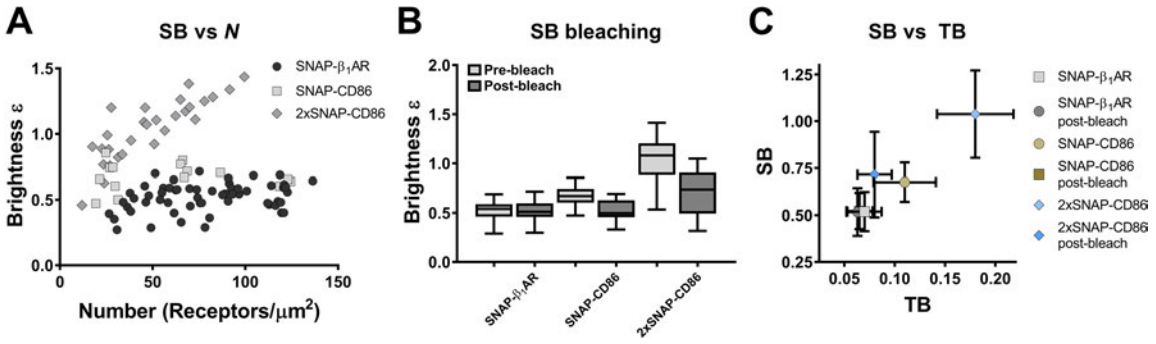

Figure 5-11. Characterization of the SNAP tagged monomeric and dimeric control constructs. (A) Box and whiskers plot of average ε values calculated by SB analysis. Each data point represents the ε and N calculated from a single cell image expressing the respective construct. (B) Box and whiskers plot of the pre- and post-bleach average ε values obtained via SB analysis. Data are given as median with its 5-95 percentiles. (C) Comparison of the average ε values calculated from SB and TB analyses before and after photobleaching. Each data point is the average ε value with SD. Each dataset is obtained from at least 3 independent experiments for each condition.

In conclusion, these results confirmed that both the C-terminal EYFP tag and an N-terminal SNAP tag can be used reliably for SB and TB analyses. Moreover, β_1AR with either of these tags serves greatly as a monomeric control construct, and a double EYFP tagged version of the β_1AR serves well as a dimeric control.

5.2.2. Oligomerization Analysis of CXCR7

Using the monomeric and dimeric controls established, the oligomeric status of CXCR7 was studied. For this, a CXCR7 construct with a C terminally EYFP tag was used. When transiently expressed in HEK293AD cells, the CXCR7-EYFP fluorescence was observed mainly as membrane, near membrane and intracellular clusters, and only a very small, hardly distinguishable CXCR7-EYFP signal was observed on the cell surface (Figure 5-12A). SB analysis on these images resulted in very high brightness values that reported an artificial, highly oligomeric organization ($\varepsilon = 5.02 \pm 1.76$ SD). Applying an intensity threshold during SB analysis helped to eliminate the high intensity clusters and provided a more homogeneous membrane area selection (Figure 5-12B). Membrane areas with more homogeneous CXCR7-EYFP signal resulted in brightness values closer to the monomeric control ($\varepsilon_{\beta 1AR} = 1.78 \pm 0.35$), yet revealed the presence of roughly 30% of CXCR7 as dimers ($\varepsilon_{CXCR7} = 1.72 \pm 0.38$) (Figure 5-12C).

In order to overcome the intracellular fluorescence from CXCR7-EYFP, and to analyze the oligomerization of the surface localized CXCR7, an N-terminally SNAP tagged CXCR7 construct was used. Cells expressing SNAP-β_1AR or SNAP-CXCR7 were labeled with SNAP Surface Alexa Fluor 488, and confocal imaging for SB was performed. Confocal images showed that right after a 20-minute SNAP labeling, SNAP-CXCR7 still formed clusters on the basolateral membrane (Figure 5-12D), yet to a lesser extent compared to that of CXCR7-EYFP. Excluding the obvious CXCR7 clusters, SB analysis of SNAP-CXCR7 showed that the average oligomer size of this receptor was approximately 1.3 ($\varepsilon = 1.52 \pm 0.25$ SD), suggesting again that this receptor is organized essentially as monomers with a 30% fraction of dimers on the cell surface (Figure 5-12F).

Together, these results suggest that CXCR7-EYFP is localized mainly at intracellular domains of HEK293AD cells, which did not allow a reliable brightness analysis of this receptor. A more confident analysis was only possible when only the surface localized SNAP-CXCR7 was used, and this construct exhibited a largely monomeric behavior in SB analysis.

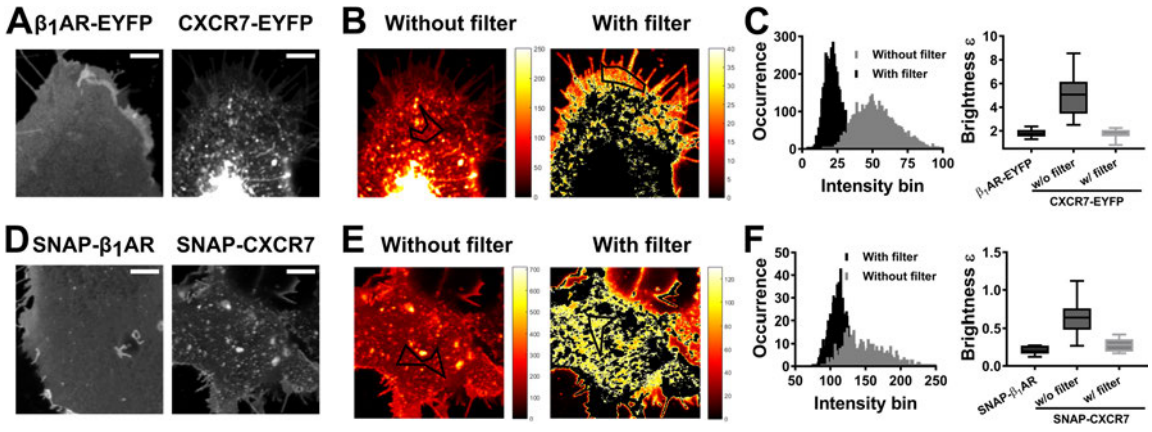

Figure 5-12. Oligomerization analysis of CXCR7 by spatial brightness. (A and D) SB images of HEK293AD cells expressing β1AR-EYFP (A left) CXCR7-EYFP (A right), SNAP-β_1AR (D left) and SNAP-CXCR7 (D right). (B and E) Intensity heat map of a cell expressing (B) CXCR7-EYFP and (E) SNAP-CXCR7 before (left) and after (right) applying an intensity threshold prior to SB analysis. (C and F) Intensity distributions of the ROIs from B and E used for SB analysis. A normal distribution is observed for threshold applied CXCR7-EYFP images, which allowed proper N and B calculations. Without filter, intensity distributions appeared as mixed normal distributions due to the contribution of high intensity clusters. (C) Box and whiskers plot showing oligomer size of CXCR7-EYFP calculated from SB analysis. Whiskers show the 5-95 percentile of the median. Data was obtained from at least 3 independent experiments.

5.2.3. Oligomerization Analysis of CXCR4

5.2.3.1. Evaluating the Endogenous Expression of CXCR4 in Cell Lines

Before exploring the oligomerization of CXCR4, the first step was to evaluate the endogenous levels of CXCR4 in the cells lines that were to be used in brightness experiments. For this purpose, HEK293AD and CHO-K1 cells were assessed. Cells seeded on glass coverslips in 6-well plates were transfected with either CXCR4-ECFP, or β_1AR-ECFP. Twenty-four hours after transfection, cells were labeled with an Alexa Fluor 488-conjugated CXCR4 antibody, which binds to the N-terminus of CXCR4. Upon labeling, basolateral membranes of the cells were imaged with the SB protocol. While both HEK293AD and CHO-K1 cells expressing CXCR4-ECFP also displayed the fluorescence signal from the antibody (Figure 5-13A and C), cells expressing β_1AR-ECFP displayed antibody signal at background level (Figure 5-13B and D). These results confirm that endogenous CXCR4 expression in both cell types investigated here are below the detection

limit of brightness analysis, which corresponds to less than approximately 5 CXCR4 copies per μm^2 membrane area.

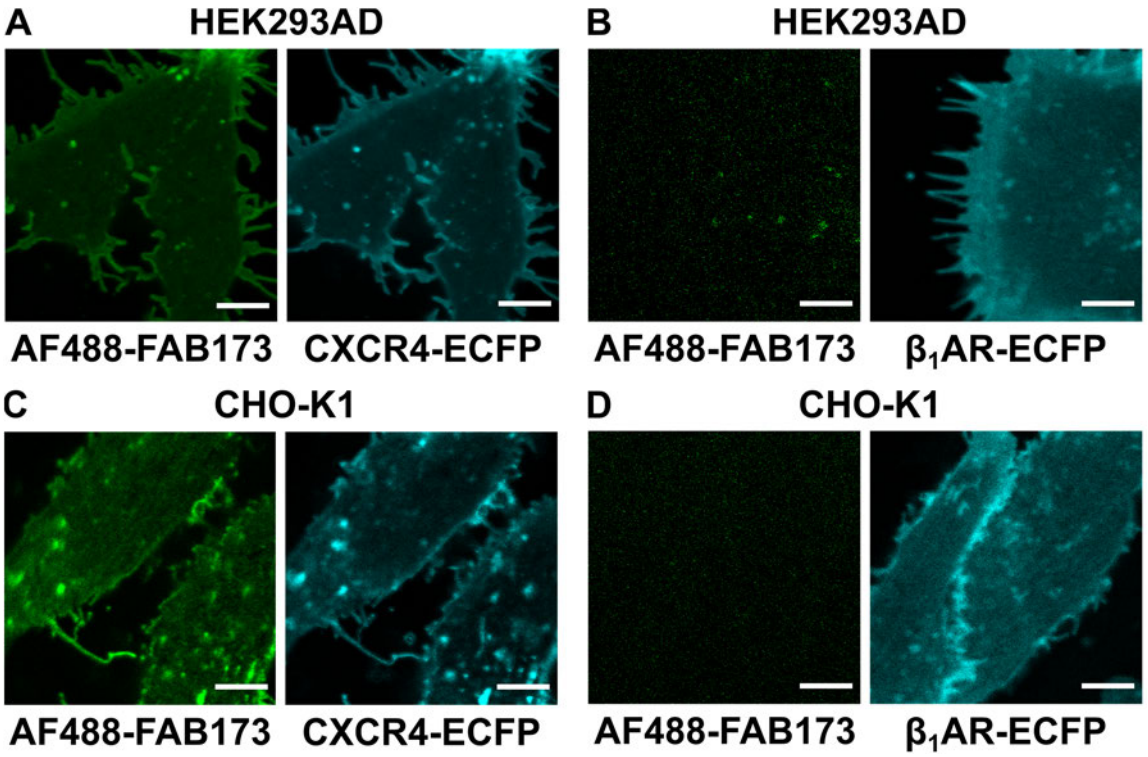

Figure 5-13. Immunocytochemistry-based assessment of endogenous CXCR4 expression in HEK293AD and CHO-K1 cells. Cells were transfected with CXCR4-ECFP (A and C) or β_1AR-ECFP (B and D) and then were labeled with the AlexaFluor488 labeled CXCR4 antibody (FAB173G). Image acquisition settings used for SB was employed. In CXCR4-ECFP overexpressing cells, the antibody detected the CXCR4 epitope (A and C, green channel). In β_1AR-ECFP expressing cells, no analyzable fluorescent signal was detected in the green channel, indicating that CXCR4 expression was below the detection levels of SpIDA (i.e. below 5 receptors/μm^2 membrane area (3,500 receptors/cell). Images are representative of 3 independent immunocytochemistry experiments. Scale bar (white): 5µm.

5.2.3.2. Evaluating the Oligomerization of CXCR4 Using Brightness Analysis

Having the cell lines and the monomeric / dimeric controls validated, the next step was assessing the CXCR4 oligomerization using brightness analysis. For this, firstly, HEK293AD cells transiently expressing CXCR4-EYFP, β_1AR-EYFP or β_1AR-2xEYFP were imaged. SB analysis of these cells at different receptor expression levels displayed a consistent brightness for β_1AR-EYFP and β_1AR-2xEYFP. On the other hand, for CXCR4-EYFP, a density-dependent increase was observed. Normalizing all brightness values to

the average brightness of the monomeric control, β_1AR-EYFP demonstrated a consistent monomeric and dimeric organization of β_1AR-EYFP and β_1AR-2xEYFP, respectively, at every expression level ranging from 10 to 150 receptors/μm^2 membrane area (Figure 5-14A). On the other hand, while CXCR4-EYFP was strictly dimeric at expression levels above 70 receptors/μm^2, this organization shifted towards less abundance of dimers and more monomers as the expression levels decreased (Figure 5-14A). Quantification of CXCR4-EYFP oligomeric state at densities between 10-30 receptors/ μm^2 displayed an average oligomer size between monomeric and dimeric value (Figure 5-14C), while the receptor showed a dimeric assembly within the range of 85-150 receptors per μm^2 (Figure 5-14D). These results suggests a density dependence of CXCR4 dimerization. In order to quantify this concentration dependence, the oligomeric state values of CXCR4-EYFP were averaged within certain density intervals. After adding the average oligomer size value from the TIRF experiment, these values were plotted against the log average *N* value. Fitting a Hill equation to this plot resulted in a dissociation constant of about 30 molecules per μm^2 for CXCR4 dimerization (Figure 5-14B).

In order to understand whether the concentration dependence of CXCR4 dimerization is specific to HEK293AD cells, SB experiments were performed also in CHO-K1 cell lines, which originate from the species of hamster. In line with the results from the HEK293AD cells, CXCR4-EYFP displayed a concentration dependent increase in brightness when expressed in CHO-K1 cells (Figure 5-15A and B). These results together suggest that CXCR4-EYFP dimerization is not limited to one cell line. Since the endogenous CXCR4 levels in both cell lines are below the range that could be detected by the brightness analysis (which means that they are below 5 receptors per μm^2 membrane area), it can be stated that the low brightness observed at low CXCR4-EYFP expression levels is not caused by a competition on dimerization between the endogenous, unlabeled CXCR4 and exogenously expressed CXCR4-EYFP.

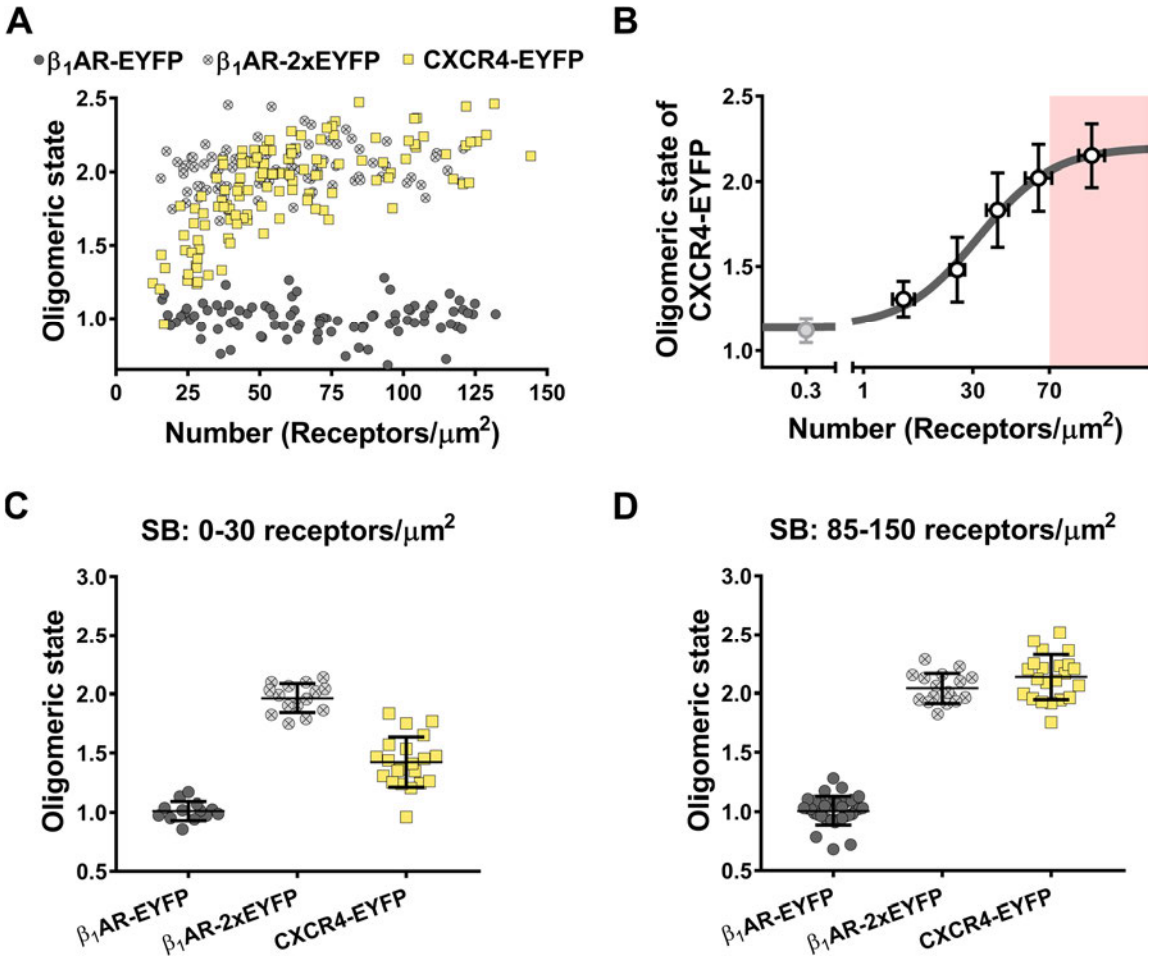

Figure 5-14. Spatial brightness analysis of CXCR4 oligomerization. (A) Measured average oligomeric state as a function of fluorescent particle number. Each data point represents the brightness value obtained from a single cell, normalized to the average brightness of the monomeric control β_1AR-EYFP. (B) Binned average oligomeric state values from single molecule (grey circle) and SpIDA data (white circles) as a function of receptor number per μm^2 membrane area. A sigmoidal curve (dark grey) fitting yielded the dimer dissociation constant of 33.6 (27.5-39.6) receptors/μm^2 (Mean and CI). The fitted line saturated at 2.21 (1.97-2.39) (Mean and CI). The shaded pink area marks the range of oncogenic CXCR4 levels. (C) Scatter dot plot representing the oligomeric states (C) between 0-30 receptors per μm^2 average oligomer states for β_1AR-EYFP: 1.01 ± 0.08, β_1AR-2xEYFP: 1.97 ± 0.12 and CXCR4-EYFP: 1.42 ± 0.21, and (D) between 85-150 receptors β_1AR-EYFP: 1.01 ± 0.12, β_1AR-2xEYFP: 2.04 ± 0.13 and CXCR4-EYFP: 2.14 ± 0.19 (mean ± SD).

It was previously shown that a number of fluorescent proteins can be prone to aggregation through dimerization, in the cytosol or at different cellular compartments (Cranfill et al., 2016). Performing brightness experiments with a fluorescent protein that is highly dimerization prone might cause observing false dimers/oligomers. Thus, it was essential to rule out any contribution of EYFP dimerization on the dimeric behavior of CXCR4. To test this, SB analysis was performed with the SNAP-CXCR4 construct. After

labeling SNAP-CXCR4 with SNAP Surface Alexa Fluor 288, SB imaging and analysis was performed. These experiments also confirmed that SNAP-CXCR4 is dimeric at high expression levels, and this dimerization is again dependent on SNAP-CXCR4 concentration, similar to what was observed for CXCR4-EYFP (Figure 5-15C and D). In conclusion, these results using different cell types, different labeling methods and different controls suggest that CXCR4 exhibits a density-dependent dimeric behavior.

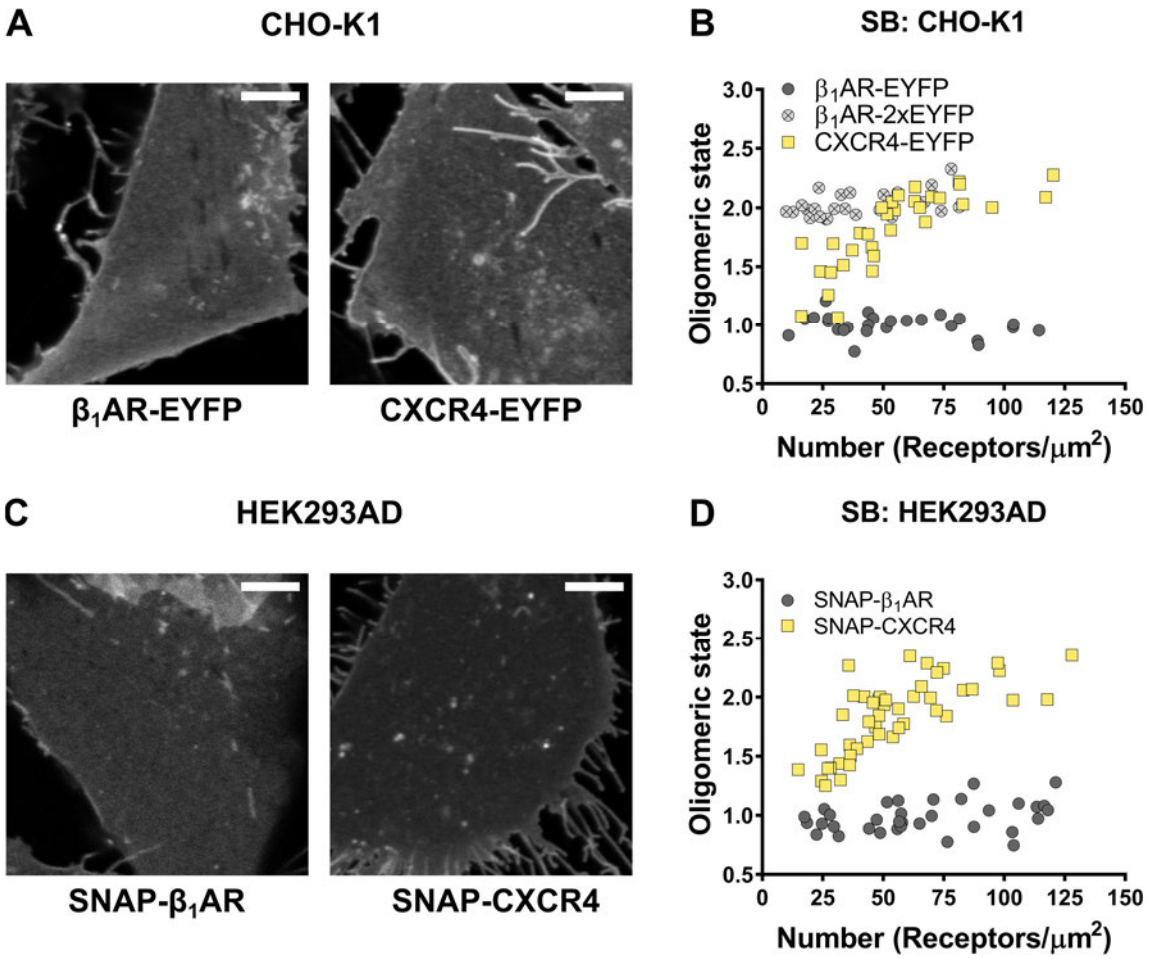

Figure 5-15. SB analysis of CXCR4 in a non-human cell line and with a different label. (A) Representative confocal images of the basolateral membranes of CHO-K1 cells expressing β_1AR-EYFP (left) or CXCR4-EYFP (right). (B) Oligomeric state of the controls and CXCR4-EYFP in CHO-K1 cells, plotted as a function of receptor density. Each data point represents the *N* and ε values calculated from a single cell and ε value and normalized to the monomeric control. (C) Representative confocal images of the basolateral membranes of HEK293AD cells expressing Snap Surface AF488 labeled SNAP-β_1AR (left) or SNAP-CXCR4 (right). (D) Density-dependence of brightness for SNAP-CXCR4 and SNAP-β_1AR expressed and imaged in HEK293AD cells. Data points are obtained as in (B). Confocal image scale bar (white): 5μm.

As mentioned previously, the presence of a protein (unlabeled, or labeled with a different fluorophore than which brightness is measured for) that competes for oligomerization with CXCR4 promotes a decrease in the number of CXCR4 homodimer. As a result, the observed dimeric brightness for CXCR4 would diminish (Figure 5-16A). Thus, this would confirm that the observed dimeric CXCR4-EYFP brightness is a result of real dimerization. To test this, HEK293AD cells were co-transfected with β_1AR-EYFP and SNAP-β_1AR, or with CXCR4-EYFP and SNAP-CXCR4. After labeling with SNAP Surface Alexa Fluor 647, SB measurements were performed and EYFP brightness was analyzed. Compared to β_1AR-EYFP alone, expression of SNAP-β_1AR alongside β_1AR-EYFP did not reduce the brightness of β_1AR-EYFP, confirming that even at the expression levels studied here, β_1AR is truly monomeric. On the other hand, co-expressing SNAP-CXCR4 with CXCR4-EYFP remarkably reduced the dimeric CXCR4-EYFP brightness, supporting that at high expression levels CXCR4-EYFP is truly dimeric (Figure 5-16B).

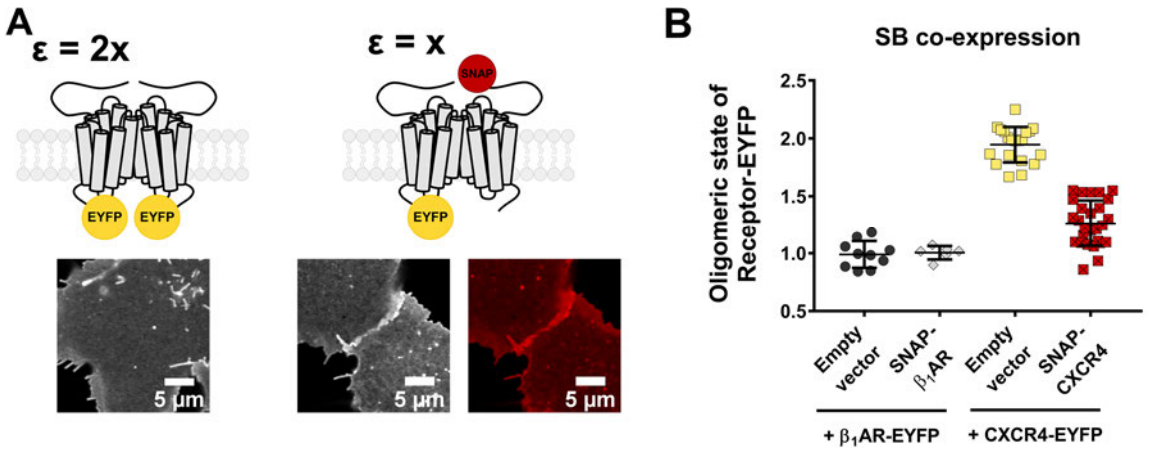

Figure 5-16. Spatial brightness analysis of dimer dilution by coexpression. (A) Schematics of the dimer dilution experiments: SNAP-CXCR4 dimerization with CXCR4-EYFP (upper right) results in lower ε than a CXCR4-EYFP homodimer (upper left). Representative images of HEK293AD cells co-expressing CXCR4-EYFP (lower right, grey) + SNAP-CXCR4 labeled with SNAP Surface 647 (lower right, red), and CXCR4-EYFP (lower left, grey) + empty vector as negative control. (B) SB analysis of HEK293AD cells co-expressing β_1AR-EYFP + vehicle (dark grey), β_1AR-EYFP + SNAP-β_1AR (light grey), CXCR4-EYFP + empty vector (yellow) and CXCR4-EYFP + SNAP-CXCR4 (red). The data are displayed with mean ± SD from 3 independent experiments.

5.2.4. Validation of CXCR4 Dimerization Using FRET Acceptor Photobleaching

Although brightness-based methods can robustly report the average oligomeric status of GPCRs, they have a number of limitations. For example, compared to RET methods, FFS based methods do not report direct interactions. Rather, FFS associates co-diffusion of particles to oligomerization. Therefore, if two (or more) protomers of a GPCR, without necessarily interacting, bind to a common partner and diffuse, they may appear as oligomeric complexes on brightness analysis. To test whether this may be the reason that CXCR4 appears dimeric on brightness analysis, the FRET acceptor photobleaching, which directly assess specific protein-protein interactions, was used as an independent method. This method provides the average FRET efficiency between donor and acceptor fluorophores, as measured upon photobleaching of the acceptor fluorophore. Since FRET occurs in distances shorter than 10 nm, it reliably reports direct protein-protein interactions.

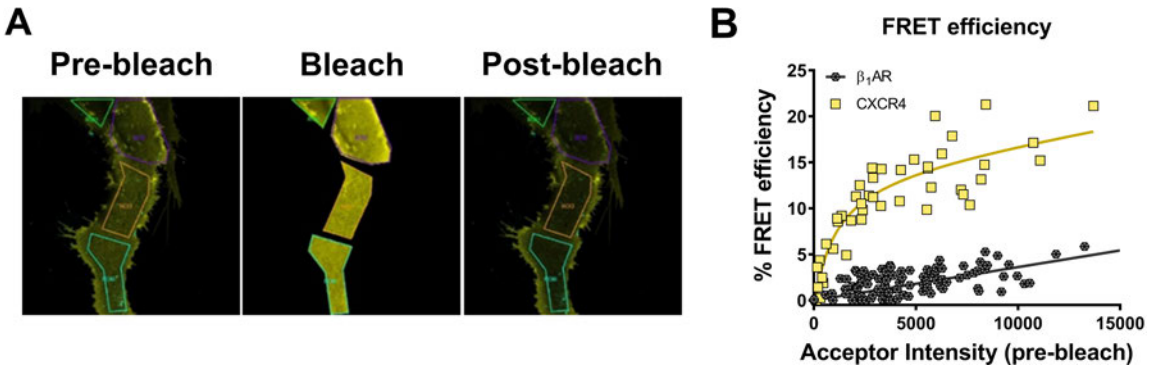

Figure 5-17. FRET Acceptor Photobleaching analysis of CXCR4 dimerization. (A) A representative acceptor photobleaching routine using the confocal microscope. After identifying a cell that expressed both donor and acceptor fluorophores, a snapshot of the donor and acceptor channel was taken before and after acceptor photobleaching. To calculate the FRET efficiency, percentage increase in the fluorescence intensity of the donor channel was calculated. (B) FRET acceptor photobleaching experiment in HEK293AD cells co-expressing CXCR4-ECFP and CXCR4-EYFP (yellow) or β_1AR-ECFP and β_1AR-EYFP (grey). Each data point is obtained from a single cell. For each dataset, a total binding fit and a straight line fit were compared and the best fit was applied.

To measure CXCR4 homodimerization using FRET AB, HEK AD cells transiently transfected with CXCR4-ECFP and CXCR4-EYFP were used. As control, cells expressing β_1AR-ECFP and β_1AR-EYFP were assessed. The FRET efficiency was measured on the

basolateral cell membranes, avoiding the heterogeneities (Figure 5-17A). After measurement, FRET efficiency values from each cell were plotted against acceptor fluorescence intensity. In this plot, a hyperbolic increase of FRET efficiency values as a function acceptor intensity was observed for CXCR4-ECFP and CXCR4-EYFP, implying specific CXCR4-CXCR4 interactions (Vilardaga et al., 2008). On the other hand, FRET efficiency results obtained from β_1AR expressing cells displayed a linear increase as a function acceptor intensity, which indicates nonspecific interaction between β_1AR-ECFP and β_1AR-EYFP as a function acceptor intensity (Figure 5-17B).

5.2.5. Agonist-Mediated Changes in CXCR4 Oligomerization

Previous studies on diverse GPCRs suggested distinct effects of ligands on receptor oligomerization (Ge et al., 2017; Martínez-Muñoz, Rodríguez-Frade, et al., 2018). Therefore, having confirmed the dimeric footprint of CXCR4 at high expression, the effect of CXCR4 ligands on receptor quaternary organization was assessed next. For this, SB analysis was used in HEK293AD cells expressing CXCR4-EYFP. For these experiments, cells expressing more than 50 receptors/μm^2 were used, as at this expression level CXCR4 is prevalently dimeric. Firstly, the effect of the agonist, CXCL12, was assessed. Cells expressing CXCR4-EYFP were treated with saturating concentrations of CXCL12 (100 nM), and brightness was assessed at different time points. After 1 min of agonist stimulation, the already-dimeric status of CXCR4 did not change remarkably. However, at later time points, CXCR4 cluster formation was observed at up to 5 molecules per cluster in average (Figure 5-18A). Moreover, stimulation with different concentrations of CXCL12 for 20 minutes revealed distinct oligomerization profiles: While 1 nM of CXCL12 did not alter the basal dimeric status, 10 nM CXCL12 increased the oligomer size to roughly trimers on average, and 100 nM CXCL12 further increased the cluster size (Figure 5-18A). It is known that agonist stimulation activates GPCRs, which prompts β-arrestin recruitment and subsequent internalization of the receptor. To understand whether the agonist induced CXCR4 clusters were associated with internalization, CXCR4-EYFP was imaged with mCherry labeled μ2 subunit of the adaptor protein 2 (mCherry-AP2μ2), which is a protein used as a clathrin coated pit (CCP) marker (Pearse et al., 2000). Imaging the basolateral membranes of HEK293AD cells after 100 nM CXCL12 stimulation for 20 min revealed

that a large number of CXCR4-EYFP clusters co-localized with AP2µ2-mCherry, indicating that these clusters may be in the process of being internalized (Figure 5-18B).

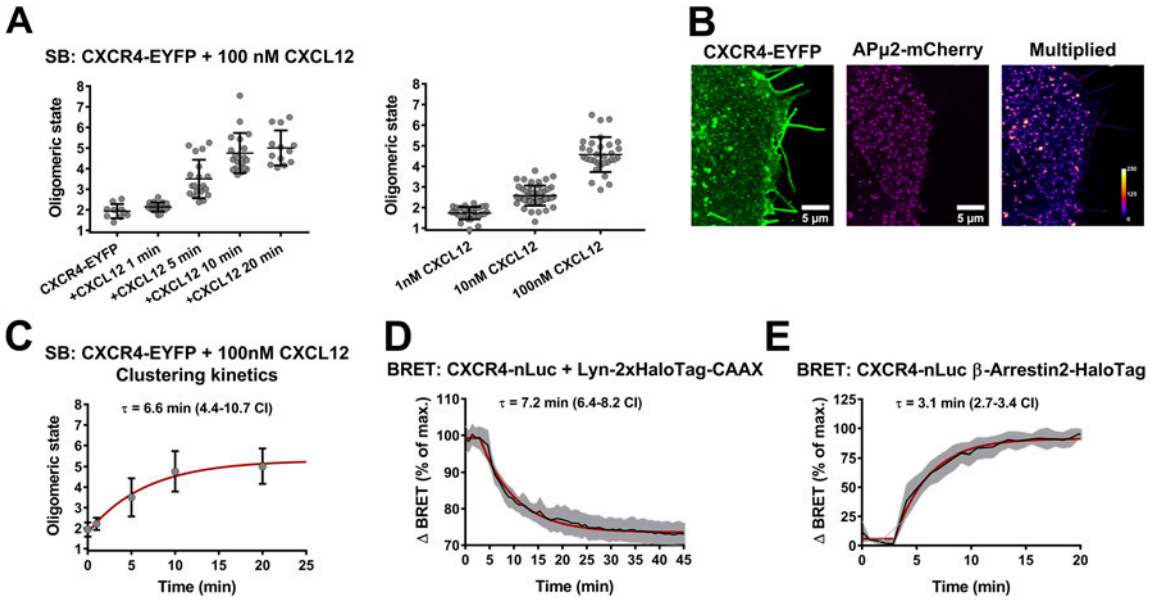

Figure 5-18. Agonist-mediated clustering of CXCR4. (A and B) SpIDA-based brightness measurement of CXCR4-EYFP as a time-course with 100 nM CXCL12 (A) and effect of different concentrations of CXCL12 measured after 20 minutes of ligand exposure (B). Each data point represents monomer-normalized brightness value obtained from a single cell. Data is shown with mean ± SD. (C) Representative confocal microscopy image of CXCR4-EYFP and AP2µ2-mCherry after 20 min exposure to 100 nM CXCL12. Merge image displays colocalization of CXC4 clusters with AP2µ2. (D) Kinetic representation of CXCR4 clustering via CXCL12. Each data point represents the mean ± SD of the data in A. (E and F) Kinetic BRET measurement of β-arrestin2 recruitment (E) and receptor internalization (F) after stimulation with 100 nM CXCL12. Data is shown as mean (black curves) ± SD (gray shades) from 3 independent plate reader experiments (D, E and F). Tau values were obtained by fitting an "exponential decay followed by plateau" function (red curves).

Next, the kinetics of receptor clustering, β-arrestin recruitment and internalization processes were assessed in order to understand the temporal relations of these processes. In order to measure β-arrestin recruitment to CXCR4, a BRET based receptor-arrestin interaction assay was used. HEK293AD cells were transfected with CXCR4-nLuc and β-arrestin2-HaloTag, then they were labeled with HaloTag 618 dye, and measurements were performed in a 96-well plate. Similarly, CXCR4 internalization was measured using another BRET based assay in HEK293AD cells at 96-well plate format, in which the non-specific interaction of CXCR4 with a membrane-bound, non-internalizing protein construct was used. This construct is made up of two HaloTag proteins separated by a 60 nm

rigid protein linker, an N-terminal membrane targeting sequence of Lyn and a C-terminal membrane targeting CAAX (C, cysteine; A, any aliphatic amino acid; X, any amino acid) motif, and is dubbed as Lyn-2xHalo-CAAX. Both BRET measurements were performed in a kinetic manner upon addition of 100 nM CXCL12. Analyzing time traces of β-arrestin recruitment and internalization revealed that the temporal kinetics of CXCR4 clustering (Figure 5-18C) and internalization (Figure 5-18D) were in good correlation, while the kinetics of arrestin recruitment (Figure 5-18E) preceded both. Together, these results agree that formation of CXCR4 higher order oligomers correlate both in time and space with the internalization process of CXCR4.

5.2.6. Effect of Antagonists/Inverse Agonists in CXCR4 Oligomerization

Next, the effect of diverse inhibitors of CXCR4 were measured. The word "diverse" here addresses to structural/chemical diversity of the inhibitors used: the bicyclam antagonist AMD3100, the N-pyridinylmethylene cyclam antagonist AMD3465, the isothiourea derivate small molecule IT1t, the cyclic peptides LY2510924 and FC131, and a recently characterized nanobody VUN401. In cells treated for 20 minutes with individual ligands, SB analysis of CXCR4-EYFP showed ligand specific changes in oligomerization (Figure 5-20A): The cyclam antagonists AMD3100 (Figure 5-19A) and AMD3465 (Figure 5-19B) did not alter the basal dimeric status. Only a slight decrease was observed with TC14012 (Figure 5-19C). While LY2510924 (Figure 5-19D) and IT1t (Figure 5-19E) significantly decreased the basal dimeric status, FC131 (Figure 5-19F) and the nanobody VUN401 (Figure 5-19G) completely disrupted CXCR4 dimerization.

As the next step, the kinetics of dimer disruption by IT1t, FC131 and VUN401 was assessed using SB. For this, cells expressing CXCR4-EYFP in a coverslip was stimulated with one of the ligands, and SB images of different cells were acquired each 30 seconds. Here, a bottom density threshold was set during the analysis in order to ensure that the cells analyzed exhibited concentrations at which CXCR4-EYFP is dimeric (>50 receptors/μm^2 membrane area). Results of this experiment showed that all ligands were able to induce

dimer destabilization within the first 30 seconds of stimulation. The equilibrium was observed with a τ-value of 50 s (30 to 84 CI) for FC131 and τ of 46 s (30 to 72 CI) for IT1t, while the nanobody VUN401 exhibited a more rapid dimer disruption, with a τ of 17 s (0 to 50 CI).

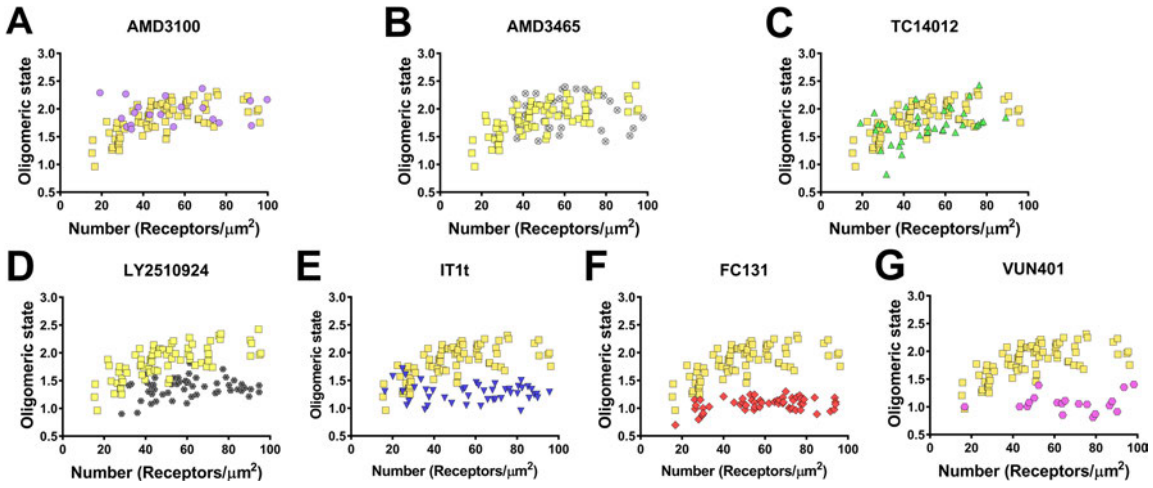

Figure 5-19. : Density dependence of CXCR4-EYFP brightness under antagonist treatment. (A-E) Normalized brightness values from cells expressing CXCR4-EYFP and treated with 10μM AMD3100 (A) and 10μM AMD3465 (B), 10μM TC14012 (C), 100nM LY2510924 (D), 10μM IT1t (E), 10μM FC131 (F), and 10μM VUN401 (G). Each data point represents the monomer control-normalized brightness value from single cells.

Temporal brightness analysis of CXCR4-EYFP with ligands was also performed to verify the effects of the ligands. Results from both TB and SB analysis were in good correlation for all tested ligands (Figure 5-20C). Because TB and SB analysis are based on the same mathematical theory, an independent assay was needed to verify the ligand effects on CXCR4 dimerization. For this purpose, FRET acceptor photobleaching (FRET AB) was used. This time, before evaluating the FRET efficiency, cells expressing CXCR4-EYFP and CXCR4 ECFP were treated with the ligands that reduced CXCR4 dimerization significantly in brightness analyses. Results showed that the FRET efficiencies at increasing acceptor intensities exhibited a linear increase that could not be fit to a hyperbola, indicating a diminished CXCR4-CXCR4 interaction. On the other hand, FRET efficiencies with LY2510924 could be fit with a hyperbolic function, but the dissociation constant (K_d) of the fit was 20,587 intensity units (IU), which is approximately 30 times lower compared to which observed for basal condition (K_d = 700 IU), indicating a reduced, but still apparent

CXCR4 homodimerization (Figure 5-20D). Together, FRET AB results also support the conclusions of brightness analyses and suggests a true dimeric organization of CXCR4.

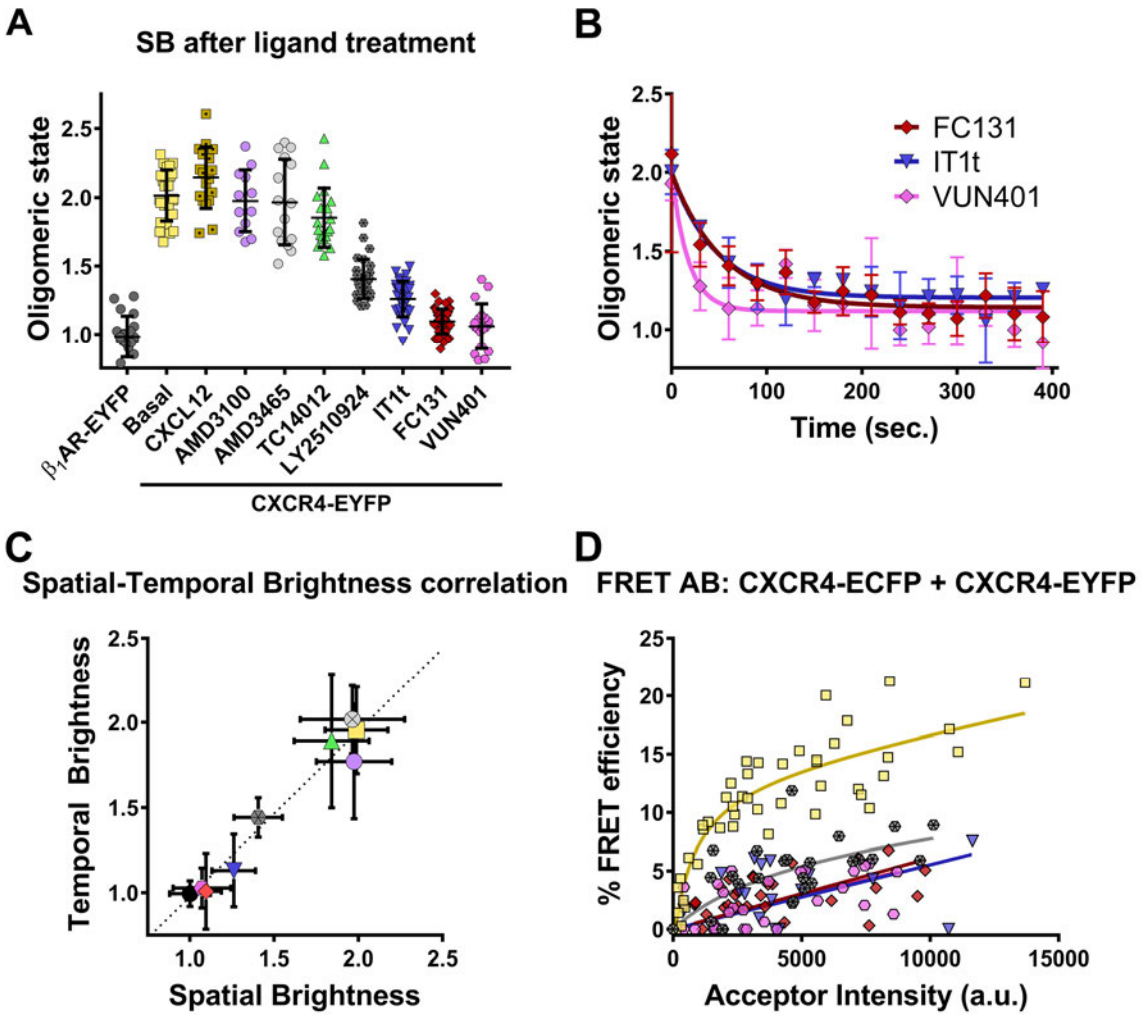

Figure 5-20. Antagonist-mediated modulation of CXCR4 dimerization. (A) SB analysis of HEK293AD cells expressing β_1AR-EYFP or CXCR4-EYFP, and CXCR4-EYFP after 20 minutes of incubation with ligands: 10 µM AMD3100, 10 µM AMD3465, 10 µM TC14012, 100 nM LY2510924, 10 µM IT1t, 10 µM FC131 and 1 µM VUN401. Each data point is a brightness value from one cell normalized to the monomer control, given with mean ± SD. (B) SB kinetics of dimer destabilization by VUN401, IT1t and FC131. Different cells were imaged for SpIDA analysis for 20 minutes at 30 second intervals upon ligand addition. Plotted mean ± SD data over time were fitted to a mono-exponential decay function. (C) Correlation of average oligomeric states (with SD) obtained from SpIDA (x-axis) and temporal brightness measurements (y-axis). Color code of the data points is the same as in Fig. 3A. Black straight line is the linear fit of the data (slope: 0.94 (0.873-1.014 CI)), representing the degree of correlation for two methods. (D) FRET acceptor photobleaching experiment in HEK293AD cells co-expressing CXCR4-ECFP and CXCR4-EYFP. Each data point is obtained from a single cell. Color code of the data points is the same as in Figure 3A. All data were obtained from at least 3 experiments per condition.

When summed up, all these results with TB, SB and FRET AB suggests a distinct, ligand specific modulation of CXCR4 dimerization. While T14012 induces only a modest decrease of dimerization, LY2510924 and IT1t disrupts dimers more prominently. However, the other cyclic peptide FC131 and the nanobody VUN401 disrupts the dimers completely and leads to an absolute monomeric equilibrium. Two small molecules containing cyclam moieties, AMD3100 and AMD3465 do not change the basal dimeric organization of CXCR4.

5.2.7. Molecular Determinants of CXCR4 Oligomerization

Having observed that ligands affect basal CXCR4 dimerization to different extends, the next question was what causes this distinct profile. To understand this, the possible contribution of a number of factors regarding CXCR4 activity and interactions in light of ligands were assessed.

5.2.7.1. Contribution of CXCR4 Activity

First, the possible contribution of CXCR4 activity on basal receptor dimerization was assessed. Since CXCR4 is a Gi-coupled GPCR, a FRET-based Gi_2 activation biosensor was used to measure the receptor activity. This biosensor reports Gi_2 protein activation as a decrease in FRET response that is mediated by separation of donor/acceptor labeled Gα and Gβγ subunits (Figure 5-21A). As expected, stimulation of cells expressing CXCR4 and the Gi_2 sensor with 100 nM CXCL12 produced a 13% decrease in FRET, while stimulation with vehicle (HBSS) did not induce any detectable FRET change, indicating agonist mediated Gi_2 sensor activation. AMD3100, AND3465 and VUN401 did not induce any FRET change at saturating concentrations. In stark contrast, the inhibitors TC14012, LY2510924, IT1t and FC131 induced an increase in FRET, indicating inactivation of the Gi_2 sensor (Figure 5-21B). These results implied a certain basal Gi_2 activity in cells expressing CXCR4, which can be reversed with a number of CXCR4 inhibitors. To further test this basal activity, cells expressing Gi_2 sensor and CXCR4 were treated with Pertussis toxin (PTx, an inhibitor of Gαi activity) or vehicle overnight, and basal BRET ratios were

measured. Compared to the cells treated with vehicle, a roughly 5% higher basal FRET ratio was observed in cells treated with PTx (Figure 5-21B, black line). These results indicate that CXCR4 expression causes a certain level of basal activity on the Gi_2 protein, which can be reversed by stimulation with PTx, or the CXCR4 inhibitors TC14012, LY2510924, IT1t or FC131.

To further understand whether these ligands are truly inverse agonists, Gi_2 biosensor experiments were performed in the presence of a constitutively active mutant of CXCR4 (CAM CXCR4, produced by mutating Asp119$^{3.35}$ to Ser (N119$^{3.35}$S). Cells expressing CAM CXCR4 exhibited roughly 15% lower basal FRET ratio in the Gi_2 sensor compared to which observed in cells expressing wild type CXCR4 (WT CXCR4), confirming the constitutive activity of the N119$^{3.35}$S mutant (Figure 5-21C). CXCL12 and AMD3100 further decreased FRET roughly by 3-4% with this mutant, while AMD3465 and VUN401 did not induce a remarkable change in FRET. On the other hand, TC14012, LY2510924, IT1t and FC131 produced a prominent increase in FRET, suggesting that these ligands act as inverse agonists both on the WT and CAM CXCR4 (Figure 5-21D). Despite being as effective as the other ligands on the CAM CXCR4 basal activity, TC14012 was only a weak inverse agonist on the WT CXCR4 at the G protein level, while AMD3100 acted as a partial agonist.

In order to understand further details of ligand effects on CXCR4 downstream signaling, CXCR4-G protein interaction was assessed using a BRET based measurement between CXCR4-nLuc and $G\gamma_2$ proteins. In this assay, the agonist CXCL12 induced a concentration dependent BRET decrease (Figure 5-22A). AMD3100 and AMD3465 did not induce any BRET change at any concentrations tested. In contrast, all other ligands induced a concentration dependent BRET increase with varying potency and efficacy values. Surprisingly, VUN401 produced the largest BRET increase compared to the other ligands. This suggests that, despite not affecting the basal Gi_2 activity at all, VUN401 still induces a conformational change between CXCR4 and the G protein (Figure 5-22B).

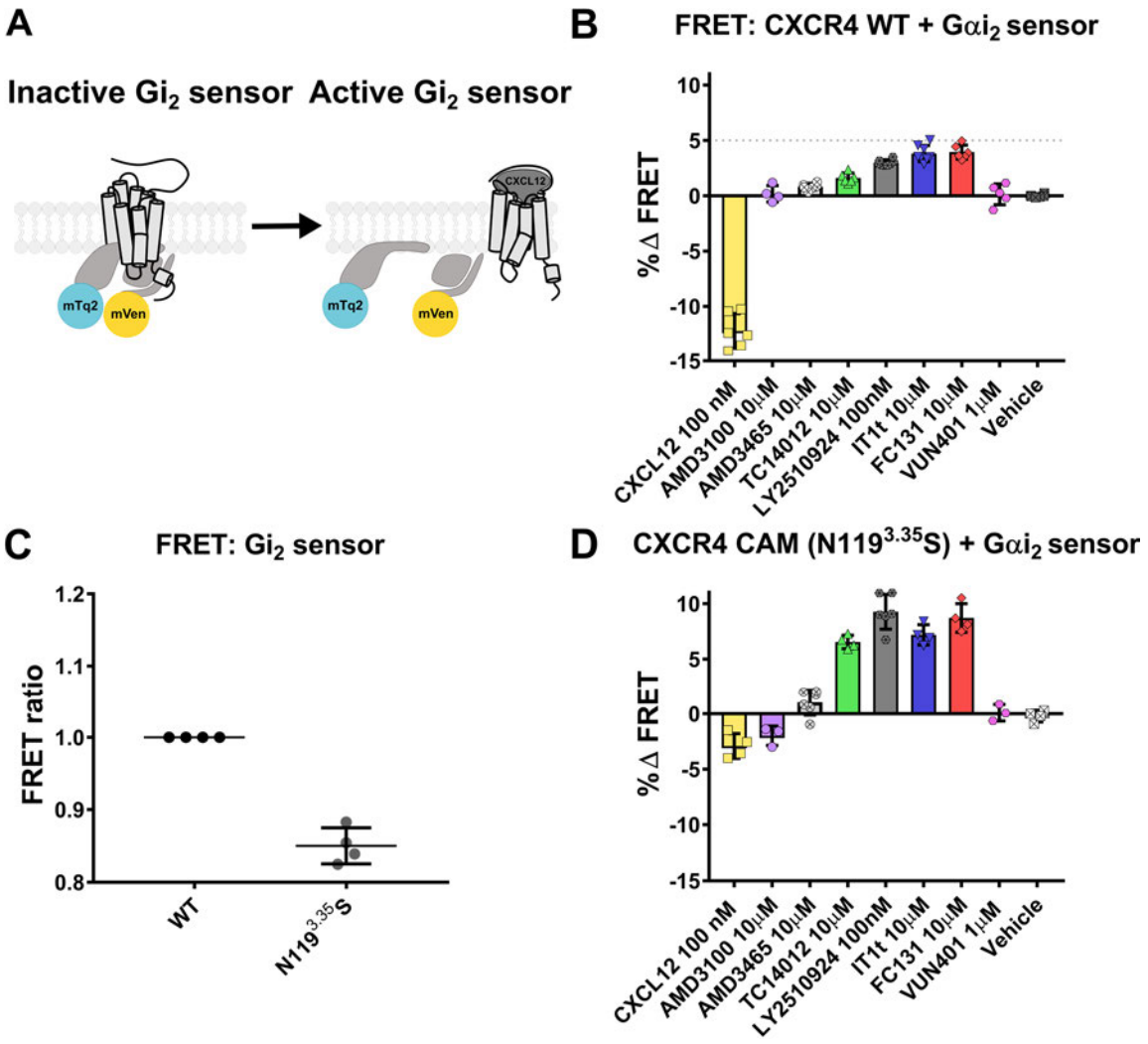

Figure 5-21. Constitutive G protein activation by CXCR4. (A) Schematics of the FRET based Gi_2 activation measurement. Gi_2 sensor is in the high FRET conformation at the resting state. CXCL12 binding to CXCR4 induces a lower FRET state of the sensor. (B) %FRET changes in the Gi_2 sensor by CXCR4 ligands. Scatter dot plots with bars show % average FRET changes in 20 minutes after the addition of different ligands. The grey line represents the average ΔFRET resulting from PTx treatment. (B) Data points represent FRET ratios of Gi_2 FRET sensor co-expressed with either WT CXCR4 (black) or CAM CXCR4 (grey) and normalized to the data from WT CXCR4 of the same plate. $N119^{3.35}S$ mutant mediates higher basal activity of Gi_2 protein than WT CXCR4, as it displays a lower FRET ratio at basal state. (C) Measurement of Gi activation by CAM CXCR4 using the Gi_2 FRET sensor with different CXCR4 ligands. Scatter dot plots with bars represent ligand mediated FRET change (mean ± SD) relative to basal in mean with SD of at least 3 different plate reader experiments.

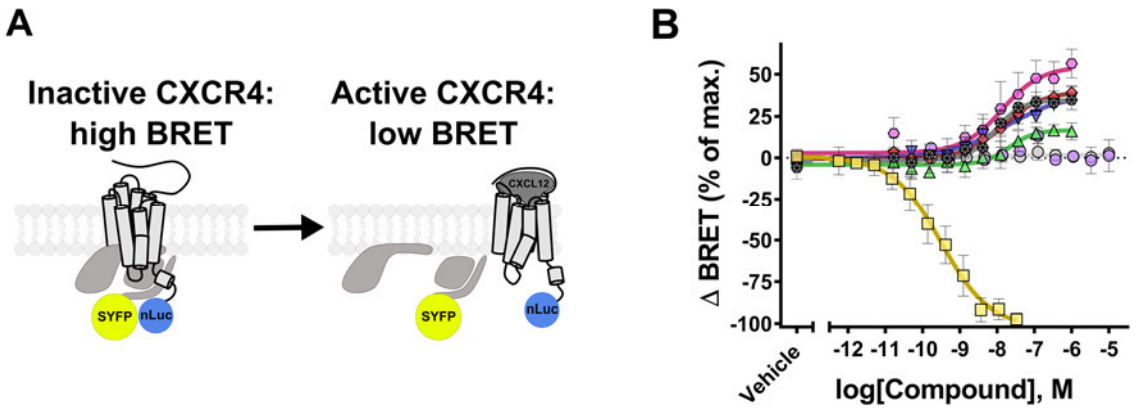

Figure 5-22. Ligand mediated modulation of CXCR4-Gγ_2 interactions by means of BRET. (A) Schematics of the BRET measurement between CXCR4-nLuc and Gγ_2-SYFP. At the basal state, CXCR4-nLuc and Gγ_2-SYFP are at BRET distance. CXCL12 binding to CXCR4-nLuc results in a decrease in BRET. (B) Concentration-response curves obtained by fitting the data to a four-parameter Hill equation. Obtained pEC_{50} values: CXCL12: 9.5 (9.7 to 9.3 CI); LY2510924: 8.1 (8.2 to -7.9 CI); TC14012: 7.7 (8.0 to 7.3 CI); IT1t: 7.8 (8.3 to 5.7 CI); VUN401: 7.9 (8.3 to 6.6 CI). Color code of the data points is the same as in Figure 3A. Data points at each concentration show the mean ± SD from at least 3 independent plate reader experiments.

The general conclusion regarding the Gi_2 activity analysis is that a number of CXCR4 ligands inhibits the basal activity of the receptor to varying levels, while some of the ligands behave as pure antagonists. In light of these results, the effects of ligands on dimerization and basal activity were compared. Simply, the average oligomer status was plotted against the percentage of inhibition in basal activity for each ligand. This plot displayed a clear positive correlation between the dimeric status and basal activity of CXCR4 under diverse ligand treatment (Figure 5-23). Simulating a linear fit with ideal conditions (zero basal activity corresponding to monomeric CXCR4 and 100% basal activity to dimeric receptor, thus the slope of the line is 1) and the experimental fit resulted in a nearly identical slope, verifying the high correlation between the basal activity and dimeric organization of CXCR4. The only ligand that deviated from this correlation was the nanobody VUN401. While VUN401 disrupted CXCR4 dimers efficiently, it failed to produce any change on the CXCR4 basal activity, yet induced conformational changes between the receptor and the G protein.

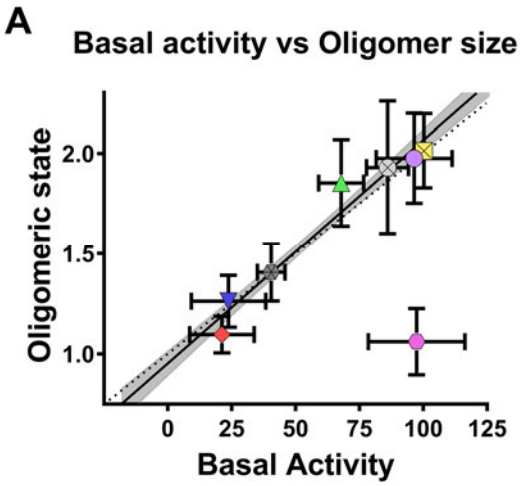

Figure 5-23. Correlation plot of CXCR4 basal activity and oligomeric state. Oligomeric state values were obtained from the data given with SD error bars in Figure 5-20A. Basal activity data (with SD error bars) was generated by normalizing the data in Figure 5-21B to %ΔFRET of PTx (as 0%) and vehicle treatment (as 100%). The dotted line shows the assumed pseudo-correlation, and the black line is the actual fit (VUN401 was identified as an outlier of the 95% CI (in grey). Color code of the data points is the same as in Figure 3A.

5.2.7.2. Contribution of G proteins and β-arrestins

Results of the previous section suggested a positive correlation between CXCR4 activity and dimerization. Therefore, the next question was whether the intracellular signal transducers that couple to CXCR4 may play a role in dimer formation. Upon agonist binding, CXCR4 can activate Gi proteins. Moreover, a baseline Gi protein activation mediated by CXCR4 is already present. Next to this, β-arrestin1 and 2 are recruited to agonist bound CXCR4. Therefore, CXCR4 oligomer state was assessed in the absence of Gα protein subunits or β-arrestins. To do so, SB analysis on CXCR4-EYFP was performed in HEK293 cells devoid of all genes encoding functional Gαs, Gαq, Gαi, and Gα12/13 proteins (ΔGα HEK293) or β-arrestin1/2 (Δβarr HEK293). In both cell lines, CXCR4 still displayed a dimeric organization at expression levels above 50 receptors/μm^2 membrane area. Moreover, IT1t, FC131 and VUN401 were still able to disrupt these dimers, while AMD3100 and TC14012 did not cause any remarkable dimer disruption: a similar pattern also observed in cells expressing all Gα subunits and β-arrestin1/2 proteins (Figure 5-24).

In conclusion, these results suggested that the absence of Gα subunits or β-arrestin1/2 did not affect the dimeric status of CXCR4 at high expression levels.

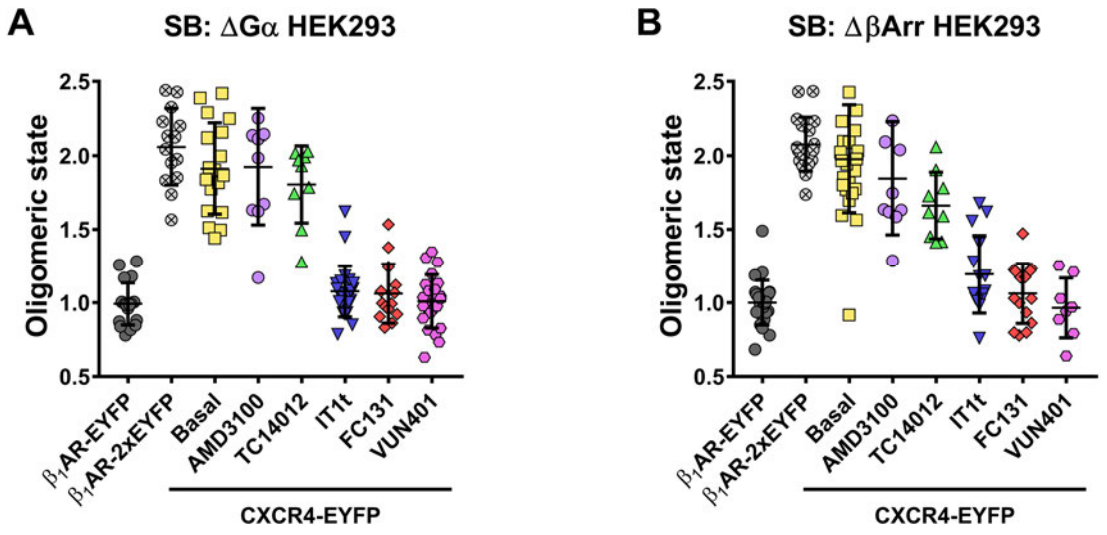

Figure 5-24. Oligomerization analysis of CXCR4-EYFP in cells lacking functional Gα subunits or β-arrestins. SB analysis in HEK293 cells devoid of Gα subunits (A) or β-arrestin1/2 (B). Analyzed are β_1AR-EYFP, β_1AR-2xEYFP and CXCR4-EYFP at basal level, and CXCR4-EYFP post-exposure to the ligands for 20 minutes at concentrations given in Fig. 5A. Each data point represents the oligomeric state calculated from one cell. Each dataset is given with mean ± SD.

5.2.7.3. Contribution of Ligand Binding Modes

Previous sections suggested a pattern correlating the ligand effect on receptor dimerization and basal activity. In order to understand whether ligand binding modes have any impact on these actions, bioinformatics analyses were performed. Using the crystal structure of CXCR4 (PDB ID: 3OE0), docking experiments were performed under the guidance of the experimental data, where binding of CXCR4 ligands on different binding pocket mutants were tested. Thus, the obtained binding poses reflect the experimentally observed structure-activity relationship. This approach revealed binding poses of each ligand (Figure 5-25A), and that the CXCR4 residues that interact with ligands could be grouped in two sub pockets and an extracellular domain, which were previously described by structural analyses (Figure 5-25C).

According to the observed binding poses, the nanobody VUN401 is accommodated on the extracellular moieties of CXCR4, forming a specific contact with the R30$^{1.24}$ residue (Figure 5-25B). AMD3100 (Figure 5-25D and Figure 5-26A), AMD3465 (Figure 5-25E and Figure 5-26B) and TC14012 (Figure 5-25F and Figure 5-26C) appear to be accommodated almost exclusively in the major binding pocket forming specific interactions with the acidic residues Asp171$^{4.60}$ of the TM4 and Asp262$^{6.58}$ of the TM6. In contrast, the ligands that reduced CXCR4 dimerization and inhibited the basal activity form contacts with the minor pocket residues. IT1t (Figure 5-25H and Figure 5-26E) is exclusively accommodated in the minor pocket, interacting with the TM2 residues Trp94$^{2.60}$, Asp97$^{2.63}$, and Tyr116$^{3.32}$. FC131 (Figure 5-25G and Figure 5-26D) exhibited a hybrid binding mode, forming interactions with the residues in both sub pockets: its L-Arg^{2} residue extends toward the minor pocket to form an ionic contact with Asp97$^{2.63}$ (TM2) and it forms a cation pi interaction with Tyr116$^{3.32}$ of the major pocket. It was not possible to find an experimentally validated binding pose of the other dimer destabilizing ligand, LY2510924, due to the lack of binding experiments with this ligand on different binding pocket mutants of CXCR4. Yet, in the only publication in which LY2510924 is described, this ligand is shown to exhibit a hybrid binding, similar to that of FC131. It is shown that LY2510924 extends towards the minor pocket by forming contact with His113$^{3.29}$ and Glu288$^{7.39}$ residues, and binds to the major pocket via interactions with Asp187$^{45.51}$, Arg188$^{45.52}$, Tyr190$^{45.54}$, and Gln200$^{5.39}$ (Figure 5-26F).

Overall, the ligand poses on CXCR4 crystal structure display a pattern that correlates with the ligand-mediated effects on receptor dimerization and basal activity: The ligands that form contacts with the minor pocket residues are the ones that effectively disrupt CXCR4 dimers and diminish the basal Gi_2 activity. On the other hand, ligands that are not able to induce significant changes in basal CXCR4 dimerization and baseline Gi_2 activity exclusively bind to the major pocket of the receptor.

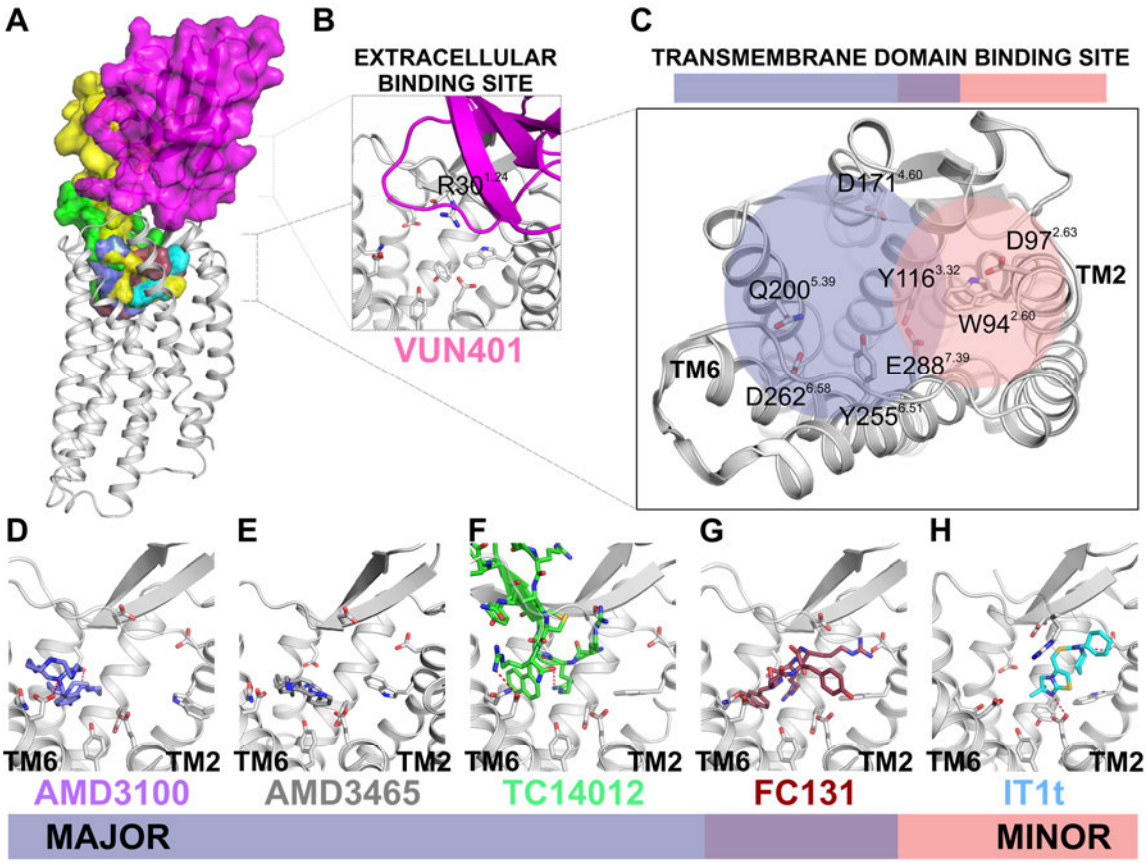

I

Ligand \ Residue	R1.24	D4.60	Q5.39	Y6.51	D6.58	Y3.32	E7.39	W2.60	D2.63
AMD3100		■			■		■		
AMD3465		■			■		■		
TC14012		■	■		■				
IT1t						■	■	■	■
FC131		■		■		■			■
VUN401	■								

Figure 5-25. Binding modes of different CXCR4 ligands. (A) Overview of the CXCR4 crystal structure (PDB ID: 3OE0, grey cartoon) with docked VUN401 (magenta), TC14012 (green), AMD3100 (purple), FC131 (brown), CXCL12 (yellow), and IT1t (cyan), seen detailed in (B), (D), (E), (F) and (G). (B) Zoom-in view of the transmembrane domain binding site of CXCR4, where no VUN401 interactions are observed. VUN401 binds in view of the extracellular vestibule of CXCR4 and its epitope has been matched to the residue $R30^{1.24}$ in the CXCR4 N-terminus. (C) Top view of the CXCR4 transmembrane domain binding site, which can be divided into a minor pocket comprised by TM1-3 and TM7 (rose), and a major pocket, comprised by TM3-7 (purple). The side-chains of residues that have been experimentally validated to interact with CXCR4 ligands are presented in sticks in all binding mode representations. (D-G) Binding mode representations based on literature data of TC14012 (based on co-crystallized ligand CVX-15) (D), AMD3100 (E), FC131 (F) and IT1t (G). Images were placed from left to right to visualize the binding pose shift from major to minor pocket. (H) Overview of the CXCR4 residues that are in contact with ligands.

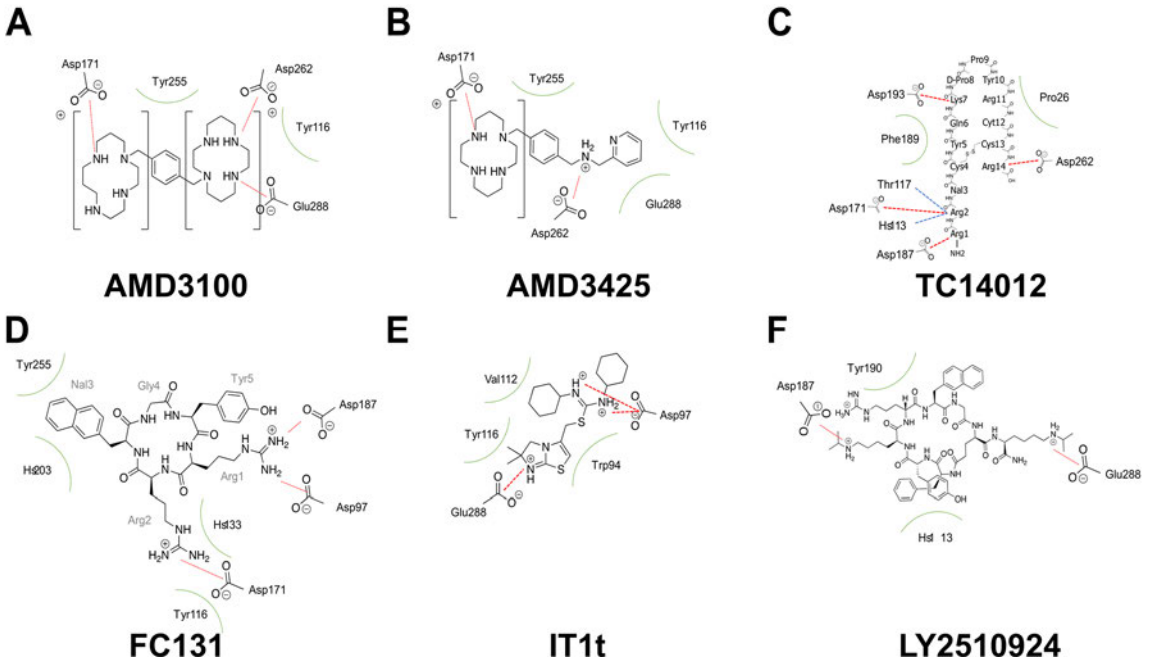

Figure 5-26. 2-D maps of ligand receptor interactions. (A-F) Ligand-receptor interaction sites as retrieved from docking. Each residue of CXCR4 that forms contact with the ligands is shown with their specific interaction types. Ionic interactions between residues and ligand atoms are shown with red lines, and hydrophobic interactions are shown as green arches.

To test experimentally whether the minor pocket binding indeed plays a role in modulating receptor dimerization, the minor pocket residue tyrosine (Y) 116 was mutated to serine (S) ($Y116^{3.32}S$), as this residue appears to be critical for FC131 and IT1t binding. Then, the oligomeric state of this mutant was assessed using SB. At densities above 60 molecules/μm^2 membrane area, $Y116^{3.32}S$ displayed a highly dimeric behavior. While 100 nM IT1t or FC131 were able to disrupt dimerization of WT CXCR4, these ligands were remarkably less efficient in destabilizing the $Y116^{3.32}S$ dimers (Figure 5-27).

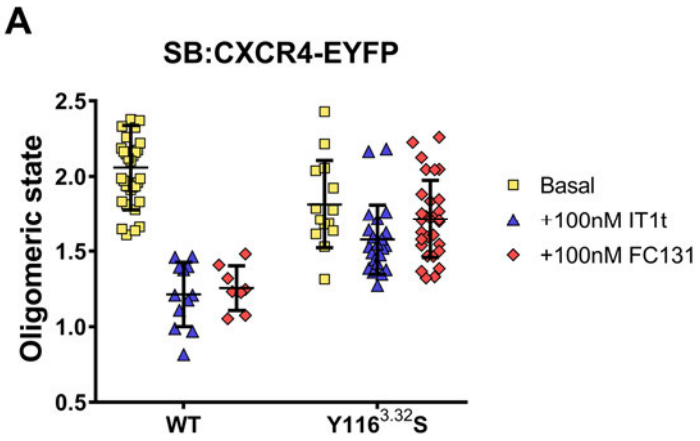

Figure 5-27. SB analysis of the WT CXCR4 and Y116$^{3.35}$S variant (yellow), after 20 minutes of incubation 100 nM IT1t (blue) and 10 µM FC131 (red). Each data point represents a brightness value from one cell normalized to the monomer control, given with mean ± SD as error bars. Data were obtained from at least 3 experiments per condition.

All together, these results demonstrated a correlation between the ligand binding mode in the transmembrane pockets and their ability to modulate the receptor dimerization.

5.2.7.4. Contribution of Receptor Conformations

Results of the previous sections suggest that CXCR4 exhibits a baseline Gi_2 signaling at the basal state. In class A GPCRs, basal activity is thought to be mediated by the shift of the equilibrium of receptor conformations towards the active conformation. In line with this, a number of ligands inhibit the basal CXCR4 signaling, which implies a shift of equilibrium towards inactive receptor conformation. Moreover, these ligands also disrupt receptor dimerization to distinct levels. In view of these observations, it can be hypothesized that 1) either the basally active receptor conformation is responsible for dimer formation, or 2) dimerization is responsible for receptor basal activity. The recent work of Wescott et al., in which distinct residues that control ligand binding, receptor activation and effector coupling were identified, aided in selecting the correct residues for mutagenesis. Among these residues, the TM6 residues valine (V) 242$^{6.38}$ and leucine (L) 246$^{6.42}$ reside in the center of the conserved signaling motifs of GPCRs and were proposed to regulate the micro switches that modulate CXCR4 activation by interacting with side chains of TM helices 5, 6, and 7 (Figure 5-28A). Therefore, the V242 to aspartate mutant

(V242$^{6.38}$D) and L246 to proline (L246$^{6.42}$P) were generated and these mutants were tested in terms of basal activity and dimerization.

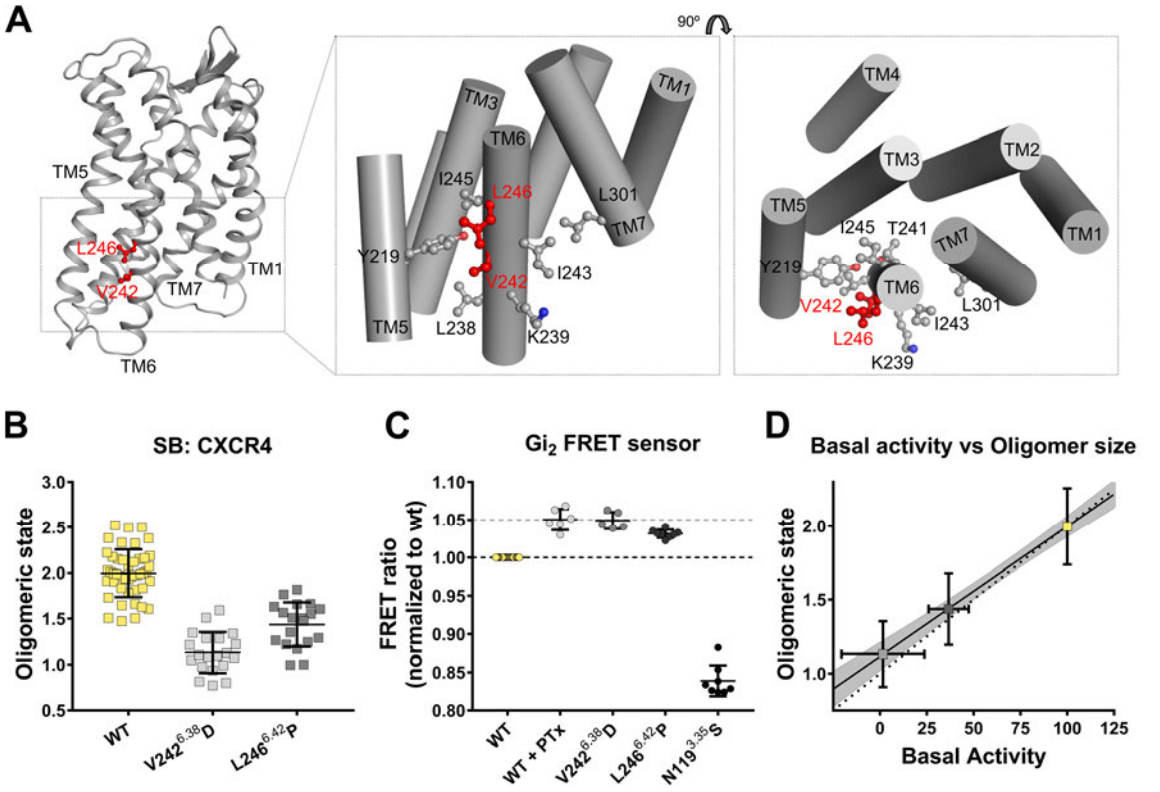

Figure 5-28. CXCR4 V242$^{6.38}$D and the L246$^{6.42}$P mutants are monomeric and display no basal or ligand-induced activity. (A) Position of the V242$^{6.38}$ residue on CXCR4 model (Ngo et al., 2020). V242$^{6.38}$ interacts with other TM6 residues (shown as sticks) and form a hydrophobic network that stabilize the micro switch residues on TM5 and 7 (shown as sticks), viewed from side (middle panel) and top (right panel). (B) SpIDA shows that the V242$^{6.38}$D mutant (light grey) is mainly monomeric and the L246$^{6.42}$P is largely monomeric in comparison to the WT CXCR4 (yellow). (C) V242$^{6.38}$D and L246$^{6.42}$P mutants display higher basal FRET ratios, (lower basal G protein activity), in comparison to the WT CXCR4 (yellow) on FRET-based Gi$_2$ sensor. PTx induced increase in FRET probes the basal activity of CXCR4. (D) Correlation plot of basal activity and oligomeric state for the TM6 mutants; data with SD error bars were derived from Fig. 6B and 6C. The dotted line indicates the pseudo-correlation. The black line with 95%CI (grey shades) is the actual fit (slope m=0.009 (0.008 to 0.010 CI))

In SB experiments, the V242$^{6.38}$D mutation exhibited a completely monomeric behavior as opposed to the WT CXCR4 (Figure 5-28B). Moreover, in the Gi$_2$ activation assay this mutant showed a noticeable reduction in basal Gi$_2$ activity (Figure 5-28C). None of the ligands tested on this receptor induced a FRET change in the Gi$_2$ biosensor (Figure 5-29A), suggesting that this mutant is absolutely signaling-deficient. Likewise, the

L246$^{6.42}$P displayed a reduced brightness compared to the WT CXCR4, yet it was not as monomeric as the V242$^{6.38}$D mutant (Figure 5-28B). The basal Gi_2 signaling via the L246$^{6.42}$P mutant was also diminished compared to the WT CXCR4, yet to a lesser extent compared to the V242$^{6.38}$D mutant (Figure 5-28C). Moreover, the partial basal activity of the L246$^{6.42}$P mutant was further reduced by the inverse agonists FC131 and IT1t (Figure 5-29B). Plotting the basal activity against the dimeric status of these mutants again showed a positive correlation between the receptor basal activity and the oligomer status (R = 0.7), further confirming the connection between these two features (Figure 5-28D).

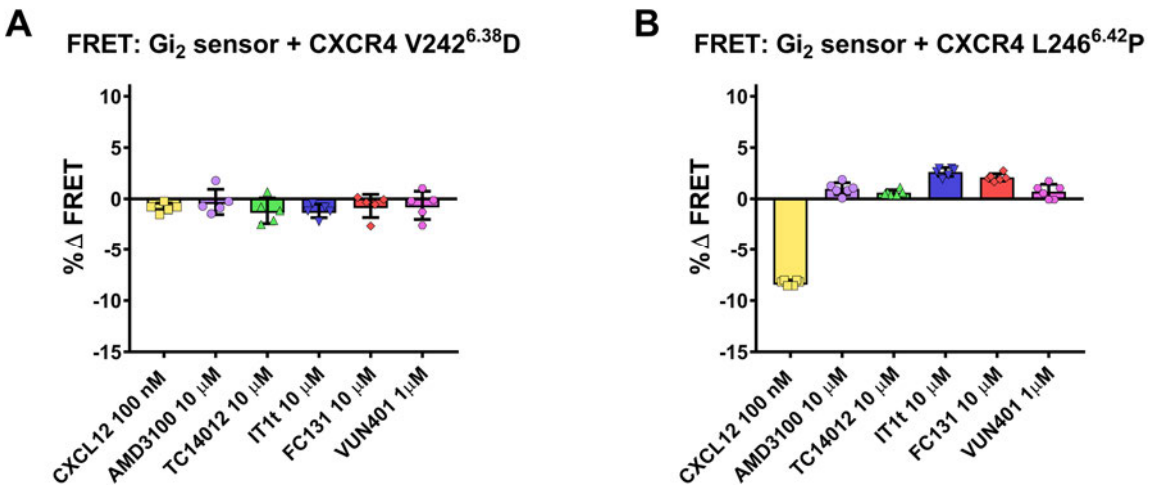

Figure 5-29. Assessment of Gi_2 protein activation by CXCR4 ligands on TM6 mutants. Measurement of Gi activation by CAM CXCR4 using the Gi_2 FRET sensor with different CXCR4 ligands for the V242$^{6.38}$D (A) and the L246$^{6.42}$P (B) mutants of the CXCR4. Scatter dot plots with bars represent ligand-mediated FRET change (mean ± SD) relative to basal in mean with SD of at least 3 different plate reader experiments.

All together, these results show that the mutations on critical micro switch residues of CXCR4 TM domains can reduce the basal signaling as well as receptor dimerization in a correlated manner. This observation suggests an important role of receptor conformation on dictating the receptor oligomer status.

5.3. Designing a Novel Biosensor to Detect CXCR4 Activation

Being in the center of immune regulation and progression of cancer and immune diseases, CXCR4 receives a great interest as a drug target. Hence, developing assays that report CXCR4 activation or signaling is crucial. Several genetically encoded biosensors and immunoassays reporting CXCR4 downstream signaling are already being used. However, only one biosensor to measure direct CXCR4 activation, which is based on an intramolecular CXCR4 FRET sensor, is available. To create a robust tool to measure CXCR4 conformational changes, two additional sensor designs were created and tested in this work.

5.3.1. BRET-Based CXCR4 Biosensor Design

The first design of choice was a BRET based intramolecular CXCR4 biosensor. This design is based on introducing a nanoluciferase (nLuc) and a HaloTag to the intracellular loops of the receptor. The design is based on the conformational changes in the transmembrane domains and relatively large distance changes at the intracellular tips of these structures. Numerous structural studies on class A GPCRs suggested that upon agonist binding these receptors undergo a number of conformational changes. The most remarkable one is the large (roughly 10 Ångström) outward movement of the intracellular tip of TM6. Therefore, inserting a nanoluciferase to the C-terminal and a HaloTag to the ICL3 of the receptor may take advantage of this large conformational rearrangement (Figure 5-30). A large number of FRET- and BRET-based biosensors based on this phenomenon were described previously, supporting the design rationale. Therefore, generating a CXCR4-based biosensor in a similar concept was expected to generate BRET signal that changes upon ligand binding and subsequent conformational changes in the receptor.

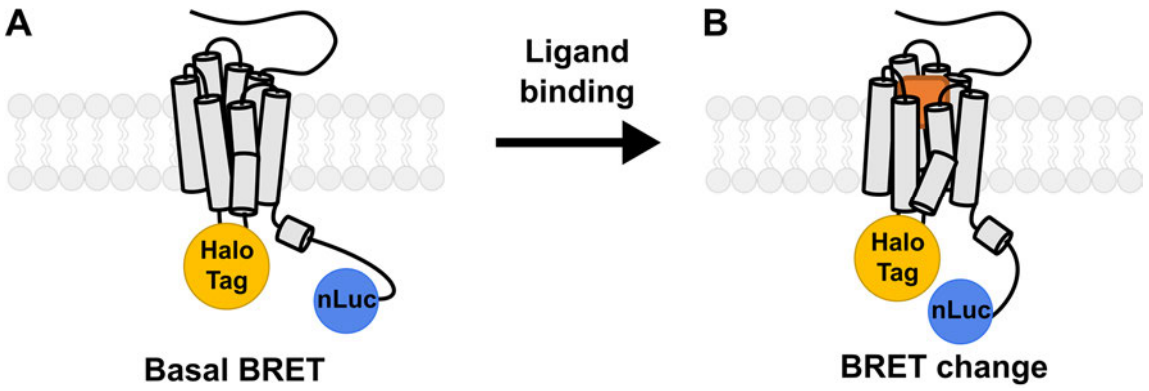

Figure 5-30. Schematic representation of the mechanism of intramolecular GPCR BRET sensors. The sensor design involves the insertion of a HaloTag to the ICL3, and a nanoluciferase (nLuc) to the end of the C terminus of the GPCR. (A) In non-ligated state, the biosensor exhibits a basal BRET signal, owing to the distance between nLuc and dye bound HaloTag. (B) Upon ligand binding to the GPCR, a series of conformational changes occur in the GPCR, which changes the orientation and the distance between the nLuc and HaloTag bound fluorescent dye. These conformational switches result in changes in BRET, which can be in positive or negative direction depending on the individual sensor used.

To generate such a CXCR4 BRET sensor, nLuc was inserted after the last residue of the C terminal, and HaloTag was introduced between the residues His228$^{5.67}$ and Ser229$^{5.68}$ (Figure 5-31A). HaloTag insertion sites were selected identical to the FRET based intramolecular CXCR4 sensor design, since the insertion of the FlAsH binding motif between His228$^{5.67}$ and Ser229$^{5.68}$ residues produced a working FRET sensor with slightly diminished G protein activity. Firstly, the absorption spectra of the cloned CXCR4 BS was assessed in 96-well plate format before and after labeling the HaloTag with the HaloTag 618 ligand. In cells, in which HaloTag is not labeled, only one absorption peak, which corresponds to nanoluciferase emission, was observed. On the other hand, cells that are labeled with HaloTag 618 ligand, two emission peaks were observed: one that corresponds to that of nanoluciferase, and another peak with smaller amplitude that corresponds to the acceptor HaloTag 618 emission, which is indicative of basal BRET (Figure 5-31B).

Next, the sensor BRET response was tested before and after adding increasing concentrations of the agonist CXCL12, as well as a number of other ligands that inhibit CXCR4. Concentration-response plots generated from these experiments revealed distinct, ligand dependent changes in BRET signal. The agonist CXCL12 induced a concentration dependent BRET increase. However, this increase did not reach to a saturation up to 10

µM CXCL12 concentrations. On the other hand, the inverse agonists FC131, IT1t, LY2510924, and TC14012 resulted in concentration dependent decrease in BRET signal with varying potency and efficacy values. In contrast, the antagonist AMD3100 caused a small but concentration dependent increase in BRET, suggesting a partial agonist activity for this ligand. Except CXCL12, all the ligands tested exhibited a saturated BRET response, which allowed calculating EC50 values for each ligand response (Figure 5-31C).

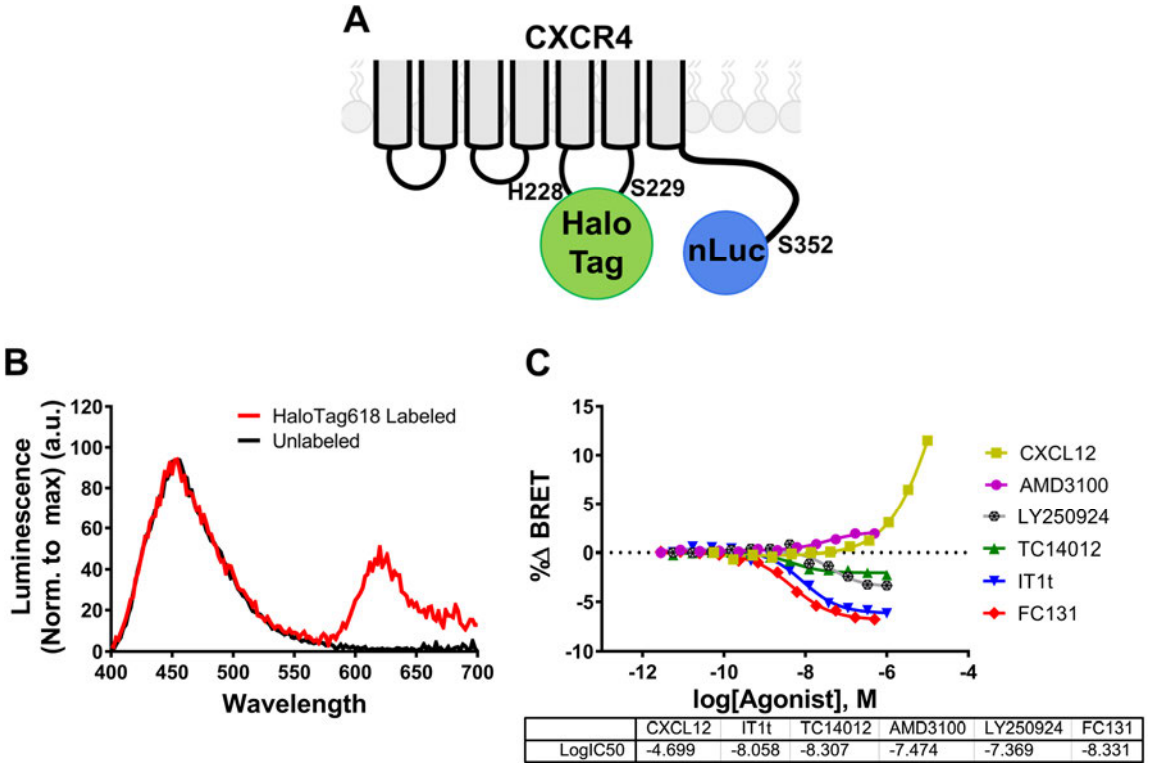

	CXCL12	IT1t	TC14012	AMD3100	LY250924	FC131
LogIC50	-4.699	-8.058	-8.307	-7.474	-7.369	-8.331

Figure 5-31. Design and evaluation of the BRET based intramolecular CXCR4 activation biosensor. (A) Topological view of the designed sensor protomer. A full length HaloTag was inserted between the residues His228 and Ser229 within the ICL3. Nanoluciferase was inserted after the last residue of the receptor C terminal, Ser352. (B) Absorption spectra of the biosensor expressed in HEK293 cells before (black line) and after (red line) labeling of the HaloTag with the Halo 618 ligand. The early peak with a maximal emission of 460 nm corresponds to the nanoluciferase emission. The late peak in the labeled condition corresponds to the HaloTag 618 emission which is an indicator of basal BRET occurrence. (C) Concentration-response plot depicting the % BRET changes observed on the CXCR4 biosensor after stimulation with various concentrations of CXCR4 ligands. Each data point is the average ± SEM of at least 3 independent experiments. Straight line on each data set is the Hill equation fit of the data, from which the $logEC_{50}$ data (below) was obtained.

To understand the temporal kinetics of the obtained responses, same BRET assay was employed in well reading format. In this format, individual wells are measured with

high temporal kinetics, and ligand addition is performed via the automatized dispenser unit of the plate reader device, which allows a continuous measurement. First, cells were stimulated with 1 µM CXCL12, and then with buffer. Here, CXCL12 induced a BRET increase with a τ value of 10 seconds, and this response went down upon addition of buffer, due to agonist dilution. When this experiment was performed with first CXCL12, and then 10 µM IT1t addition, IT1t decreased the CXCL12 induced response below the basal level. When first stimulus was performed with IT1t, a BRET decrease with a τ = 26 seconds was observed. While buffer stimulus as second injection did not change the IT1t induced response, CXCL12 partially reversed this response, revealing its agonistic activity on the biosensor (Figure 5-32).

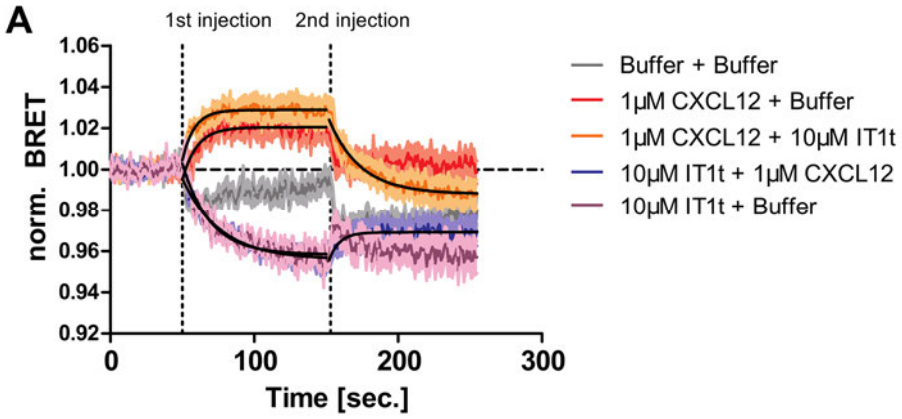

Figure 5-32. Time course analysis of ligand-induced BRET responses in CXCR4 BRET biosensor. BRET experiments were performed in HEK293 cells transiently expressing the CXCR4 BRET sensor. In order to perform a measurement with high temporal resolution, each time a single well was measured. Step-wise ligand stimulations were performed via the internal dispensers of the plate reader in order to achieve an uninterrupted measurement. Time trace data shown in the graph is the mean ± SEM of at least 3 experiments for each condition. Exponential fitting (black lines) after each ligand injection was performed to calculate the kinetics of the ligand mediated changes in BRET signal.

Altogether, a first generation intramolecular CXCR4 BRET sensor was generated and experimentally evaluated. This sensor exhibited changes in its basal BRET with all the ligands that were tested. The sensor revealed an accurate profile of agonism/antagonism/inverse agonism for all of the tested ligands. Apart from the agonist CXCL12, all ligands generated EC_{50} values that are in the range of which reported in the literature.

5.3.2. cpGFP-Based CXCR4 Biosensor Design

As a second approach to generate a biosensor that reports CXCR4 conformational changes, the cpGFP design was used. This design is also based on the outward movement of the TM6 helix upon receptor activation. It is believed that the cpGFP inserted between the TM5 and TM6 helices can undergo conformational changes due to the movements of both helices, but particularly the TM6, which results in stretching/relaxing of the cpGFP between these two helices. These movements in turn cause different assemblies of the GFP barrel and affects the chromophore microenvironment, thus producing different fluorescence intensities (Figure 5-33).

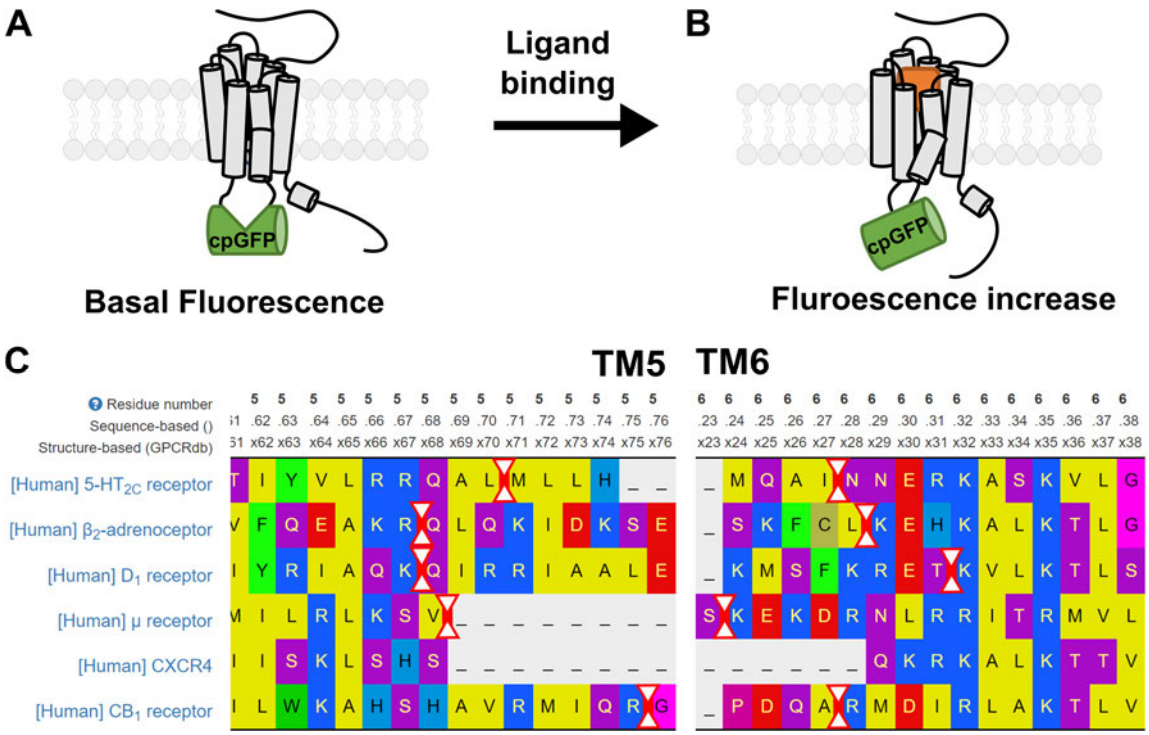

Figure 5-33. Schematic representation of cpGFP based GPCR biosensors. A cpGFP is inserted between TM5 and 6, with linkers of a few residues flanking cpGFP. Upon ligand binding to the sensor, cpGFP fluorescence increases due to the conformational changes. (C) Sequence alignment of CXCR4 with other class A GPCRs that were used as cpGFP scaffold. Red lines at TM5 and TM6 represents the sites where cpGFP with flanking linkers is inserted.

Following this phenomenon, and considering the characteristics of the previously reported cpGFP based GPCR biosensors, a CXCR4-cpGFP sensor was designed. Firstly,

a signal peptide was inserted to the N terminus of CXCR4 to increase plasma membrane targeting of the receptor. Then, the insertion site for cpGFP and the composition of the linkers flanking cpGFP were selected (Figure 5-34A). Considering the linkers from successful GPCR-cpGFP biosensors, two sets of linkers were selected: The first set of linkers come from the dLight sensor (based on the dopamine receptor D1), in which the cpGFP is flanked by the LSSLI and NHDQL residues. The second linker set comes from the Gach2.0 sensor (based on the muscarinic receptor M3), in which the cpGFP is flanked by the VEQGG and APSVADGR residues. As an initial insertion site, Gly231-His232 was selected, since these residues are in the center of the short ECL3 of CXCR4, and may undergo a large distance shift upon activation.

Fluorescence microscopy analysis of intact cells expressing the CXCR4-cpGFP variant with dLight linkers (v1) showed that this sensor was localized mainly on the cell surface, and a remarkable portion of the fluorescence signal was observed in the intracellular domains. This sensor did not exhibit any fluorescence intensity change upon addition of 10 μM CXCL12, or 10μM IT1t, suggesting that this sensor does not report the possible ligand induced conformational changes. The second sensor design that contains the Gach2.0 linkers (v2) was mainly localized on the cell surface. In contrast to the first design, CXCR4-cpGFP v2 induced a roughly 5% increase in fluorescence intensity upon treatment with 10 μM CXCL12 (Figure 5-34B and C). Next, temporal kinetics of the agonist-mediated response was measured with the assistance of a perfusion system for rapid ligand stimulation. From these experiments, a τ-value of 690 msec was observed for the fluorescence increase by 10 μM CXCL12 addition ((Figure 5-34D). These kinetics match the one observed for the recently described CXCR4 FRET sensor. Therefore, CXCR4-cpGFP v2 design was selected as the preliminary candidate for further development.

As a second line of sensor improvement, other insertion sites were selected. The insertion site of the cpGFP can be critical, since inserting this fluorophore where the largest conformational changes are observed would result in the best responses. Therefore, cpGFP with Gach2.0 linkers was inserted between His228 and Ser229 (v3) and Gln233 and

Lys234 (v4) (Figure 5-34A). Although both sensors displayed excellent membrane localization, neither of them responded to saturating concentrations of CXCL12 or IT1t (Figure 5-34C).

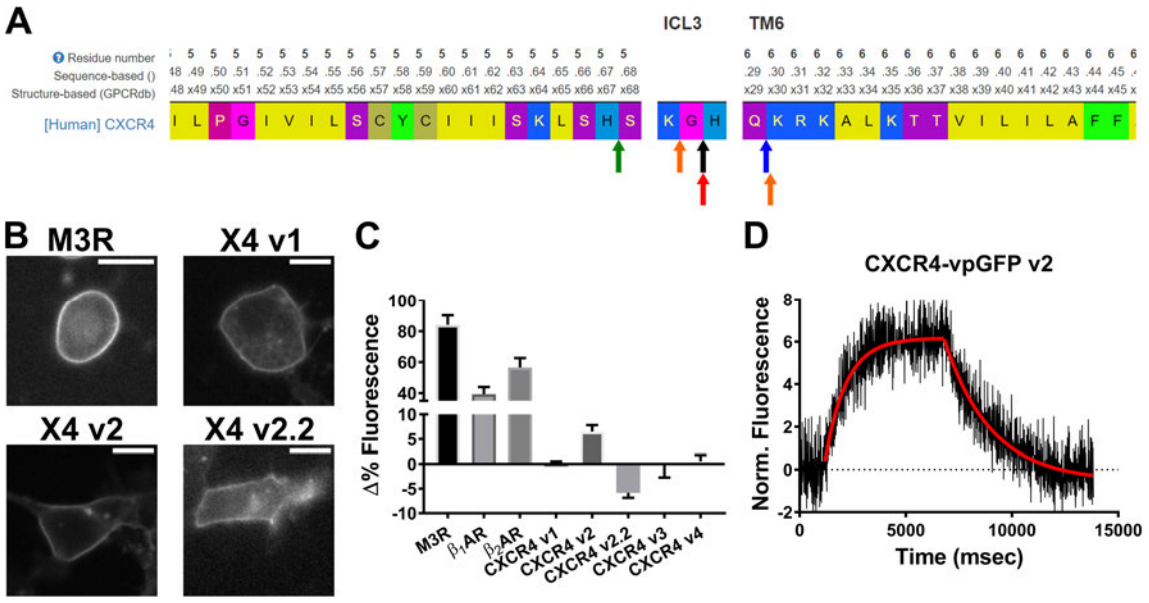

Figure 5-34. Design and experimental evaluation of CXCR4-cpGFP biosensors. (A) Sequence of CXCR4 TM5, ICL3 and TM6 residues. Arrows below show the selected insertion sites for cpGFP. Two arrows with the same color indicates that the residues in between were truncated. (B) Epi-fluorescence microscopy images of GPCR-cpGFP biosensors. Scale bar is 10 µm. (C) Bar graph shows agonist induced changes in cpGFP fluorescence. M_3R-cpGFP (Jing et al., 2018) was stimulated with 100 µM acetylcholine. β_1ARand β_2AR sensors (Patriarchi et al., 2018) were stimulated with 100 µM norepinephrine. CXCR4-cpGFP variants were stimulated with 10 µM CXCL12. Error bars indicate SEM of 3 independent experiments. (D) Representative single cell analysis of activation and deactivation kinetics of the CXCR4-cpGFP v2 sensor. Black line indicates the time trace data and red lines show the monoexponential fit of the data within the shown range to calculate activation (τ=690 ms) and deactivation (τ=1516 ms) kinetics.

As well as the insertion site, amino acid composition flanking the cpGFP and the linkers may also influence the cpGFP response. When compared by amino acid alignment, it was observed that a big portion, if not all, of the ICL3 was truncated with the intracellular "tips" of the TM5 and 6 in the successfully published GPCR-cpGFP biosensors. In most of the sensors, the linkers were flanked by a positively charged residue. In light of this, an insertion approach resembling the other GPCR-cpGFP biosensors was prepared. In this design, cpGFP flanked by the Gach2.0 (Jing et al., 2018) linkers was inserted between CXCR4 residues K230 and K234 (v2.2), as these residues align to the basic residues used

in other GPCRs for inserting the cpGFP between. CXCR4-cpGFP v2.2 displayed an unaltered membrane localization, compared to the previous versions (Figure 5-34B). In contrast to the v2, the v2.2 sensor produced a decrease in fluorescence intensity in response to 10 μM CXCL12 (Figure 5-34C).

In summary, this work led to two cpGFP-based CXCR4 biosensors, both of which responding to the agonist CXCL12 in inverse directions, reflecting the correct agonism of the sensor. The biosensor CXCR4-cpGFP v2 displays an increasing fluorescence signal in response to the agonist CXCL12, and therefore is an excellent starting point to develop CXCR4-cpGFP sensors with larger fluorescence intensity change and a better agonist affinity.

6. DISCUSSION

G protein coupled receptor oligomerization has been an attractive, yet controversial topic over the last two decades (George et al., 2002). Using diverse types of methods, contradicting conclusions have been reported in terms of oligomerization of several receptors (Isbilir et al., 2017). Despite this controversy, a growing number of evidence suggest that oligomerization may have an influence on the pharmacology of a number of receptors under certain cellular context (Ferré et al., 2014). Recent advances in high resolution single molecule microscopy, as well as fluorescence spectroscopy have served as great tools to study membrane protein complexes with great precision (Calebiro and Sungkaworn, 2018). Super resolution methods provide a resolution at single molecule level. Numerous reports using these methods suggested a largely monomeric quaternary organization of class A GPCRs, such as the β_1 adrenergic receptor (Calebiro et al., 2013), μ opioid receptor (Möller et al., 2020), muscarinic M_1 receptor (Hern et al., 2010), dopamine D_2 receptor (Tabor et al., 2016) and neurotensin 1 receptor (Dijkman et al., 2018).

Although single molecule imaging provides a great amount of quantitative information on the exact amount of receptors per complex as well as the spatio-temporal dynamics of receptor-receptor interactions, this method requires a very low, and usually sub physiological expression levels of the receptor being studied, in order to assure single molecule resolution. Thus, it does not allow addressing the effect of different expression levels on receptor oligomerization. Recent advances in fluorescent fluctuation spectroscopy have allowed the use of this technique on commercial confocal microscopes, with less complicated analysis routines, to study membrane protein oligomerization. Methods such as SpIDA, PCH and N&B have been successfully employed to decipher the oligomeric assembly of numerous GPCRs at expression levels ranging from 10 to 1000 receptors per μm^2 plasma membrane area (Briddon et al., 2018; T. Youker and Voet, 2020).

The main scope of this thesis work was to assess the oligomerization of chemokine receptors CXCR4 and CXCR7 using a well-established single molecule imaging routine,

and implementing a clear protocol to assess receptor oligomerization using molecular brightness analysis at high receptor expression levels, where concentrations exceed the single molecule resolution. Implementation of two brightness analyses with reliable monomeric controls was successfully achieved in this work. For two labeling methods, two monomeric control constructs based on β_1AR were verified with vigorous testing. Moreover, a double EYFP tagged version of the β_1AR also worked greatly as a dimeric control for the case of EYFP labeling.

First, TIRFM based single molecule microscopy revealed a highly monomeric organization of CXCR4: only 12% of the observed spots resulted in a dimeric assembly, in comparison to the monomeric control β_1AR and the dimeric control CD28. Assessing the single receptor tracks over space and time allowed characterizing the individual receptor-receptor colocalizations. This analysis revealed that CXCR4 protomers do indeed codiffuse. After deconvoluting the random, nonspecific interaction kinetics, the dimer lifetime of CXCR4 was observed in the range of ~1 second. Compared to previous single molecule data under analogous conditions (i.e. temperature), this interaction kinetics was in the same scale as observed for the neurotensin 1 receptor, which displayed a τ of 1.2 seconds of dimer lifetime. On the other hand, CXCR4 displayed longer interaction times in comparison to that of the μ opioid receptor (Möller et al., 2020) and the muscarinic M_1 receptor (Hern et al., 2010), both of which displayed interaction lifetimes of ~0.5 seconds. When interpreting the dimer kinetics data from TIRFM experiments, it is important to note that the duration of TIRF movies was between 4 and 8 seconds. Therefore, if there are any interactions that are longer than these, the software would not involve them in the analysis. On the other hand, upon interaction, if both of the molecules are photobleached, this is also not involved in the analysis. Moreover, it is also worth to note that a proportion of CXCR4 dimers at low expression levels may also be constitutive, which is also not considered in the dimerization kinetics calculations. Therefore, it is possible to speculate that a number of experimental drawbacks, which need immediate improvement, may actually cause the underestimation of dimer lifetimes of CXCR4.

Next, the goal was to use these methods to investigate the oligomerization of CXCR4 and CXCR7 at higher expression levels. Both CXCR4 and CXCR7 are expressed

in several tissue types, with varying copy numbers per cell. In particular, immune cells express from a few thousands to 150,000 copies of CXCR4 (Lee et al., 1999; Ueda et al., 1998), while cancer cells, where CXCR4 expression is usually a prognostic factor, express above 100,000 CXCR4 copies per cell (P. Guo et al., 2012; D. Liu et al., 2018; B. Wang et al., 2015). On the other hand, despite not characterized quantitatively, growing evidence suggests that cancer cells can express very high amounts of CXCR7 as well (Melo et al., 2014; Song et al., 2019; S. Xu et al., 2019). Therefore, studying the oligomerization of CXCR4 and CXCR7 at a large spectrum rather than only at low expression levels was important to understand the quaternary assembly of these receptors in greater detail. Molecular brightness methods, such as the number and brightness analysis, are well established tools for this purpose. Firstly, the application of the N&B theory was expanded from temporal domain to spatial domain. Since N&B method is based on statistical analysis of photon counts over individual pixels over time, it could in principle be applied on several pixels of a single confocal microscopy image. Firstly, this theory was tested by measuring the number of Rhodamine 6G fluorescence dye molecules within the confocal beam volume, and comparing them with the theoretical number calculated from the known concentration of the dye solutions used. This comparison showed that the spatial brightness expansion of the N&B method can precisely calculate the concentration of molecules in a well characterized beam volume.

In order to use spatial and temporal brightness methods, appropriate monomeric and dimeric controls for each labeling approach were needed. Firstly, two labeling methods were tested: 1) C-terminal EYFP tagging and 2) N-terminal SNAP tagging with Alexa Fluor 488 labeling. For EYFP tagging, β_1AR-EYFP served as a reliable monomeric control, as its brightness was lower than that of CD86-EYFP. Moreover, β_1AR-EYFP brightness was stable even after 10 frames of photobleaching. A double EYFP-tagged β_1AR worked as a robust dimeric control, with a doubled brightness value compared to β_1AR-EYFP. For SNAP tagging, SNAP-β_1AR again displayed lower, bleaching-resistant brightness in comparison to SNAP-CD86, verifying that it is indeed a reliable monomeric control for both labeling approaches. A robust outcome of the results here is that both spatial and

temporal brightness analyses resulted in correlating brightness values for the control constructs for each labeling approach. These conclusions suggest that the expansion of the N&B theory from temporal to spatial domain has proven to be working vigorously.

Next step after establishing the working protocols for brightness analyses was to apply the methods on CXCR4 and CXCR7. When tested on CXCR7 with a C terminal EYFP tag, this receptor displayed a highly intracellular localization of the fluorescence signal. This may not be surprising, as CXCR7 is an arrestin-biased, decoy oriented receptor that exhibits continuous basal internalization in several assay systems (Canals et al., 2012; K. E. Luker et al., 2010). In order to avoid the interference of intracellular CXCR7-EYFP signal on the plasma membrane signal, SNAP surface labeling approach was used, as this technique allows labeling only the receptors that are localized on the cell surface. Yet again, SNAP Surface labeled SNAP-CXCR7 still displayed clusters near the cell surface. Of note, labeling with SNAP dyes requires an incubation time of 20 minutes. Since CXCR7 is believed to be internalized constitutively, this time scale would be sufficient for labeled receptors to be internalized already, and this might cause the observed SNAP-CXCR7 clusters which are either internalized or on the path of internalization. Since clusters exhibit higher intensity values, they can be eliminated in brightness analyses by filtering out the pixels with intensity values above a certain threshold. After applying individual intensity threshold values for each image, membrane areas with more homogenous CXCR7 distribution could be analyzed. This analysis showed that CXCR7 is mainly monomeric. These results contradict others reported earlier, in which luminescence complementation, FRET and BRET were used to assess oligomerization (Kalatskaya et al., 2009; Levoye et al., 2009; H. T. Nguyen et al., 2020). It should be noted that the methods in the given studies do not assess the localization of the CXCR7 signal. Therefore, it is possible that the reported oligomer signal of CXCR7 might stem from receptor clusters in clathrin coated pits and endosomes, which CXCR7 appears to accumulate constitutively.

Molecular brightness analysis of CXCR4 at various expression levels suggested a concentration-dependent increase in the complex size for this receptor. Brightness based assessment of receptor oligomerization may suffer from receptors binding to and co-dif-

fusing with an interaction partner, without specific receptor-receptor interactions. To overcome this, a technically independent assay, FRET AB in this case, was applied, and the results of this assay further corroborated the specific interactions of CXCR4. At densities above 50,000 receptors per cell (>70 receptors per μm^2 membrane area), CXCR4 exhibited a strictly dimeric behavior. The concentration dependence of CXCR4 dimerization might be important for its physiological and pathophysiological function, as CXCR4 concentrations in functionally relevant cells are usually at the range where the receptor is dimeric. However, it is important to note that dimerization of receptors can be influenced by the cellular context (i.e. presence or absence of interaction partners, membrane composition and properties etc.). Therefore the conclusions of these results should be assessed with careful consideration.

Activation of CXCR4 with its agonist CXCL12 appeared to further increase the complex size. CXCL12 caused clusters of CXCR4, which appeared time and ligand concentration dependently. A deeper assessment showed that these clusters colocalized with the clathrin adaptor AP2. Moreover, time kinetics of the cluster formation was in good correlation with receptor internalization. CXCR4 was also still in a dimeric state very shortly after agonist stimulation. This short time scale is already necessary to reach a full G protein activation state. Therefore, it is possible to speculate that G protein activation does not require an apparent shift in CXCR4 stoichiometry. Yet, it was previously reported that CXCR4 dimers undergo a conformational rearrangement rapidly upon activation. A possible mechanism to suggest here would be that CXCL12 binding to CXCR4 induces a rapid (~600 msec) intramolecular conformational rearrangement, as well as a slower homodimer rearrangement (~2 sec). Then, activated dimers start to form clusters, which may be associated with receptor internalization. However, the interplay and interdependence of these processes are not fully understood, and require further investigation. The elegant study of Martinez-Muñoz *et al*. recently suggested that agonist induced clustering of CXCR4 mediated T cell migration, and mutants that are not able to form clusters do not activate the migration process (Martínez-Muñoz, Rodríguez-Frade, et al., 2018). This hypothesis may be true, but it is worth noting that the mutations in the study of Martinez-Muñoz *et al*. are on the TM6 residues of CXCR4, which were previously shown to strictly control the conformational changes of the receptor upon agonist binding (Wescott et al.,

2016). Therefore, it is necessary to understand better if these mutants do not form clusters because they cannot become activated, or if they cannot become activated because they cannot cluster. Answering such a question may contribute the understanding of the interplay between CXCR4 tertiary and quaternary structure during receptor activation.

Further assessment of CXCR4 dimers showed that dimerization is closely related to the receptor basal activity. A FRET-based G protein activation assay showed that CXCR4 induces basal Gi_2 protein activity, which is PTX-dependent. Moreover, CXCR4 antagonists TC14012, LY2510924, IT1t an FC131 can reduce this basal activity with varying efficacies. These ligands also reduce the high basal activity of a constitutively active CXCR4 mutant. Therefore, these ligands can be labeled as inverse agonists. Interestingly, among these inverse agonists, LY2510924, IT1t and FC131 were able to inhibit CXCR4 dimerization. Furthermore, compared to the other CXCR4 inhibitors, these 3 ligands form contacts with the CCR4 minor binding pocket. Mutating a residue within this binding pocket reduced the dimer destabilizing ability of IT1t and FC131. Therefore, it can be proposed that ligands of CXCR4 minor pocket can inhibit receptor dimerization by inhibiting the receptor basal activity. The lack of dimer destabilizing ability of TC14012 can be associated with its low efficacy on reducing the basal Gi_2 activity. In support of these observations, a great correlation was observed between the basal activity and basal dimerization of two CXCR4 mutants, $V242^{6.38}D$ and $L246^{6.42}P$. While $V242^{6.38}D$ exhibited virtually no basal activity, this mutant was also completely monomeric. $L246^{6.42}P$, on the other hand, displayed a partial basal activity, which probably reflects the partially dimeric organization of this mutant. Therefore, it is possible to speculate that the basally active CXCR4 conformation is a modulator of the receptor dimerization. Once the basal activity is inhibited, receptor stoichiometry shifts towards the prevalence of monomers. Another supportive result in regard to this observation came from the nanobody VUN401. This ligand binds exclusively to the extracellular regions of CXCR4. Probably because it does not bind to the major or minor binding pockets of CXCR4, it is not able to modulate the receptor basal activity. Yet, it disrupts receptor dimers completely. From this observation, it can be concluded that VUN401 causes a physical separation of CXCR4 dimers, owing to the large size of the ligand, and its extracellular binding mode, without affecting the receptor basal activity. This supports that it is not the receptor dimerization that modulates

receptor's basal activity. Rather, CXCR4 dimerization is a consequence of its basal activity, and inhibition of CXCR4 basal activity leads to dimer disruption.

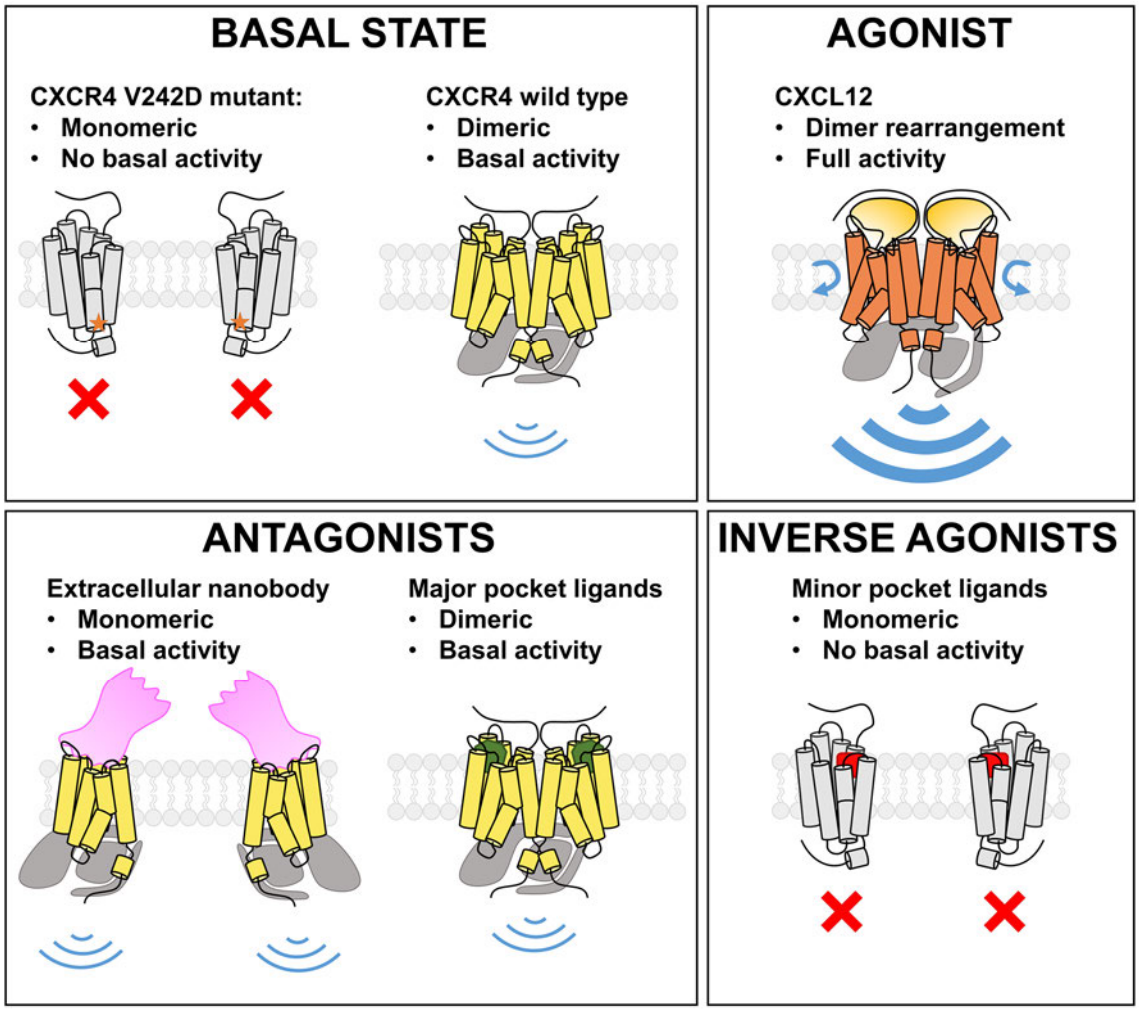

Figure 6-1. Graphical abstract of quaternary organization, pharmacological modulation and receptor conformation dependency of CXCR4 dimerization. At the basal state, CXCR4 is highly dimeric, and exhibits basal G protein activity. Mutating the V242 residue to D diminishes both receptor dimerization and basal activity. Among the ligands, the agonist CXCL12 induces a dimer rearrangement and fully activates the G protein. From the inhibitors, inverse agonists that bind to the minor pocket diminish the basal activity, thus disrupts dimers, while the major pocket ligands cannot exhibit either of these. On the other hand, the nanobody VUN401 binds to the extracellular sites and disrupts the dimers, without affecting the basal activity of CXCR4.

Upon observing how the basally active CXCR4 conformation is prone to form receptor dimers, it was crucial to assess whether the intracellular interaction partners of

CXCR4 can influence receptor dimerization. Therefore, the most obvious signaling partners were assessed: G protein α subunits and β-arrestins. Although CXCR4 is known to activate primarily Gαi, others reported that it can stimulate Gαq (Doijen et al., 2017; Soede et al., 2001) and Gα12/13 (Yagi et al., 2011) signaling as well. Therefore, assessing CXCR4 dimerization in a cell line devoid of all functional Gα subunits, as well as another that lacks both β-arrestin 1 and 2 was the choice for this approach. In both of these cell lines, CXCR4-EYFP appeared to be dimeric above 50 receptors/µm2 membrane area. Moreover, inverse agonists that disrupted CXCR4 dimers in HEK293AD cells still retained their effect in the knockout cell lines as well. From these experiments, it can be concluded that neither Gα subunits, nor β-arrestins stabilize CXCR4 dimers. However, what is not assessed here is whether these effectors affect the dimer stability at different expression levels of CXCR4. Pharmacologically, it is possible that the effectors can shift the K_d of dimer formation. The experiments here were performed already and the levels where dimerization reached the saturation, which may hinder any effect of the effectors. Therefore, more detailed assessment of the effectors may be needed to understand their effect in more detail.

To sum up, this thesis work focused on tackling the problem of CXCR4 and CXCR7 oligomerization via a tour de force of fluorescence microscopy and luminescence methods including single particle tracking, molecular brightness analysis, FRET, and BRET. The results agreeably show that exogenously expressed CXCR4 dimerizes in a density dependent fashion, and the dimerization is inhibited by stabilizing an inactive receptor conformation, either via mutations, or inverse agonists that bind the minor pocket of CXCR4. CXCR4 is a major drug target in immune diseases as well as cancer, and developing more efficient inhibitors of CXCR4 is essential in this regard. Here, the results of this work may uncover a new strategy to design drugs that target CXCR4 minor pocket, rather than only targeting the receptor dimer interface.

7. OUTLOOK

GPCR oligomerization has been studied by several groups using numerous biochemical and biophysical methods over recent decades (Guo et al., 2017). Although some of these methods, such as FRET and BRET, reports direct receptor-receptor interactions, they cannot discriminate the location of the RET signal. As a result, when a receptor accumulates in a subcellular structure, i.e. an endosome, the conclusion from such assays would be that it is an oligomeric receptor. Yet, if FRET is the method of choice for oligomerization analysis, it is recommended to use it on a confocal or TIRF microscope, where a specific cellular domain, in particular the cell membrane, may be selected, so that any RET signal that may arise from other compartments can be avoided. Yet, such methods, i.e. FRET acceptor photobleaching, as applied in this work, still does not provide a quantitative analysis of receptor oligomerization. Vigorous simulations and mathematical modeling approaches are needed to use FRET AB in a quantitative manner, which requires a high level of mathematical expertise to follow (Prasanna et al., 2014). On the other hand, biochemical methods that involve receptor solubilization in methods are rather harsh and do not always represent the native quaternary organization of GPCRs. Although more advanced biochemical methods, such as blue native polyacrylamide gel electrophoresis method, use milder detergents and retain the receptor complexes in their native states (Furness et al., 2016), this method still does not match an analysis in an intact cell. As opposed to such methods, image analysis based techniques provide more quantitative assessment of receptor quaternary organization. Among these, fluorescence fluctuation spectroscopy based methods stand out.

Here, the implementation and use of temporal and spatial brightness analysis techniques served as valuable tools to uncover several biological insights regarding CXCR4 and CXCR7 oligomerization. The work here demonstrated that these two methods could be combined with different labeling strategies, which provide a flexible platform. One important aspect to consider while designing a brightness-based measurement is to have a reliable monomeric control, which should be used as a reference while characterizing av-

erage oligomer size of each receptor of interest. The work here also describe such monomeric and dimeric control constructs, and provide a strong strategy to assess any other candidate monomeric or dimeric control construct. Another crucial aspect of brightness based analyses is the selection of the region for analysis. Cells being imaged may exhibit inhomogeneous structures, which display high intensities, such as filopodia, membrane ruffles, endosomes that are located closely to the membrane etc. Such heterogeneities should be avoided while selecting a region of interest (ROI) to be analyzed. A very good example, as shown in the work here, is the chemokine receptor CXCR7, which exhibited a highly clustered organization. The membrane located fraction of CXCR7 could only be assessed by eliminating the clusters by implementing an intensity filtering. This educated ROI selection revealed that the plasma membrane localized fraction of CXCR7 is actually monomeric, while previous reports based on RET analysis in 96-well plates suggested an oligomeric assembly of CXCR7.

Another important point is using the temporal and spatial brightness in combination. Even though both methods are simply based on the same mathematical theory, in practice their results may slightly differ. In temporal brightness, any immobile fraction persisting in individual pixels will result in zero brightness, as there will be virtually no fluorescence fluctuation. Here, using a spatial brightness approach would provide a solution. On the other hand, spatial brightness may suffer from the selection of areas with inhomogeneous intensities. This problem can also be solved during the analysis. Testing the quality of the Gaussian fit on the intensity distribution can help identifying whether any inhomogeneity was involved in the ROI. This analysis can be iterated for numerous ROIs until a convenient ROI selection has been made.

As opposed to single molecule analysis, temporal and brightness analyses provide only an average behavior of oligomerization. For example, for a species that exhibits a dimeric brightness value, it is difficult to say whether it is formed by 100% dimeric ensembles, or 50% monomeric and 50% trimeric complexes. Another extension of the N&B analysis, called fluorescence intensity fluctuation spectrometry (FIF) addressed this issue by segmenting a single confocal image and calculating brightness within each segment, in order to generate brightness spectrograms from which oligomeric species can be quantified

(Stoneman et al., 2019). Although this novel approach offers an extra magnification on the existing ensemble brightness methods, its way of handling small segments of a large ROI has been debated (Annibale and Lohse, 2020).

Chemokine receptors CXCR4 and CXCR7 are two of the main regulators of cellular migration during development and immune cell surveillance. Owing to their abundance in numerous tissues, they mediate distinct cellular signaling functions at diverse sites of the human body. Being involved in several vital processes also comes with its own price: Dysregulation of both CXCR4 and CXCR7 mediated signaling has been proven by many studies to cause cancer progression, due to cancer cell survival and metastasis (Y. Shi et al., 2020). Due to its involvement in such diseases, CXCR4 has been a valuable druggable target. Therefore, understanding the biology of this receptor is quite crucial in terms of drug development.

Here, this worked addressed the CXCR4 biology in terms of receptor organization on the cell surface. The results of this study suggested that CXCR4 can form dimers in a density dependent fashion. Moreover, this work revealed a basal G protein activity that is mediated by CXCR4. Mutations that are introduced in the TM6 residues that govern conformational changes of CXCR4 during activation process can inhibit the basal activity. This suggests that CXCR4 appears to reside in a conformation where activation is slightly favorable, which in turn causes a small but obvious basal G protein activity. A recently published computational study supported this notion. Chang *et al*. performed molecular dynamics simulations of CXCR4 conformations, and found out that the receptor displayed different conformations in the basal and IT1t bound state (Chang et al., 2020). Measuring the movement of the TM6, they found out that the apo receptor displayed a 5Å outward shift of TM6 compared to the IT1t bound state. Moreover, two mutations, L244$^{6.40}$P and L246$^{6.42}$P are able to stabilize a conformation that is similar to the IT1t bound state, both moving the TM6 inwards. Binding of the agonist CXCL12 further moved the TM6 outwards to a probably fully active state. These results suggest that the apo receptor is partially active, and IT1t binding, as well as two TM6 mutants, can shift the receptor back to a fully inactive state. The results of Chang *et* al. are in line with the observations of this thesis

work, describing a basally active CXCR4 state, which can be modulated pharmacologically and via mutations in the TM6 residues of the receptor.

Moreover, this thesis work revealed that CXCR4 dimerization is connected to the basal activity of the receptor. Dimerization could be disrupted by shifting the receptor conformation towards a more inactive direction. Clinically, the basally active conformation of CXCR4 might have a potential of targeting. Recently, a number of groups showed that the ligands of the minor pocket, thus inverse agonists, diminished auto inflammatory responses caused by CXCR4 (N. Smith et al., 2019; Zirafi et al., 2015), while the major pocket ligand, AMD3100, did not exhibit such an effect. In line with these observations, it is possible to speculate here that the anti-inflammatory effects of these CXCR4 inhibitors may be due to their inverse agonistic activity, as the neutral antagonist/partial agonist AMD3100 did not show any similar effect. Moreover, another group has recently reported that inducing a mutation to the TM6 residue of mouse CXCR4 in leukemia cells decreased the homing of these cells in bone marrow, while mutations in CXCR4 binding pocket did not have such an effect (Ramakrishnan et al., 2020). The results of this study implies that inhibiting CXCL12 binding does not completely diminish the ligand independent activity of CXCR4. Therefore, inverse agonists that exert such an inhibitory effect may also decrease cancer cell homing in the bone marrow. Bone marrow homing of cancer cells provide an environment for cancer survival and progression. Moreover, bone marrow is not an easily accessible environment for anticancer drugs (Mu et al., 2018). Therefore, any mechanism that can allow cancer stem cells, or leukemia cells out of the bone marrow can increase the targetability of these cells by chemotherapeutic drugs. This may be achieved by developing CXCR4 inverse agonists, as such ligands may not only inhibit agonist binding to the receptor, but also inhibit the basal signaling via CXCR4, thus diminishing the homing of malignant cells in the bone marrow. Possible activity of existing CXCR4 inverse agonists on this axis, especially the ones that were identified as the dimer disrupting inverse agonists in this thesis work, would be of importance to test in such *in vivo* assays in order to open up a novel therapeutic mechanism.

In summary, recent studies focusing on CXCR4 conformations and clinical implications of receptor functions suggest that CXCR4 exhibits a certain basal activity that is

clinically important. A number of drugs that are under clinical trials already target CXCR4 activity, especially in cancer. Yet, the molecular mechanism of CXCR4 activity is still not fully understood, and requires further exploration. This work focused on the effect of the quaternary structure of CXCR4 on the receptor signaling, and proposes a possible mechanism on how basal activity and inverse agonists modulate receptor oligomer size. Due to the importance of CXCR4 activity in such diseases, targeting the basal activity of CXCR4 via inverse agonists may be a relevant and potentially useful strategy as a therapeutical approach in cancer.

APPENDIX

Table A-1. Multiple comparison and significance test results for Figure 5-20.

Tukey's multiple comparisons test	Mean Diff,	95,00% CI of diff,	Significant?	Summary	Adjusted P Value
β_1AR-EYFP vs. Basal	-1,03	-1,192 to -0,8672	Yes	****	<0,0001
β_1AR-EYFP vs. CXCL12	-1,158	-1,335 to -0,9817	Yes	****	<0,0001
β_1AR-EYFP vs. IT1t	-0,2771	-0,4309 to -0,1233	Yes	****	<0,0001
β_1AR-EYFP vs. FC131	-0,112	-0,2565 to 0,03244	No	ns	0,2860
β_1AR-EYFP vs. AMD3100	-0,991	-1,19 to -0,7917	Yes	****	<0,0001
β_1AR-EYFP vs. TC14012	-0,8694	-1,043 to -0,6954	Yes	****	<0,0001
β_1AR-EYFP vs. VUN401	-0,07642	-0,2504 to 0,09752	No	ns	0,9250
β_1AR-EYFP vs. AMD3465	-0,981	-1,167 to -0,795	Yes	****	<0,0001
β_1AR-EYFP vs. LY2510924	-0,4226	-0,5809 to -0,2644	Yes	****	<0,0001
Basal vs. CXCL12	-0,1286	-0,3003 to 0,04306	No	ns	0,3343
Basal vs. IT1t	0,7525	0,6042 to 0,9008	Yes	****	<0,0001
Basal vs. FC131	0,9176	0,779 to 1,056	Yes	****	<0,0001
Basal vs. AMD3100	0,03857	-0,1565 to 0,2336	No	ns	0,9998
Basal vs. TC14012	0,1602	-0,008794 to 0,3293	No	ns	0,0796
Basal vs. VUN401	0,9532	0,7841 to 1,122	Yes	****	<0,0001
Basal vs. AMD3465	0,04859	-0,1328 to 0,23	No	ns	0,9975
Basal vs. LY2510924	0,607	0,4541 to 0,7598	Yes	****	<0,0001
CXCL12 vs. IT1t	0,8811	0,7175 to 1,045	Yes	****	<0,0001
CXCL12 vs. FC131	1,046	0,8913 to 1,201	Yes	****	<0,0001
CXCL12 vs. AMD3100	0,1672	-0,0398 to 0,3742	No	ns	0,2327
CXCL12 vs. TC14012	0,2889	0,1062 to 0,4716	Yes	****	<0,0001
CXCL12 vs. VUN401	1,082	0,8991 to 1,264	Yes	****	<0,0001
CXCL12 vs. AMD3465	0,1772	-0,01696 to 0,3714	No	ns	0,1071
CXCL12 vs. LY2510924	0,7356	0,5678 to 0,9034	Yes	****	<0,0001
IT1t vs. FC131	0,1651	0,03663 to 0,2935	Yes	**	0,0022
IT1t vs. AMD3100	-0,7139	-0,9019 to -0,5259	Yes	****	<0,0001
IT1t vs. TC14012	-0,5923	-0,7531 to -0,4314	Yes	****	<0,0001
IT1t vs. VUN401	0,2007	0,03983 to 0,3615	Yes	**	0,0035
IT1t vs. AMD3465	-0,7039	-0,8777 to -0,5301	Yes	****	<0,0001
IT1t vs. LY2510924	-0,1455	-0,2893 to -0,001813	Yes	*	0,0444
FC131 vs. AMD3100	-0,879	-1,059 to -0,6985	Yes	****	<0,0001
FC131 vs. TC14012	-0,7573	-0,9093 to -0,6054	Yes	****	<0,0001
FC131 vs. VUN401	0,03563	-0,1163 to 0,1876	No	ns	0,9991
FC131 vs. AMD3465	-0,869	-1,035 to -0,7034	Yes	****	<0,0001
FC131 vs. LY2510924	-0,3106	-0,4443 to -0,1769	Yes	****	<0,0001
AMD3100 vs. TC14012	0,1217	-0,08312 to 0,3265	No	ns	0,6699
AMD3100 vs. VUN401	0,9146	0,7098 to 1,119	Yes	****	<0,0001
AMD3100 vs. AMD3465	0,01003	-0,2051 to 0,2251	No	ns	>0,9999
AMD3100 vs. LY2510924	0,5684	0,3768 to 0,76	Yes	****	<0,0001
TC14012 vs. VUN401	0,7929	0,6127 to 0,9731	Yes	****	<0,0001
TC14012 vs. AMD3465	-0,1117	-0,3035 to 0,08018	No	ns	0,6958
TC14012 vs. LY2510924	0,4467	0,2816 to 0,6118	Yes	****	<0,0001
VUN401 vs. AMD3465	-0,9046	-1,096 to -0,7128	Yes	****	<0,0001
VUN401 vs. LY2510924	-0,3462	-0,5113 to -0,1811	Yes	****	<0,0001
AMD3465 vs. LY2510924	0,5584	0,3807 to 0,7361	Yes	****	<0,0001

Test details	Mean 1	Mean 2	Mean Diff,	SE of diff,	n1	n2	q	DF
β_1AR-EYFP vs. Basal	0,9836	2,013	-1,03	0,0508	22	25	28,66	225
β_1AR-EYFP vs. CXCL12	0,9836	2,142	-1,158	0,05524	22	18	29,65	225
β_1AR-EYFP vs. IT1t	0,9836	1,261	-0,2771	0,04813	22	32	8,142	225
β_1AR-EYFP vs. FC131	0,9836	1,096	-0,112	0,04521	22	45	3,505	225
β_1AR-EYFP vs. AMD3100	0,9836	1,975	-0,991	0,06237	22	12	22,47	225
β_1AR-EYFP vs. TC14012	0,9836	1,853	-0,8694	0,05443	22	19	22,59	225
β_1AR-EYFP vs. VUN401	0,9836	1,06	-0,07642	0,05443	22	19	1,986	225
β_1AR-EYFP vs. AMD3465	0,9836	1,965	-0,981	0,05819	22	15	23,84	225
β_1AR-EYFP vs. LY2510924	0,9836	1,406	-0,4226	0,04951	22	28	12,07	225
Basal vs. CXCL12	2,013	2,142	-0,1286	0,05372	25	18	3,386	225
Basal vs. IT1t	2,013	1,261	0,7525	0,04639	25	32	22,94	225
Basal vs. FC131	2,013	1,096	0,9176	0,04335	25	45	29,93	225
Basal vs. AMD3100	2,013	1,975	0,03857	0,06103	25	12	0,8936	225
Basal vs. TC14012	2,013	1,853	0,1602	0,05289	25	19	4,284	225
Basal vs. VUN401	2,013	1,06	0,9532	0,05289	25	19	25,48	225
Basal vs. AMD3465	2,013	1,965	0,04859	0,05676	25	15	1,211	225
Basal vs. LY2510924	2,013	1,406	0,607	0,04782	25	28	17,95	225
CXCL12 vs. IT1t	2,142	1,261	0,8811	0,0512	18	32	24,34	225
CXCL12 vs. FC131	2,142	1,096	1,046	0,04847	18	45	30,53	225
CXCL12 vs. AMD3100	2,142	1,975	0,1672	0,06477	18	12	3,651	225
CXCL12 vs. TC14012	2,142	1,853	0,2889	0,05716	18	19	7,147	225
CXCL12 vs. VUN401	2,142	1,06	1,082	0,05716	18	19	26,76	225
CXCL12 vs. AMD3465	2,142	1,965	0,1772	0,06076	18	15	4,125	225
CXCL12 vs. LY2510924	2,142	1,406	0,7356	0,0525	18	28	19,81	225
IT1t vs. FC131	1,261	1,096	0,1651	0,04019	32	45	5,808	225
IT1t vs. AMD3100	1,261	1,975	-0,7139	0,05883	32	12	17,16	225
IT1t vs. TC14012	1,261	1,853	-0,5923	0,05033	32	19	16,64	225
IT1t vs. VUN401	1,261	1,06	0,2007	0,05033	32	19	5,639	225
IT1t vs. AMD3465	1,261	1,965	-0,7039	0,05438	32	15	18,3	225
IT1t vs. LY2510924	1,261	1,406	-0,1455	0,04497	32	28	4,577	225
FC131 vs. AMD3100	1,096	1,975	-0,879	0,05646	45	12	22,02	225
FC131 vs. TC14012	1,096	1,853	-0,7573	0,04755	45	19	22,52	225
FC131 vs. VUN401	1,096	1,06	0,03563	0,04755	45	19	1,06	225
FC131 vs. AMD3465	1,096	1,965	-0,869	0,05182	45	15	23,72	225
FC131 vs. LY2510924	1,096	1,406	-0,3106	0,04183	45	28	10,5	225
AMD3100 vs. TC14012	1,975	1,853	0,1217	0,06408	12	19	2,685	225
AMD3100 vs. VUN401	1,975	1,06	0,9146	0,06408	12	19	20,18	225
AMD3100 vs. AMD3465	1,975	1,965	0,01003	0,06731	12	15	0,2106	225
AMD3100 vs. LY2510924	1,975	1,406	0,5684	0,05996	12	28	13,41	225
TC14012 vs. VUN401	1,853	1,06	0,7929	0,05639	19	19	19,89	225
TC14012 vs. AMD3465	1,853	1,965	-0,1117	0,06003	19	15	2,631	225
TC14012 vs. LY2510924	1,853	1,406	0,4467	0,05166	19	28	12,23	225
VUN401 vs. AMD3465	1,06	1,965	-0,9046	0,06003	19	15	21,31	225
VUN401 vs. LY2510924	1,06	1,406	-0,3462	0,05166	19	28	9,479	225
AMD3465 vs. LY2510924	1,965	1,406	0,5584	0,05561	15	28	14,2	225

Table A-2. Multiple comparison and significance test results for Figure 5-21.

WT CXCR4

Tukey's multiple comparisons test	Mean Diff,	95,00% CI of diff,	Sig-nifi-cant?	Sum-mary	Adjusted P Value
CXCL12 100 nM vs. AMD3100 10μM	-12,39	-13,94 to -10,83	Yes	****	<0,0001
CXCL12 100 nM vs. TC14012 10μM	-13,82	-15,21 to -12,43	Yes	****	<0,0001
CXCL12 100 nM vs. IT1t 10μM	-16,02	-17,33 to -14,72	Yes	****	<0,0001
CXCL12 100 nM vs. FC131 10μM	-16,15	-17,54 to -14,76	Yes	****	<0,0001
CXCL12 100 nM vs. VUN401 1μM	-12,34	-13,8 to -10,88	Yes	****	<0,0001
CXCL12 100 nM vs. Vehicle	-12,2	-13,59 to -10,81	Yes	****	<0,0001
CXCL12 100 nM vs. AMD3465 10μM	-13,03	-14,42 to -11,64	Yes	****	<0,0001
CXCL12 100 nM vs. LY2510924 100nM	-15,19	-16,49 to -13,89	Yes	****	<0,0001
AMD3100 10μM vs. TC14012 10μM	-1,432	-2,986 to 0,1233	No	ns	0,0930
AMD3100 10μM vs. IT1t 10μM	-3,637	-5,112 to -2,162	Yes	****	<0,0001
AMD3100 10μM vs. FC131 10μM	-3,766	-5,321 to -2,211	Yes	****	<0,0001
AMD3100 10μM vs. VUN401 1μM	0,04596	-1,57 to 1,662	No	ns	>0,9999
AMD3100 10μM vs. Vehicle	0,1917	-1,363 to 1,747	No	ns	>0,9999
AMD3100 10μM vs. AMD3465 10μM	-0,6396	-2,194 to 0,9152	No	ns	0,9141
AMD3100 10μM vs. LY2510924 100nM	-2,799	-4,274 to -1,324	Yes	****	<0,0001
TC14012 10μM vs. IT1t 10μM	-2,205	-3,506 to -0,9044	Yes	****	<0,0001
TC14012 10μM vs. FC131 10μM	-2,334	-3,725 to -0,9437	Yes	****	<0,0001
TC14012 10μM vs. VUN401 1μM	1,477	0,01891 to 2,936	Yes	*	0,0450
TC14012 10μM vs. Vehicle	1,623	0,2325 to 3,014	Yes	*	0,0116
TC14012 10μM vs. AMD3465 10μM	0,7919	-0,5988 to 2,183	No	ns	0,6481
TC14012 10μM vs. LY2510924 100nM	-1,368	-2,669 to -0,06705	Yes	*	0,0325
IT1t 10μM vs. FC131 10μM	-0,1291	-1,43 to 1,172	No	ns	>0,9999
IT1t 10μM vs. VUN401 1μM	3,683	2,31 to 5,056	Yes	****	<0,0001
IT1t 10μM vs. Vehicle	3,828	2,528 to 5,129	Yes	****	<0,0001
IT1t 10μM vs. AMD3465 10μM	2,997	1,696 to 4,298	Yes	****	<0,0001
IT1t 10μM vs. LY2510924 100nM	0,8373	-0,367 to 2,042	No	ns	0,3853
FC131 10μM vs. VUN401 1μM	3,812	2,353 to 5,27	Yes	****	<0,0001
FC131 10μM vs. Vehicle	3,958	2,567 to 5,348	Yes	****	<0,0001
FC131 10μM vs. AMD3465 10μM	3,126	1,736 to 4,517	Yes	****	<0,0001
FC131 10μM vs. LY2510924 100nM	0,9664	-0,3344 to 2,267	No	ns	0,2994
VUN401 1μM vs. Vehicle	0,1457	-1,313 to 1,604	No	ns	>0,9999
VUN401 1μM vs. AMD3465 10μM	-0,6856	-2,144 to 0,773	No	ns	0,8358
VUN401 1μM vs. LY2510924 100nM	-2,845	-4,219 to -1,472	Yes	****	<0,0001
Vehicle vs. AMD3465 10μM	-0,8313	-2,222 to 0,5594	No	ns	0,5876
Vehicle vs. LY2510924 100nM	-2,991	-4,292 to -1,69	Yes	****	<0,0001
AMD3465 10μM vs. LY2510924 100nM	-2,16	-3,461 to -0,8589	Yes	****	<0,0001

Test details	Mean 1	Mean 2	Mean Diff,	SE of diff,	n1	n2	q	DF
CXCL12 100 nM vs. AMD3100 10µM	-12,21	0,1758	-12,39	0,4779	6	4	36,66	46
CXCL12 100 nM vs. TC14012 10µM	-12,21	1,607	-13,82	0,4274	6	6	45,72	46
CXCL12 100 nM vs. IT1t 10µM	-12,21	3,813	-16,02	0,3998	6	8	56,68	46
CXCL12 100 nM vs. FC131 10µM	-12,21	3,942	-16,15	0,4274	6	6	53,45	46
CXCL12 100 nM vs. VUN401 1µM	-12,21	0,1298	-12,34	0,4483	6	5	38,93	46
CXCL12 100 nM vs. Vehicle	-12,21	-0,01588	-12,2	0,4274	6	6	40,35	46
CXCL12 100 nM vs. AMD3465 10µM	-12,21	0,8154	-13,03	0,4274	6	6	43,1	46
CXCL12 100 nM vs. LY2510924 100nM	-12,21	2,975	-15,19	0,3998	6	8	53,72	46
AMD3100 10µM vs. TC14012 10µM	0,1758	1,607	-1,432	0,4779	4	6	4,236	46
AMD3100 10µM vs. IT1t 10µM	0,1758	3,813	-3,637	0,4533	4	8	11,34	46
AMD3100 10µM vs. FC131 10µM	0,1758	3,942	-3,766	0,4779	4	6	11,14	46
AMD3100 10µM vs. VUN401 1µM	0,1758	0,1298	0,04596	0,4966	4	5	0,1309	46
AMD3100 10µM vs. Vehicle	0,1758	-0,01588	0,1917	0,4779	4	6	0,5672	46
AMD3100 10µM vs. AMD3465 10µM	0,1758	0,8154	-0,6396	0,4779	4	6	1,893	46
AMD3100 10µM vs. LY2510924 100nM	0,1758	2,975	-2,799	0,4533	4	8	8,733	46
TC14012 10µM vs. IT1t 10µM	1,607	3,813	-2,205	0,3998	6	8	7,8	46
TC14012 10µM vs. FC131 10µM	1,607	3,942	-2,334	0,4274	6	6	7,724	46
TC14012 10µM vs. VUN401 1µM	1,607	0,1298	1,477	0,4483	6	5	4,661	46
TC14012 10µM vs. Vehicle	1,607	-0,01588	1,623	0,4274	6	6	5,371	46
TC14012 10µM vs. AMD3465 10µM	1,607	0,8154	0,7919	0,4274	6	6	2,62	46
TC14012 10µM vs. LY2510924 100nM	1,607	2,975	-1,368	0,3998	6	8	4,839	46
IT1t 10µM vs. FC131 10µM	3,813	3,942	-0,1291	0,3998	8	6	0,4567	46
IT1t 10µM vs. VUN401 1µM	3,813	0,1298	3,683	0,422	8	5	12,34	46
IT1t 10µM vs. Vehicle	3,813	-0,01588	3,828	0,3998	8	6	13,54	46
IT1t 10µM vs. AMD3465 10µM	3,813	0,8154	2,997	0,3998	8	6	10,6	46
IT1t 10µM vs. LY2510924 100nM	3,813	2,975	0,8373	0,3702	8	8	3,199	46
FC131 10µM vs. VUN401 1µM	3,942	0,1298	3,812	0,4483	6	5	12,03	46
FC131 10µM vs. Vehicle	3,942	-0,01588	3,958	0,4274	6	6	13,09	46
FC131 10µM vs. AMD3465 10µM	3,942	0,8154	3,126	0,4274	6	6	10,34	46
FC131 10µM vs. LY2510924 100nM	3,942	2,975	0,9664	0,3998	6	8	3,418	46
VUN401 1µM vs. Vehicle	0,1298	-0,01588	0,1457	0,4483	5	6	0,4596	46
VUN401 1µM vs. AMD3465 10µM	0,1298	0,8154	-0,6856	0,4483	5	6	2,163	46
VUN401 1µM vs. LY2510924 100nM	0,1298	2,975	-2,845	0,422	5	8	9,535	46
Vehicle vs. AMD3465 10µM	-0,01588	0,8154	-0,8313	0,4274	6	6	2,751	46
Vehicle vs. LY2510924 100nM	-0,01588	2,975	-2,991	0,3998	6	8	10,58	46
AMD3465 10µM vs. LY2510924 100nM	0,8154	2,975	-2,16	0,3998	6	8	7,64	46

CAM CXCR4

Tukey's multiple comparisons test	Mean Diff,	95,00% CI of diff,	Signifi-cant?	Sum-mary	Adjusted P Value
CXCL12 100 nM vs. AMD3100 10µM	-0,9164	-3,716 to 1,883	No	ns	0,9703
CXCL12 100 nM vs. TC14012 10µM	-9,449	-12,04 to -6,858	Yes	****	<0,0001
CXCL12 100 nM vs. IT1t 10µM	-10,09	-12,68 to -7,501	Yes	****	<0,0001
CXCL12 100 nM vs. FC131 10µM	-11,62	-14,21 to -9,025	Yes	****	<0,0001
CXCL12 100 nM vs. VUN401 1µM	-2,995	-5,794 to -0,1954	Yes	*	0,0290
CXCL12 100 nM vs. Vehicle	-2,689	-5,28 to -0,09713	Yes	*	0,0374
CXCL12 100 nM vs. AMD3465 10µM	-3,938	-6,303 to -1,572	Yes	***	0,0002
CXCL12 100 nM vs. LY2510924 100nM	-12,17	-14,53 to -9,802	Yes	****	<0,0001
AMD3100 10µM vs. TC14012 10µM	-8,533	-11,33 to -5,734	Yes	****	<0,0001
AMD3100 10µM vs. IT1t 10µM	-9,176	-11,98 to -6,377	Yes	****	<0,0001
AMD3100 10µM vs. FC131 10µM	-10,7	-13,5 to -7,901	Yes	****	<0,0001
AMD3100 10µM vs. VUN401 1µM	-2,078	-5,071 to 0,9143	No	ns	0,3613
AMD3100 10µM vs. Vehicle	-1,772	-4,571 to 1,027	No	ns	0,4811
AMD3100 10µM vs. AMD3465 10µM	-3,021	-5,613 to -0,4296	Yes	*	0,0132
AMD3100 10µM vs. LY2510924 100nM	-11,25	-13,84 to -8,66	Yes	****	<0,0001
TC14012 10µM vs. IT1t 10µM	-0,6436	-3,235 to 1,948	No	ns	0,9948
TC14012 10µM vs. FC131 10µM	-2,167	-4,758 to 0,4245	No	ns	0,1593
TC14012 10µM vs. VUN401 1µM	6,455	3,656 to 9,254	Yes	****	<0,0001
TC14012 10µM vs. Vehicle	6,761	4,169 to 9,352	Yes	****	<0,0001
TC14012 10µM vs. AMD3465 10µM	5,512	3,146 to 7,877	Yes	****	<0,0001
TC14012 10µM vs. LY2510924 100nM	-2,719	-5,084 to -0,353	Yes	*	0,0152
IT1t 10µM vs. FC131 10µM	-1,523	-4,115 to 1,068	No	ns	0,5764
IT1t 10µM vs. VUN401 1µM	7,098	4,299 to 9,897	Yes	****	<0,0001
IT1t 10µM vs. Vehicle	7,404	4,813 to 9,996	Yes	****	<0,0001
IT1t 10µM vs. AMD3465 10µM	6,155	3,79 to 8,521	Yes	****	<0,0001
IT1t 10µM vs. LY2510924 100nM	-2,075	-4,441 to 0,2906	No	ns	0,1214
FC131 10µM vs. VUN401 1µM	8,622	5,823 to 11,42	Yes	****	<0,0001
FC131 10µM vs. Vehicle	8,928	6,336 to 11,52	Yes	****	<0,0001
FC131 10µM vs. AMD3465 10µM	7,679	5,313 to 10,04	Yes	****	<0,0001
FC131 10µM vs. LY2510924 100nM	-0,5517	-2,917 to 1,814	No	ns	0,9966
VUN401 1µM vs. Vehicle	0,3059	-2,493 to 3,105	No	ns	>0,9999
VUN401 1µM vs. AMD3465 10µM	-0,943	-3,534 to 1,649	No	ns	0,9459
VUN401 1µM vs. LY2510924 100nM	-9,173	-11,76 to -6,582	Yes	****	<0,0001
Vehicle vs. AMD3465 10µM	-1,249	-3,615 to 1,117	No	ns	0,7023
Vehicle vs. LY2510924 100nM	-9,479	-11,84 to -7,114	Yes	****	<0,0001
AMD3465 10µM vs. LY2510924 100nM	-8,23	-10,35 to -6,114	Yes	****	<0,0001

Test details	Mean 1	Mean 2	Mean Diff,	SE of diff,	n1	n2	q	DF
CXCL12 100 nM vs. AMD3100 10µM	-2,91	-1,993	-0,9164	0,8366	4	3	1,549	29
CXCL12 100 nM vs. TC14012 10µM	-2,91	6,54	-9,449	0,7745	4	4	17,25	29
CXCL12 100 nM vs. IT1t 10µM	-2,91	7,183	-10,09	0,7745	4	4	18,43	29
CXCL12 100 nM vs. FC131 10µM	-2,91	8,707	-11,62	0,7745	4	4	21,21	29
CXCL12 100 nM vs. VUN401 1µM	-2,91	0,08496	-2,995	0,8366	4	3	5,062	29
CXCL12 100 nM vs. Vehicle	-2,91	-0,221	-2,689	0,7745	4	4	4,909	29
CXCL12 100 nM vs. AMD3465 10µM	-2,91	1,028	-3,938	0,707	4	6	7,876	29
CXCL12 100 nM vs. LY2510924 100nM	-2,91	9,258	-12,17	0,707	4	6	24,34	29
AMD3100 10µM vs. TC14012 10µM	-1,993	6,54	-8,533	0,8366	3	4	14,42	29
AMD3100 10µM vs. IT1t 10µM	-1,993	7,183	-9,176	0,8366	3	4	15,51	29
AMD3100 10µM vs. FC131 10µM	-1,993	8,707	-10,7	0,8366	3	4	18,09	29
AMD3100 10µM vs. VUN401 1µM	-1,993	0,08496	-2,078	0,8943	3	3	3,286	29
AMD3100 10µM vs. Vehicle	-1,993	-0,221	-1,772	0,8366	3	4	2,996	29
AMD3100 10µM vs. AMD3465 10µM	-1,993	1,028	-3,021	0,7745	3	6	5,516	29
AMD3100 10µM vs. LY2510924 100nM	-1,993	9,258	-11,25	0,7745	3	6	20,54	29
TC14012 10µM vs. IT1t 10µM	6,54	7,183	-0,6436	0,7745	4	4	1,175	29
TC14012 10µM vs. FC131 10µM	6,54	8,707	-2,167	0,7745	4	4	3,957	29
TC14012 10µM vs. VUN401 1µM	6,54	0,08496	6,455	0,8366	4	3	10,91	29
TC14012 10µM vs. Vehicle	6,54	-0,221	6,761	0,7745	4	4	12,34	29
TC14012 10µM vs. AMD3465 10µM	6,54	1,028	5,512	0,707	4	6	11,02	29
TC14012 10µM vs. LY2510924 100nM	6,54	9,258	-2,719	0,707	4	6	5,438	29
IT1t 10µM vs. FC131 10µM	7,183	8,707	-1,523	0,7745	4	4	2,782	29
IT1t 10µM vs. VUN401 1µM	7,183	0,08496	7,098	0,8366	4	3	12	29
IT1t 10µM vs. Vehicle	7,183	-0,221	7,404	0,7745	4	4	13,52	29
IT1t 10µM vs. AMD3465 10µM	7,183	1,028	6,155	0,707	4	6	12,31	29
IT1t 10µM vs. LY2510924 100nM	7,183	9,258	-2,075	0,707	4	6	4,151	29
FC131 10µM vs. VUN401 1µM	8,707	0,08496	8,622	0,8366	4	3	14,57	29
FC131 10µM vs. Vehicle	8,707	-0,221	8,928	0,7745	4	4	16,3	29
FC131 10µM vs. AMD3465 10µM	8,707	1,028	7,679	0,707	4	6	15,36	29
FC131 10µM vs. LY2510924 100nM	8,707	9,258	-0,5517	0,707	4	6	1,103	29
VUN401 1µM vs. Vehicle	0,08496	-0,221	0,3059	0,8366	3	4	0,5172	29
VUN401 1µM vs. AMD3465 10µM	0,08496	1,028	-0,943	0,7745	3	6	1,722	29
VUN401 1µM vs. LY2510924 100nM	0,08496	9,258	-9,173	0,7745	3	6	16,75	29
Vehicle vs. AMD3465 10µM	-0,221	1,028	-1,249	0,707	4	6	2,498	29
Vehicle vs. LY2510924 100nM	-0,221	9,258	-9,479	0,707	4	6	18,96	29
AMD3465 10µM vs. LY2510924 100nM	1,028	9,258	-8,23	0,6324	6	6	18,41	29

Table 0-3. Statistical outlier analysis and of the linear fit on Figure 5-23:

Straight line	
Best-fit values	
YIntercept	0,9528
Slope	0,01112
Std. Error	
YIntercept	0,03084
Slope	0,0004855
95% CI (profile likelihood)	
YIntercept	0,8919 to 1,014
Slope	0,01016 to 0,01208
Goodness of Fit	
Degrees of Freedom	158
R square	0,7686
Absolute Sum of Squares	5,946
Sy.x	0,194
Number of points	
# of X values	179
# Y values analyzed	179
Outliers (excluded, Q=1%)	**1**

REFERENCES

Ahlquist, R. P., 1948, "A Study of the Adrenotropic Receptors", *The American journal of physiology*, Vol. 153, No. 3, pp. 586–600.

Ahlquist, R. P., 1973, "Adrenergic Receptors: A Personal and Practical View", *Perspectives in Biology and Medicine*, Vol. 17, No. 1, pp. 119–122.

Albizu, L., M. Cottet, M. Kralikova, S. Stoev, R. Seyer, I. Brabet, T. Roux, H. Bazin, E. Bourrier, … T. Durroux, 2010, "Time-Resolved FRET between GPCR Ligands Reveals Oligomers in Native Tissues", *Nature Chemical Biology*, Vol. 6, No. 8, pp. 587–594.

Alexander, R. W., J. N. Davis, and R. J. Lefkowitz, 1975, "Direct Identification and Characterisation of β-Adrenergic Receptors in Rat Brain", *Nature*, Vol. 258, No. 5534, pp. 437–440.

Ali, S., H. Robertson, J. H. Wain, J. D. Isaacs, G. Malik, and J. A. Kirby, 2005, "A Non-Glycosaminoglycan-Binding Variant of CC Chemokine Ligand 7 (Monocyte Chemoattractant Protein-3) Antagonizes Chemokine-Mediated Inflammation", *The Journal of Immunology*, Vol. 175, No. 2, pp. 1257–1266.

Angers, S., A. Salahpour, E. Joly, S. Hilairet, D. Chelsky, M. Dennis, and M. Bouvier, 2000, "Detection of B2-Adrenergic Receptor Dimerization in Living Cells Using Bioluminescence Resonance Energy Transfer (BRET)", *Proceedings of the National Academy of Sciences of the United States of America*, Vol. 97, No. 7, pp. 3684–3689.

Annibale, P., and M. J. Lohse, 2020, "Spatial heterogeneity in molecular brightness",

Nature Methods, Vol. 17, No. 3, pp. 273–275.

Arai, R., H. Ueda, A. Kitayama, N. Kamiya, and T. Nagamune, 2001, "Design of the Linkers Which Effectively Separate Domains of a Bifunctional Fusion Protein", *Protein Engineering*, Vol. 14, No. 8, pp. 529–532.

Arimont, M., S. L. Sun, R. Leurs, M. Smit, I. J. P. De Esch, and C. De Graaf, 2017, "Structural Analysis of Chemokine Receptor-Ligand Interactions", *Journal of Medicinal Chemistry*, Vol. 60, No. 12, pp. 4735–4779.

Arimont, M., M. Van Der Woude, R. Leurs, H. F. Vischer, C. De Graaf, and S. Nijmeijer, 2019, "Identification of Key Structural Motifs Involved in 7 Transmembrane Signaling of Adhesion GPCRs", *ACS Pharmacology and Translational Science*, Vol. 2, No. 2, pp. 101–113.

Armando, S., J. Quoyer, V. Lukashova, A. Maiga, Y. Percherancier, N. Heveker, J. P. Pin, L. Prézeau, and M. Bouvier, 2014, "The Chemokine CXC4 and CC2 Receptors Form Homo- and Heterooligomers That Can Engage Their Signaling G-Protein Effectors and Barrestin", *FASEB Journal*, Vol. 28, No. 10, pp. 4509–4523.

Asano, S., K. Kitatani, M. Taniguchi, M. Hashimoto, K. Zama, S. Mitsutake, Y. Igarashi, H. Takeya, J. Kigawa, … T. Okazaki, 2012, "Regulation of Cell Migration by Sphingomyelin Synthases: Sphingomyelin in Lipid Rafts Decreases Responsiveness to Signaling by the CXCL12/CXCR4 Pathway", *Molecular and Cellular Biology*, Vol. 32, No. 16, pp. 3242–3252.

Asher, W. B., P. Geggier, M. D. Holsey, G. T. Gilmore, A. K. Pati, J. Meszaros, D. S. Terry, S. Mathiasen, M. J. Kaliszewski, … J. A. Javitch, 2021, "Single-Molecule FRET Imaging of GPCR Dimers in Living Cells.", *Nature methods*, pp. 1–9.

Attramadal, H., J. L. Arriza, C. Aoki, T. M. Dawson, J. Codina, M. M. Kwatra, S. H. Snyder, M. G. Caron, and R. J. Lefkowitz, 1992, "β-Arrestin2, a Novel Member of the Arrestin/β-Arrestin Gene Family", *Journal of Biological Chemistry*, Vol. 267, No. 25, pp. 17882–17890.

Ayoub, M. A., C. Couturier, E. Lucas-Meunier, S. Angers, P. Fossier, M. Bouvier, and R. Jockers, 2002, "Monitoring of Ligand-Independent Dimerization and Ligand-Induced Conformational Changes of Melatonin Receptors in Living Cells by Bioluminescence Resonance Energy Transfer", *Journal of Biological Chemistry*, Vol. 277, No. 24, pp. 21522–21528.

Baba, K., A. Benleulmi-Chaachoua, A. S. Journé, M. Kamal, J. L. Guillaume, S. Dussaud, F. Gbahou, K. Yettou, C. Liu, … G. Tosini, 2013, "Heteromeric MT1/MT2 Melatonin Receptors Modulate Photoreceptor Function", *Science Signaling*, Vol. 6, No. 296, pp. ra89–ra89.

Babcock, G. J., M. Farzan, and J. Sodroski, 2003, "Ligand-Independent Dimerization of CXCR4, a Principal HIV-1 Coreceptor", *Journal of Biological Chemistry*, Vol. 278, No. 5, pp. 3378–3385.

Bachelerie, Francoise, A. Ben-Baruch, A. M. Burkhardt, C. Combadiere, J. M. Farber, G. J. Graham, R. Horuk, A. H. Sparre-Ulrich, M. Locati, … A. Zlotnik, 2014, "International union of pharmacology. LXXXIX. Update on the extended family of chemokine receptors and introducing a new nomenclature for atypical chemokine receptors", *Pharmacological Reviews*, Vol. 66, No. 1, pp. 1–79.

Bachelerie, Françoise, G. J. Graham, M. Locati, A. Mantovani, P. M. Murphy, R. Nibbs, A. Rot, S. Sozzani, and M. Thelen, 2014, "New nomenclature for atypical chemokine receptors", *Nature Immunology*, Vol. 15, No. 3, pp. 207–208.

Bagher, A. M., M. E. M. Kelly, and E. M. Denovan-Wright, 2019, "Combining SRET2 and BiFC to Study GPCR Heteromerization and Protein–Protein Interactions", *Methods in Molecular Biology* ,Vol. 1947, pp. 199–215.

Bai, M., S. Trivedi, and E. M. Brown, 1998, "Dimerization of the Extracellular Calcium-Sensing Receptor (CaR) on the Cell Surface of CaR-Transfected HEK293 Cells", *Journal of Biological Chemistry*, Vol. 273, No. 36, pp. 23605–23610.

Balabanian, K., B. Lagane, S. Infantino, K. Y. C. Chow, J. Harriague, B. Moepps, F. Arenzana-Seisdedos, M. Thelen, and F. Bachelerie, 2005, "The Chemokine SDF-1/CXCL12 Binds to and Signals through the Orphan Receptor RDC1 in T Lymphocytes", *Journal of Biological Chemistry*, Vol. 280, No. 42, pp. 35760–35766.

Balabanian, K., B. Lagane, J. L. Pablos, L. Laurent, T. Planchenault, O. Verola, C. Lebbe, D. Kerob, A. Dupuy, … F. Bachelerie, 2005, "WHIM Syndromes with Different Genetic Anomalies Are Accounted for by Impaired CXCR4 Desensitization to CXCL12", *Blood*, Vol. 105, No. 6, pp. 2449–2457.

Ballesteros, J. A., and H. Weinstein, 1995, "Integrated Methods for the Construction of Three-Dimensional Models and Computational Probing of Structure-Function Relations in G Protein-Coupled Receptors", *Methods in Neurosciences*, Vol. 25, No. C, pp. 366–428.

Beletkaia, E., S. F. Fenz, W. Pomp, B. E. Snaar-Jagalska, P. W. C. Hogendoorn, and T. Schmidt, 2016, "CXCR4 Signaling Is Controlled by Immobilization at the Plasma Membrane", *Biochimica et Biophysica Acta - Molecular Cell Research*, Vol. 1863, No. 4, pp. 607–616.

Beliu, G., S. Altrichter, R. Guixà-González, M. Hemberger, I. Brauer, A.-K. Dahse, N. Scholz, R. Wieduwild, A. Kuhlemann, … T. Langenhan, 2021, "Tethered Agonist

Exposure in Intact Adhesion/Class B2 GPCRs through Intrinsic Structural Flexibility of the GAIN Domain", *Molecular Cell*, Vol. 81, No. 5, pp. 905- 921.e5.

Benovic, J. L., R. H. Strasser, M. G. Caron, and R. J. Lefkowitz, 1986, "β-Adrenergic Receptor Kinase: Identification of a Novel Protein Kinase That Phosphorylates the Agonist-Occupied Form of the Receptor", *Proceedings of the National Academy of Sciences of the United States of America*, Vol. 83, No. 9, pp. 2797–2801.

Berahovich, R. D., B. A. Zabel, S. Lewén, M. J. Walters, K. Ebsworth, Y. Wang, J. C. Jaen, and T. J. Schall, 2014, "Endothelial Expression of CXCR7 and the Regulation of Systemic CXCL12 Levels", *Immunology*, Vol. 141, No. 1, pp. 111–122.

Bettler, B., K. Kaupmann, J. Mosbacher, and M. Gassmann, 2004, "Molecular structure and physiological functions of GABAB receptors", *Physiological Reviews*, Vol. 84, No. 3, pp. 835–867.

Birnbaumer, L., and M. Rodbell, 1969, "Adenyl Cyclase in Fat Cells. II. Hormone Receptors.", *Journal of Biological Chemistry*, Vol. 244, No. 13, pp. 3477–3482.

Black, J. W., and J. S. Stephenson, 1962, "Pharmacology of a New Adrenergic Beta-Receptor-Blocking Compound (Nethalide)", *The Lancet*, Vol. 280, No. 7251, pp. 311–314.

Bleul, C. C., M. Farzan, H. Choe, C. Parolin, I. Clark-Lewis, J. Sodroski, and T. A. Springer, 1996, "The Lymphocyte Chemoattractant SDF-1 Is a Ligand for LESTR/Fusin and Blocks HIV-1 Entry", *Nature*, Vol. 382, No. 6594, pp. 829–833.

Bock, A., P. Annibale, C. Konrad, A. Hannawacker, S. E. Anton, I. Maiellaro, U. Zabel, S. Sivaramakrishnan, M. Falcke, and M. J. Lohse, 2020, "Optical Mapping of CAMP

Signaling at the Nanometer Scale", *Cell*, Vol. 182, No. 6, pp. 1519- 1530.e17.

Bokoch, G. M., T. Katada, J. K. Northup, M. Ui, and A. G. Gilman, 1984, "Purification and Properties of the Inhibitory Guanine Nucleotide-Binding Regulatory Component of Adenylate Cyclase.", *Journal of Biological Chemistry*, Vol. 259, No. 6, pp. 3560–3567.

Bonham, L. W., C. M. Karch, C. C. Fan, C. Tan, E. G. Geier, Y. Wang, N. Wen, I. J. Broce, Y. Li, … A. B. Singleton, 2018, "CXCR4 Involvement in Neurodegenerative Diseases", *Translational Psychiatry*, Vol. 8, No. 1,.

Bouvier, M., and T. E. Hébert, 2014, "CrossTalk proposal: Weighing the evidence for Class A GPCR dimers, the evidence favours dimers", *Journal of Physiology*, Vol. 592, No. 17, pp. 2439–2441.

Briddon, S. J., L. E. Kilpatrick, and S. J. Hill, 2018, "Studying GPCR Pharmacology in Membrane Microdomains: Fluorescence Correlation Spectroscopy Comes of Age", *Trends in Pharmacological Sciences*, Vol.39, No. 2, pp. 158–174.

Brock, C., N. Oueslati, S. Soler, L. Boudier, P. Rondard, and J. P. Pin, 2007, "Activation of a Dimeric Metabotropic Glutamate Receptor by Intersubunit Rearrangement", *Journal of Biological Chemistry*, Vol. 282, No. 45, pp. 33000–33008.

Broxmeyer, H. E., L. Kohli, C. H. Kim, Y. Lee, C. Mantel, S. Cooper, G. Hangoc, M. Shaheen, X. Li, and D. W. Clapp, 2003, "Stromal Cell-Derived Factor-1/CXCL12 Directly Enhances Survival/Antiapoptosis of Myeloid Progenitor Cells through CXCR4 and Gαi Proteins and Enhances Engraftment of Competitive, Repopulating Stem Cells", *Journal of Leukocyte Biology*, Vol. 73, No. 5, pp. 630–638.

Bünemann, M., M. Frank, and M. J. Lohse, 2003, "Gi Protein Activation in Intact Cells Involves Subunit Rearrangement Rather than Dissociation", *Proceedings of the National Academy of Sciences of the United States of America*, Vol. 100, No. 26, pp. 16077–16082.

Burg, J. S., J. R. Ingram, A. J. Venkatakrishnan, K. M. Jude, A. Dukkipati, E. N. Feinberg, A. Angelini, D. Waghray, R. O. Dror, … K. C. Garcia, 2015, "Structural Basis for Chemokine Recognition and Activation of a Viral G Protein-Coupled Receptor", *Science*, Vol. 347, No. 6226, pp. 1113–1117.

Burns, J. M., B. C. Summers, Y. Wang, A. Melikian, R. Berahovich, Z. Miao, M. E. T. Penfold, M. J. Sunshine, D. R. Littman, … T. J. Schall, 2006, "A Novel Chemokine Receptor for SDF-1 and I-TAC Involved in Cell Survival, Cell Adhesion, and Tumor Development", *Journal of Experimental Medicine*, Vol. 203, No. 9, pp. 2201–2213.

Busillo, J. M., S. Armando, R. Sengupta, O. Meucci, M. Bouvier, and J. L. Benovic, 2010, "Site-Specific Phosphorylation of CXCR4 Is Dynamically Regulated by Multiple Kinases and Results in Differential Modulation of CXCR4 Signaling", *Journal of Biological Chemistry*, Vol. 285, No. 10, pp. 7805–7817.

Calebiro, D., V. O. Nikolaev, M. C. Gagliani, T. De Filippis, C. Dees, C. Tacchetti, L. Persani, and M. J. Lohse, 2009, "Persistent CAMP-Signals Triggered by Internalized G-Protein-Coupled Receptors", *PLoS Biology*, Vol. 7, No. 8, pp. e1000172.

Calebiro, D., F. Rieken, J. Wagner, T. Sungkaworn, U. Zabel, A. Borzi, E. Cocucci, A. Zürn, and M. J. Lohse, 2013, "Single-Molecule Analysis of Fluorescently Labeled G-Protein-Coupled Receptors Reveals Complexes with Distinct Dynamics and Organization", *Proceedings of the National Academy of Sciences of the United States of America*, Vol. 110, No. 2, pp. 743–748.

Calebiro, D., and T. Sungkaworn, 2018, "Single-Molecule Imaging of GPCR Interactions", *Trends in Pharmacological Sciences*, Vol. 39, No. 2, pp. 109–122.

Calizo, R. C., and S. Scarlata, 2013, "Discrepancy between Fluorescence Correlation Spectroscopy and Fluorescence Recovery after Photobleaching Diffusion Measurements of G-Protein-Coupled Receptors", *Analytical Biochemistry*, Vol. 440, No. 1, pp. 40–48.

Canals, M., D. J. Scholten, S. de Munnik, M. K. L. Han, M. J. Smit, and R. Leurs, 2012, "Ubiquitination of CXCR7 Controls Receptor Trafficking", *PLoS ONE*, Vol. 7, No. 3, pp. e34192.

Caron, M. G., L. E. Limbird, and R. J. Lefkowitz, 1979, "Biochemical characterization of the BETA-adrenergic receptor of the frog erythrocyte", *Molecular and Cellular Biochemistry*, Vol. 28, No. 1–3, pp. 45–66.

Carriba, P., G. Navarro, F. Ciruela, S. Ferré, V. Casadó, L. Agnati, A. Cortés, J. Mallol, K. Fuxe, … R. Franco, 2008, "Detection of Heteromerization of More than Two Proteins by Sequential BRET-FRET", *Nature Methods*, Vol. 5, No. 8, pp. 727–733.

Cerione, R. A., B. Strulovici, J. L. Benovic, R. J. Lefkowitz, and M. G. Caron, 1983, "Pure β-Adrenergic Receptor: The Single Polypeptide Confers Catecholamine Responsiveness to Adenylate Cyclase", *Nature*, Vol. 306, No. 5943, pp. 562–566.

Chabre, M., P. Deterre, and B. Antonny, 2009, "The Apparent Cooperativity of Some GPCRs Does Not Necessarily Imply Dimerization", *Trends in Pharmacological Sciences*, Vol. 30, No. 4, pp. 182–187.

Chakraborty, H., M. Jafurulla, A. H. A. Clayton, and A. Chattopadhyay, 2018, "Exploring

Oligomeric State of the Serotonin1A Receptor Utilizing Photobleaching Image Correlation Spectroscopy: Implications for Receptor Function", *Faraday Discussions*, Vol. 207, , pp. 409–421.

Chang, C. C., J. W. Liou, K. T. P. Dass, Y. T. Li, S. J. Jiang, S. F. Pan, Y. C. Yeh, and H. J. Hsu, 2020, "Internal Water Channel Formation in CXCR4 Is Crucial for Gi-Protein Coupling upon Activation by CXCL12", *Communications Chemistry*, Vol. 3, No. 1, pp. 1–12.

Charette, N., P. Holland, J. Frazer, H. Allen, and D. J. Dupré, 2011, "Dependence on Different Rab GTPases for the Trafficking of CXCR4 and CCR5 Homo or Heterodimers between the Endoplasmic Reticulum and Plasma Membrane in Jurkat Cells", *Cellular Signalling*, Vol. 23, No. 11, pp. 1738–1749.

Chatterjee, S., B. Behnam Azad, and S. Nimmagadda, 2014, "The intricate role of CXCR4 in cancer", In *Advances in Cancer Research*, Vol. 124, pp. 31–82.

Chen, Y., J. D. Müller, P. T. C. So, and E. Gratton, 1999, "The Photon Counting Histogram in Fluorescence Fluctuation Spectroscopy", *Biophysical Journal*, Vol. 77, No. 1, pp. 553–567.

Chuang, D. M., and E. Costa, 1979, "Evidence for Internalization of the Recognition Site of β-Adrenergic Receptors during Receptor Subsensitivity Induced by (-)-Isoproterenol", *Proceedings of the National Academy of Sciences of the United States of America*, Vol. 76, No. 6, pp. 3024–3028.

Clark-Lewis, I., C. Schumacher, M. Baggiolini, and B. Moser, 1991, "Structure-Activity Relationships of Interleukin-8 Determined Using Chemically Synthesized Analogs: Critical Role of NH2-Terminal Residues and Evidence for Uncoupling of Neutrophil Chemotaxis, Exocytosis, and Receptor Binding Activities", *Journal of Biological*

Chemistry, Vol. 266, No. 34, pp. 23128–23134.

Clark, A. J., 1933, "The Mode of Action of Drugs on Cells.", *Nature*, No. 132, pp. 695.

Conley-LaComb, M. K., L. Semaan, R. Singareddy, Y. Li, E. I. Heath, S. Kim, M. L. Cher, and S. R. Chinni, 2016, "Pharmacological Targeting of CXCL12/CXCR4 Signaling in Prostate Cancer Bone Metastasis", *Molecular Cancer*, Vol. 15, No. 1, pp. 68.

Constantin, G., M. Majeed, C. Giagulli, L. Piccio, J. Y. Kim, E. C. Butcher, and C. Laudanna, 2000, "Chemokines Trigger Immediate B2 Integrin Affinity and Mobility Changes: Differential Regulation and Roles in Lymphocyte Arrest under Flow", *Immunity*, Vol. 13, No. 6, pp. 759–769.

Contento, R. L., B. Molon, C. Boularan, T. Pozzan, S. Manes, S. Marullo, and A. Viola, 2008, "CXCR4-CCR5: A Couple Modulating T Cell Functions", *Proceedings of the National Academy of Sciences of the United States of America*, Vol. 105, No. 29, pp. 10101–10106.

Craig Venter, J., M. D. Adams, E. W. Myers, P. W. Li, R. J. Mural, G. G. Sutton, H. O. Smith, M. Yandell, C. A. Evans, … X. Zhu, 2001, "The Sequence of the Human Genome", *Science*, Vol. 291, No. 5507, pp. 1304–1351.

Cranfill, P. J., B. R. Sell, M. A. Baird, J. R. Allen, Z. Lavagnino, H. M. De Gruiter, G. J. Kremers, M. W. Davidson, A. Ustione, and D. W. Piston, 2016, "Quantitative Assessment of Fluorescent Proteins", *Nature Methods*, Vol. 13, No. 7, pp. 557–562.

Crump, M. P., J. H. Gong, P. Loetscher, K. Rajarathnam, A. Amara, F. Arenzana-Seisdedos, J. L. Virelizier, M. Baggiolini, B. D. Sykes, and I. Clark-Lewis, 1997, "Solution Structure and Basis for Functional Activity of Stromal Cell-Derived Factor-

1; Dissociation of CXCR4 Activation from Binding and Inhibition of HIV-1", *EMBO Journal*, Vol. 16, No. 23, pp. 6996–7007.

Cutrale, F., D. Rodriguez, V. Hortigüela, C. L. Chiu, J. Otterstrom, S. Mieruszynski, A. Seriola, E. Larrañaga, A. Raya, … S. Ojosnegros, 2019, "Using Enhanced Number and Brightness to Measure Protein Oligomerization Dynamics in Live Cells", *Nature Protocols*, Vol. 14, No. 2, pp. 616–638.

Cvejic, S., and L. A. Devi, 1997, "Dimerization of the δ Opioid Receptor: Implication for a Role in Receptor Internalization", *Journal of Biological Chemistry*, Vol. 272, No. 43, pp. 26959–26964.

Daaka, Y., J. A. Pitcher, M. Richardson, R. H. Stoffel, J. D. Robishaw, and R. J. Lefkowitz, 1997, "Receptor and Gβγ Isoform-Specific Interactions with G Protein-Coupled Receptor Kinases", *Proceedings of the National Academy of Sciences of the United States of America*, Vol. 94, No. 6, pp. 2180–2185.

Dale, H. H., 1906, "On Some Physiological Actions of Ergot", *The Journal of Physiology*, Vol. 34, No. 3, pp. 163–206.

Dale, H. H., 1922, "The Value of Ergot in Obstetrical and Gynæcological Practice; with Special Reference to Its Present Position in the British Pharmacopœia.", *Proceedings of the Royal Society of Medicine*, Vol. 16, pp. 1–7.

De Lean, A., J. M. Stadel, and R. J. Lefkowitz, 1980, "A Ternary Complex Model Explains the Agonist-Specific Binding Properties of the Adenylate Cyclase-Coupled β-Adrenergic Receptor", *Journal of Biological Chemistry*, Vol. 255, No. 15, pp. 7108–7117.

Décaillot, F. M., M. A. Kazmi, Y. Lin, S. Ray-Saha, T. P. Sakmar, and P. Sachdev, 2011, "CXCR7/CXCR4 Heterodimer Constitutively Recruits β-Arrestin to Enhance Cell Migration", *Journal of Biological Chemistry*, Vol. 286, No. 37, pp. 32188–32197.

Degorce, F., A. Card, S. Soh, E. Trinquet, G. P. Knapik, and B. Xie, 2009, "HTRF: A technology tailored for drug discovery - A review of theoretical aspects and recent applications", *Current Chemical Genomics*, Vol. 3, No. 1, pp. 22–32.

Delgado, D. M., T. C. Møller, J. Ster, J. Giraldo, D. Maurel, X. Rovira, P. Scholler, J. M. Zwier, J. Perroy, … J. P. Pin, 2017, "Pharmacological Evidence for a Metabotropic Glutamate Receptor Heterodimer in Neuronal Cells", *eLife*, Vol. 6, .

Devree, B. T., J. P. Mahoney, G. A. Vélez-Ruiz, S. G. F. Rasmussen, A. J. Kuszak, E. Edwald, J. J. Fung, A. Manglik, M. Masureel, … R. K. Sunahara, 2016, "Allosteric Coupling from G Protein to the Agonist-Binding Pocket in GPCRs", *Nature*, Vol. 535, No. 7610, pp. 182–186.

Digman, M. A., R. Dalal, A. F. Horwitz, and E. Gratton, 2008, "Mapping the Number of Molecules and Brightness in the Laser Scanning Microscope", *Biophysical Journal*, Vol. 94, No. 6, pp. 2320–2332.

Dijkman, P. M., O. K. Castell, A. D. Goddard, J. C. Munoz-Garcia, C. De Graaf, M. I. Wallace, and A. Watts, 2018, "Dynamic Tuneable G Protein-Coupled Receptor Monomer-Dimer Populations", *Nature Communications*, Vol. 9, No. 1, pp. 1710.

Dixon, R. A. F., B. K. Kobilka, D. J. Strader, J. L. Benovic, H. G. Dohlman, T. Frielle, M. A. Bolanowski, C. D. Bennett, E. Rands, … C. D. Strader, 1986, "Cloning of the Gene and CDNA for Mammalian β-Adrenergic Receptor and Homology with Rhodopsin", *Nature*, Vol. 321, No. 6065, pp. 75–79.

Doijen, J., T. Van Loy, W. De Haes, B. Landuyt, W. Luyten, L. Schoofs, and D. Schols, 2017, "Signaling Properties of the Human Chemokine Receptors CXCR4 and CXCR7 by Cellular Electric Impedance Measurements", *PLoS ONE*, Vol. 12, No. 9.

Döring, Y., L. Pawig, C. Weber, and H. Noels, 2014, "The CXCL12/CXCR4 Chemokine Ligand/Receptor Axis in Cardiovascular Disease", *Frontiers in Physiology*, Vol. 5.

Dorsch, S., K. N. Klotz, S. Engelhardt, M. J. Lohse, and M. Bünemann, 2009, "Analysis of Receptor Oligomerization by FRAP Microscopy", *Nature Methods*, Vol. 6, No. 3, pp. 225–230.

Du, Y., N. M. Duc, S. G. F. Rasmussen, D. Hilger, X. Kubiak, L. Wang, J. Bohon, H. R. Kim, M. Wegrecki, … K. Y. Chung, 2019, "Assembly of a GPCR-G Protein Complex", *Cell*, Vol. 177, No. 5, pp. 1232- 1242.e11.

Duan, J., D. dan Shen, X. E. Zhou, P. Bi, Q. feng Liu, Y. xia Tan, Y. wen Zhuang, H. bing Zhang, P. yu Xu, … Y. Jiang, 2020, "Cryo-EM Structure of an Activated VIP1 Receptor-G Protein Complex Revealed by a NanoBiT Tethering Strategy", *Nature Communications*, Vol. 11, No. 1, pp. 1–10.

Dupré, D. J., M. Robitaille, R. V. Rebois, and T. E. Hébert, 2009, "The Role of Gβγ Subunits in the Organization, Assembly, and Function of GPCR Signaling Complexes", *Annual Review of Pharmacology and Toxicology*, Vol. 49, pp. 31–56.

Ehrenberg, M., and R. Rigler, 1974, "Rotational Brownian Motion and Fluorescence Intensify Fluctuations", *Chemical Physics*, Vol. 4, No. 3, pp. 390–401.

Ehrlich, P., and J. Morgenroth, 1900, "Über Hämolysine", *Dritte Mitheilung. Berl. Klin. Wschr*, Vol. 37, pp. 453–458.

El Moustaine, D., S. Granier, E. Doumazane, P. Scholler, R. Rahmeh, P. Bron, B. Mouillac, J. L. Banères, P. Rondard, and J. P. Pin, 2012, "Distinct Roles of Metabotropic Glutamate Receptor Dimerization in Agonist Activation and G-Protein Coupling", *Proceedings of the National Academy of Sciences of the United States of America*, Vol. 109, No. 40, pp. 16342–16347.

Ellaithy, A., J. Gonzalez-Maeso, D. A. Logothetis, and J. Levitz, 2020, "Structural and Biophysical Mechanisms of Class C G Protein-Coupled Receptor Function", *Trends in Biochemical Sciences*, Vol. 45, No. 12, pp. 1049–1064.

Farrens, D. L., C. Altenbach, K. Yang, W. L. Hubbell, and H. G. Khorana, 1996, "Requirement of Rigid-Body Motion of Transmembrane Helices for Light Activation of Rhodopsin", *Science*, Vol. 274, No. 5288, pp. 768–770.

Feinstein, T. N., V. L. Wehbi, J. A. Ardura, D. S. Wheeler, S. Ferrandon, T. J. Gardella, and J. P. Vilardaga, 2011, "Retromer Terminates the Generation of CAMP by Internalized PTH Receptors", *Nature Chemical Biology*, Vol. 7, No. 5, pp. 278–284.

Felce, J. H., S. L. Latty, R. G. Knox, S. R. Mattick, Y. Lui, S. F. Lee, D. Klenerman, and S. J. Davis, 2017, "Receptor Quaternary Organization Explains G Protein-Coupled Receptor Family Structure", *Cell Reports*, Vol. 20, No. 11, pp. 2654–2665.

Feng, Y., C. C. Broder, P. E. Kennedy, and E. A. Berger, 1996, "HIV-1 Entry Cofactor: Functional CDNA Cloning of a Seven-Transmembrane, G Protein-Coupled Receptor", *Science*, Vol. 272, No. 5263, pp. 872–877.

Ferrandon, S., T. N. Feinstein, M. Castro, B. Wang, R. Bouley, J. T. Potts, T. J. Gardella, and J. P. Vilardaga, 2009, "Sustained Cyclic AMP Production by Parathyroid Hormone Receptor Endocytosis", *Nature Chemical Biology*, Vol. 5, No. 10, pp. 734–742.

Ferré, S., V. Casadó, L. A. Devi, M. Filizola, R. Jockers, M. J. Lohse, G. Milligan, J. P. Pin, and X. Guitart, 2014, "G protein-coupled receptor oligomerization revisited: Functional and pharmacological perspectives", *Pharmacological Reviews*, Vol. 66, No. 2, pp. 413–434.

Fong, A. M., R. T. Premont, R. M. Richardson, Y. R. A. Yu, R. J. Lefkowitz, and D. D. Patel, 2002, "Defective Lymphocyte Chemotaxis in β-Arrestin2- and GRK6-Deficient Mice", *Proceedings of the National Academy of Sciences of the United States of America*, Vol. 99, No. 11, pp. 7478–7483.

Fonseca, J. M., and N. A. Lambert, 2009, "Instability of a Class A G Protein-Coupled Receptor Oligomer Interface", *Molecular Pharmacology*, Vol. 75, No. 6, pp. 1296–1299.

Foord, S. M., T. I. Bonner, R. R. Neubig, E. M. Rosser, J. P. Pin, A. P. Davenport, M. Spedding, and A. J. Harmar, 2005, "International Union of Pharmacology. XLVI. G protein-coupled receptor list", *Pharmacological Reviews*, Vol. 57, No. 2, pp. 279–288.

Förster, T., 1946, "Energiewanderung Und Fluoreszenz", *Die Naturwissenschaften*, Vol. 33, No. 6, pp. 166–175.

Frank, M., L. Thümer, M. J. Lohse, and M. Bünemann, 2005, "G Protein Activation without Subunit Dissociation Depends on a Gαi-Specific Region", *Journal of Biological Chemistry*, Vol. 280, No. 26, pp. 24584–24590.

Fraser, C. M., and J. C. Venter, 1982, "The Size of the Mammalian Lung B2-Adrenergic Receptor as Determined by Target Size Analysis and Immunoaffinity Chromatography", *Biochemical and Biophysical Research Communications*, Vol. 109, No. 1, pp. 21–29.

Fredriksson, R., M. C. Lagerström, L. G. Lundin, and H. B. Schiöth, 2003, "The G-Protein-Coupled Receptors in the Human Genome Form Five Main Families. Phylogenetic Analysis, Paralogon Groups, and Fingerprints", *Molecular Pharmacology*, Vol. 63, No. 6, pp. 1256–1272.

Freitas, C., A. Desnoyer, F. Meuris, F. Bachelerie, K. Balabanian, and V. Machelon, 2014, "The relevance of the chemokine receptor ACKR3/CXCR7 on CXCL12-mediated effects in cancers with a focus on virus-related cancers", *Cytokine and Growth Factor Reviews*, Vol. 25, No. 3, pp. 307–316.

Furness, S. G. B., Y. L. Liang, C. J. Nowell, M. L. Halls, P. J. Wookey, E. Dal Maso, A. Inoue, A. Christopoulos, D. Wootten, and P. M. Sexton, 2016, "Ligand-Dependent Modulation of G Protein Conformation Alters Drug Efficacy", *Cell*, Vol. 167, No. 3, pp. 739- 749.e11.

Gandia, J., J. Galino, O. B. Amaral, A. Soriano, C. Lluís, R. Franco, and F. Ciruela, 2008, "Detection of Higher-Order G Protein-Coupled Receptor Oligomers by a Combined BRET-BiFC Technique", *FEBS Letters*, Vol. 582, No. 20, pp. 2979–2984.

Gao, X., G. A. Enten, A. J. DeSantis, B. F. Volkman, V. Gaponenko, and M. Majetschak, 2020, "Characterization of Heteromeric Complexes between Chemokine (C-X-C Motif) Receptor 4 and A1-Adrenergic Receptors Utilizing Intermolecular Bioluminescence Resonance Energy Transfer Assays", *Biochemical and Biophysical Research Communications*, Vol. 528, No. 2, pp. 368–375.

Ge, B., J. Lao, J. Li, Y. Chen, Y. Song, and F. Huang, 2017, "Single-Molecule Imaging Reveals Dimerization/Oligomerization of CXCR4 on Plasma Membrane Closely Related to Its Function", *Scientific Reports*, Vol. 7, No. 1, pp. 1–9.

Geiger, and Hesse, 1833, "Darstellung Des Atropins", *Annalen der Pharmacie*, Vol. 5, No.

1, pp. 43–81.

Geng, Y., M. Bush, L. Mosyak, F. Wang, and Q. R. Fan, 2013, "Structural Mechanism of Ligand Activation in Human GABA B Receptor", *Nature*, Vol. 504, No. 7479, pp. 254–259.

George, S. R., B. F. O'Dowd, and S. P. Lee, 2002, "G-protein-coupled receptor oligomerization and its potential for drug discovery", *Nature Reviews Drug Discovery*, Vol.1, No. 10, pp. 808–820.

Gerrard, A. W., 1875, "Alkaloid and Active Principle of Jaborandi", *The Pharmaceutical Journal and Translations*, Vol. 5, pp. 865.

Gether, U., S. Lin, and B. K. Kobilka, 1995, "Fluorescent Labeling of Purified B2 Adrenergic Receptor. Evidence for Ligand-Specific Conformational Changes", *Journal of Biological Chemistry*, Vol. 270, No. 47, pp. 28268–28275.

Godbole, A., S. Lyga, M. J. Lohse, and D. Calebiro, 2017, "Internalized TSH Receptors En Route to the TGN Induce Local Gs-Protein Signaling and Gene Transcription", *Nature Communications*, Vol. 8, No. 1, pp. 1–15.

Gong, J. H., and I. Clark-Lewis, 1995, "Antagonists of Monocyte Chemoattractant Protein 1 Identified by Modification of Functionally Critical Nh2-Terminal Residues", *Journal of Experimental Medicine*, Vol. 181, No. 2, pp. 631–640.

Gregorio, G. G., M. Masureel, D. Hilger, D. S. Terry, M. Juette, H. Zhao, Z. Zhou, J. M. Perez-Aguilar, M. Hauge, … S. C. Blanchard, 2017, "Single-Molecule Analysis of Ligand Efficacy in B2AR-G-Protein Activation", *Nature*, Vol. 547, No. 7661, pp. 68–73.

Griffith, J. W., C. L. Sokol, and A. D. Luster, 2014, "Chemokines and chemokine receptors: Positioning cells for host defense and immunity", *Annual Review of Immunology*, Vol. 31, No. 1, pp. 659–702.

Grisshammer, R., 2020, "The Quest for High-Resolution G Protein-Coupled Receptor-G Protein Structures", *Proceedings of the National Academy of Sciences of the United States of America*, Vol. 117, No. 13, pp. 6971–6973.

Grundmann, M., N. Merten, D. Malfacini, A. Inoue, P. Preis, K. Simon, N. Rüttiger, N. Ziegler, T. Benkel, … E. Kostenis, 2018, "Lack of Beta-Arrestin Signaling in the Absence of Active G Proteins", *Nature Communications*, Vol. 9, No. 1, pp. 1–16.

Grushevskyi, E. O., T. Kukaj, R. Schmauder, A. Bock, U. Zabel, T. Schwabe, K. Benndorf, and M. J. Lohse, 2019, "Stepwise Activation of a Class C GPCR Begins with Millisecond Dimer Rearrangement", *Proceedings of the National Academy of Sciences of the United States of America*, Vol. 116, No. 20, pp. 10150–10155.

Guo, H., S. An, R. Ward, Y. Yang, Y. Liu, X. X. Guo, Q. Hao, and T. R. Xu, 2017, ""Methods used to study the oligomeric structure of G-protein-coupled receptors", *Bioscience Reports*, Vol. 37, No. 2.

Guo, P., J. O. You, J. Yang, M. A. Moses, and D. T. Auguste, 2012, "Using Breast Cancer Cell CXCR4 Surface Expression to Predict Liposome Binding and Cytotoxicity", *Biomaterials*, Vol. 33, No. 32, pp. 8104–8110.

Guo, W., E. Urizar, M. Kralikova, J. C. Mobarec, L. Shi, M. Filizola, and J. A. Javitch, 2008, "Dopamine D2 Receptors Form Higher Order Oligomers at Physiological Expression Levels", *EMBO Journal*, Vol. 27, No. 17, pp. 2293–2304.

Hamatake, M., T. Aoki, Y. Futahashi, E. Urano, N. Yamamoto, and J. Komano, 2009, "Ligand-Independent Higher-Order Multimerization of CXCR4, a G-Protein-Coupled Chemokine Receptor Involved in Targeted Metastasis", *Cancer Science*, Vol. 100, No. 1, pp. 95–102.

Hamdan, F. F., Y. Percherancier, B. Breton, and M. Bouvier, 2006, "Monitoring Protein-Protein Interactions in Living Cells by Bioluminescence Resonance Energy Transfer (BRET)", *Current Protocols in Neuroscience*, Vol. 34, No. 1.

Hammad, M. M., Y. Q. Kuang, R. Yan, H. Allen, and D. J. Dupre, 2010, "Na+/H+ Exchanger Regulatory Factor-1 Is Involved in Chemokine Receptor Homodimer CCR5 Internalization and Signal Transduction but Does Not Affect CXCR4 Homodimer or CXCR4-CCR5 Heterodimer", *Journal of Biological Chemistry*, Vol. 285, No. 45, pp. 34653–34664.

Han, Y., I. S. Moreira, E. Urizar, H. Weinstein, and J. A. Javitch, 2009, "Allosteric Communication between Protomers of Dopamine Class a GPCR Dimers Modulates Activation", *Nature Chemical Biology*, Vol. 5, No. 9, pp. 688–695.

Hanson, S. M., E. V. Gurevich, S. A. Vishnivetskiy, M. R. Ahmed, X. Song, and V. V. Gurevich, 2007, "Each Rhodopsin Molecule Binds Its Own Arrestin", *Proceedings of the National Academy of Sciences of the United States of America*, Vol. 104, No. 9, pp. 3125–3128.

Hanyaloglu, A. C., R. M. Seeber, T. A. Kohout, R. J. Lefkowitz, and K. A. Eidne, 2002, "Homo- and Hetero-Oligomerization of Thyrotropin-Releasing Hormone (TRH) Receptor Subtypes: Differential Regulation of β-Arrestins 1 and 2", *Journal of Biological Chemistry*, Vol. 277, No. 52, pp. 50422–50430.

Harada, K., M. Ito, X. Wang, M. Tanaka, D. Wongso, A. Konno, H. Hirai, H. Hirase, T.

Tsuboi, and T. Kitaguchi, 2017, "Red Fluorescent Protein-Based CAMP Indicator Applicable to Optogenetics and in Vivo Imaging", *Scientific Reports*, Vol. 7, No. 1,.

Harvey, C. D., A. G. Ehrhardt, C. Cellurale, H. Zhong, R. Yasuda, R. J. Davis, and K. Svoboda, 2008, "A Genetically Encoded Fluorescent Sensor of ERK Activity", *Proceedings of the National Academy of Sciences of the United States of America*, Vol. 105, No. 49, pp. 19264–19269.

Hauser, A. S., M. M. Attwood, M. Rask-Andersen, H. B. Schiöth, and D. E. Gloriam, 2017, "Trends in GPCR Drug Discovery: New Agents, Targets and Indications", *Nature Reviews Drug Discovery*, Vol. 16, No. 12, pp. 829–842.

Hauser, M. A., K. Schaeuble, I. Kindinger, D. Impellizzieri, W. A. Krueger, C. R. Hauck, O. Boyman, and D. F. Legler, 2016, "Inflammation-Induced CCR7 Oligomers Form Scaffolds to Integrate Distinct Signaling Pathways for Efficient Cell Migration", *Immunity*, Vol. 44, No. 1, pp. 59–72.

Hayasaka, H., D. Kobayashi, H. Yoshimura, E. E. Nakayama, T. Shioda, and M. Miyasaka, 2015, "The HIV-1 Gp120/CXCR4 Axis Promotes CCR7 Ligand-Dependent CD4 T Cell Migration: CCR7 Homo- and CCR7/CXCR4 Hetero-Oligomer Formation as a Possible Mechanism for up-Regulation of Functional CCR7", *PLoS ONE*, Vol. 10, No. 2, pp. e0117454.

Hebert, B., S. Costantino, and P. W. Wiseman, 2005, "Spatiotemporal Image Correlation Spectroscopy (STICS) Theory, Verification, and Application to Protein Velocity Mapping in Living CHO Cells", *Biophysical Journal*, Vol. 88, No. 5, pp. 3601–3614.

Hebert, T. E., S. Moffett, J. P. Morello, T. P. Loisel, D. G. Bichet, C. Barret, and M. Bouvier, 1996, "A Peptide Derived from a β 2-Adrenergic Receptor Transmembrane Domain Inhibits Both Receptor Dimerization and Activation", *Journal of Biological*

Chemistry, Vol. 271, No. 27, pp. 16384–16392.

Hein, P., M. Frank, C. Hoffmann, M. J. Lohse, and M. Bünemann, 2005, "Dynamics of Receptor/G Protein Coupling in Living Cells", *EMBO Journal*, Vol. 24, No. 23, pp. 4106–4114.

Hemmerich, S., C. Paavola, A. Bloom, S. Bhakta, R. Freedman, D. Grunberger, J. Krstenansky, S. Lee, D. McCarley, … K. Jarnagin, 1999, "Identification of Residues in the Monocyte Chemotactic Protein-1 That Contact the MCP-1 Receptor, CCR2", *Biochemistry*, Vol. 38, No. 40, pp. 13013–13025.

Hereld, D., and P. N. Devreotes, 1993, "The CAMP Receptor Family of Dictyostelium", *International Review of Cytology*, Vol. 137, , pp. 35–47.

Hern, J. A., A. H. Baig, G. I. Mashanov, B. Birdsall, J. E. T. Corrie, S. Lazareno, J. E. Molloy, and N. J. M. Birdsall, 2010, "Formation and Dissociation of M1 Muscarinic Receptor Dimers Seen by Total Internal Reflection Fluorescence Imaging of Single Molecules", *Proceedings of the National Academy of Sciences of the United States of America*, Vol. 107, No. 6, pp. 2693–2698.

Hernandez, P. A., R. J. Gorlin, J. N. Lukens, S. Taniuchi, J. Bohinjec, F. Francois, M. E. Klotman, and G. A. Diaz, 2003, "Mutations in the Chemokine Receptor Gene CXCR4 Are Associated with WHIM Syndrome, a Combined Immunodeficiency Disease", *Nature Genetics*, Vol. 34, No. 1, pp. 70–74.

Hernanz-Falcón, P., J. M. Rodríguez-Frade, A. Serrano, D. Juan, A. del Sol, S. F. Soriano, F. Roncal, L. Gómez, A. Valencia, … M. Mellado, 2004, "Identification of Amino Acid Residues Crucial for Chemokine Receptor Dimerization", *Nature Immunology*, Vol. 5, No. 2, pp. 216–223.

Herrick-Davis, K., E. Grinde, A. Cowan, and J. E. Mazurkiewicz, 2013, "Fluorescence Correlation Spectroscopy Analysis of Serotonin, Adrenergic, Muscarinic, and Dopamine Receptor Dimerization: The Oligomer Number Puzzle", *Molecular Pharmacology*, Vol. 84, No. 4, pp. 630–642.

Herrick-Davis, K., E. Grinde, T. Lindsley, M. Teitler, F. Mancia, A. Cowan, and J. E. Mazurkiewicz, 2015, "Native Serotonin 5-HT2C Receptors Are Expressed as Homodimers on the Apical Surface of Choroid Plexus Epithelial Cells", *Molecular Pharmacology*, Vol. 87, No. 4, pp. 660–673.

Herrick-Davis, K., E. Grinde, and J. E. Mazurkiewicz, 2004, "Biochemical and Biophysical Characterization of Serotonin 5-HT2C Receptor Homodimers on the Plasma Membrane of Living Cells", *Biochemistry*, Vol. 43, No. 44, pp. 13963–13971.

Herrick-Davis, K., B. A. Weaver, E. Grinde, and J. E. Mazurkiewicz, 2006, "Serotonin 5-HT2C Receptor Homodimer Biogenesis in the Endoplasmic Reticulum: Real-Time Visualization with Confocal Fluorescence Resonance Energy Transfer", *Journal of Biological Chemistry*, Vol. 281, No. 37, pp. 27109–27116.

Heuninck, J., C. P. Viciano, A. Işbilir, B. Caspar, D. Capoferri, S. J. Briddon, T. Durroux, S. J. Hill, M. J. Lohse, … C. Hoffmann, 2019, "Context-dependent signaling of CXC chemokine receptor 4 and atypical chemokine receptor 3", *Molecular Pharmacology*, Vol. 96, No. 6, pp. 778–793.

Hildebrandt, J. D., J. Codina, R. Risinger, and L. Birnbaumer, 1984, "Identification of a γ Subunit Associated with the Adenylyl Cyclase Regulatory Proteins N(s) and N(I)", *Journal of Biological Chemistry*, Vol. 259, No. 4, pp. 2039–2042.

Hilger, D., K. K. Kumar, H. Hu, M. F. Pedersen, E. S. O'Brien, L. Giehm, C. Jennings, G. Eskici, A. Inoue, … B. K. Kobilka, 2020, "Structural Insights into Differences in G

Protein Activation by Family A and Family B GPCRs", *Science*, Vol. 369, No. 6503, pp. eaba3373.

Hill, A. V., 1913, "The Combinations of Haemoglobin with Oxygen and with Carbon Monoxide. I", *Biochemical Journal*, Vol. 7, No. 5, pp. 471–480.

Hislop, J. N., and M. Von Zastrow, 2011, "Analysis of GPCR Localization and Trafficking", *Methods in Molecular Biology*, Vol. 746, pp. 425–440.

Hokin, M. R., and L. E. Hokin, 1989, "The Journal of Biological Chemistry, Volume 203, 1953: Enzyme Secretion and the Incorporation of P32 into Phospholipides of Pancreas Slices.", *Nutrition Reviews*, Vol. 47, No. 6, pp. 170–172.

Holmes, W. E., J. Lee, W. J. Kuang, G. C. Rice, and W. I. Wood, 1991, "Structure and Functional Expression of a Human Interleukin-8 Receptor", *Science*, Vol. 253, No. 5025, pp. 1278–1280.

Hoogewerf, A. J., G. S. V. Kuschert, A. E. I. Proudfoot, F. Borlat, I. Clark-Lewis, C. A. Power, and T. N. C. Wells, 1997, "Glycosaminoglycans Mediate Cell Surface Oligomerization of Chemokines", *Biochemistry*, Vol. 36, No. 44, pp. 13570–13578.

Huang, J., S. Chen, J. J. Zhang, and X. Y. Huang, 2013, "Crystal Structure of Oligomeric β 1-Adrenergic G Protein-Coupled Receptors in Ligand-Free Basal State", *Nature Structural and Molecular Biology*, Vol. 20, No. 4, pp. 419–425.

Hughes, C. E., and R. J. B. Nibbs, 2018, "A guide to chemokines and their receptors", *FEBS Journal*, Vol. 285, No. 16, pp. 2944–2971.

Humpert, M. L., M. Tzouros, S. Thelen, A. Bignon, A. Levoye, F. Arenzana-Seisdedos,

K. Balabanian, F. Bachelerie, H. Langen, and M. Thelen, 2012, "Complementary Methods Provide Evidence for the Expression of CXCR7 on Human B Cells", *Proteomics*, Vol. 12, No. 12, pp. 1938–1948.

Hurevich, M., M. Ratner-Hurevich, Y. Tal-Gan, D. E. Shalev, S. Z. Ben-Sasson, and C. Gilon, 2013, "Backbone Cyclic Helix Mimetic of Chemokine (C-C Motif) Receptor 2: A Rational Approach for Inhibiting Dimerization of G Protein-Coupled Receptors", *Bioorganic and Medicinal Chemistry*, Vol. 21, No. 13, pp. 3958–3966.

Ilien, B., N. Glasser, J. P. Clamme, P. Didier, E. Piemont, R. Chinnappan, S. B. Daval, J. L. Galzi, and Y. Mely, 2009, "Pirenzepine Promotes the Dimerization of Muscarinic M1 Receptors through a Three-Step Binding Process", *Journal of Biological Chemistry*, Vol. 284, No. 29, pp. 19533–19543.

Infantino, S., B. Moepps, and M. Thelen, 2006, "Expression and Regulation of the Orphan Receptor RDC1 and Its Putative Ligand in Human Dendritic and B Cells", *The Journal of Immunology*, Vol. 176, No. 4, pp. 2197–2207.

Irannejad, R., V. Pessino, D. Mika, B. Huang, P. B. Wedegaertner, M. Conti, and M. Von Zastrow, 2017, "Functional Selectivity of GPCR-Directed Drug Action through Location Bias", *Nature Chemical Biology*, Vol. 13, No. 7, pp. 799–806.

Isaikina, P., C. J. Tsai, N. Dietz, F. Pamula, A. Grahl, K. N. Goldie, R. Guixà-González, G. F. X. Schertler, O. Hartley, … S. Grzesiek, 2020, "Structural basis of the activation of the CC chemokine receptor 5 by a chemokine agonist", *bioRxiv*.

Işbilir, A., J. Möller, M. Arimont, V. Bobkov, C. Perpiñá-Viciano, C. Hoffmann, A. Inoue, R. Heukers, C. de Graaf, … M. J. Lohse, 2020, "Advanced Fluorescence Microscopy Reveals Disruption of Dynamic CXCR4 Dimerization by Subpocket-Specific Inverse Agonists", *Proceedings of the National Academy of Sciences of the United States of*

America, Vol. 117, No. 46, pp. 29144–29154.

Isbilir, A., J. Möller, A. Bock, U. Zabel, P. Annibale, and M. J. Lohse, 2017, "Visualization of Class A GPCR Oligomerization by Image-Based Fluorescence Fluctuation Spectroscopy", *bioRxiv*.

Işbilir, A., R. Serfling, J. Möller, R. Thomas, C. De Faveri, U. Zabel, M. Scarselli, A. G. Beck-Sickinger, A. Bock, … P. Annibale, 2021, "Determination of G-Protein–Coupled Receptor Oligomerization by Molecular Brightness Analyses in Single Cells", *Nature Protocols*, Vol. 16, No. 3, pp. 1419–1451.

Isik, N., D. Hereld, and T. Jin, 2008, "Fluorescence Resonance Energy Transfer Imaging Reveals That Chemokine-Binding Modulates Heterodimers of CXCR4 and CCR5 Receptors", *PLoS ONE*, Vol. 3, No. 10.

Issafras, H., S. Angers, S. Bulenger, C. Blanpain, M. Parmentier, C. Labbé-Jullié, M. Bouvier, and S. Marullo, 2002, "Constitutive Agonist-Independent CCR5 Oligomerization and Antibody-Mediated Clustering Occurring at Physiological Levels of Receptors", *Journal of Biological Chemistry*, Vol. 277, No. 38, pp. 34666–34673.

Jaeger, K., S. Bruenle, T. Weinert, W. Guba, J. Muehle, T. Miyazaki, M. Weber, A. Furrer, N. Haenggi, … J. Standfuss, 2019, "Structural Basis for Allosteric Ligand Recognition in the Human CC Chemokine Receptor 7", *Cell*, Vol. 178, No. 5, pp. 1222- 1230.e10.

Jakubík, J., A. Randáková, N. Chetverikov, E. E. El-Fakahany, and V. Doležal, 2020, "The Operational Model of Allosteric Modulation of Pharmacological Agonism", *Scientific Reports*, Vol. 10, No. 1, pp. 14421.

Janetopoulos, C., T. Jin, and P. Devreotes, 2001, "Receptor-Mediated Activation of Heterotrimeric G-Proteins in Living Cells", *Science*, Vol. 291, No. 5512, pp. 2408–2411.

Jin, J., F. Momboisse, G. Boncompain, F. Koensgen, Z. Zhou, N. Cordeiro, F. Arenzana-Seisdedos, F. Perez, B. Lagane, … A. Brelot, 2018, "CCR5 Adopts Three Homodimeric Conformations That Control Cell Surface Delivery", *Science Signaling*, Vol. 11, No. 529, pp. 2869.

Jing, M., P. Zhang, G. Wang, J. Feng, L. Mesik, J. Zeng, H. Jiang, S. Wang, J. C. Looby, … Y. Li, 2018, "A Genetically Encoded Fluorescent Acetylcholine Indicator for in Vitro and in Vivo Studies", *Nature Biotechnology*, Vol. 36, No. 8, pp. 726–737.

Joost, P., and A. Methner, 2002, "Phylogenetic Analysis of 277 Human G-Protein-Coupled Receptors as a Tool for the Prediction of Orphan Receptor Ligands.", *Genome biology*, Vol. 3, No. 11, pp. 1–16.

Kalatskaya, I., Y. A. Berchiche, S. Gravel, B. J. Limberg, J. S. Rosenbaum, and N. Heveker, 2009, "AMD3100 Is a CXCR7 Ligand with Allosteric Agonist Properties", *Molecular Pharmacology*, Vol. 75, No. 5, pp. 1240–1247.

Kallikourdis, M., A. E. Trovato, F. Anselmi, A. Sarukhan, G. Roselli, L. Tassone, R. Badolato, and A. Viola, 2013, "The CXCR4 Mutations in WHIM Syndrome Impair the Stability of the T-Cell Immunologic Synapse", *Blood*, Vol. 122, No. 5, pp. 666–673.

Kasai, R. S., K. G. N. Suzuki, E. R. Prossnitz, I. Koyama-Honda, C. Nakada, T. K. Fujiwara, and A. Kusumi, 2011, "Full Characterization of GPCR Monomer-Dimer Dynamic Equilibrium by Single Molecule Imaging", *Journal of Cell Biology*, Vol. 192, No. 3, pp. 463–480.

Kauk, M., and C. Hoffmann, 2018, "Intramolecular and Intermolecular FRET Sensors for GPCRs – Monitoring Conformational Changes and Beyond", *Trends in Pharmacological Sciences*, Vol. 29, No. 2, pp. 123–135.

Kawai, T., B. Sun, H. Yoshino, D. Feng, Y. Suzuki, M. Fukazawa, S. Nagao, D. B. Wainscott, A. D. Showalter, … K. W. Sloop, 2020, "Structural Basis for GLP-1 Receptor Activation by LY3502970, an Orally Active Nonpeptide Agonist", *Proceedings of the National Academy of Sciences of the United States of America*, Vol. 117, No. 47, pp. 29959–29967.

Kent, R. S., A. De Lean, and R. J. Lefkowitz, 1980, "A Quantitative Analysis of Beta-Adrenergic Receptor Interactions: Resolution of High and Low Affinity States of the Receptor by Computer Modeling of Ligand Binding Data", *Molecular Pharmacology*, Vol. 17, No. 1, pp. 14–23.

Kilpatrick, L. E., S. J. Briddon, and N. D. Holliday, 2012, "Fluorescence Correlation Spectroscopy, Combined with Bimolecular Fluorescence Complementation, Reveals the Effects of β-Arrestin Complexes and Endocytic Targeting on the Membrane Mobility of Neuropeptide Y Receptors", *Biochimica et Biophysica Acta - Molecular Cell Research*, Vol. 1823, No. 6, pp. 1068–1081.

Klarenbeek, J., J. Goedhart, A. Van Batenburg, D. Groenewald, and K. Jalink, 2015, "Fourth-Generation Epac-Based FRET Sensors for CAMP Feature Exceptional Brightness, Photostability and Dynamic Range: Characterization of Dedicated Sensors for FLIM, for Ratiometry and with High Affinity", *PLoS ONE*, Vol. 10, No. 4.

Kleist, A. B., A. E. Getschman, J. J. Ziarek, A. M. Nevins, P. A. Gauthier, A. Chevigné, M. Szpakowska, and B. F. Volkman, 2016, "New paradigms in chemokine receptor signal transduction: Moving beyond the two-site model", *Biochemical*

Pharmacology. Vol. 114, pp. 53–68.

Kniazeff, J., A. S. Bessis, D. Maurel, H. Ansanay, L. Prézeau, and J. P. Pin, 2004, "Closed State of Both Binding Domains of Homodimeric MGlu Receptors Is Required for Full Activity", *Nature Structural and Molecular Biology*, Vol. 11, No. 8, pp. 706–713.

Kniazeff, J., L. Prézeau, P. Rondard, J. P. Pin, and C. Goudet, 2011, "Dimers and beyond: The functional puzzles of class C GPCRs", *Pharmacology and Therapeutics*, Vol. 130, No. 1, pp. 9–25.

Knight, K. M., S. Ghosh, S. L. Campbell, T. J. Lefevre, R. H. J. Olsen, A. V. Smrcka, N. H. Valentin, G. Yin, N. Vaidehi, and H. G. Dohlman, 2020, "A Universal Allosteric Mechanism for G Protein Activation.", *bioRxiv*.

Kobilka, B. K., R. A. F. Dixon, T. Frielle, H. G. Dohlman, M. A. Bolanowski, I. S. Sigal, T. L. Yang-Feng, U. Francke, M. G. Caron, and R. J. Lefkowitz, 1987, "cDNA for the Human B2-Adrenergic Receptor: A Protein with Multiple Membrane-Spanning Domains and Encoded by a Gene Whose Chromosomal Location Is Shared with That of the Receptor for Platelet-Derived Growth Factor", *Proceedings of the National Academy of Sciences of the United States of America*, Vol. 84, No. 1, pp. 46–50.

Kobilka, B. K., H. Matsui, T. S. Kobilka, T. L. Yang-Feng, U. Francke, M. G. Caron, R. J. Lefkowitz, and J. W. Regan, 1987, "Cloning, Sequencing, and Expression of the Gene Coding for the Human Platelet A2-Adrenergic Receptor", *Science*, Vol. 238, No. 4827, pp. 650–656.

Koehl, A., H. Hu, D. Feng, B. Sun, Y. Zhang, M. J. Robertson, M. Chu, T. S. Kobilka, T. Laermans, … B. K. Kobilka, 2019, "Structural Insights into the Activation of Metabotropic Glutamate Receptors", *Nature*, Vol. 566, No. 7742, pp. 79–84.

Kooistra, A. J., S. Mordalski, G. Pándy-Szekeres, M. Esguerra, A. Mamyrbekov, C. Munk, G. M. Keserű, and D. E. Gloriam, 2021, "GPCRdb in 2021: Integrating GPCR Sequence, Structure and Function", *Nucleic Acids Research*, Vol. 49, No. D1, pp. D335–D343.

Krasel, C., M. Bünemann, K. Lorenz, and M. J. Lohse, 2005, "β-Arrestin Binding To the B2-Adrenergic Receptor Requires Both Receptor Phosphorylation and Receptor Activation", *Journal of Biological Chemistry*, Vol. 280, No. 10, pp. 9528–9535.

Krumm, B., and B. L. Roth, 2020, "A Structural Understanding of Class B GPCR Selectivity and Activation Revealed", *Structure*, Vol. 28, No. 3, pp. 277–279.

Kuang, Y. Q., N. Charette, J. Frazer, P. J. Holland, K. M. Attwood, G. Dellaire, and D. J. Dupré, 2012, "Dopamine Receptor-Interacting Protein 78 Acts as a Molecular Chaperone for CCR5 Chemokine Receptor Signaling Complex Organization", *PLoS ONE*, Vol. 7, No. 7, pp. 40522.

Kühn, H., 1978, "Light-Regulated Binding of Rhodopsin Kinase and Other Proteins to Cattle Photoreceptor Membranes", *Biochemistry*, Vol. 17, No. 21, pp. 4389–4395.

Kühn, H., S. W. Hall, and U. Wilden, 1984, "Light-Induced Binding of 48-KDa Protein to Photoreceptor Membranes Is Highly Enhanced by Phosphorylation of Rhodopsin", *FEBS Letters*, Vol. 176, No. 2, pp. 473–478.

Kumar, A., T. D. Humphreys, K. N. Kremer, P. S. Bramati, L. Bradfield, C. E. Edgar, and K. E. Hedin, 2006, "CXCR4 Physically Associates with the T Cell Receptor to Signal in T Cells", *Immunity*, Vol. 25, No. 2, pp. 213–224.

Kunishima, N., Y. Shimada, Y. Tsuji, T. Sato, M. Yamamoto, T. Kumasaka, S. Nakanishi,

H. Jingami, and K. Morikawa, 2000, "Structural Basis of Glutamate Recognition by a Dimeric Metabotropic Glutamate Receptor", *Nature*, Vol. 407, No. 6807, pp. 971–977.

Kuschen, G. S. V., F. Coulin, C. A. Power, A. E. I. Proudfoot, R. E. Hubbard, A. J. Hoogewerf, and T. N. C. Wells, 1999, "Glycosaminoglycans Interact Selectively with Chemokines and Modulate Receptor Binding and Cellular Responses", *Biochemistry*, Vol. 38, No. 39, pp. 12959–12968.

Kuszak, A. J., S. Pitchiaya, J. P. Anand, H. I. Mosberg, N. G. Walter, and R. K. Sunahara, 2009, "Purification and Functional Reconstitution of Monomeric μ-Opioid Receptors. Allosteric Modulation of Agonists Binding by Gi2", *Journal of Biological Chemistry*, Vol. 284, No. 39, pp. 26732–26741.

Labrecque, J., V. Anastassov, G. Lau, M. Darkes, R. Mosi, and S. P. Fricker, 2005, "The Development of an Europium-GTP Assay to Quantitate Chemokine Antagonist Interactions for CXCR4 and CCR5", *Assay and Drug Development Technologies*, Vol. 3, No. 6, pp. 637–648.

Ladenburg, A., 1881, "Die Natürlich Vorkommenden Mydriatisch Wirkenden Alkaloïde", *Justus Liebigs Annalen der Chemie*, Vol. 206, No. 3, pp. 274–307.

Lagane, B., K. Y. C. Chow, K. Balabanian, A. Levoye, J. Harriague, T. Planchenault, F. Baleux, N. Gunera-Saad, F. Arenzana-Seisdedos, and F. Bachelerie, 2008, "CXCR4 Dimerization and 2-Arrestin Mediated Signaling Account for the Enhanced Chemotaxis to CXCL12 in WHIM Syndrome", *Blood*, Vol. 112, No. 1, pp. 34–44.

Lally, C. C. M., B. Bauer, J. Selent, and M. E. Sommer, 2017, "C-Edge Loops of Arrestin Function as a Membrane Anchor", *Nature Communications*, Vol. 8.

Lam, W., A. C. Yeung, I. M. Chu, and P. K. S. Chan, 2010, "Profiles of Cytokine and Chemokine Gene Expression in Human Pulmonary Epithelial Cells Induced by Human and Avian Influenza Viruses", *Virology Journal*, Vol. 7, No. 1, pp. 344.

Lambert, N. A., and J. A. Javitch, 2014, "CrossTalk opposing view: Weighing the evidence for class A GPCR dimers, the jury is still out", *Journal of Physiology*, Vol. 592, No. 12, pp. 2443–2445.

Lamichhane, R., J. J. Liu, G. Pljevaljcic, K. L. White, E. Der Van Schans, V. Katritch, R. C. Stevens, K. Wüthrich, and D. P. Millar, 2015, "Single-Molecule View of Basal Activity and Activation Mechanisms of the G Protein-Coupled Receptor B2 AR", *Proceedings of the National Academy of Sciences of the United States of America*, Vol. 112, No. 46, pp. 14254–14259.

Langley, J. N., 1905, "On the Reaction of Cells and of Nerve-endings to Certain Poisons, Chiefly as Regards the Reaction of Striated Muscle to Nicotine and to Curari", *The Journal of Physiology*, Vol. 33, No. 4–5, pp. 374–413.

Lao, J., H. He, X. Wang, Z. Wang, Y. Song, B. Yang, N. Ullahkhan, B. Ge, and F. Huang, 2017, "Single-Molecule Imaging Demonstrates Ligand Regulation of the Oligomeric Status of CXCR4 in Living Cells", *Journal of Physical Chemistry B*, Vol. 121, No. 7, pp. 1466–1474.

Latorraca, N. R., J. K. Wang, B. Bauer, R. J. L. Townshend, S. A. Hollingsworth, J. E. Olivieri, H. E. Xu, M. E. Sommer, and R. O. Dror, 2018, "Molecular Mechanism of GPCR-Mediated Arrestin Activation", *Nature*, Vol. 557, No. 7705, pp. 452–456.

Lavington, S., and A. Watts, 2020, "Lipid nanoparticle technologies for the study of G protein-coupled receptors in lipid environments", *Biophysical Reviews*, Vol. 12, No. 6, pp. 1287–1302.

Leach, K., and K. J. Gregory, 2017, "Molecular insights into allosteric modulation of Class C G protein-coupled receptors", *Pharmacological Research*, Vol. 116, pp. 105–118.

Leach, K., P. M. Sexton, and A. Christopoulos, 2007, "Allosteric GPCR Modulators: Taking Advantage of Permissive Receptor Pharmacology", *Trends in Pharmacological Sciences*, Vol. 28, No. 8, pp. 382–389.

Lebon, G., T. Warne, and C. G. Tate, 2012, "Agonist-bound structures of G protein-coupled receptors", *Current Opinion in Structural Biology*, Vol. 22, No. 4, pp. 482–490.

Lee, B., M. Sharron, L. J. Montaner, D. Weissman, and R. W. Doms, 1999, "Quantification of CD4, CCR5, and CXCR4 Levels on Lymphocyte Subsets, Dendritic Cells, and Differentially Conditioned Monocyte-Derived Macrophages", *Proceedings of the National Academy of Sciences of the United States of America*, Vol. 96, No. 9, pp. 5215–5220.

Lefkowitz, R. J., J. Roth, W. Pricer, and I. Pastan, 1970, "ACTH Receptors in the Adrenal: Specific Binding of ACTH-125I and Its Relation to Adenyl Cyclase.", *Proceedings of the National Academy of Sciences of the United States of America*, Vol. 65, No. 3, pp. 745–752.

Levitz, J., C. Habrian, S. Bharill, Z. Fu, R. Vafabakhsh, and E. Y. Isacoff, 2016, "Mechanism of Assembly and Cooperativity of Homomeric and Heteromeric Metabotropic Glutamate Receptors", *Neuron*, Vol. 92, No. 1, pp. 143–159.

Levoye, A., K. Balabanian, F. Baleux, F. Bachelerie, and B. Lagane, 2009, "CXCR7 Heterodimerizes with CXCR4 and Regulates CXCL12-Mediated G Protein Signaling", *Blood*, Vol. 113, No. 24, pp. 6085–6093.

Levoye, A., J. Dam, M. A. Ayoub, J. L. Guillaume, C. Couturier, P. Delagrange, and R. Jockers, 2006, "The Orphan GPR50 Receptor Specifically Inhibits MT1 Melatonin Receptor Function through Heterodimerization", *EMBO Journal*, Vol. 25, No. 13, pp. 3012–3023.

Levoye, A., J. M. Zwier, A. Jaracz-Ros, L. Klipfel, M. Cottet, D. Maurel, S. Bdioui, K. Balabanian, L. Prézeau, … F. Bachelerie, 2015, "A Broad G Protein-Coupled Receptor Internalization Assay That Combines SNAP-Tag Labeling, Diffusion-Enhanced Resonance Energy Transfer, and a Highly Emissive Terbium Cryptate", *Frontiers in Endocrinology*, Vol. 6.

Lewitt, M., 1902, "Yohimbin (Spiegel), Ein Neues Alkaloid, Specificum Gegen Impotenz (Schluss Aus No. 47.)", *Deutsche Medizinische Wochenschrift*, Vol. 28, No. 48, pp. 870–871.

Liang, Y. L., M. Khoshouei, A. Glukhova, S. G. B. Furness, P. Zhao, L. Clydesdale, C. Koole, T. T. Truong, D. M. Thal, … D. Wootten, 2018, "Phase-Plate Cryo-EM Structure of a Biased Agonistbound Human GLP-1 Receptor-Gs Complex", *Nature*, Vol. 555, No. 7694, pp. 121–125.

Liang, Y. L., M. Khoshouei, M. Radjainia, Y. Zhang, A. Glukhova, J. Tarrasch, D. M. Thal, S. G. B. Furness, G. Christopoulos, … P. M. Sexton, 2017, "Phase-Plate Cryo-EM Structure of a Class B GPCR-G-Protein Complex", *Nature*, Vol. 546, No. 7656, pp. 118–123.

Liauw, B. W. H., H. S. Afsari, and R. Vafabakhsh, 2021, "Conformational Rearrangement during Activation of a Metabotropic Glutamate Receptor", *Nature Chemical Biology*, Vol. 17, No. 3, pp. 291–297.

Liebscher, I., J. Schön, S. C. Petersen, L. Fischer, N. Auerbach, L. M. Demberg, A. Mogha,

M. Cöster, K. U. Simon, … T. Schöneberg, 2014, "A Tethered Agonist within the Ectodomain Activates the Adhesion G Protein-Coupled Receptors GPR126 and GPR133", *Cell Reports*, Vol. 9, No. 6, pp. 2018–2026.

Limbird, L. E., P. De Meyts, and R. J. Lefkowitz, 1975, "β-Adrenergic Receptors: Evidence for Negative Cooperativity", *Biochemical and Biophysical Research Communications*, Vol. 64, No. 4, pp. 1160–1168.

Liu, D., P. Guo, C. McCarthy, B. Wang, Y. Tao, and D. Auguste, 2018, "Peptide Density Targets and Impedes Triple Negative Breast Cancer Metastasis", *Nature Communications*, Vol. 9, No. 1, pp. 1–11.

Liu, J., Z. Zhang, D. Moreno-Delgado, J. A. R. Dalton, X. Rovira, A. Trapero, C. Goudet, A. Llebaria, J. Giraldo, … J. P. Pin, 2017, "Allosteric Control of an Asymmetric Transduction in a g Protein-Coupled Receptor Heterodimer", *eLife*, Vol. 6.

Liu, K., L. Wu, S. Yuan, M. Wu, Y. Xu, Q. Sun, S. Li, S. Zhao, T. Hua, and Z. J. Liu, 2020, "Structural Basis of CXC Chemokine Receptor 2 Activation and Signalling", *Nature*, Vol. 585, No. 7823, pp. 135–140.

Liu, Q., H. Chen, T. Ojode, X. Gao, S. Anaya-O'Brien, N. A. Turner, J. Ulrick, R. DeCastro, C. Kelly, … D. H. McDermott, 2012, "WHIM Syndrome Caused by a Single Amino Acid Substitution in the Carboxy-Tail of Chemokine Receptor CXCR4", *Blood*, Vol. 120, No. 1, pp. 181–189.

Liu, X., S. Ahn, A. W. Kahsai, K. C. Meng, N. R. Latorraca, B. Pani, A. J. Venkatakrishnan, A. Masoudi, W. I. Weis, … B. K. Kobilka, 2017, "Mechanism of Intracellular Allosteric β 2 AR Antagonist Revealed by X-Ray Crystal Structure", *Nature*, Vol. 548, No. 7668, pp. 480–484.

Lohse, M. J., J. L. Benovic, J. Codina, M. G. Caron, and R. J. Lefkowitz, 1990, "β-Arrestin: A Protein That Regulates β-Adrenergic Receptor Function", *Science*, Vol. 248, No. 4962, pp. 1547–1550.

Lohse, M. J., and D. Calebiro, 2013, "Cell biology: Receptor signals come in waves", *Nature*, Vol. 495, No. 7442, pp. 457–458

Lohse, M. J., V. O. Nikolaev, P. Hein, C. Hoffmann, J. P. Vilardaga, and M. Bünemann, 2008, "Optical Techniques to Analyze Real-Time Activation and Signaling of G-Protein-Coupled Receptors", *Trends in Pharmacological Sciences*, Vol. 29, No. 3, pp. 159–165.

Lomasney, J. W., L. M. F. Leeb-Lundberg, S. Cotecchia, J. W. Regan, J. F. DeBernardis, M. G. Caron, and R. J. Lefkowitz, 1986, "Mammalian A1-Adrenergic Receptor. Purification and Characterization of the Native Receptor Ligand Binding Subunit", *Journal of Biological Chemistry*, Vol. 261, No. 17, pp. 7710–7716.

Lorenz, K., M. J. Lohse, and U. Quitterer, 2003, "Protein Kinase C Switches the Raf Kinase Inhibitor from Raf-1 to GRK-2", *Nature*, Vol. 426, No. 6966, pp. 574–579.

Łukasiewicz, S., E. Błasiak, A. Faron-Górecka, A. Polit, M. Tworzydło, A. Górecki, Z. Wasylewski, and M. Dziedzicka-Wasylewska, 2007, "Fluorescence Studies of Homooligomerization of Adenosine A2A and Serotonin 5-HT1A Receptors Reveal the Specificity of Receptor Interactions in the Plasma Membrane", *Pharmacological Reports*, Vol. 59, No. 4, pp. 379–392.

Luker, K. E., J. M. Steele, L. A. Mihalko, P. Ray, and G. D. Luker, 2010, "Constitutive and Chemokine-Dependent Internalization and Recycling of CXCR7 in Breast Cancer Cells to Degrade Chemokine Ligands", *Oncogene*, Vol. 29, No. 32, pp. 4599–4610.

Luker, Kathryn E., M. Gupta, and G. D. Luker, 2009, "Imaging Chemokine Receptor Dimerization with Firefly Luciferase Complementation", *The FASEB Journal*, Vol. 23, No. 3, pp. 823–834.

Luttrell, L. M., J. Wang, B. Plouffe, J. S. Smith, L. Yamani, S. Kaur, P. Y. Jean-Charles, C. Gauthier, M. H. Lee, … R. J. Lefkowitz, 2018, "Manifold Roles of β-Arrestins in GPCR Signaling Elucidated with SiRNA and CRISPR/Cas9", *Science Signaling*, Vol. 11, No. 549, pp. 7650.

Ma, Q., D. Jones, P. R. Borghesani, R. A. Segal, T. Nagasawa, T. Kismimoto, R. T. Bronson, and T. A. Springer, 1998, "Impaired B-Lymphopoiesis, Myelopoiesis, and Derailed Cerebellar Neuron Migration in CXCR4- and SDF-1-Deficient Mice", *Proceedings of the National Academy of Sciences of the United States of America*, Vol. 95, No. 16, pp. 9448–9453.

Ma, S., Q. Shen, L. H. Zhao, C. Mao, X. E. Zhou, D. D. Shen, P. W. de Waal, P. Bi, C. Li, … H. E. Xu, 2020, "Molecular Basis for Hormone Recognition and Activation of Corticotropin-Releasing Factor Receptors", *Molecular Cell*, Vol. 77, No. 3, pp. 669-680.e4.

Maeda, R., M. Hiroshima, T. Yamashita, A. Wada, S. Nishimura, Y. Sako, Y. Shichida, and Y. Imamoto, 2014, "Single-Molecule Observation of the Ligand-Induced Population Shift of Rhodopsin, A G-Protein-Coupled Receptor", *Biophysical Journal*, Vol. 106, No. 4, pp. 915–924.

Magde, D., E. Elson, and W. W. Webb, 1972, "Thermodynamic Fluctuations in a Reacting System Measurement by Fluorescence Correlation Spectroscopy", *Physical Review Letters*, Vol. 29, No. 11, pp. 705–708.

Mancia, F., Z. Assur, A. G. Herman, R. Siegel, and W. A. Hendrickson, 2008, "Ligand

Sensitivity in Dimeric Associations of the Serotonin 5HT2c Receptor", *EMBO Reports*, Vol. 9, No. 4, pp. 363–369.

Manglik, A., A. C. Kruse, T. S. Kobilka, F. S. Thian, J. M. Mathiesen, R. K. Sunahara, L. Pardo, W. I. Weis, B. K. Kobilka, and S. Granier, 2012, "Crystal Structure of the μ-Opioid Receptor Bound to a Morphinan Antagonist", *Nature*, Vol. 485, No. 7398, pp. 321–326.

Mantovani, A., 1999, "The chemokine system: Redundancy for robust outputs", *Immunology Today*, Vol. 20, No. 6, pp. 254–257.

Marinissen, M. J., and J. S. Gutkind, 2001, "G-protein-coupled receptors and signaling networks: Emerging paradigms", *Trends in Pharmacological Sciences*, Vol. 22, No. 7, pp. 368–376.

Marsango, S., M. C. Bonaccorsi Di Patti, D. Barra, and R. Miele, 2011, "Evidence That Prokineticin Receptor 2 Exists as a Dimer in Vivo", *Cellular and Molecular Life Sciences*, Vol. 68, No. 17, pp. 2919–2929.

Marsango, S., G. Caltabiano, M. Jiménez-Rosés, M. J. Millan, J. D. Pediani, R. J. Ward, and G. Milligan, 2017, "A Molecular Basis for Selective Antagonist Destabilization of Dopamine D3 Receptor Quaternary Organization", *Scientific Reports*, Vol. 7, No. 1,.

Martínez-Muñoz, L., R. Barroso, S. Y. Dyrhaug, G. Navarro, P. Lucas, S. F. Soriano, B. Vega, C. Costas, M. Ángeles Muñoz-Fernández, … M. Mellado, 2014, "CCR5/CD4/CXCR4 Oligomerization Prevents HIV-1 Gp120IIIB Binding to the Cell Surface", *Proceedings of the National Academy of Sciences of the United States of America*, Vol. 111, No. 19, pp. E1960–E1969.

Martínez-Muñoz, L., J. M. Rodríguez-Frade, R. Barroso, C. Ó. S. Sorzano, J. A. Torreño-Pina, C. A. Santiago, C. Manzo, P. Lucas, E. M. García-Cuesta, … M. Mellado, 2018, "Separating Actin-Dependent Chemokine Receptor Nanoclustering from Dimerization Indicates a Role for Clustering in CXCR4 Signaling and Function", *Molecular Cell*, Vol. 70, No. 1, pp. 106- 119.e10.

Martínez-Muñoz, L., R. Villares, J. L. Rodríguez-Fernández, J. M. Rodríguez-Frade, and M. Mellado, 2018, "Remodeling our concept of chemokine receptor function: From monomers to oligomers", *Journal of Leukocyte Biology*, Vol. 104, No. 2, pp. 323–331.

Martínez Muñoz, L., P. Lucas, G. Navarro, A. I. Checa, R. Franco, C. Martínez-A., J. M. Rodríguez-Frade, and M. Mellado, 2009, "Dynamic Regulation of CXCR1 and CXCR2 Homo- and Heterodimers", *The Journal of Immunology*, Vol. 183, No. 11, pp. 7337–7346.

Maslov, I., O. Volkov, P. Khorn, P. Orekhov, A. Gusach, P. Kuzmichev, A. Gerasimov, A. Luginina, Q. Coucke, … V. Borshchevskiy, 2020, "Sub-millisecond conformational dynamics of the A2A adenosine receptor revealed by single-molecule FRET", *bioRxiv*.

Masuho, I., N. K. Skamangas, B. S. Muntean, and K. A. Martemyanov, 2021, "Diversity of the Gβγ Complexes Defines Spatial and Temporal Bias of GPCR Signaling", *Cell Systems*, Vol. 12, No. 4, pp.324–337.e5.

Matthews, C., and F. P. Cordelières, 2010, "MetroloJ : an ImageJ plugin to help monitor microscopes' health.", *Image Use Develope Conference*

Mayer M R. an M J Stone 2001 "Identificatio o Recepto Bindin an Activatio Determinant i th N-Termina an N-Loo Region o th C Chemokin Eotaxin"

Journal of Biological Chemistry, Vol. 276, No. 17, pp. 13911–13916.

McEwen, D. P., K. R. Gee, H. C. Kang, and R. R. Neubig, 2001, "Fluorescent BODIPY-GTP Analogs: Real-Time Measurement of Nucleotide Binding to G Proteins", *Analytical Biochemistry*, Vol. 291, No. 1, pp. 109–117.

Mehta, S., Y. Zhang, R. H. Roth, J. fan Zhang, A. Mo, B. Tenner, R. L. Huganir, and J. Zhang, 2018, "Single-Fluorophore Biosensors for Sensitive and Multiplexed Detection of Signalling Activities", *Nature Cell Biology*, Vol. 20, No. 10, pp. 1215–1225.

Melo, R. D. C. C., A. L. Longhini, C. L. Bigarella, M. O. Baratti, F. Traina, P. Favaro, P. D. M. Campos, and S. T. O. Saad, 2014, "CXCR7 Is Highly Expressed in Acute Lymphoblastic Leukemia and Potentiates CXCR4 Response to CXCL12", *PLoS ONE*, Vol. 9, No. 1.

Merlen, C., N. Farhat, X. Luo, D. Chatenet, A. Tadevosyan, L. R. Villeneuve, M. A. Gillis, S. Nattel, E. Thorin, … B. G. Allen, 2013, "Intracrine Endothelin Signaling Evokes IP3-Dependent Increases in Nucleoplasmic Ca2+ in Adult Cardiac Myocytes", *Journal of Molecular and Cellular Cardiology*, Vol. 62, , pp. 189–202.

Métayé, T., H. Gibelin, R. Perdrisot, and J. L. Kraimps, 2005, "Pathophysiological roles of G-protein-coupled receptor kinases", *Cellular Signalling*, Vol. 17, No. 8, pp. 917–928.

Meyrath, M., M. Szpakowska, J. Zeiner, L. Massotte, M. P. Merz, T. Benkel, K. Simon, J. Ohnmacht, J. D. Turner, … A. Chevigné, 2020, "The Atypical Chemokine Receptor ACKR3/CXCR7 Is a Broad-Spectrum Scavenger for Opioid Peptides", *Nature Communications*, Vol. 11, No. 1, pp. 1–16.

Miao, Z., K. E. Luker, B. C. Summers, R. Berahovich, M. S. Bhojani, A. Rehemtulla, C. G. Kleer, J. J. Essner, A. Nasevicius, … T. J. Schall, 2007, "CXCR7 (RDC1) Promotes Breast and Lung Tumor Growth in Vivo and Is Expressed on Tumor-Associated Vasculature", *Proceedings of the National Academy of Sciences of the United States of America*, Vol. 104, No. 40, pp. 15735–15740.

Mo, G. C. H., B. Ross, F. Hertel, P. Manna, X. Yang, E. Greenwald, C. Booth, A. M. Plummer, B. Tenner, … J. Zhang, 2017, "Genetically Encoded Biosensors for Visualizing Live-Cell Biochemical Activity at Super-Resolution", *Nature Methods*, Vol. 14, No. 4, pp. 427–434.

Möller, J., A. Isbilir, T. Sungkaworn, B. Osberg, C. Karathanasis, V. Sunkara, E. O. Grushevskyi, A. Bock, P. Annibale, … M. J. Lohse, 2020, "Single-Molecule Analysis Reveals Agonist-Specific Dimer Formation of μ-Opioid Receptors", *Nature Chemical Biology*, Vol. 16, No. 9, pp. 946–954.

Møller, T. C., J. Hottin, C. Clerté, J. M. Zwier, T. Durroux, P. Rondard, L. Prézeau, C. A. Royer, J. P. Pin, … J. Kniazeff, 2018, "Oligomerization of a G Protein-Coupled Receptor in Neurons Controlled by Its Structural Dynamics", *Scientific Reports*, Vol. 8, No. 1, pp. 1–15.

Montpas, N., G. St-Onge, N. Nama, D. Rhainds, B. Benredjem, M. Girard, G. Hickson, V. Pons, and N. Heveker, 2018, "Ligand-Specific Conformational Transitions and Intracellular Transport Are Required for Atypical Chemokine Receptor 3–Mediated Chemokine Scavenging", *Journal of Biological Chemistry*, Vol. 293, No. 3, pp. 893–905.

Moore, C. A. C., S. K. Milano, and J. L. Benovic, 2007, "Regulation of receptor trafficking by GRKs and arrestins", *Annual Review of Physiology*, Vol. 69, No. 1, 451–482.

Mu, C. F., J. Shen, J. Liang, H. S. Zheng, Y. Xiong, Y. H. Wei, and F. Li, 2018, Targeted drug delivery for tumor therapy inside the bone marrow, *Biomaterials*, Vol. 155, pp. 191–202.

Mueller, W., D. Schütz, F. Nagel, S. Schulz, and R. Stumm, 2013, "Hierarchical Organization of Multi-Site Phosphorylation at the CXCR4 C Terminus", *PLoS ONE*, Vol. 8, No. 5, pp. e64975.

Mukherjee, C., M. G. Caron, and R. J. Lefkowitz, 1975, "Catecholamine Induced Subsensitivity of Adenylate Cyclase Associated with Loss of β Adrenergic Receptor Binding Sites", *Proceedings of the National Academy of Sciences of the United States of America*, Vol. 72, No. 5, pp. 1945–1949.

Murakami, M., and T. Kouyama, 2008, "Crystal Structure of Squid Rhodopsin", *Nature*, Vol. 453, No. 7193, pp. 363–367.

Murphy, P. M., and H. L. Tiffany, 1991, "Cloning of Complementary DNA Encoding a Functional Human Interleukin-8 Receptor", *Science*, Vol. 253, No. 5025, pp. 1280–1283.

Nair, A., P. Chauhan, B. Saha, and K. F. Kubatzky, 2019, "Conceptual evolution of cell signaling", *International Journal of Molecular Sciences*, Vol. 20, No. 13.

Namkung, Y., C. Le Gouill, V. Lukashova, H. Kobayashi, M. Hogue, E. Khoury, M. Song, M. Bouvier, and S. A. Laporte, 2016, "Monitoring G Protein-Coupled Receptor and β-Arrestin Trafficking in Live Cells Using Enhanced Bystander BRET", *Nature Communications*, Vol. 7, No. 1, pp. 1–12.

Nash, C. A., W. Wei, R. Irannejad, and A. V. Smrcka, 2019, "Golgi Localized Bi-

Adrenergic Receptors Stimulate Golgi PI4P Hydrolysis by PLCε to Regulate Cardiac Hypertrophy", *eLife*, Vol. 8.

Naumann, U., E. Cameroni, M. Pruenster, H. Mahabaleshwar, E. Raz, H. G. Zerwes, A. Rot, and M. Thelen, 2010, "CXCR7 Functions as a Scavenger for CXCL12 and CXCL11", *PLoS ONE*, Vol. 5, No. 2,.

Neves, M., A. Fumagalli, J. van den Bor, P. Marin, M. J. Smit, and F. Mayor, 2019, "The Role of ACKR3 in Breast, Lung, and Brain Cancer", *Molecular Pharmacology*, Vol. 96, No. 6, pp. 819–825.

Nevins, A. M., and A. Marchese, 2018, "Detecting cell surface expression of the g protein-coupled receptor CXCR4", In *Methods in Molecular Biology*, Vol. 1722, pp. 151–164.

Ngo, T., B. S. Stephens, M. Gustavsson, L. G. Holden, R. Abagyan, T. M. Handel, and I. Kufareva, 2020, "Crosslinking-Guided Geometry of a Complete CXC Receptor-Chemokine Complex and the Basis of Chemokine Subfamily Selectivity", *PLoS Biology*, Vol. 18, No. 4, pp. e3000656.

Nguyen, A. H., A. R. B. Thomsen, T. J. Cahill, R. Huang, L. Y. Huang, T. Marcink, O. B. Clarke, S. Heissel, A. Masoudi, … R. J. Lefkowitz, 2019, "Structure of an Endosomal Signaling GPCR–G Protein–β-Arrestin Megacomplex", *Nature Structural and Molecular Biology*, Vol. 26, No. 12, pp. 1123–1131.

Nguyen, H. T., A. Reyes-Alcaraz, H. J. Yong, L. P. Nguyen, H. K. Park, A. Inoue, C. S. Lee, J. Y. Seong, and J. I. Hwang, 2020, "CXCR7: A β-Arrestin-Biased Receptor That Potentiates Cell Migration and Recruits β-Arrestin2 Exclusively through Gβγ Subunits and GRK2", *Cell and Bioscience*, Vol. 10, No. 1, pp. 134.

Nikolaev, V. O., M. Bünemann, L. Hein, A. Hannawacker, and M. J. Lohse, 2004, "Novel Single Chain CAMP Sensors for Receptor-Induced Signal Propagation", *Journal of Biological Chemistry*, Vol. 279, No. 36, pp. 37215–37218.

Nimchinsky, E. A., P. R. Hof, W. G. M. Janssen, J. H. Morrison, and C. Schmauss, 1997, "Expression of Dopamine D3 Receptor Dimers and Tetramers in Brain and in Transfected Cells", *Journal of Biological Chemistry*, Vol. 272, No. 46, pp. 29229–29237.

Nuber, S., U. Zabel, K. Lorenz, A. Nuber, G. Milligan, A. B. Tobin, M. J. Lohse, and C. Hoffmann, 2016, "β-Arrestin Biosensors Reveal a Rapid, Receptor-Dependent Activation/Deactivation Cycle", *Nature*, Vol. 531, No. 7596, pp. 661–664.

O'Hayre, M., K. Eichel, S. Avino, X. Zhao, D. J. Steffen, X. Feng, K. Kawakami, J. Aoki, K. Messer, … J. S. Gutkind, 2017, "Genetic Evidence That B-Arrestins Are Dispensable for the Initiation of B2-Adrenergic Receptor Signaling to ERK", *Science Signaling*, Vol. 10, No. 484.

Oberlin, E., A. Amara, F. Bachelerie, C. Bessia, J. L. Virelizier, F. Arenzana- Seisdedos, O. Schwartz, J. M. Heard, I. Clark-Lewis, … B. Moser, 1996, "The CXC Chemokine SDF-1 Is the Ligand for LESTR/Fusin and Prevents Infection by T-Cell-Line-Adapted HIV-1", *Nature*, Vol. 382, No. 6594, pp. 833–835.

Ohta, Y., T. Furuta, T. Nagai, and K. Horikawa, 2018, "Red Fluorescent CAMP Indicator with Increased Affinity and Expanded Dynamic Range", *Scientific Reports*, Vol. 8, No. 1.

Olofsson, L., S. Felekyan, E. Doumazane, P. Scholler, L. Fabre, J. M. Zwier, P. Rondard, C. A. M. Seidel, J. P. Pin, and E. Margeat, 2014, "Fine Tuning of Sub-Millisecond Conformational Dynamics Controls Metabotropic Glutamate Receptors Agonist

Efficacy", *Nature Communications*, Vol. 5, No. 1, pp. 1–12.

Olsen, R. H. J., J. F. DiBerto, J. G. English, A. M. Glaudin, B. E. Krumm, S. T. Slocum, T. Che, A. C. Gavin, J. D. McCorvy, … R. T. Strachan, 2020, "TRUPATH, an Open-Source Biosensor Platform for Interrogating the GPCR Transducerome", *Nature Chemical Biology*, Vol. 16, No. 8, pp. 841–849.

Oswald, C., M. Rappas, J. Kean, A. S. Doré, J. C. Errey, K. Bennett, F. Deflorian, J. A. Christopher, A. Jazayeri, … F. H. Marshall, 2016, "Intracellular Allosteric Antagonism of the CCR9 Receptor", *Nature*, Vol. 540, No. 7633, pp. 462–465.

Overton, M. C., and K. J. Blumer, 2000, "G-Protein-Coupled Receptors Function as Oligomers in Vivo", *Current Biology*, Vol. 10, No. 6, pp. 341–344.

Øvrevik, J., M. Låg, J. A. Holme, P. E. Schwarze, and M. Refsnes, 2009, "Cytokine and Chemokine Expression Patterns in Lung Epithelial Cells Exposed to Components Characteristic of Particulate Air Pollution", *Toxicology*, Vol. 259, No. 1–2, pp. 46–53.

Paavola, K. J., J. R. Stephenson, S. L. Ritter, S. P. Alter, and R. A. Hall, 2011, "The N Terminus of the Adhesion G Protein-Coupled Receptor GPR56 Controls Receptor Signaling Activity", *Journal of Biological Chemistry*, Vol. 286, No. 33, pp. 28914–28921.

Pándy-Szekeres, G., C. Munk, T. M. Tsonkov, S. Mordalski, K. Harpsøe, A. S. Hauser, A. J. Bojarski, and D. E. Gloriam, 2018, "GPCRdb in 2018: Adding GPCR Structure Models and Ligands", *Nucleic Acids Research*, Vol. 46, No. D1, pp. D440–D446.

Papasergi-Scott, M. M., M. J. Robertson, A. B. Seven, O. Panova, J. M. Mathiesen, and G.

Skiniotis, 2020, "Structures of Metabotropic GABAB Receptor", *Nature*, Vol. 584, No. 7820, pp. 310–314.

Park, S. H., B. B. Das, F. Casagrande, Y. Tian, H. J. Nothnagel, M. Chu, H. Kiefer, K. Maier, A. A. De Angelis, … S. J. Opella, 2012, "Structure of the Chemokine Receptor CXCR1 in Phospholipid Bilayers", *Nature*, Vol. 491, No. 7426, pp. 779–783.

Parmar, V. K., E. Grinde, J. E. Mazurkiewicz, and K. Herrick-Davis, 2017, "Beta2-Adrenergic Receptor Homodimers: Role of Transmembrane Domain 1 and Helix 8 in Dimerization and Cell Surface Expression", *Biochimica et Biophysica Acta - Biomembranes*, Vol. 1859, No. 9, pp. 1445–1455.

Patel, R. C., U. Kumar, D. C. Lamb, J. S. Eid, M. Rocheville, M. Grant, A. Rani, T. Hazlett, S. C. Patel, … Y. C. Patel, 2002, "Ligand Binding to Somatostatin Receptors Induces Receptor-Specific Oligomer Formation in Live Cells", *Proceedings of the National Academy of Sciences of the United States of America*, Vol. 99, No. 5, pp. 3294–3299.

Patel, R. C., D. C. Lange, and Y. C. Patel, 2002, "Photobleaching Fluorescence Resonance Energy Transfer Reveals Ligand-Induced Oligomer Formation of Human Somatostatin Receptor Subtypes", *Methods*, Vol. 27, No. 4, pp. 340–348.

Patriarchi, T., J. R. Cho, K. Merten, M. W. Howe, A. Marley, W. H. Xiong, R. W. Folk, G. J. Broussard, R. Liang, … L. Tian, 2018, "Ultrafast Neuronal Imaging of Dopamine Dynamics with Designed Genetically Encoded Sensors", *Science*, Vol. 360, No. 6396,.

Pearse, B. M., C. J. Smith, and D. J. Owen, 2000, "Clathrin coat construction in endocytosis", *Current Opinion in Structural Biology*, Vol. 10, No. 2, pp. 220–228.

Pellissier, L. P., G. Barthet, F. Gaven, E. Cassier, E. Trinquet, J. P. Pin, P. Marin, A. Dumuis, J. Bockaert, … S. Claeysen, 2011, "G Protein Activation by Serotonin Type 4 Receptor Dimers: Evidence That Turning on Two Protomers Is More Efficient", *Journal of Biological Chemistry*, Vol. 286, No. 12, pp. 9985–9997.

Percherancier, Y., Y. A. Berchiche, I. Slight, R. Volkmer-Engert, H. Tamamura, N. Fujii, M. Bouvier, and N. Heveker, 2005, "Bioluminescence Resonance Energy Transfer Reveals Ligand-Induced Conformational Changes in CXCR4 Homo- and Heterodimers", *Journal of Biological Chemistry*, Vol. 280, No. 11, pp. 9895–9903.

Perpiñá-Viciano, C., A. Işbilir, A. Zarca, B. Caspar, L. E. Kilpatrick, S. J. Hill, M. J. Smit, M. J. Lohse, and C. Hoffmann, 2020, "Kinetic Analysis of the Early Signaling Steps of the Human Chemokine Receptor CXCR4", *Molecular Pharmacology*, Vol. 98, No. 2, pp. 72–87.

Petersen, N. O., P. L. Höddelius, P. W. Wiseman, O. Seger, and K. E. Magnusson, 1993, "Quantitation of Membrane Receptor Distributions by Image Correlation Spectroscopy: Concept and Application", *Biophysical Journal*, Vol. 65, No. 3, pp. 1135–1146.

Pfeuffer, T., and E. J. M. Helmreich, 1975, "Activation of Pigeon Erythrocyte Membrane Adenylate Cyclase by Guanylnucleotide Analogues and Separation of a Nucleotide Binding Protein", *Journal of Biological Chemistry*, Vol. 250, No. 3, pp. 867–876.

Pierce, K. L., R. T. Premont, and R. J. Lefkowitz, 2002, "Seven-transmembrane receptors", *Nature Reviews Molecular Cell Biology*, Vol. 3, No. 9, pp. 639–650.

Pin, J. P., and B. Bettler, 2016, "Organization and functions of mGlu and GABA B receptor complexes", *Nature*, Vol. 540, No. 7631, pp. 60–68.

Pin, J. P., T. Galvez, and L. Prézeau, 2003, "Evolution, structure, and activation mechanism of family 3/C G-protein-coupled receptors", *Pharmacology and Therapeutics*, Vol. 98, No. 3, pp. 325–354.

Pitcher, J. A., E. S. Payne, C. Csortos, A. A. Depaoli-Roach, and R. J. Lefkowitz, 1995, "The G-Protein-Coupled Receptor Phosphatase: A Protein Phosphatase Type 2A with a Distinct Subcellular Distribution and Substrate Specificity", *Proceedings of the National Academy of Sciences of the United States of America*, Vol. 92, No. 18, pp. 8343–8347.

Plotkin, J., S. E. Prockop, A. Lepique, and H. T. Petrie, 2003, "Critical Role for CXCR4 Signaling in Progenitor Localization and T Cell Differentiation in the Postnatal Thymus", *The Journal of Immunology*, Vol. 171, No. 9, pp. 4521–4527.

Pohl, S. L., L. Birnbaumer, and M. Rodbell, 1971, "The Glucagon-Sensitive Adenyl Cyclase System in Plasma Membranes of Rat Liver. I. Properties.", *Journal of Biological Chemistry*, Vol. 246, No. 6, pp. 1849–1856.

Prasanna, X., A. Chattopadhyay, and D. Sengupta, 2014, "Cholesterol Modulates the Dimer Interface of the B2- Adrenergic Receptor via Cholesterol Occupancy Sites", *Biophysical Journal*, Vol. 106, No. 6, pp. 1290–1300.

Prihandoko, R., S. J. Bradley, A. B. Tobin, and A. J. Butcher, 2015, "Determination of GPCR Phosphorylation Status: Establishing a Phosphorylation Barcode", *Current Protocols in Pharmacology*, Vol. 2015, pp. 2.13.1-2.13.26.

Proudfoot, A. E. I., T. M. Handel, Z. Johnson, E. K. Lau, P. LiWang, I. Clark-Lewis, F. Borlat, T. N. C. Wells, and M. H. Kosco-Vilbois, 2003, "Glycosaminoglycan Binding and Oligomerization Are Essential for the in Vivo Activity of Certain Chemokines", *Proceedings of the National Academy of Sciences of the United States of America*,

Vol. 100, No. 4, pp. 1885–1890.

Proudfoot, A. E. I., C. A. Power, A. J. Hoogewerf, M. O. Montjovent, F. Borlat, R. E. Offord, and T. N. C. Wells, 1996, "Extension of Recombinant Human RANTES by the Retention of the Initiating Methionine Produces a Potent Antagonist", *Journal of Biological Chemistry*, Vol. 271, No. 5, pp. 2599–2603.

Proudfoot, A. E. I., and M. Uguccioni, 2016, "Modulation of chemokine responses: Synergy and cooperativity", *Frontiers in Immunology*, Vol. 7, No. MAY, pp. 183.

Puchert, M., F. Pelkner, G. Stein, D. N. Angelov, J. Boltze, D. C. Wagner, F. Odoardi, A. Flügel, W. J. Streit, and J. Engele, 2017, "Astrocytic Expression of the CXCL12 Receptor, CXCR7/ACKR3 Is a Hallmark of the Diseased, but Not Developing CNS", *Molecular and Cellular Neuroscience*, Vol. 85, pp. 105–118.

Purgert, C. A., Y. Izumi, Y. J. I. Jong, V. Kumar, C. F. Zorumski, and K. L. O'Malley, 2014, "Intracellular MGluR5 Can Mediate Synaptic Plasticity in the Hippocampus", *Journal of Neuroscience*, Vol. 34, No. 13, pp. 4589–4598.

Pyo, R. T., J. Sui, A. Dhume, J. Palomeque, B. C. Blaxall, G. Diaz, J. Tunstead, D. E. Logothetis, R. J. Hajjar, and A. D. Schecter, 2006, "CXCR4 Modulates Contractility in Adult Cardiac Myocytes", *Journal of Molecular and Cellular Cardiology*, Vol. 41, No. 5, pp. 834–844.

Qi, X., L. Friedberg, R. De Bose-Boyd, T. Long, and X. Li, 2020, "Sterols in an Intramolecular Channel of Smoothened Mediate Hedgehog Signaling", *Nature Chemical Biology*, Vol. 16, No. 12, pp. 1368–1375.

Qian, H., and E. L. Elson, 1990, "Distribution of Molecular Aggregation by Analysis of

Fluctuation Moments", *Proceedings of the National Academy of Sciences of the United States of America*, Vol. 87, No. 14, pp. 5479–5483.

Qin, L., I. Kufareva, L. G. Holden, C. Wang, Y. Zheng, C. Zhao, G. Fenalti, H. Wu, G. W. Han, … T. M. Handel, 2015, "Crystal Structure of the Chemokine Receptor CXCR4 in Complex with a Viral Chemokine", *Science*, Vol. 347, No. 6226, pp. 1117–1122.

Quinn, K. E., D. I. Mackie, and K. M. Caron, 2018, "Emerging Roles of Atypical Chemokine Receptor 3 (ACKR3) in Normal Development and Physiology", *Cytokine*, Vol. 109, pp. 17–23.

Rajagopal, S., J. Kim, S. Ahn, S. Craig, C. M. Lam, N. P. Gerard, C. Gerard, and R. J. Lefkowitz, 2010, "β-Arrestin- But Not G Protein-Mediated Signaling by the "Decoy" Receptor CXCR7", *Proceedings of the National Academy of Sciences of the United States of America*, Vol. 107, No. 2, pp. 628–632.

Ramakrishnan, R., P. Peña-Martínez, P. Agarwal, M. Rodriguez-Zabala, M. Chapellier, C. Högberg, M. Eriksson, D. Yudovich, M. Shah, … M. Järås, 2020, "CXCR4 Signaling Has a CXCL12-Independent Essential Role in Murine MLL-AF9-Driven Acute Myeloid Leukemia", *Cell Reports*, Vol. 31, No. 8.

Rasmussen, S. G. F., B. T. Devree, Y. Zou, A. C. Kruse, K. Y. Chung, T. S. Kobilka, F. S. Thian, P. S. Chae, E. Pardon, … B. K. Kobilka, 2011, "Crystal Structure of the β 2 Adrenergic Receptor-Gs Protein Complex", *Nature*, Vol. 477, No. 7366, pp. 549–557.

Ray, P., L. A. Mihalko, N. L. Coggins, P. Moudgil, A. Ehrlich, K. E. Luker, and G. D. Luker, 2012, "Carboxy-Terminus of CXCR7 Regulates Receptor Localization and Function", *International Journal of Biochemistry and Cell Biology*, Vol. 44, No. 4, pp. 669–678.

Regan, J. W., N. Barden, R. J. Lefkowitz, M. G. Caron, R. M. DeMarinis, A. J. Krog, K. G. Holden, W. D. Matthews, and J. P. Hieble, 1982, "Affinity Chromatography of Human Platelet α 2-Adrenergic Receptors", *Proceedings of the National Academy of Sciences of the United States of America*, Vol. 79, No. 23 I, pp. 7223–7227.

Regard, J. B., I. T. Sato, and S. R. Coughlin, 2008, "Anatomical Profiling of G Protein-Coupled Receptor Expression", *Cell*, Vol. 135, No. 3, pp. 561–571.

Ribas, C., P. Penela, C. Murga, A. Salcedo, C. García-Hoz, M. Jurado-Pueyo, I. Aymerich, and F. Mayor, 2007, The G protein-coupled receptor kinase (GRK) interactome: Role of GRKs in GPCR regulation and signaling, *Biochimica et Biophysica Acta - Biomembranes*, Vol. 1768, No. 4, pp. 913–922.

Rivero-Müller, A., Y. Y. Chou, I. Ji, S. Lajic, A. C. Hanyaloglu, K. Jonas, N. Rahman, T. H. Ji, and I. Huhtaniemi, 2010, "Rescue of Defective G Protein - Coupled Receptor Function in Vivo by Intermolecular Cooperation", *Proceedings of the National Academy of Sciences of the United States of America*, Vol. 107, No. 5, pp. 2319–2324.

Robiquet, P.-J., 1832, "Nouvelle Observations Sur Les Principaux Produits de l'opium", *Ann. Chim. Phys*, Vol. 51, No. 2, pp. 225–267.

Robison, G. A., R. W. Butcher, and E. W. Sutherland, 1967, "Adenyl Cyclase As an Adrenergic Receptor", *Annals of the New York Academy of Sciences*, Vol. 139, No. 3, pp. 703–723.

Rocheville, M., D. C. Lange, U. Kumar, R. Sasi, R. C. Patel, and Y. C. Patel, 2000, "Subtypes of the Somatostatin Receptor Assemble as Functional Homo- and Heterodimers", *Journal of Biological Chemistry*, Vol. 275, No. 11, pp. 7862–7869.

Rodbell, M., 1980, "The Role of Hormone Receptors and GTP-Regulatory Proteins in Membrane Transduction", *Nature*, Vol. 284, No. 5751, pp. 17–22.

Rodríguez-Frade, J. M., G. Del Real, A. Serrano, P. Hernanz-Falcón, S. F. Soriano, A. J. Vila-Coro, A. M. De Ana, P. Lucas, I. Prieto, … M. Mellado, 2004, "Blocking HIV-1 Infection via CCR5 and CXCR4 Receptors by Acting in Trans on the CCR2 Chemokine Receptor", *EMBO Journal*, Vol. 23, No. 1, pp. 66–76.

Romano, C., W. L. Yang, and K. L. O'Malley, 1996, "Metabotropic Glutamate Receptor 5 Is a Disulfide-Linked Dimer", *Journal of Biological Chemistry*, Vol. 271, No. 45, pp. 28612–28616.

Ross, E. M., and A. G. Gilman, 1977, "Resolution of Some Components of Adenylate Cyclase Necessary for Catalytic Activity", *Journal of Biological Chemistry*, Vol. 252, No. 20, pp. 6966–6969.

Rozwandowicz-Jansen, A., J. Laurila, E. Martikkala, H. Frang, I. Hemmilä, M. Scheinin, P. Hänninen, and H. Härmä, 2010, "Homogeneous GTP Binding Assay Employing QRET Technology", *Journal of Biomolecular Screening*, Vol. 15, No. 3, pp. 261–267.

Salahpour, A., S. Angers, J. F. Mercier, M. Lagacé, S. Marullo, and M. Bouvier, 2004, "Homodimerization of the B2-Adrenergic Receptor as a Prerequisite for Cell Surface Targeting", *Journal of Biological Chemistry*, Vol. 279, No. 32, pp. 33390–33397.

Sánchez-Martín, L., P. Sánchez-Mateos, and C. Cabañas, 2013, "CXCR7 impact on CXCL12 biology and disease", *Trends in Molecular Medicine*, Vol. 19, No. 1, pp. 12–22.

Santos, R., O. Ursu, A. Gaulton, A. P. Bento, R. S. Donadi, C. G. Bologa, A. Karlsson, B. Al-Lazikani, A. Hersey, … J. P. Overington, 2016, "A Comprehensive Map of Molecular Drug Targets", *Nature Reviews Drug Discovery*, Vol. 16, No. 1, pp. 19–34.

Sartania, N., S. Appelbe, J. D. Pediani, and G. Milligan, 2007, "Agonist Occupancy of a Single Monomeric Element Is Sufficient to Cause Internalization of the Dimeric B2-Adrenoceptor", *Cellular Signalling*, Vol. 19, No. 9, pp. 1928–1938.

Scholten, D. J., M. Canals, D. Maussang, L. Roumen, M. J. Smit, M. Wijtmans, C. De Graaf, H. F. Vischer, and R. Leurs, 2012, "Pharmacological modulation of chemokine receptor function", *British Journal of Pharmacology*, Vol. 165, No. 6, pp. 1617–1643.

Schöneberg, T., M. Hofreiter, A. Schulz, and H. Römpler, 2007, "Learning from the Past: Evolution of GPCR Functions", *Trends in Pharmacological Sciences*, Vol. 28, No. 3, pp. 117–121.

Seidel, L., B. Zarzycka, S. A. Zaidi, V. Katritch, and I. Coin, 2017, "Structural Insight into the Activation of a Class B G-Protein-Coupled Receptor by Peptide Hormones in Live Human Cells", *eLife*, Vol. 6.

Sertuerner, F., 1817, "Ueber Das Morphium, Eine Neue Salzfähige Grundlage, Und Die Mekonsäure, Als Hauptbestandtheile Des Opiums", *Annalen der Physik*, Vol. 55, No. 1, pp. 56–89.

Sezgin, E., F. Schneider, S. Galiani, I. Urbančič, D. Waithe, B. C. Lagerholm, and C. Eggeling, 2019, "Measuring Nanoscale Diffusion Dynamics in Cellular Membranes with Super-Resolution STED–FCS", *Nature Protocols*, Vol. 14, No. 4, pp. 1054–1083.

Shaik, M. M., H. Peng, J. Lu, S. Rits-Volloch, C. Xu, M. Liao, and B. Chen, 2019, "Structural Basis of Coreceptor Recognition by HIV-1 Envelope Spike", *Nature*, Vol. 565, No. 7739, pp. 318–323.

Shi, G., S. Partida-Sánchez, R. S. Misra, M. Tighe, M. T. Borchers, J. J. Lee, M. I. Simon, and F. E. Lund, 2007, "Identification of an Alternative Gαq-Dependent Chemokine Receptor Signal Transduction Pathway in Dendritic Cells and Granulocytes", *Journal of Experimental Medicine*, Vol. 204, No. 11, pp. 2705–2718.

Shi, Y., D. J. Riese, and J. Shen, 2020, "The Role of the CXCL12/CXCR4/CXCR7 Chemokine Axis in Cancer", *Frontiers in Pharmacology*, Vol. 11, pp. 1969.

Shimada, I., T. Ueda, Y. Kofuku, M. T. Eddy, and K. Wüthrich, 2018, "GPCR drug discovery: Integrating solution NMR data with crystal and cryo-EM structures", *Nature Reviews Drug Discovery*, Vol. 18, No. 1, pp. 55–64.

Shorr, R. G. L., R. J. Lefkowitz, and M. G. Caron, 1981, "Purification of the β-Adrenergic Receptor. Identification of the Hormone Binding Subunit", *Journal of Biological Chemistry*, Vol. 256, No. 11, pp. 5820–5826.

Sierro, F., C. Biben, L. Martínez-Muñoz, M. Mellado, R. M. Ransohoff, M. Li, B. Woehl, H. Leung, J. Groom, … F. Mackay, 2007, "Disrupted Cardiac Development but Normal Hematopoiesis in Mice Deficient in the Second CXCL12/SDF-1 Receptor, CXCR7", *Proceedings of the National Academy of Sciences of the United States of America*, Vol. 104, No. 37, pp. 14759–14764.

Smith, J. S., T. F. Pack, A. Inoue, C. Lee, K. Zheng, I. Choi, D. S. Eiger, A. Warman, X. Xiong, … S. Rajagopal, 2021, "Noncanonical Scaffolding of Gai and B-Arrestin by G Protein-Coupled Receptors", *Science*, Vol. 371, No. 6534.

Smith, N., M. P. Rodero, N. Bekaddour, V. Bondet, Y. B. Ruiz-Blanco, M. Harms, B. Mayer, B. Badder-Meunier, P. Quartier, … J. P. Herbeuval, 2019, "Control of TLR7-Mediated Type i IFN Signaling in PDCs through CXCR4 Engagement-A New Target for Lupus Treatment", *Science Advances*, Vol. 5, No. 7, pp. eaav9019.

Soave, M., B. Kellam, J. Woolard, S. J. Briddon, and S. J. Hill, 2020, "NanoBiT Complementation to Monitor Agonist-Induced Adenosine A1 Receptor Internalization", *SLAS Discovery*, Vol. 25, No. 2, pp. 186–194.

Soede, R. D. M., I. S. Zeelenberg, Y. M. Wijnands, M. Kamp, and E. Roos, 2001, " Stromal Cell-Derived Factor-1-Induced LFA-1 Activation During In Vivo Migration of T Cell Hybridoma Cells Requires G q/11 , RhoA, and Myosin, as Well as G i and Cdc42 ", *The Journal of Immunology*, Vol. 166, No. 7, pp. 4293–4301.

Sohy, D., M. Parmentier, and J. Y. Springael, 2007, "Allosteric Transinhibition by Specific Antagonists in CCR2/CXCR4 Heterodimers", *Journal of Biological Chemistry*, Vol. 282, No. 41, pp. 30062–30069.

Sohy, D., H. Yano, P. de Nadai, E. Urizar, A. Guillabert, J. A. Javitch, M. Parmentier, and J. Y. Springael, 2009, "Hetero-Oligomerization of CCR2, CCR5, and CXCR4 and the Protean Effects of “Selective” Antagonists", *Journal of Biological Chemistry*, Vol. 284, No. 45, pp. 31270–31279.

Solt, A. S., M. J. Bostock, B. Shrestha, P. Kumar, T. Warne, C. G. Tate, and D. Nietlispach, 2017, "Insight into Partial Agonism by Observing Multiple Equilibria for Ligand-Bound and Gs-Mimetic Nanobody-Bound B1-Adrenergic Receptor", *Nature Communications*, Vol. 8, No. 1, pp. 1–12.

Song, Z. Y., F. Wang, S. X. Cui, Z. H. Gao, and X. J. Qu, 2019, "CXCR7/CXCR4 Heterodimer-Induced Histone Demethylation: A New Mechanism of Colorectal

Tumorigenesis", *Oncogene*, Vol. 38, No. 9, pp. 1560–1575.

Sprang, S. R., 2010, "Structures of heterotrimeric g proteins and their complexes", *Handbook of Cell Signaling,* Vol. 1, pp. 119–128.

Springael, J. Y., P. N. Le Minh, E. Urizar, S. Costagliola, G. Vassart, and M. Parmentier, 2006, "Allosteric Modulation of Binding Properties between Units of Chemokine Receptor Homo- and Hetero-Oligomers", *Molecular Pharmacology*, Vol. 69, No. 5, pp. 1652–1661.

Srivastava, M., and N. O. Petersen, 1996, "Image Cross-Correlation Spectroscopy: A New Experimental Biophysical Approach to Measurement of Slow Diffusion of Fluorescent Molecules", *Methods in Cell Science*, Vol. 18, No. 1, pp. 47–54.

Stadel, J. M., P. Nambi, R. G. L. Shorr, D. F. Sawyer, M. G. Caron, and R. J. Lefkowitz, 1983, "Catecholamine-Induced Desensitization of Turkey Erythrocyte Adenylate Cyclase Is Associated with Phosphorylation of the β-Adrenergic Receptor", *Proceedings of the National Academy of Sciences of the United States of America*, Vol. 80, No. 11 I, pp. 3173–3177.

Starling, E. H., 1905, "The Croonian Lectures ON THE CHEMICAL CORRELATION OF THE FUNCTIONS OF THE BODY.", *The Lancet*, Vol. 166, No. 4275, pp. 339–341.

Steiner, A. L., C. W. Parker, and D. M. Kipnis, 1972, "Radioimmunoassay for Cyclic Nucleotides. I. Preparation of Antibodies and Iodinated Cyclic Nucleotides.", *Journal of Biological Chemistry*, Vol. 247, No. 4, pp. 1106–1113.

Stephens, B., an T M Handel 2013 "Chemokin recepto oligomerizatio an allostery"

*Progress in Molecular Biology and Translational Science,*Vol. 115, pp. 375–420). Elsevie B.V

Sternweis P C. J K Northup M D Smigel an A G Gilman 1981 "Th Regulator Componen o Adenylat Cyclase Purificatio an Properties." *Journa o Biologica Chemistry* Vol 256 No 22 pp 11517–11526

Stokes G G. 1852 "XXX O th Chang o Refrangibilit o Light" *Philosophica Transaction o th Roya Societ o London* Vol 142 pp 463–562

Stoneman M R. G Biener R J Ward J D Pediani D Badu A Eis I Popa G Milligan an V Raicu 2019 " Genera Metho t Quantif Ligand-Drive Oligomerizatio fro Fluorescence-Base Images" *Natur Methods* Vol 16 No 6 pp 493–496

Stumm R. an V Höllt 2007 "CX chemokin recepto regulate neurona migratio an axona pathfindin i th developin nervou system Implication fo neurona regeneratio i th adul brain" *Journa o Molecula Endocrinology* Vol 28 No 3–4 pp 377–382

Sugiyama T. H Kohara M Noda an T Nagasawa 2006 "Maintenanc o th Hematopoieti Ste Cel Poo b CXCL12-CXCR Chemokin Signalin i Bon Marro Stroma Cel Niches" *Immunity* Vol 25 No 6 pp 977–988

Sungkaworn T. M L Jobin K Burnecki A Weron M J Lohse an D Calebiro 2017 "Single-Molecul Imagin Reveal Receptor- Protei Interaction a Cel Surfac Ho Spots" *Nature* Vol 550 No 7677 pp 543–547

Sutherland . ., an . W. Rall 19 7, "The ro er ies of an adenine ribonucleotide

produced with cellular particles, ATP, Mg++, and epinephrine or glucagon", *Journa f t e Americ n Chemic l Societ* . Americ n Chemic l Societ .

Sutherlan , . W , a d . . Ral , 195 , "Fractionati n a d Characterizati n f a Cycl c Adeni e Ribonucleoti e Form d y Tiss e Particles. , *T e Journ l f biologic l chemistr* , Vo . 23 , N . , p . 1077–109 .

. Youke , R , a d . Voe , 202 , Fluorescen e Fluctuati n Techniqu s f r t e Investigati n f Structure-Functi n Relationshi s f G-Protein-Coupl d Receptor , n *Fluorescen e Metho s f r Investigati n f Livi g Cel s a d Microorganism* .

Tabo , A , . Weisenburge , . Banerje , . Purkayasth , . . Kaind , . Hübne , . We , . . Gröme , . Kornhube , … . Gmeine , 201 , "Visualizati n a d Ligand-Induc d Modulati n f Dopami e Recept r Dimerizati n t t e Sing e Molecu e Level , *Scientif c Report* , Vo . , N . , p . 3323 .

Tachiban , K , . Hirot , . Iizas , . Yoshid , . Kawabat , . Kataok , . Kitamur , . Matsushim , . Yoshid , … . Nagasaw , 199 , "T e Chemoki e Recept r CXC 4 s Essenti l f r Vascularizati n f t e Gastrointestin l Tract , *Natur* , Vo . 39 , N . 668 , p . 591–59 .

Tadevosya , A , . Létournea , . Folc , . Douce , . . Villeneuv , . . Mamarbach , . Pétri , . . Héber , . Fournie , … . Natte , 201 , "Photoreleasab e Ligan s o Stu y Intracri e Angiotens n I Signalling , *Journ l f Physiolog* , Vo . 59 , N . , p . 521–53 .

Takahash , A , . Camach , . . Lechleite , a d . Herma , 199 , "Measureme t f intracellul r calcium , *Physiologic l Review* , Vo . 7 , N . , p . 1089–112 .

Takahashi, K., K. Tsuchida, Y. Tanabe, M. Masu, and S. Nakanishi, 1993, "Role of the Large Extracellular Domain of Metabotropic Glutamate Receptors in Agonist Selectivity Determination", *Journal of Biological Chemistry*, Vol. 268, No. 26, pp. 19341–19345.

Takeda, S., S. Kadowaki, T. Haga, H. Takaesu, and S. Mitaku, 2002, "Identification of G Protein-Coupled Receptor Genes from the Human Genome Sequence", *FEBS Letters*, Vol. 520, No. 1–3, pp. 97–101.

Tan, Q., Y. Zhu, J. Li, Z. Chen, G. W. Han, I. Kufareva, T. Li, L. Ma, G. Fenalti, … B. Wu, 2013, "Structure of the CCR5 Chemokine Receptor-HIV Entry Inhibitor Maraviroc Complex", *Science*, Vol. 341, No. 6152, pp. 1387–1390.

Tan, W., D. Martin, and J. S. Gutkind, 2006, "The Gα13-Rho Signaling Axis Is Required for SDF-1-Induced Migration through CXCR", *Journal of Biological Chemistry*, Vol. 281, No. 51, pp. 39542–39549.

Tanaka, T., W. Nomura, T. Narumi, A. Masuda, and H. Tamamura, 2010, "Bivalent Ligands of CXCR4 with Rigid Linkers for Elucidation of the Dimerization State in Cells", *Journal of the American Chemical Society*, Vol. 132, No. 45, pp. 15899–15901.

Taylor, M. J., D. Perrais, and C. J. Merrifield, 2011, "A High Precision Survey of the Molecular Dynamics of Mammalian Clathrin-Mediated Endocytosis", *PLoS Biology*, Vol. 9, No. 3.

Teicher, B. A., and S. P. Fricker, 2010, "CXCL12 (SDF-1)/CXCR4 pathway in cancer", *Clinical Cancer Research*, Vol. 16, No. 11, pp. 2927–2931.

Torossian, F., A. Anginot, A. Chabanon, D. Clay, B. Guerton, C. Desterke, L. Boutin, S. Marullo, M. G. H. Scott, … M. C. Le Bousse-Kerdilès, 2014, "CXCR7 Participates in CXCL12-Induced CD34+ Cell Cycling through b-Arrestin-Dependent Akt Activation", *Blood*, Vol. 123, No. 2, pp. 191–202.

Toth, P. T., D. Ren, and R. J. Miller, 2004, "Regulation of CXCR4 Receptor Dimerization by the Chemokine SDF-1α and the HIV-1 Coat Protein Gp120: A Fluorescence Resonance Energy Transfer (FRET) Study", *Journal of Pharmacology and Experimental Therapeutics*, Vol. 310, No. 1, pp. 8–17.

Trampont, P. C., A. C. Tosello-Trampont, Y. Shen, A. K. Duley, A. E. Sutherland, T. P. Bender, D. R. Littman, and K. S. Ravichandran, 2010, "CXCR4 Acts as a Costimulator during Thymic B-Selection", *Nature Immunology*, Vol. 11, No. 2, pp. 162–170.

Tripathi, A., P. G. Vana, T. S. Chavan, L. I. Brueggemann, K. L. Byron, N. I. Tarasova, B. F. Volkman, V. Gaponenko, and M. Majetschak, 2015, "Heteromerization of Chemokine (C-X-C Motif) Receptor 4 with A1A/B -Adrenergic Receptors Controls Adrenergic A1 Receptor Function", *Proceedings of the National Academy of Sciences of the United States of America*, Vol. 112, No. 13, pp. E1659–E1668.

Ueda, H., O. M. Z. Howard, M. C. Grimm, S. B. Su, W. Gong, G. Evans, F. W. Ruscetti, J. J. Oppenheim, and J. M. Wang, 1998, "HIV-1 Envelope Gp41 Is a Potent Inhibitor of Chemoattractant Receptor Expression and Function in Monocytes", *Journal of Clinical Investigation*, Vol. 102, No. 4, pp. 804–812.

Uings, I. J., and S. N. Farrow, 2000, "Cell receptors and cell signalling", *Journal of Clinical Pathology - Molecular Pathology*, Vol. 53, No. 6, pp. 295–299.

Vafabakhsh, R., J. Levitz, and E. Y. Isacoff, 2015, "Conformational Dynamics of a Class

C G-Protein-Coupled Receptor", *Nature*, Vol. 524, No. 7566, pp. 497–501.

Van Unen, J., A. D. Stumpf, B. Schmid, N. R. Reinhard, P. L. Hordijk, C. Hoffmann, T. W. J. Gadella, and J. Goedhart, 2016, "A New Generation of FRET Sensors for Robust Measurement of Gαi1, Gαi2 and Gαi3 Activation Kinetics in Single Cells", *PLoS ONE*, Vol. 11, No. 1, pp. e0146789.

Vauquelin, G., P. Geynet, J. Hanoune, and A. D. Strosberg, 1977, "Isolation of Adenylate Cyclase-Free, β-Adrenergic Receptor from Turkey Erythrocyte Membranes by Affinity Chromatography", *Proceedings of the National Academy of Sciences of the United States of America*, Vol. 74, No. 9, pp. 3710–3714.

Vauquelin, G., P. Geynet, J. Hanoune, and A. D. Strosberg, 1979, "Affinity Chromatography of the B-Adrenergic Receptor from Turkey Erythrocytes", *European Journal of Biochemistry*, Vol. 98, No. 2, pp. 543–556.

Velazhahan, V., N. Ma, G. Pándy-Szekeres, A. J. Kooistra, Y. Lee, D. E. Gloriam, N. Vaidehi, and C. G. Tate, 2021, "Structure of the Class D GPCR Ste2 Dimer Coupled to Two G Proteins", *Nature*, Vol. 589, No. 7840, pp. 148–153.

Vicente-Manzanares, M., M. Rey, D. R. Jones, D. Sancho, M. Mellado, J. M. Rodriguez-Frade, M. A. del Pozo, M. Yáñez-Mó, A. M. de Ana, … F. Sánchez-Madrid, 1999, "Involvement of Phosphatidylinositol 3-Kinase in Stromal Cell-Derived Factor-1 Alpha-Induced Lymphocyte Polarization and Chemotaxis.", *Journal of immunology (Baltimore, Md. : 1950)*, Vol. 163, No. 7, pp. 4001–12.

Vidi, P. A., J. A. Przybyla, C. D. Hu, and V. J. Watts, 2010, Visualization of G protein-coupled receptor (GPCR) Interactions in living cells using bimolecular fluorescence complementation (BiFC), *Current Protocols in Neuroscience*. NIH Public Access.

Vila-Coro, A. J., 2000, "HIV-1 Infection through the CCR5 Receptor Is Blocked by Receptor Dimerization", *Proceedings of the National Academy of Sciences*, Vol. 97, No. 7, pp. 3388–3393.

Vila-Coro, A. J., J. M. Rodríguez-Frade, A. M. De Ana, M. C. Moreno-Ortíz, C. Martínez-A., and M. Mellado, 1999a, "The Chemokine SDF-lα Triggers CXCR4 Receptor Dimerization and Activates the JAK/STAT Pathway", *The FASEB Journal*, Vol. 13, No. 13, pp. 1699–1710.

Vila-Coro, A. J., J. M. Rodríguez-Frade, A. M. De Ana, M. C. Moreno-Ortíz, C. Martínez-A., and M. Mellado, 1999b, "The Chemokine SDF-lα Triggers CXCR4 Receptor Dimerization and Activates the JAK/STAT Pathway", *The FASEB Journal*, Vol. 13, No. 13, pp. 1699–1710.

Vilardaga, J. P., M. Bünemann, C. Krasell, M. Castro, and M. J. Lohse, 2003, "Measurement of the Millisecond Activation Switch of G Protein-Coupled Receptors in Living Cells", *Nature Biotechnology*, Vol. 21, No. 7, pp. 807–812.

Vilardaga, J. P., V. O. Nikolaev, K. Lorenz, S. Ferrandon, Z. Zhuang, and M. J. Lohse, 2008, "Conformational Cross-Talk between A2A-Adrenergic and μ-Opioid Receptors Controls Cell Signaling", *Nature Chemical Biology*, Vol. 4, No. 2, pp. 126–131.

Vilardaga, J. P., R. Steinmeyer, G. S. Harms, and M. J. Lohse, 2005, "Molecular Basis of Inverse Agonism in a G Protein-Coupled Receptor", *Nature Chemical Biology*, Vol. 1, No. 1, pp. 25–28.

Vincent, K., V. M. Cornea, Y. J. I. Jong, A. Laferriere, N. Kumar, A. Mickeviciute, J. S. T. Fung, P. Bandegi, A. Ribeiro-Da-Silva, … T. J. Coderre, 2016, "Intracellular MGluR5 Plays a Critical Role in Neuropathic Pain", *Nature Communications*, Vol. 7.

Wall, M. A., D. E. Coleman, E. Lee, J. A. Iñiguez-Lluhi, B. A. Posner, A. G. Gilman, and S. R. Sprang, 1995, "The Structure of the G Protein Heterotrimer Giα1β1γ2", *Cell*, Vol. 83, No. 6, pp. 1047–1058.

Wang, B., P. Guo, and D. T. Auguste, 2015, "Mapping the CXCR4 Receptor on Breast Cancer Cells", *Biomaterials*, Vol. 57, pp. 161–168.

Wang, C., H. Wu, T. Evron, E. Vardy, G. W. Han, X. P. Huang, S. J. Hufeisen, T. J. Mangano, D. J. Urban, … R. C. Stevens, 2014, "Structural Basis for Smoothened Receptor Modulation and Chemoresistance to Anticancer Drugs", *Nature Communications*, Vol. 5, No. 1, pp. 1–11.

Wang, J., L. He, C. A. Combs, G. Roderiquez, and M. A. Norcross, 2006, "Dimerization of CXCR4 in Living Malignant Cells: Control of Cell Migration by a Synthetic Peptide That Reduces Homologous CXCR4 Interactions", *Molecular Cancer Therapeutics*, Vol. 5, No. 10, pp. 2474–2483.

Wani, N. A., M. W. Nasser, D. K. Ahirwar, H. Zhao, Z. Miao, K. Shilo, and R. K. Ganju, 2014, "C-X-C Motif Chemokine 12/C-X-C Chemokine Receptor Type 7 Signaling Regulates Breast Cancer Growth and Metastasis by Modulating the Tumor Microenvironment", *Breast Cancer Research*, Vol. 16, No. 3.

Ward, R. J., J. D. Pediani, A. G. Godin, and G. Milligan, 2015, "Regulation of Oligomeric Organization of the Serotonin 5-Hydroxytryptamine 2C (5-HT2C) Receptor Observed by Spatial Intensity Distribution Analysis", *Journal of Biological Chemistry*, Vol. 290, No. 20, pp. 12844–12857.

Wasilko, D. J., Z. L. Johnson, M. Ammirati, Y. Che, M. C. Griffor, S. Han, and H. Wu, 2020, "Structural Basis for Chemokine Receptor CCR6 Activation by the Endogenous Protein Ligand CCL20", *Nature Communications*, Vol. 11, No. 1, pp. 1–

9.

Weis, W. I., and B. K. Kobilka, 2018, "The Molecular Basis of G Protein-Coupled Receptor Activation", *Annual Review of Biochemistry*, Vol. 87, No. 1, pp. 879–919.

Wescott, M. P., I. Kufareva, C. Paes, J. R. Goodman, Y. Thaker, B. A. Puffer, E. Berdougo, J. B. Rucker, T. M. Handel, and B. J. Doranz, 2016, "Signal Transmission through the CXC Chemokine Receptor 4 (CXCR4) Transmembrane Helices", *Proceedings of the National Academy of Sciences of the United States of America*, Vol. 113, No. 35, pp. 9928–9933.

Wheeler, D., W. B. Sneddon, B. Wang, P. A. Friedman, and G. Romero, 2007, "NHERF-1 and the Cytoskeleton Regulate the Traffic and Membrane Dynamics of G Protein-Coupled Receptors", *Journal of Biological Chemistry*, Vol. 282, No. 34, pp. 25076–25087.

White, C. W., H. K. Vanyai, H. B. See, E. K. M. Johnstone, and K. D. G. Pfleger, 2017, "Using NanoBRET and CRISPR/Cas9 to Monitor Proximity to a Genome-Edited Protein in Real-Time", *Scientific Reports*, Vol. 7, No. 1, pp. 1–14.

White, K. L., M. T. Eddy, Z. G. Gao, G. W. Han, T. Lian, A. Deary, N. Patel, K. A. Jacobson, V. Katritch, and R. C. Stevens, 2018, "Structural Connection between Activation Microswitch and Allosteric Sodium Site in GPCR Signaling", *Structure*, Vol. 26, No. 2, pp. 259- 269.e5.

Whorton, M. R., B. Jastrzebska, P. S. H. Park, D. Fotiadis, A. Engel, K. Palczewski, and R. K. Sunahara, 2008, "Efficient Coupling of Transducin to Monomeric Rhodopsin in a Phospholipid Bilayer", *Journal of Biological Chemistry*, Vol. 283, No. 7, pp. 4387–4394.

Williams, L. T., D. Mullikin, and R. J. Lefkowitz, 1976, "Identification of α Adrenergic Receptors in Uterine Smooth Muscle Membranes by [3H]Dihydroergocryptine Binding", *Journal of Biological Chemistry*, Vol. 251, No. 22, pp. 6915–6923.

Wolf-Ringwall, A. L., P. W. Winter, J. Liu, A. K. Van Orden, D. A. Roess, and B. G. Barisas, 2011, "Restricted Lateral Diffusion of Luteinizing Hormone Receptors in Membrane Microdomains", *Journal of Biological Chemistry*, Vol. 286, No. 34, pp. 29818–29827.

Wolfe, B. L., and J. A. Trejo, 2007,éClathrin-dependent mechanisms of G protein-coupled receptor endocytosis", *Traffic* Vol 8 No 5 pp 462–470

Wootten D. J Simms L J Miller A Christopoulos an P M Sexton 2013 "Pola Transmembran Interaction Driv Formatio o Ligand-Specifi an Signa Pathway-Biase Famil Protein-Couple Recepto Conformations" *Proceeding o th Nationa Academ o Science o th Unite State o America* Vol 110 No 13 pp 5211–5216

Wu B. E Y T Chien C D Mol G Fenalti W Liu V Katritch R Abagyan A Brooun P Wells R C Stevens 2010 "Structure o th CXCR chemokin GPC wit small-molecul an cycli peptid antagonists" *Science* Vol 330 No 6007 pp 1066–1071

Wu H. D Wacker M Mileni V Katritch G W Han E Vardy W Liu A A Thompson X P Huang R C Stevens 2012 "Structur o th Huma κ-Opioi Recepto i Comple wit JDTic" *Nature* Vol 485 No 7398 pp 327–332

Wyatt R. an J Sodroski 1998 "Th HIV- Envelop Glycoproteins Fusogens Antigens an Immunogens" *Science* Vol 280 No 5371 pp 1884–1888

Xu, J., Y. Hu, J. Kaindl, P. Risel, H. Hübner, S. Maeda, X. Niu, H. Li, P. Gmeiner, … B. K. Kobilka, 2019, "Conformational Complexity and Dynamics in a Muscarinic Receptor Revealed by NMR Spectroscopy", *Molecular Cell*, Vol. 75, No. 1, pp. 53-65.e7.

Xu, S., J. Tang, C. Wang, J. Liu, Y. Fu, and Y. Luo, 2019, "CXCR7 Promotes Melanoma Tumorigenesis via Src Kinase Signaling", *Cell Death and Disease*, Vol. 10, No. 3,.

Xu, T. R., R. J. Ward, J. D. Pediani, and G. Milligan, 2011, "The Orexin OX 1 Receptor Exists Predominantly as a Homodimer in the Basal State: Potential Regulation of Receptor Organization by Both Agonist and Antagonist Ligands", *Biochemical Journal*, Vol. 439, No. 1, pp. 171–183.

Xue, L., Q. Sun, H. Zhao, X. Rovira, S. Gai, Q. He, J. P. Pin, J. Liu, and P. Rondard, 2019, "Rearrangement of the Transmembrane Domain Interfaces Associated with the Activation of a GPCR Hetero-Oligomer", *Nature Communications*, Vol. 10, No. 1, pp. 2765.

Yagi, H., W. Tan, P. Dillenburg-Pilla, S. Armando, P. Amornphimoltham, M. Simaan, R. Weigert, A. A. Molinolo, M. Bouvier, and J. S. Gutkind, 2011, "Cancer Biology: A Synthetic Biology Approach Reveals a CXCR4-G 13-Rho Signaling Axis Driving Transendothelial Migration of Metastatic Breast Cancer Cells", *Science Signaling*, Vol. 4, No. 191, pp. ra60–ra60.

Yanagawa, M., M. Hiroshima, Y. Togashi, M. Abe, T. Yamashita, Y. Shichida, M. Murata, M. Ueda, and Y. Sako, 2018, "Single-Molecule Diffusion-Based Estimation of Ligand Effects on G Protein-Coupled Receptors", *Science Signaling*, Vol. 11, No. 548,.

Yin, S., M. J. Noetzel, K. A. Johnson, R. Zamorano, N. Jalan-Sakrikar, K. J. Gregory, P.

Jeffrey Conn, and C. M. Niswender, 2014, "Selective Actions of Novel Allosteric Modulators Reveal Functional Heteromers of Metabotropic Glutamate Receptors in the CNS", *Journal of Neuroscience*, Vol. 34, No. 1, pp. 79–94.

Zamai, M., A. Trullo, E. Arza, U. Cavallaro, and V. R. Caiolfa, 2019, "Oligomerization Dynamics of Cell Surface Receptors in Living Cells by Total Internal Reflection Fluorescence Microscopy Combined with Number and Brightness Analysis", *Journal of Visualized Experiments*, Vol. 2019, No. 153, pp. e60398.

Zarca, A., C. Perez, J. van den Bor, J. P. Bebelman, J. Heuninck, R. J. F. de Jonker, T. Durroux, H. F. Vischer, M. Siderius, and M. J. Smit, 2021, "Differential Involvement of ACKR3 C-Tail in β-Arrestin Recruitment, Trafficking and Internalization", *Cells*, Vol. 10, No. 3, pp. 618.

Zhang, Y., B. Sun, D. Feng, H. Hu, M. Chu, Q. Qu, J. T. Tarrasch, S. Li, T. Sun Kobilka, … G. Skiniotis, 2017, "Cryo-EM Structure of the Activated GLP-1 Receptor in Complex with a G Protein", *Nature*, Vol. 546, No. 7657, pp. 248–253.

Zheng, Y., G. W. Han, R. Abagyan, B. Wu, R. C. Stevens, V. Cherezov, I. Kufareva, and T. M. Handel, 2017, "Structure of CC Chemokine Receptor 5 with a Potent Chemokine Antagonist Reveals Mechanisms of Chemokine Recognition and Molecular Mimicry by HIV", *Immunity*, Vol. 46, No. 6, pp. 1005- 1017.e5.

Zheng, Y., L. Qin, N. V. O. Zacarías, H. De Vries, G. W. Han, M. Gustavsson, M. Dabros, C. Zhao, R. J. Cherney, … T. M. Handel, 2016, "Structure of CC Chemokine Receptor 2 with Orthosteric and Allosteric Antagonists", *Nature*, Vol. 540, No. 7633, pp. 458–461.

Zhong, C., and J. Schleifenbaum, 2019, "Genetically Encoded Calcium Indicators: A New Tool in Renal Hypertension Research", *Frontiers in Medicine*, Vol. 6, , pp. 128.

Zhou, Q., D. Yang, M. Wu, Y. Guo, W. Guo, L. Zhong, X. Cai, A. Dai, W. Jang, … S. Zhao, 2019, "Common Activation Mechanism of Class a GPCRs", *eLife*, Vol. 8.

Zhukovsky, M. A., S. Basmaciogullari, B. Pacheco, L. Wang, N. Madani, H. Haim, and J. Sodroski, 2010, "Thermal Stability of the Human Immunodeficiency Virus Type 1 (HIV-1) Receptors, CD4 and CXCR4, Reconstituted in Proteoliposomes", *PLoS ONE*, Vol. 5, No. 10.

Zirafi, O., K. A. Kim, L. Ständker, K. B. Mohr, D. Sauter, A. Heigele, S. F. Kluge, E. Wiercinska, D. Chudziak, … J. Münch, 2015, "Discovery and Characterization of an Endogenous CXCR4 Antagonist", *Cell Reports*, Vol. 11, No. 5, pp. 737–747.

Zlotnik, A., and O. Yoshie, 2000, "Chemokines: A new classification system and their role in immunity", *Immunity*, Vol. 12, No. 2 pp. 121–127.

Zou, Y. R., A. H. Kottman, M. Kuroda, I. Taniuchi, and D. R. Littman, 1998, "Function of the Chemokine Receptor CXCR4 in Heaematopolesis and in Cerebellar Development", *Nature*, Vol. 393, No. 6685, pp. 595–599.

Zürn, A., U. Zabel, J. P. Vilardaga, H. Schindelin, M. J. Lohse, and C. Hoffmann, 2009, "Fluorescence Resonance Energy Transfer Analysis of α 2a- Adrenergic Receptor Activation Reveals Distinct Agonist-Specific Conformational Changes", *Molecular Pharmacology*, Vol. 75, No. 3, pp. 534–541.

CURRICULUM VITAE

ACKNOWLEDGMENTS

First, I would like to thank my primary supervisor Prof. Dr. Martin J. Lohse for giving me the fantastic opportunity of working under his guidance. I learned an ocean-full of science from him, not only during the time he was my supervisor, but also before; when I was reading the publications from his group during my master's. I am very thankful to Prof. Lohse for showing great interest to even a tiny bit of the data I presented him, any time of the year and no matter how busy he was. It still impresses me every day how even a small feedback from him turns on so many lightbulbs in my head. For this, I would feel very lucky if I managed to learn how to think even a little bit like him. I am also deeply grateful to Prof. Lohse for being very supportive, not only with my project, but also personally to me along this journey. Thanks to him, I learned how to be think independently in science, but also how to collaborate with others when necessary. I am especially thankful to Prof. Lohse for introducing me to many valuable members of the GPCR community, which helped me immensely to break the shy in me and have the chance to discuss science with the experts all around the world.

I am immensely grateful to Prof. Markus Sauer for always being available to evaluate and follow the progress of my PhD. Prof. Sauer has always been the fastest to respond whenever I needed to organize a meeting or paperwork, even at a short notice and during difficult times, which made many things easy for me.

I would like to thank Prof. Martine Smit for all the unique opportunities she provided to me and to the whole ONCORNET group. Martine put up an amazing program and brought together the nicest, smartest and the most friendly group of people possible, and she worked endlessly to push every individual of this community forward. I am also very happy that she always treated me as one of her own students, and that she was always available to discuss my projects. I would like to thank also to all of my ONCORNET colleagues for being great collaborators and knowing how to make science a fun place. Specially, I would like to thank Chris de Graaf, Marta Arimont and Vladimir Bobkov for all

the work they did to bring up a great manuscript together with me. Many thanks to Dr. Steve Briddon for his feedbacks on several parts of this thesis. I would also like to thank to Prof. Tracy Handel for giving very critical and valuable feedback on my project from the first day she noticed it. I am very thankful to her for providing me several materials to assess my questions from different angles. I am also very thankful to Prof. Moritz Bünemann for providing me a life-changing opportunity in his lab in Marburg, which has been a key factor in my career. I am lucky to have taken my very first steps into the pharmacology field under his guidance, and I feel very grateful for his continuous support.

A huge part of the credit goes to my parents; Bektaş and Muammer İşbilir, for having their support and trust with me in anything I ever did. I could not be happier with the way they brought me up. I am very thankful to them for only expecting me to be myself. I am also very grateful to have my sister, Arzu, by my side, whenever I struggled and needed support. My cousins, Dilek, Fırat, Eray, Ersin and İdil have always been like siblings. They are one of the big reasons I am enjoying the life, and I cannot wait to spend the summer with them again. Demet, I know that you are looking down to us from heaven, with a glass of maracuja juice in your hand. I will always remember how cool and full-of-energy you were. My another brother, Hamid Hamzeiy also deserves a huge thank you for always being one of the most genuine and the least awkward friend, and also being a very inspirational scientist at the same time.

An endless amount of thanks go to my lab-mates, who were not only great collaborators and mentors in the lab, but also one of the best group of people I know. Thank you, Jan Möller and Eugene Grushevskyi Hannes Schihada, for helping me sharpen my math skills, but especially for being my best friends in these years. Another set of thanks for Katarina Nemec, Selma Anton, Ruth Pareja and Atakan Aydın for being great friends and colleagues in and out the lab, and, Bärbel Pohl, Marlies Grieben, Ulrike Zabel and Moni Frank for always helping me finding my way in the lab. I would like to thank the past and present members of AG Lohse for the great working atmosphere they created in the lab.

I am deeply thankful to my partner in crime, Mykolė Kasperavičiūtė, for always being near and present, no matter how much I annoyed her with science at home. Without Mykolė, this journey would not have been as joyful and fruitful as it has been.

Finally, I would like to thank anyone whose road somehow crossed with mine during my PhD in the last few years. Every small thing I learned from each one of you made my journey just better. So thank you all very much.